

FIBRE OPTIC SENSORS AND BEHAVIOUR IN CONCRETE AT EARLY AGE

THÈSE N° 2186 (2000)

PRÉSENTÉE AU DÉPARTEMENT DE GÉNIE CIVIL

ÉCOLE POLYTECHNIQUE FÉDÉRALE DE LAUSANNE

POUR L'OBTENTION DU GRADE DE DOCTEUR ÈS SCIENCES TECHNIQUES

PAR

Branko GLIŠIĆ

Ingénieur civil diplômé à l'université de Belgrade
Mathématicien diplômé à l'université de Belgrade
de nationalité yougoslave et origine serbe

acceptée sur proposition du jury:

Prof. L. Pflug, directeur de thèse
Prof. A. Del Grosso, corapporteur
Prof. M. Petronijević, corapporteur
Prof. F. H. Wittmann, corapporteur
Prof. A. Muttoni, corapporteur
Dr J.-G. Hammerschlag, corapporteur
Dr D. Inaudi, corapporteur

Lausanne, EPFL
2000

*To my parents,
father Dragomir and mother Dragica*

**МОЈИМ РОДИТЕЉИМА,
ОЦУ ДРАГОМИРУ И МАЈЦИ ДРАГИЦИ**

*Butterflies and dinosaurs
date from the same epoch...*

*Recent research leads scientists to the conclusion that butterflies
have survived because they have been equipped with better sensors
than dinosaurs, and thus are able to adapt to environmental changes.*

*Should we build structures with
a butterfly or dinosaur destiny?*

Préface

Si 40 siècles contemplaient les soldats de Napoléon du haut des pyramides de Gizeh, c'est parce que la conception de ces ouvrages offrait toute garantie de stabilité et de pérennité, élaborés qu'ils étaient pour traverser l'éternité. La forme de l'ouvrage et le matériau utilisé correspondaient parfaitement à cette vocation éternelle voulue par le maître d'œuvre.

De nos jours, la destination des ouvrages s'est fortement diversifiée mais les exigences de stabilité et de pérennité restent comparables - la notion d'éternité s'étant adaptée à notre perception du temps. Garantie dans une large mesure lors de l'emploi du granit ou du calcaire, cette pérennité peut être affectée lors du recours à des matériaux d'usage plus récent comme l'acier ou le béton. Fatigue, corrosion, microfissures ou carbonatation constituent autant d'agents susceptibles de réduire les propriétés du matériau et de conduire à terme à une dégradation marquée de l'ouvrage.

Dans le cas particulier du béton, les conditions prévalant lors de sa mise en place influent grandement la qualité finale du produit et par conséquent la tenue de l'ouvrage au cours du temps. Il importe donc de contrôler, de manière précise et continue, les tout premiers moments de la mise en place de ce matériau, commun mais fort complexe, d'en suivre l'évolution dans le temps, et d'y déceler le cas échéant les indices de défauts naissants.

Le mérite de Monsieur Glisic est d'avoir imaginé puis mis en œuvre un capteur d'une extrême sensibilité, susceptible de suivre l'évolution dimensionnelle du béton dès l'instant où, pâte amorphe, ce matériau est coulé en place. Ce mérite doit être souligné car la mise en œuvre d'un tel capteur, outre la phase proprement inventive inhérente à toute nouveauté, comporte le développement et l'application d'un savoir faire allant de la préparation du capteur proprement dit à sa mise en place in situ; cette dernière phase est particulièrement délicate eu égard à l'environnement hostile d'un chantier de génie civil.

Par ailleurs, Monsieur Glisic ne s'est pas contenté de l'aspect matériel ou expérimental, à eux seuls remarquables; il a également développé un module numérique destiné à simuler le comportement au très jeune âge du béton. Là également, il s'agit d'une modélisation inédite, dont l'adéquation aux phénomènes observés et mesurés a été dûment attestée. Cette double approche, théorique et expérimentale, témoigne d'une discipline rigoureuse dans la démarche scientifique de conception d'abord, puis d'étude détaillée des phénomènes complexes qui entrent en jeu.

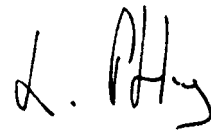
En effet, la mise en œuvre d'une telle instrumentation implique la maîtrise de techniques fort différentes : optique pour le principe de mesure, mécanique appliquée pour l'exploitation des mesures, informatique pour le stockage des informations, la modélisation numérique et le traitement des grandeurs mesurées, chimie pour la prise en compte et le contrôle de l'évolution du béton de l'état liquide à l'état solide, en attachant une importance particulière à l'évolution temporelle de la phase pâteuse.

Pour répondre à d'autres besoins spécifiques en matière de contrôle non destructif, le candidat a également conçu et développé d'autres capteurs inédits; ces capteurs ont tous été implantés in situ et leurs résultats contrôlés à l'aide de méthodes indépendantes. Pour chacun de ces

types de capteurs, le candidat a dû concevoir puis mettre en œuvre un dispositif inédit, en mesure d'exploiter le principe de fonctionnement basé sur l'interférométrie en basse cohérence, mais dont la configuration devait être adaptée à l'environnement imposé. C'est ainsi qu'ont été élaborés :

- Les capteurs longs (jusqu'à 40 de longueur de base) destinés au contrôle des micro-déplacements des barrages.
- Les capteurs "feuilles", installés sur un substrat en ruban souple et destinés au contrôle de déformation de membranes (application destinée à l'Exposition Nationale, entre autres).
- Le capteur de déplacement utilisé pour le contrôle de déplacement du tube du LHC du CERN. Ce tube est confiné à une température voisine du zéro absolu (1.4° K) et le contrôle de son positionnement nécessite une technique totalement nouvelle.

Par le sérieux et la pertinence de son apport, Monsieur Glisic s'inscrit de manière remarquable dans la lignée de jeunes chercheurs enthousiastes et créatifs dont j'ai eu l'honneur et le privilège de diriger les premiers travaux.



Prof. L. Pflug

Outline

Préface	xii
Acknowledgements	xi
Summary	xv
Version abrégée	xvii
Zusammenfassung	xix
Резиме	xxi
Table of contents	xxiii
1 Introduction	1
2 SOFO monitoring system	15
3 Concrete at early and very early age	21
4 Numerical models for Standard Sensor and concrete at very early age	37
5 Interaction of Standard Sensor and concrete at early and very early age	55
6 Characterisation of concrete at early and very early age	85
7 Advanced sensor designs	117
8 Conclusions	147
9 Bibliography	149
Appendix: Monitoring system - basic notions	a1
Curriculum vitae	
Published papers	

Acknowledgements

This thesis was mainly done at the Laboratory of Stress Analysis (IMAC) of the Swiss Federal Institute of Technology, Lausanne (EPFL) under direction of Prof. Léopold Pflug. Nevertheless, portions of the work were carried out in other institutions or in-situ, and many people were contributed in different ways to its successful completion.

I would especially like to thank:

- | | |
|--|---|
| Prof. Léopold Pflug
IMAC-EPFL,
Director of thesis | For his enthusiasm, support, encouragement, and generosity, for the autonomy he allowed me in research and for the unique work ambience he created at IMAC |
| Prof. Jean-Claud Badoux
President of the EPFL | For his encouragement, support, comprehension and for the scholarship he provided |
| Dr Daniele Inaudi
Smartec SA, IMAC-EPFL | For including me in the SOFO project, supervising my work from beginning to end, for correction to the final thesis document, as well as his support, encouragement, friendship, comprehension and for being member of the jury of this thesis |
| Dr Samuel Vurpillot
Smartec SA, IMAC-EPFL | For introducing me in the IMAC laboratory, for his help and excellent advise which improved my thesis better, for support, encouragement and friendship, for exchange of comics, and for discovering high mountains, water sports, single malts and Gag's bar |
| Olivier Bernard
MCS-EPFL | For his support, help and precious advise concerning research on concrete at very early age, belief in my work, collaboration during the tests and friendship |
| Raymond Délez
IMAC-EPFL | For his precious help, advise and mechanical knowledge which was indispensable for the realisation of several tests in the laboratory as well as in-situ, for transport to building sites and for his friendship and great days he offered me in the Vallais |
| Dr Pierre Mivelaz
MCS-EPFL | For their support, and precious advise concerning research on the concrete at very early age, encouragement and collaboration during the test program |
| Dr Jean Marc Ducret
ICOM-EPFL | |
| Prof. Zivota Perisic
University of Belgrade, Dean of
Faculty of Civil Engineering | For his support, encouragement and recommendations which offered me the possibility to come to the EPFL |

- Jean Hugon**
Bruno Gay-Des-Combes
Electricité d'Emosson SA
- For their collaboration, kindness, helpfulness, interest in the Long Sensor development and my work, for being friendly as well as for making each visit to the Emosson dam instructive, pleasant and exciting
- Jean-Marie Rouiller**
Olivier Dumas
Bertrand Daubord
and Electricité d'Emosson SA
- For their support, interest in fibre optic sensors technology, for financial support and for making the Emosson dam available for Long Sensor implementation
- Smartec SA**
IMM SA
- For the enthusiasm, support, interest in my work and collaboration during realisation of tests
- Prof. Ian Smith**
- For their advise and corrections that have considerably increased the quality of the final document
- Dr Ruth Stalker**
Pascal Kronenberg
Bernd Domer
IMAC-EPFL
- Sandra Lloret Berrera**
- For her advise, corrections and extremely critical (almost pessimistic) spirit that have considerably increased the quality of the thesis, for help in the SOFO laboratory and during installation of the Displacement Sensor as well as for her help during fabrication of sensors for purposes of her thesis
- Eduardo Kessi**
and Créatex SA
- For the support, interest in my work and collaboration during development of the Membrane Sensor
- Dr Francois Bay**
Pierre-Olivier Bouchard
Ecole des mines de Paris
Jean-Albert Ferrez
ROSO-EPFL
- For their support as well as for their help and collaboration on the numerical modelling
- Juan Garcia Perez**
Jacques Billan
Walter Scandale
and LHC-CERN
- For their enthusiasm, support, interest and belief in fibre optic sensing technology, and collaboration during development of the Displacement Sensor
- Dr Pieter Volgers**
IMAC-EPFL
- For his support, help in numerical modelling, friendship and instructive discussions with *pain au chocolat* every morning
- Sirine Fakra**
- For her enthusiasm and help during realisation and testing of the Displacement Sensor as well as for her particular charm with which she weakened and lost different parts of IMAC's equipment
- Prof. Bishwajit Bhattacharjee**
Delhi University of Technology,
Nicolas Simon
IBAP-EPFL
- For his enthusiasm as well as collaboration and help during development and testing of the Stiff Sensor

Yves Putallaz
Michaël Benouaich
Alexandre Destraz
Claire Scholtes
Students - EPFL

For their help and collaboration during the realisation of different tests that considerably contributed to the thesis

Prof. Mira Petronijevic
University of Belgrade

For her support, corrections to the final document and for being a member of the jury of this thesis

Prof. Eugen Brühwiler
Roland Gysler
and **MCS-EPFL**

For their help and advise during the realisation of different projects and for the use of their tests for my purposes

Prof. Marc Badoux
Dr Jean Paul Jaccoud
Blaise Fleury
and **IBAP-EPFL**

Christian Monney
Alexandre Blanc
Miguel Navarro Gomez
and **ICOM-EPFL**

Gilbert Steinmann
Frédéric Mayoraz
LMS-EPFL

Dr Parviz Navi
LMC-EPFL

Prof. Andrea Del Grosso
University of Genoa

For their corrections, advise and for being members of the jury of this thesis

Prof. Folker H. Wittmann
IBWK-ETHZ

Prof. Aurelio Muttoni
IBAP-EPFL

Dr Jean-Gabriel
Hammerschlag
TFB SA

Alain Herzog
IMAC-EPFL

For his wonderful photos, for making me "star" in the Flash journal, for football, for sharing the office with me and for asking me each morning: "Comment ça va?"

All members of Mala Srpska
Zajednica and notably
Ljubica, Sandra and Dragan,
Jelena and Laurent,
Bojana and Zoran,
Maja and Igi, Tanja, Bora,
Cane and Despot

For their support, encouragement, friendship, advise, suppers, as well as for the first steps and great days in "Serbian Diaspora"

All members of IMAC and notably

Prof. Léopold Pflug

Dr Daniele Inaudi

Dr Samuel Vurpillot

Raymond Délez

Denis Clément

Michel Cherbuliez

Etienne Fest

Charles Gilliard

Martine Baudin

Yvan Robert-Nicoud

Prof. Ian Smith

Sandra Lloret Berrera

Dr Ruth Stalker

Pascal Kronenberg

Bernd Domer

For their support, encouragement, friendship, advise, corrections, uniquely pleasant work ambience, as well as for making easier my first steps in Switzerland, IMAC's football team, *fêtes*, ski-days (in mountain or on water), and for offering me a wonderful four years in Lausanne

Father Dragomir Glisic

Mother Dragica Glisic

For their support, encouragement, belief in me and love

Tanja Kragic

For her encouragement, support, love in good and patience and comprehension in less good moments

I would like to thank once more all of these people and all of the many others that contributed even a small amount of their time, patience and energy for the successful realisation of this thesis.

Summary

Civil structures are important to society. For durable and safe service lives, good design, quality construction as well as appropriate management during service are important goals of structural engineering. Measurement and monitoring are often essential parts of managing activities. Therefore, monitoring structures from construction to the end of service may be useful. For concrete structures, this includes monitoring during the early age.

Early age of concrete includes the period that begins with pouring and finishes when the thermal processes due to hydration are calmed. The period within early age during which the concrete is not hardened is called very early age. Thermal processes, caused by hydration of cement, generate unavoidable early and very early age deformation that is the origin of premature cracking of concrete. Recent research shows that early age cracking significantly increases the vulnerability of structures to environmental effects that attack concrete and rebars. Such effects damage structures, thereby reducing their long-term capacity and durability. Therefore it is important to understand and monitor early and very early age deformation.

The deformation measurement system, based on the low coherence interferometry in fibre optic sensors, has already been developed at IMAC-EPFL. This system has been applied and verified on several structures in Switzerland and Europe. The sensor, usually employed for in-situ monitoring, is called the Standard Sensor, for the purposes of this thesis.

The Standard Sensor can be used in a wide variety of applications and materials. However, there are some cases where it can not be applied. Its application may be limited by its dimensions, by the mechanical properties of materials of the host structure or by extreme environmental conditions (low ambient temperature and pressure).

This work is closely related to the monitoring system cited above. Generally two groups of problems are treated: monitoring of concrete structures at early and very early age and monitoring of special structures for cases where application of the Standard Sensor is not possible.

The phenomenon of very early age deformation is assessed three ways. Firstly, a numerical model describing the evolution of thermal expansion coefficient is developed in order to understand the generation of very early age deformations. Then the interaction between the Standard Sensor and very early age concrete is numerically modelled and experimentally examined in order to estimate whether or not the Standard Sensor is able to measure very early age deformation of concrete. Since a positive response is obtained, the third assessment, characterisation of concrete at very early age, is performed.

In order to extend the use of the monitoring system to special cases when use of Standard Sensor is not possible, four advanced sensors have been developed in this work. The Membrane Sensor is for use on laminated materials (e.g. membrane roofing). The Long Sensor has a measurement gauge length of several tens of meters. Its purpose is the measurement of deformations in massive and large structures (dams, tunnels). The aim of the Stiff Sensor is to determine the hardening time of concrete. Finally, the Displacement Sensor is used to measure large displacements over short gauge lengths even when it is exposed to extreme environmental conditions (temperature of 1.9 K and vacuum).

Version abrégée

Les structures de génie civil jouent un rôle important dans la vie d'un pays. Pour garantir leur durabilité ainsi que leur exploitation, une construction de qualité aussi bien qu'une gestion optimale durant l'exploitation doivent être des objectifs prioritaires. Mesures et auscultation sont souvent considérés comme la clef de cette gestion efficace. Cette auscultation débute dès la mise en place du béton.

Le jeune âge du béton est défini par la période comprise entre le bétonnage et l'instant où les processus thermiques liés à l'hydratation deviennent négligeables. Le très jeune âge est défini comme la période durant laquelle le béton n'est pas encore durci. Les processus thermiques, engendrés par l'hydratation du béton, génèrent inévitablement une déformation qui est à l'origine de la fissuration prématurée du béton. Les recherches récentes ont montré que la fissuration au jeune âge augmente la vulnérabilité des structures face aux influences nuisibles de l'environnement, agressant le béton et l'armature, endommageant la structure et réduisant ainsi la durabilité et la capacité à long terme des structures. La mesure des déformations au jeune et très jeune âge permettra ainsi de mieux comprendre les causes des variations dimensionnelles néfastes apparaissant dans ces phases.

Un système de mesure de capteurs à fibres optiques basé sur l'interférométrie à basse cohérence a été développé à l'IMAC-EPFL. Ce système, appliqué sur différents ouvrages en Suisse et en Europe, présente des nombreux avantages quant à la mesure des variations dimensionnelle du béton.

Le Capteur Standard (Standard Sensor) utilisé dans une large gamme d'applications et de matériaux, présente toutefois des lacunes dans certains domaines: cas des variations de phase des matériaux, utilisation des matériaux non - traditionnels et application dans des conditions extrêmes (basse température et pression).

Le travail fourni dans cette thèse est étroitement liée à ce système de mesure. Deux domaines y sont traités: L'auscultation du béton au jeune et très jeune âge et auscultation des ouvrages spéciaux, dans les cas où l'utilisation du Capteur Standard n'est pas possible.

Les problèmes concernant l'auscultation au très jeune âge ont été divisés en trois domaines. Développement d'un modèle numérique décrivant l'évolution du coefficient de la dilatation thermique. L'analyse de l'interaction entre le Capteur Standard et le béton au très jeune âge a été défini par des méthodes numériques et expérimentales. Finalement, la caractérisation du béton au très jeune âge a été réalisée.

L'extension de l'utilisation du Capteur Standard aux cas extrêmes à nécessité le développement de quatre Capteurs Spéciaux: Le Capteur à ruban (Membrane Sensor) destiné à mesurer les déformations des matériaux laminés (par ex. toiture en toile). Le Capteur Long (Long Sensor) muni d'une base de mesure de plusieurs dizaines de mètres, mesurant les déformations dans des ouvrages larges et massifs (barrages, tunnels). Le Capteur Rigide (Stiff Sensor) dont l'intérêt est l'identification du point de rigidification du béton. Finalement, le Capteur à grand déplacements (Displacement Sensor) utilisé pour mesurer déplacements sur une plage courte exposé dans des conditions d'environnement extrême (température de 1.9K et sous vide).

L'auteur espère ainsi que le présent travail contribuera à éteindre notre connaissance du comportement réel des ouvrages.

Zusammenfassung

Bauwerke sind wichtige Investitionsgüter unserer Gesellschaft. Eine sichere Bemessung, qualitativ hochwertige Bauausführung so wie ein entsprechendes Facility-Management stellen die Nutzung des Gebäudes über seine geplante Lebensdauer sicher. Der Einsatz von Mess- und Überwachungssystemen erleichtert die Planung von Instandhaltungsaktivitäten und ist deshalb von der Fertigstellung bis an das Lebensende des Bauwerks zu empfehlen. Bei Betonbauten beinhaltet dies zusätzlich die Überwachung des Betons im jungen Alter.

Der Begriff junger Beton bezeichnet die Zeitperiode vom Betonieren bis zum Abklingen der durch die Hydratation bedingten thermischen Prozesse. Der Zeitraum innerhalb des jungen Alters, in welcher sich der Beton noch nicht verfestigt hat, wird als sehr junges Alter bezeichnet. Thermische Prozesse, die durch die Hydratation des Zements verursacht sind, haben unausweichlich Verformungen im sehr jungen und im jungen Alter zur Folge, welche die Ursache von vorzeitiger Rissbildung sind. Forschungsprojekte haben gezeigt, dass die Rissbildung im jungen Alter die Verletzbarkeit des Bauwerks durch äussere Einflüsse, welche den Beton ebenso wie die Bewehrung angreifen, drastisch erhöht. Solche Einflüsse beschädigen Bauwerke und beeinträchtigen damit ihr Langzeitverhalten und ihre Dauerhaftigkeit. Es ist deshalb wichtig, Verformungen im junge Alter und im sehr jungen Alter zu verstehen und zu überwachen.

Das am IMAC (EPFL) entwickelte Verformungsmesssystem wurde bereits zur Überwachung von zahlreichen Bauwerken in der Schweiz und im Ausland eingesetzt und hat sich dabei bestens bewährt. Es beruht auf Glasfasersensoren, die mittels optischer Interferometrie in nieder Kohärenz gelesen werden. Der Sensor, hauptsächlich zur in-situ Überwachung eingesetzt, wird im Rahmen dieser Arbeit „Standardsensor“ genannt.

Obwohl der Standardsensor für ein weites Gebiet von Anwendungen und Materialien einsetzbar ist, gibt es Fälle, für die er ungeeignet ist. Seine Anwendung ist beispielsweise limitiert durch seine Grösse, durch Materialeigenschaften des zu überwachenden Bauwerks und durch extreme äussere Einflüsse (z.B. tiefe Temperaturen und niedriger Luftdruck).

Diese Arbeit ist eng mit dem zuvor erwähnten Messsystem verknüpft. Grundsätzlich werden zwei Probleme behandelt: Die Überwachung von Betonelementen im jungen und sehr jungen Alter, und die Überwachung von speziellen Bauwerken wo der Standardsensor nicht eingesetzt werden kann.

Die Auswertung des Phänomens der Verformungen im sehr jungen Alter geschieht in drei Phasen. Erstens wird ein numerisches Model entwickelt, das die Evolution des thermischen Ausdehnungskoeffizienten beschreibt und damit die Entstehung von Verformungen im sehr jungen Alter modelliert. In der zweiten Phase wird die Interaktion zwischen dem Standardsensor und dem sehr jungem Beton numerisch modelliert. Der Vergleich mit experimentell gewonnenen Daten soll belegen, dass der Standardsensor in der Lage ist, Betonverformungen im sehr jungen Alter zu messen. An letzter Stelle wird der Beton im sehr jungen Alter charakterisiert.

Damit das Überwachungssystems in Fällen, in denen der Einsatz von Standardsensoren unmöglich ist, angewendet werden kann, wurden im Rahmen dieser Arbeit vier neuartige Sensoren entwickelt. Der „Membransensor“ wird bei geschichteten Materialien (z.B. Membranbedachungen) eingesetzt. Der „lange Sensor“ verfügt über eine Messlänge zwischen 30 und 40 Metern, grössere Messlängen sind allerdings möglich. Er wird zur Überwachung von Verformungen in grossen Massivbauten (z.B. Staumauern und Tunnel) verwendet. Das Einsatzgebiet des „steifen Sensors“ ist die Bestimmung der Verfestigungsdauer von Beton. Der „Verschiebungssensor“ wird bei der Messung von weiten Verschiebungen über kurze Messdistanzen angewendet, er ist von besonderem Interesse bei extremen äusseren Bedingungen (Temperatur 1.9 K und Vakuum).

Резиме

Грађевинске конструкције имају значајну улогу у свакој заједници. Зато су важни циљеви грађевинарства да им обезбеди дуготрајну и сигурну употребу не само кроз добар дизајн и квалитетну израду, него и кроз адекватно одржавање, управљање и контролу. Мерење деформација и праћење рада конструкција (Monitoring или Auscultation) су често интегрисани у те три активности. Праћење рада конструкција је свакако најбоље започети непосредно након градње конструкције и спроводити га до окончања њене употребе. На тај начин, у случају бетонских конструкција, праћење је спроведено и током младих дана бетона.

Период који почиње непосредно након ливења бетона и који се завршава са смиривањем термичких процеса у бетону изазваних процесом хидратације, назива се млади дани (early age). Период који је укључен у младе дане, а током ког је бетон још увек неочврсно, назива се веома млади дани (very early age). Термички процеси имају као неизбежну последицу генерисање деформације током младих и веома младих дана која је узрок преране појаве прслина на бетону. Новија истраживања показују да прерана појава прслина значајно смањује отпорност бетона према агресивним материјама из околине које могу изазвати његову деструкцију као и корозију арматуре, и на тај начин битно смањити дуготрајност и каснију носивост конструкције. Зато је неопходно разумети механизме и пратити еволуцију деформације у младим и веома младим данима.

Систем за праћење деформација, заснован на приципу ниске кохереције у сензорима од оптичких влакана, развијен је у лабораторији ИМАС-EPFL и доказан на различитим типовима конструкција у Швајцарској и Европи. Сензор који је коришћен у тим приликама назива се стандардни сензор (Standard Sensor).

Стандардни сензор може бити примењен за праћење деформација на широком спектру конструкција, али ипак постоје случајеви када је немогуће применити га. Ово ограничење у употреби стандардног сензора углавном је последица његових димензија, механичких особина материјала од ког је конструкција направљена или екстремним условима околине у којој се конструкција налази (нпр. ниска температура или притисак).

Тема ове тезе је уско везана са наведеним системом за праћење деформација. Генерално гледано, истраживања су подељена у две групе: праћење деформација на бетонским конструкцијама током младих и веома младих дана и праћење деформација на специјалним типовима конструкција у случајевима у којима је немогуће применити стандардни сензор.

Група истраживања која се тичу праћења деформација бетона у младим и веома младим данима подељена је у три подгрупе. Најпре је развијен нумерички модел који описује еволуцију коефицијента термичке дилатације бетона како би се разумео процес генерисања деформације током младих и веома младих дана. Затим су извршене нумеричка анализа и експериментално испитивање интеракције између стандардног сензора и бетона, са циљем да се оцени да ли се датим сензором могу мерити деформације током веома младих дана. Коначно, када је претходно истраживање дало позитиван одговор, извршена је карактеризација бетона у младим и веома младим данима.

Друга група истраживања обухвата развој и проверу четири нова сензора. Сензор за мембране (Membrane sensor) намењен је мерењу деформација на танким мембранским конструкцијама (нпр. кровови од пластичних платана). Дуги сензор (Long Sensor) има мерну базу дугу више десетина метара и његова намена је мерење деформација на масивним конструкцијама (нпр. бране и тунели). Крути сензор (Stiff Sensor) је намењен регистовању времена очвршћавања бетона. Коначно сензор за померања (Displacement Sensor) намењен је мерењу великих померања са малом мерном базом у екстремним амбијенталним условима (температура од 1.9 К и вакуум).

Table of contents

Préface	xii
Acknowledgements	xi
Summary	xv
Version abrégée	xvii
Zusammenfassung	xix
Резиме	xxi
1 Introduction	1
1.1 Monitoring of structures	1
1.2 Motivations, objectives and the specific context of this thesis	2
1.3 Monitoring of concrete structures	6
1.3.1 Introduction	6
1.3.2 Importance of structural monitoring	6
1.3.3 Required performances of new monitoring systems	9
1.3.4 Importance of monitoring of concrete at early and very early age	10
1.3.5 SOFO measurement system	11
1.4 References	12
2 SOFO monitoring system	15
2.1 Introduction	15
2.2 Main components and functional principle of the SOFO system	15
2.3 Standard Sensor - description	16
2.4 SOFO sensor measurement	17
2.5 Performances of SOFO system	18
2.6 References	19
3 Concrete at early and very early age	21
3.1 Introduction	21
3.2 Composition of concrete	21
3.3 Hydration process	22
3.4 Thermal effects	23
3.5 Maturity	24
3.6 Setting, solidification and hardening	25
3.7 Early and very early age of concrete, hardening time	26
3.8 Evolution of mechanical properties of concrete - description	26
3.9 Mechanical properties of concrete at very early age - initial stiffness and strength	27
3.10 Deformation of concrete at early and very early age	30
3.11 Concluding remarks	34
3.12 References	34
4 Numerical models for Standard Sensor and concrete at very early age	37
4.1 Introduction	37
4.2 Numerical model for Standard Sensor	37
4.3 Simplified numerical model for concrete at very early age	39
4.3.1 Introduction	39
4.3.2 Composite and Multiphase models	39
4.3.3 Development of Extended Multiphase (EM) model	43
4.4 Concluding remarks	53

4.5 References	53
5 Interaction of Standard Sensor and concrete at early and very early age	55
5.1 Introduction	55
5.2 Numerical modelling of sensor-concrete interaction	56
5.2.1 Introduction	56
5.2.2 Concrete composition	57
5.2.3 2D FEM modelling at meso-level	57
5.2.4 3D FEM modelling at macro-level	60
5.2.5 Results and discussion	62
5.2.6 Summary	68
5.3 Experimental estimation of concrete-sensor interaction	68
5.3.1 Introduction	68
5.3.2 Laboratory tests	69
5.3.3 Results and discussion	78
5.3.4 Summary	80
5.4 Other system applied for in-situ monitoring of concrete at very early age	81
5.5 Concluding remarks	82
5.6 References	82
6 Characterisation of concrete at early and very early age	85
6.1 Introduction	85
6.2 Monitoring of total early age deformation of concrete	85
6.2.1 Typical deformation of concrete at early and very early age	85
6.2.2 Monitoring in laboratory conditions	87
6.2.3 In-situ monitoring	91
6.2.4 Summary	93
6.3 Monitoring of hardening time of concrete	94
6.3.1 Introduction	94
6.3.2 Hardening time of concrete in case of hybrid structures	95
6.3.3 Hardening time of concrete in general case	98
6.3.4 Summary	103
6.4 TEC evolution monitoring at very early age	104
6.4.1 Introduction	104
6.4.2 Principle of experiment	104
6.4.3 Laboratory monitoring of TEC evolution	105
6.4.4 Summary	114
6.6 Concluding remarks	114
6.7 References	115
7 Advanced sensor designs	117
7.1 Introduction	117
7.2 Membrane Sensor	117
7.3 Long Sensor	126
7.4 Stiff Sensor	132
7.5 Displacement Sensor	137
7.6 Concluding remarks	145
7.7 References	146
8 Conclusions	147
9 Bibliography	149

Appendix: Monitoring system - basic notions	a1
A1 Introduction	a1
A2 What is a measurement?	a1
A3 Direct and indirect measurement	a2
A4 Error of a measurement	a2
A5 Measurement system	a3
A6 Time dependant measurement - absolute and relative measurement	a4
A7 Monitoring system	a4
A8 Properties of a measurement system: sensitivity, resolution, precision, dynamic range and drift	a5
A9 Deformation sensor	a6
A10 Static and dynamic deformation	a7
A11 Choice of the monitoring system	a8
A12 References	a8

Curriculum vitae

Published papers

1 Introduction

1.1 Monitoring of structures

Civil structures are omnipresent in every society, regardless of culture, religion, geographical location and economical development. It is difficult to imagine a society without buildings, roads, rails, bridges, tunnels, dams and power plants. Structures affect human, social, ecological, economical, cultural and aesthetic aspects of societies and associated activities contribute considerably to the gross internal product (GIP) (in 1998 in Switzerland, architecture, engineering and construction investments accounts for 41 billions of Swiss Francs [1]). Therefore good design, quality construction as well as durable and safe exploitation of civil structures are goals of structural engineering.

Malfunctioning of civil structures often has serious consequences. The most serious is an accident involving human victims. Even when there is no loss of life, populations suffer if infrastructure is partially or completely out of service. Collapse of certain structures, such as nuclear power plants, may provoke serious ecological pollution. The economic impact of structural deficiency is twofold: direct and indirect. The direct impact is reflected by costs of reconstruction while the indirect impact involves losses in the other branches of the economy. Fully collapse of historical monuments, such as old stone bridges and cathedrals, represent an irretrievable cultural loss for society.

The most safe and durable structures are usually structures that are well managed. Measurement and monitoring often have essential roles in management activities.

Several monitoring systems have been developed for monitoring of civil structures (bridges, dams, tunnels, etc.) that are constructed from standard construction materials such as concrete, steel and timber (see Appendix). Such monitoring systems are not appropriate in certain situations. For example, it is important to monitor the evolution of deformation of concrete structures during the very early age. However traditional deformation monitoring systems are not applicable to non-hardened concrete. Also for non-typical structures and structures built of non-standard materials, utilisation of such monitoring systems is often impossible due to aspects such as material properties, geometry and environmental conditions.

In this thesis, challenges related to structural monitoring are addressed in two ways: characterisation of concrete structures at very early age, and the development of sensors for specific advanced applications.

1.2 Motivations, objectives and the specific context of this thesis

Motivations

The principal motivations for this work has been inspired from three sources. The first source is the importance of in-situ deformation monitoring during all phases of a structure's life, from the construction, to the end of service (see Section 1.3). The second source originates from importance of monitoring and characterisation of concrete structures at early and very early age (see Sections 1.3 and Chapter 3). The third source is a desire to extend a novel monitoring system called SOFO (see Section 1.3 and Chapter 2), to non-traditional applications. The system is based on low-coherence interferometry in fibre optic sensors. When the sensor employed traditionally, it is named the Standard Sensor for the purposes of this thesis. The discussion concerning the motivation of this work is further developed in Section 1.3.

In Table 1.2.1 the scope of successful applications is resumed through comparison of the SOFO system with other monitoring systems prior to this research. In the table, monitoring systems are divided into two sets: those applicable to typical structures (bridges, dams, tunnels etc.) and made out of standard construction materials (concrete, steel and wood), and those monitoring systems that are designed for special applications (structures whose dimensions, construction material or environmental conditions do not permit utilisation of a traditional monitoring system). Structures are considered to be existing or new. It is important to emphasise that the monitoring of new concrete structures includes the very early age period.

<i>Civil structures</i>	<i>Standard structures</i>						<i>Special applications</i>	
	<i>Concrete</i>		<i>Steel</i>		<i>Wood</i>		<i>SOFO</i>	<i>Other</i>
	<i>SOFO</i>	<i>Other</i>	<i>SOFO</i>	<i>Other</i>	<i>SOFO</i>	<i>Other</i>		
<i>Existing</i>	4	4	4	4	4	4	?	8
<i>New</i>	?	8	4	4	4	4	?	8

SOFO - SOFO system, Other - Other monitoring systems,

4 - Successful application, 8- No application, ? - Application possible but not confirmed

*Table 1.2.1: Scope of successful applications.
This thesis focuses on application where a ? is noted*

Further discussion concerning the motivation of this work is provided in Section 1.3.

Scope, objectives and original contribution

Results of four tasks are reported in this thesis:

- *Numerical modelling of evolution of concrete thermal expansion coefficient*
- *Estimation of interaction between the Standard Sensor and concrete at very early age*
- *Characterisation of concrete at very early age using the Standard Sensor*
- *Development of sensors for special applications*

The first task is related to the second. In order to estimate numerically the interaction between the Standard Sensor and concrete at very early age, an existing multiphase model is used for numerical modelling of Young modulus and Poisson coefficient. However, no appropriate model has been found for the evolution of thermal expansion coefficients (TEC) for concrete. Therefore an original numerical model was developed (see Chapter 4).

The aim of the second task is to examine whether the Standard Sensor can be used for measuring deformations in concrete at very early age. This original and new research consists of numerical simulations and laboratory experiments (see Chapter 5).

In the third task, procedures for determining and monitoring important characteristics of concrete at early and very early age are developed. Characteristics such as deformation, hardening time and evolution of thermal expansion coefficient (see Chapters 3 and 6) are studied. Aside from scientific contribution (see below), the results of this research in this domain will contribute to establishment of new standard procedures.

The fourth task is consecrated to the development of special sensors for use in cases when application of the Standard Sensor is not possible. Four new sensors are developed: the Long Sensor for measurements with measurement basis longer than 10 metres, the Membrane Sensor destined to measure the deformations of thin plastic membranes, the Stiff Sensor whose purpose is the determination of the hardening time of concrete and the Displacement Sensor for measurement in extreme environmental conditions (temperature of 1.4K and vacuum).

Completion of these tasks has resulted in the following scientific contributions:

- ***Increased knowledge concerning the real behaviour of concrete at very early age***
- ***Characterisation of concrete at very early age***
- ***Development and calibration of numerical models that describe this characterisation***
- ***Understanding of real behaviour of special civil structures***

Research related to the interaction between the Standard Sensor and very early age concrete, as well as the successful development of sensors for special applications will extend the domain of application of fibre optic monitoring system. Thus, the deficiencies presented in Table 1.2.1 will be improved (question marks in Table 1.2.1 will be replaced with ticks).

The following contributions are the main sources of originality in this thesis:

- ***A numerical model for evolution of concrete thermal expansion properties***
- ***Providing for very early age deformation measurement, hardening time measurement and thermal expansion coefficient evolution measurement***
- ***Development of sensors with greater performance than the Standard Sensor (Long Sensor) and development of sensors for special applications (Membrane Sensor, Stiff Sensor and Displacement Sensor)***

Specific context of thesis

This work is part of the research performed by the SOFO group at EPFL. The aim of the SOFO group is to develop a complete monitoring system using fibre optics. Three areas of activities define the research. The first area involves development of the reading unit; the second area focuses on new sensors; and the third area concerns the analysis of data obtained by the SOFO system. The areas of the SOFO group activities are shown in Figure 1.2.2.

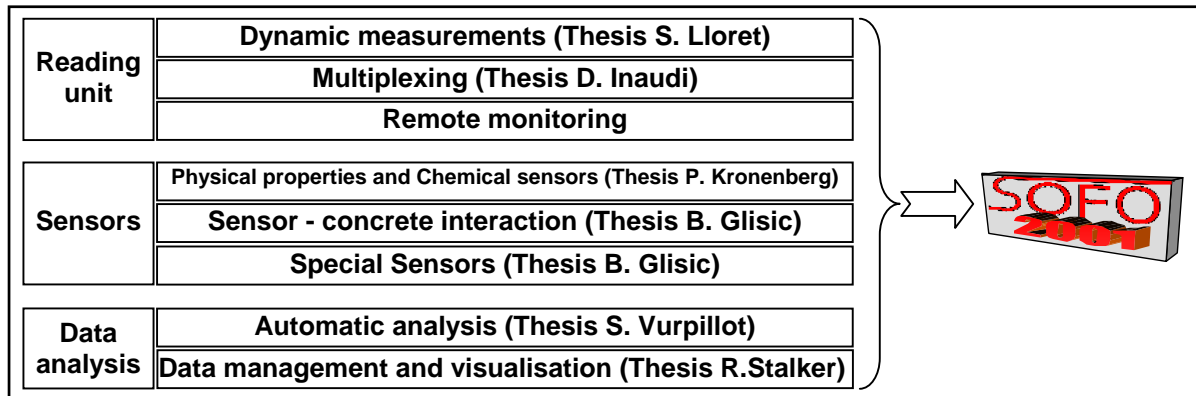


Figure 1.2.2: This thesis in the Context of the SOFO group activities

Guide

To facilitate reading of this document, we present briefly the content of each Chapter. In this way, the reader can consult rapidly specific topics of interest.

- In the continuation of the first Chapter, we develop the topics related to motivation for this thesis. We explain in more detail the general importance of monitoring, monitoring of concrete structures at early and very early age and aspects of the SOFO monitoring system.
- The technical presentation of the SOFO monitoring system, its functional principle, components and performances are given in the second Chapter.
- The third Chapter introduces the reader to notions related to concrete at early and very early age. The hydration process and its effects on mechanical properties and deformation are presented in this Chapter. Particular attention is devoted to making a distinction between very early age and early age as well as between the origins of the early age deformation and the very early age deformation.
- In the fourth Chapter, numerical models of the sensor and the mechanical behaviour of concrete are described. In this Chapter, a new model for the thermal expansion coefficient is developed. This model and the following three Chapters are original contribution of this thesis.
- The interaction between the Standard Sensor and concrete is presented in Chapter 5. This interaction is modelled numerically and studied experimentally.

- The sixth Chapter contains a characterisation of the early and very early age concrete. Monitoring results of the early and very early age deformation as well as determination of hardening time and thermal expansion coefficient evolution are presented in this Chapter.
- The development and application of four special sensors are given in the seventh Chapter. The Long Sensor is used for displacement monitoring of large structures; the Membrane Sensor for monitoring of membrane structures; the Stiff Sensor for monitoring of hardening time of concrete and the Displacement Sensor for monitoring of displacement in extreme environmental conditions, including an application to the Large Hadron Collider (LHC) at CERN.

Each Chapter finishes with relevant references. The conclusions and bibliography are in Chapters 8 and 9. Finally, basic notions related to monitoring systems are presented in an appendix. The structure of the thesis, the interactions between Chapters and original work of the author are presented in Figure 1.1.2.1.

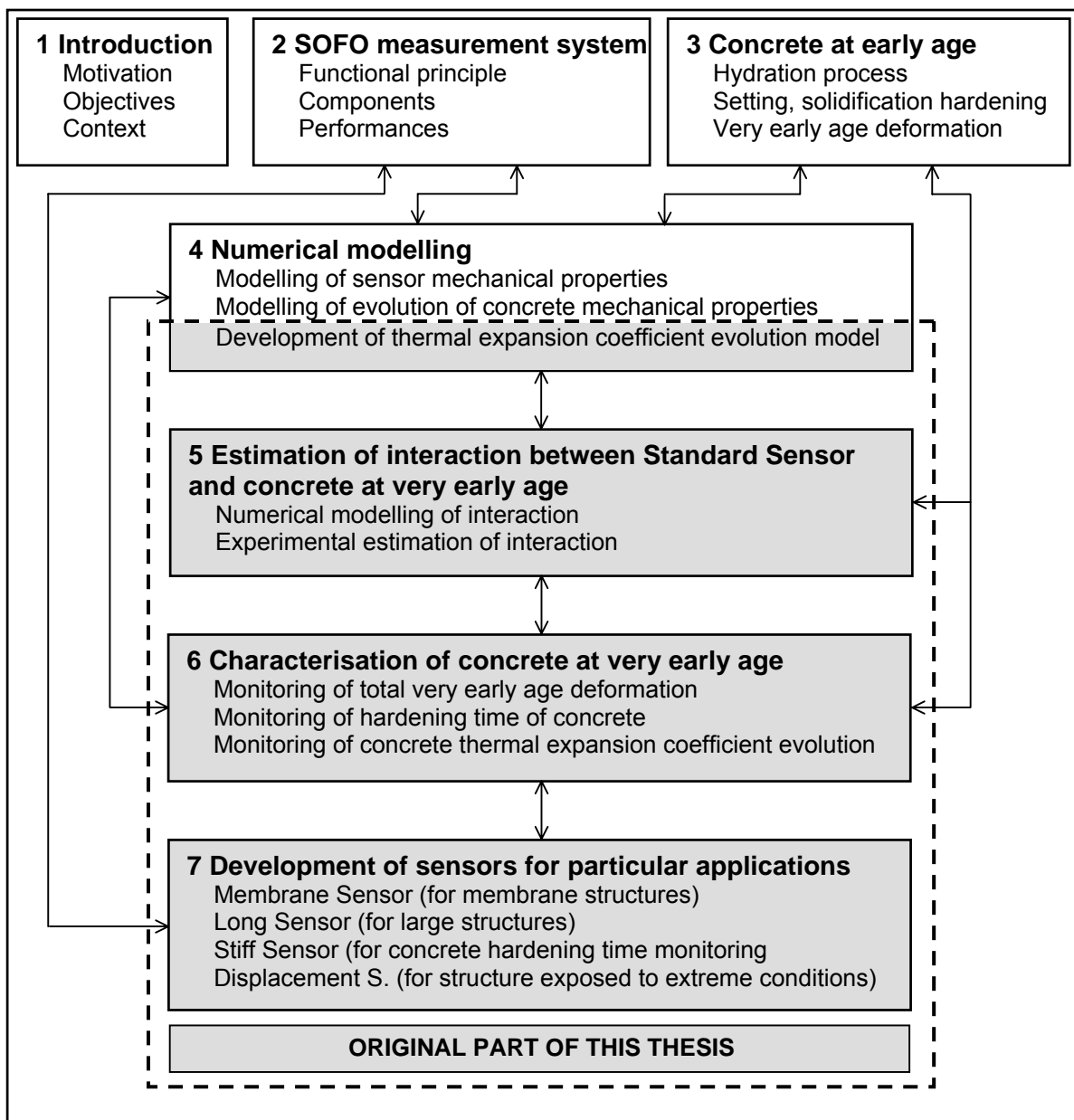


Figure 1.1.2.2: Structure of thesis

1.3 Monitoring of concrete structures

1.3.1 Introduction

The aim of this Section is to expand upon the motivation for this work. The importance of structural monitoring and more specifically, monitoring of concrete structures at early and very early age as well as a brief presentation of the SOFO monitoring system are presented in this Section.

1.3.2 Importance of structural monitoring

Monitoring (or auscultation) of structures involves recording of parameters during certain periods. These parameters are related to the structural material and to the structure itself. In both cases they can be physical, mechanical or chemical. Table 1.3.2.1 resumes the most important material and structural parameters for monitoring.

<i>Category of parameter</i>	<i>Material parameter</i>	<i>Structural parameter</i>
<i>Physical</i>	Porosity, temperature, humidity	Temperature, humidity
<i>Mechanical</i>	Elastic module, thermal expansion coefficient, Poisson ratio, strength (compressive, tensional or shear), cracking	Stress, strain, deformation, displacement, load, mechanical degradation
<i>Chemical</i>	Chemical composition, chemical degradation (chloride concentration and carbonatation penetration in concrete, oxidation of steel, oxidation of rebars, decaying of timber)	Chemical degradation

Table 1.3.2.1: The most usually monitored parameters in civil engineering

The main components of a monitoring systems are sensors, carriers of information, reading unit analysers, interfaces and data managing subsystems. The purpose of each part of the system is explained in the Appendix. In the next paragraphs we will explain, through examples, why monitoring is important.

Monitoring during construction of new structure

Construction is a very delicate phase in the life of structures. For concrete structures, material properties change through ageing. It is important to know whether or not the required values are achieved and maintained. Defects (e.g. premature cracking) that arise during construction may have serious consequences on structural performance. Monitoring data help engineers to understand the real behaviour of the structure and this leads to better estimates of real performance and more appropriate remedial actions. Important information obtained through monitoring during construction includes the following:

- Estimation of hardening time of concrete in order to estimate when shrinkage stresses begin to be generated;

- Deformation measurements during early age of concrete in order to estimate self-stressing and risk of premature cracking. When structures are constructed in successive phases, measurement can help to improve the composition of concrete when necessary [2];
- Optimisation between two successive phases of pouring due to evaluation of cure in previous phases;
- For prestressed structure, deformation monitoring of cables helps to adjust prestressing forces;
- For pre-fabricated structures, sensors may be useful for quality control;
- Monitoring of foundation settlement helps to understand the origins of built-in stresses;
- Damage caused by unusual loads such as thunderstorm or earthquakes during construction may influence the ultimate performance of structures;
- Optimal regulation of structural position during erection [3]
- Knowledge improvement and calibration of models. These last two aspects are treated separately in further paragraphs.

Installation of monitoring systems during construction phases allows monitoring to be carried out during the whole life of the structure. Since most structures have to be inspected several times during the service [4], the best way to decrease the costs of monitoring and inspection is to install the monitoring system from the beginning.

Monitoring during testing of structure

Some structures have to be tested before service for safety reasons. At this stage, required performance levels of structures have to be reached. Typical examples are bridges and stadiums: the load is positioned on critical places (following the influence lines) and the parameters of interest (such as deformation, strain, displacement, rotation of section and cracks opening) are measured [5]. Tests are performed in order to understand the real behaviour of the structure and to compare it with theoretical estimates. Monitoring during this phase can be used to calibrate numerical models that describe the behaviour of structures.

Monitoring during service of structure

The service phase is the most important period in the life of a structure. During this phase, construction materials are subjected to degradation by ageing. Concrete cracks and creeps, steel oxidises and may crack due to fatigue loading. The degradation of materials is caused by mechanical (loads higher than theoretically assumed) and physico-chemical factors (corrosion of steel, penetration of salts and chlorides in concrete, freezing of concrete etc.). As a consequence of material degradation, the capacity, durability and safety of structure decrease.

Monitoring during service provides information on structural behaviour under predicted loads [6], and also registers the effects of unpredicted overloading. Data obtained by monitoring are useful for damage detection, evaluation of safety and determination of the residual capacity of structures. Early damage detection is particularly important because it leads to appropriate and timely interventions. If the damage is not detected, it continues to propagate and the structure no longer guarantees required performance levels. Late detection of damage results in either

very elevated refurbishment costs [7] or, in some cases, the structure has to be closed and dismantled. In seismic areas the importance of monitoring is most critical.

Subsequent auscultation of a structure that has not been monitored during its construction can serve as a basis for understanding of present and for prediction of future structural behaviour [8]. This is discussed next.

Monitoring after refurbishing or strengthening of structure

Material degradation and/or damage are often the reasons for refurbishing existing structures. Also, new functional requirements for a structure (e.g. enlarging of bridges) leads to requirements for strengthening. If strengthening elements are made of new concrete, a good interaction of new concrete with the existing structure has to be assured. Early age deformation of new concrete creates built-in stresses and bad cohesion causes delamination of the new concrete, thereby erasing the beneficial effects of the repair efforts. Since new concrete elements observed separately represent new structures, the reasons for monitoring them are the same as for new structures. The determination of the success of refurbishment or strengthening is an additional justification [2].

Monitoring during dismantling of structures

When the structure does no longer respond to required performances and the costs of reparation or strengthening are excessively high, the ultimate life-span of the structure is attained and the structure should be dismantled. Monitoring helps to dismantle structures safely and successfully.

Knowledge improvement

Understanding the real behaviour of structures is an essential task in civil engineering. Structures are classified according to criteria such as construction material (concrete, steel, wood), situation (underground or surface), purpose (hyrotechnical structures, bridges, transport), etc. Structural diversity due to factors such as geographical region, environmental influences, soil properties, loads etc. makes absolute behavioural knowledge impossible: there are no two identical structures.

A good way to enlarge knowledge of structural performance is to monitor their behaviour. That's why monitoring during the complete lives of structures, from construction to the end of service, is of interest from the theoretical point of view as well as from the point of view of structure management. Theories need to be tested, and an excellent method to test theories describing the civil structures is monitoring [9]. For structures built of unusual materials (e.g. roofs composed of thin plastic membranes or tensegrity structures [10]) monitoring is an effective way to comprehend the real behaviour and to refine behavioural theories.

Calibration of models

To compute and design a structure, accurate values of parameters related to material, mechanical properties and to the static system are indispensable. Modelling of structures is often performed using finite element methods. Modelling of the correlation of stress with deformation is difficult if there are material and structural non-linearities. Concrete is a visco-elastic material that changes its mechanical properties by ageing. Therefore, it is difficult to

predict the evolution of its properties. Numerical prediction based on the analysis of concrete component properties is practically impossible due to the complexity and the variety of cases and parameters. Calibrated models are therefore easier, faster and more accurate than non-calibrated numerical models, regardless of their complexity [11].

Monitoring the evolution of parameters is a unique method to calibrate numerical models. Since parameters change, not only during the early age of structure, but also afterwards, due to degradation, it is of interest to monitor their evolution during the life of the structure.

1.3.3 Required performances of new monitoring systems

The importance of monitoring is presented in the previous paragraphs. Different monitoring systems already exist and are in use in civil engineering. Visual inspection is presently the most utilised method of monitoring. Its limitations [8] support needs for more sophisticated auscultation. The development of new monitoring systems continues. In this paragraph, we describe the performance required from new systems.

Safety aspects

The new system must provide information that guarantee a safe and functional exploitation of the structure and allow timely intervention when necessary. The determinant factors for such kind of monitoring are the monitoring strategy and the performance of the monitoring system. While the best monitoring strategy depends on engineers, the performance of monitoring systems depends on technology.

Technological aspects

New technologies permit development of very sophisticated devices for use in monitoring. The new systems have to be more performant than the existing (higher precision and resolution, longer life, lower drift and dimensions) or applicable in areas where adequate systems do not exist. In order to ensure structural safety, a modern monitoring system has to be easy to use, fast to install, durable, reliable, independent from human intervention, fully automatic and insensitive to external influences (temperature, electro-magnetic fields, humidity etc.).

Economical aspects

The economical aspect refers to the relation between the investment and the economical gains obtained from monitoring. Important structures should be monitored. There are two approaches: periodic inspections and permanent monitoring.

In the first case, a conceivable intervention (repairing, refurbishing or temporary closing) can be undertaken only after the inspection. The costs of intervention may be elevated, especially when intervention is not undertaken in time. Moreover, the cost of inspection itself can be high if a monitoring system that requires qualified personnel is employed. The investment in maintenance of the structure, using periodical inspections as a means of control, can exceed the cost of a new structure [7,12].

Permanent monitoring offers greater possibilities for timely interventions. Monitoring systems are best employed if they are present on structures from construction to dismantling. Of course, engineers decide the schedule of measurements. Using permanent monitoring, the disadvantages of periodical inspection can be avoided. Using permanent monitoring as a mean of control may decrease the maintenance cost by 10% [13].

Esthetical aspects

Many old and new structures are considered to be part of the historical and cultural heritage of society. Some of them need to be monitored in order to prevent damage or to undertake repair. Monitoring equipment can affect the esthetical appearance of structures. Therefore it is recommended to use an "invisible" monitoring system i.e., to hide it from the eye of spectator.

1.3.4. Importance of monitoring of concrete at early and very early age

Concrete is the most used construction material and the percentage of concrete structures is over 50% in Switzerland [14]. Durability of concrete structures strongly depends on early age behaviour of the structure [15]. For these reasons, in this Chapter, we focus on monitoring of concrete structure during early and very early age.

Hydration is a complex physico-chemical exothermal process. During hydration, the water-cement suspension transforms to hardened cement paste; strength and stiffness of concrete increase; a considerable amount of heat is discharged; and early age deformation occurs. The deformation due to hydration is caused by hydration heating and cooling and by material transition to hardened cement paste (autogenous deformation). Hydration and its consequences are described in details in Chapter 3.

Early age deformation is often restrained by previously poured parts of structure, or by other structural elements (steel or old concrete in case of hybrid structures, walls, foundations etc.). Therefore at early age, residual tensile and compressive stresses are generated. Residual tensile stresses, generated before the tensile strength of concrete is fully developed, cause early age cracking.

Recent studies and research [16, 17, 18] have shown that early age cracking of concrete can significantly increase the vulnerability of structures to noxious environmental influences. The cracks form "open doors" to the infiltration and penetration of noxious substances such as chlorides [19] and sulphate water [20]. These substances attack the concrete and rebars, and damage the structure, thereby reducing its long-term capacity and durability.

Figure 1.3.4.1 [11] shows the influence of early age cracking on durability for a hybrid old concrete-new concrete structure. Even small gains in concrete performance during very early age, have a consequence of extending considerably the life span of the structure.

How does one evaluate the risk of the early age cracking? Generally there are two approaches, numerical simulation and monitoring. Numerical simulations are very complicated because of the problem complexity. They may be successful [11], only after calibration provided by measurements (notably of concrete parameters as elastic module, strength, creeping ratio etc.). Data collected by early age monitoring represent a unique source of information for understanding the real concrete behaviour.

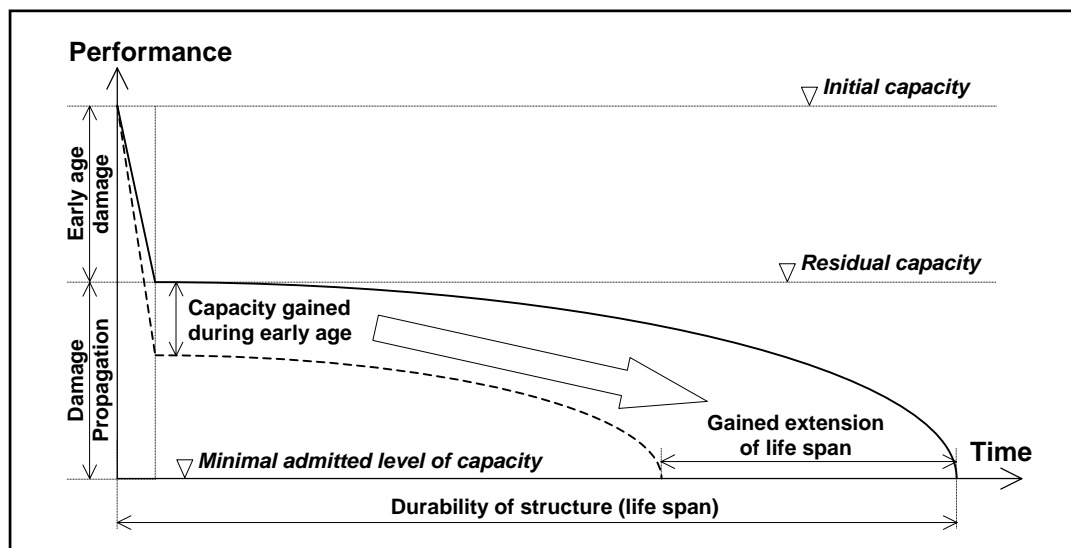


Figure 1.3.4.1: Influence of the early age damage on the durability of an old concrete-new concrete hybrid structure [11]

It is recommended to start deformation monitoring of concrete structures from the moment of concrete pouring. In this way, the whole history of deformation is collected. This includes the very early age deformation which is generated while the concrete is still not hardened. For this purpose, it is necessary to provide the monitoring system with sensors that are capable of such measurements.

1.3.5 SOFO monitoring system

The deformation monitoring system named SOFO (French acronym of "Surveillance d'Ouvrage par Fibres Optiques" - "Monitoring of Structures by Optical Fibers") has been developed at the Stress Analysis Laboratory of the Swiss Federal Institute of Technology (IMAC-EPFL) [21]. It is based on fibre optic technology and is capable of monitoring of micrometer deformations over measurement bases up to a few meters. It is particularly adapted to measure civil structures built with conventional civil engineering materials (concrete, steel and timber). Since 1993 it has been successfully practiced in different types of structures such as bridges, tunnels and piles (e.g. [2, 22]). Performance data are presented more in details in Chapter 2. Here we note that this performance corresponds well to the requirements discussed in Section 1.3.3.

SOFO sensors can be applied externally, attached to the surface of the structure, but also, and more important, they can be applied internally, embedded in fresh concrete. Installation of sensors before the pouring of concrete is an obligatory condition for deformation monitoring at very early age. The second obligatory condition is a good transfer of deformation from concrete to the sensor. Traditional sensors have certain stiffness (see Appendix and Section 5.4) and it is difficult to estimate what is really measured during the very early age: the real deformation of concrete or something between the concrete deformation and sensor deformation. This aspect is examined in this thesis (see Chapter 5).

A typical application of the SOFO system to a civil structure is presented in Figure 1.3.5.1. The system is independent and fully automated.

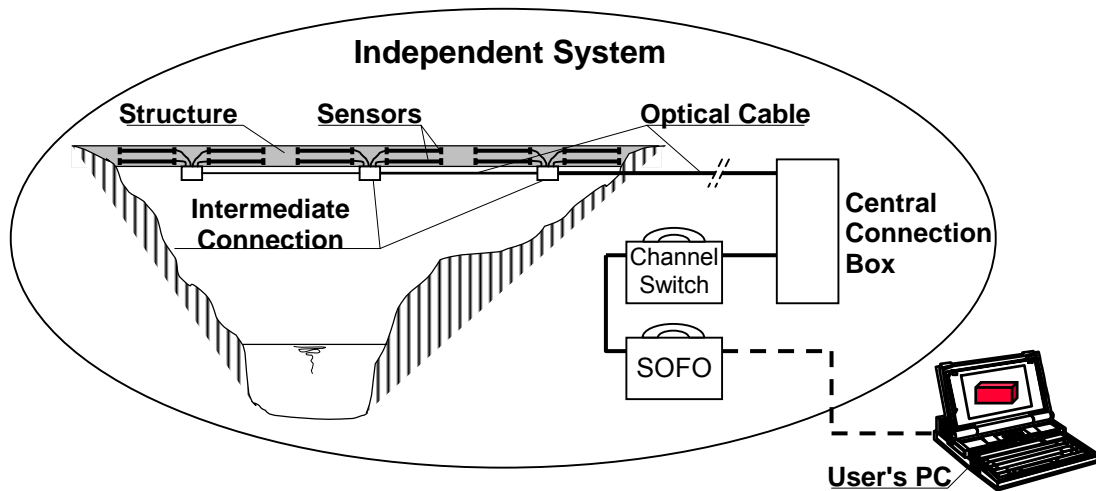


Figure 1.3.5.1: Concept of the SOFO monitoring system

The SOFO monitoring system has already been validated for a large range of applications. There are however, domains where it is not possible to apply the system due to the dimension and shape of the Standard Sensors or due to particularities of the structure (material and extreme environmental conditions).

1.4 References

- [1] www.statistik.admin.ch/stat_ch/ber09/fufr09.htm, Official WEB site of Swiss Federal Statistic Office
- [2] Inaudi D., Vurpillot S., Glisic B., Kronenberg P., LLoret S., *Long-term Monitoring of a Concrete Bridge with 100+ Fiber Optic Long-gage Sensors*, SPIE's International Symposium on Nondestructive Evaluation Techniques for Aging Infrastructure & Manufacturing, , Vol. 3587, Pages 50-59, Newport Beach, USA, 3-5, March 1999
- [3] Vohra S.T., Althouse B., Johnson G., Vurpillot S., Inaudi D., *Quasi-Static Strain Monitoring During the "Push" Phase of a Box-Grider Bridge Using Fiber Bragg Grating Sensors*, European Workshop on Fiber Optic Sensors, Peebles, Scotland, July 1998
- [4] SIA 462, Swiss norms
- [5] Hassan M., *Critères découlant d'essais de charge pour l'évaluation du comportement des ponts en béton et pour le choix de la précontrainte*, Ph.D. Thesis N° 1296, EPFL, Lausanne, Switzerland, 1994
- [6] Vurpillot S. *Analyse automatisée des systèmes de mesure de déformation pour l'auscultation des structures*, Ph.D. Thesis N° 1982, EPFL, Lausanne, Switzerland, 1999

-
- [7] Radojicic A, Bailey S., Brühwiler E., *Consideration of the Serviceability Limit State in a Time Dependant Probabilistic Cost Model*, in "Application of Statistics and Probability", Vol. 2, pp 605-612, Balkema, Rotterdam, Netherlands, 1999
- [8] Vurpillot S., Krueger G., Benouaich D., Clément D., Inaudi D., *Vertical Deflection of a Pre-Stressed Concrete Bridge Obtained Using Deformation Sensors and Inclinator Measurements*, ACI Structural Journal, Vol. 95, No. 5, September-October 1998
- [9] Markey I. F., *Enseignements tirés d'observations des déformations de ponts en béton et d'analyses non linéaires*, Ph.D. Thesis N° 1194, EPFL, Lausanne, Switzerland, 1993
- [10] Fest E., Smith I., *Construction et modélisation des structures tensegrités*, , Rapport Technique, IMAC - EPFL, Lausanne, Switzerland, 1999
- [11] Bernard O., *Comportement à long terme des éléments de structures formés de bétons d'âges différents*, Ph.D. Thesis, EPFL, Lausanne, Switzerland, 2000 (to be published)
- [12] Frangopol D. M., Estes A. C., Augusti G., Ciampoli M., *Optimal bridge management based on lifetime reliability and life-cycle cost*, Short course on the Safety of Existing Bridges, ICOM&MCS, pp 112-120, EPFL, Lausanne, Switzerland, 1998
- [13] Bertoincini A., Hammerschlag J.-G., *Personal communication*, February 2000
- [14] Walther R., Miehlbradt M., *Dimensionnement des structures en béton, Traité de génie civil*, Vol.7 pp. 3, Presses polytechniques et universitaires Romandes, Lausanne, 1990
- [15] Baron J., Ollivier J.-P., (sous la direction de), *La durabilité des bétons*, Presses de LCPC, Paris, France, 1992
- [16] Tazawa E., Iida K., *Mechanism of thermal stress generation due to hydration heat of concrete*, Transactions of the Japan Concrete Institute, 1983, vol. 5, p.p. 119-126
- [17] *Thermal Cracking in Concrete at Early Age*, RILEM International Symposium, Munich, Germany, 1994
- [18] *Limitation de la fissuration au jeune age du béton dans des structures hybrides*, research report, MCS, IMAC et ICOM, EPFL, Lausanne, Switzerland, 2000 (to be published)
- [19] Nagesh M., Bhattacharjee B., *Modelling of Chloride Diffusion in Concrete and Determination of Diffusion Coefficients*, ACI Materials Journal, Vol. 95, N°2, April 1998
- [20] Hammerschlag J.-G., *Mécanismes des réactions alcalis-granulats et leurs effets sur la structure du béton*, Service de recherches et conseils techniques de l'industrie suisse du ciment, 1999
- [21] Inaudi D., *Fiber Optic Sensor Network for the Monitoring of Civil Structures*, Ph.D. Thesis N°1612, EPFL, Lausanne, Switzerland, 1997
- [22] Glisic B., Badoux M., Jaccoud J.-P., Inaudi D., *Monitoring A Subterranean Structure with the SOFO System*, 1st International Conference Long Road and Rail Tunnels, November 29 - December 1, 1999, Basel, Switzerland

2 SOFO Monitoring system

2.1 Introduction

The SOFO [1, 2] deformation monitoring system was developed at IMAC-EPFL in 1993. Since then, it has been used for laboratory tests and for in-situ monitoring, applied to different type of structures such as bridges, tunnels, walls, piles, dams and historical monuments (churches) [3, 4, 5]. It is particularly well adapted to measure civil structures built with conventional materials (concrete, steel and timber).

The SOFO deformation monitoring system is central in this thesis. The research and development presented in this work is intimately linked to the SOFO system, since based on measurements provided by the SOFO system. The aim of this chapter is to briefly present its components, functional principle and characteristics.

2.2 Main components and functional principle of SOFO system

The SOFO measurement system is based on low coherence interferometry in single-mode optical fibres. The three main elements of the system are the SOFO reading unit, the SOFO fibre optic sensors and the data acquisition and management software: SOFO DB [1]. Following the definitions given in Appendix, a monitoring system consist of sensors, carriers of information, reading unit, analyser, interface and management subsystems. Table 2.2.1 and Figure 1.3.5.1 present how all these components are combined in the case of the SOFO system.

<i>Monitoring system components</i>	<i>SOFO elements</i>
Sensors	SOFO sensors
Carriers of information	Passive zone of the SOFO sensor, optical cable (see Appendix)
Reading unit	SOFO reading unit
Analyser	
Interface	(Portable) PC with software SOFO DB
Measurement management subsystem	SOFO DB Software

Table 2.2.1: SOFO elements

The SOFO components as well as the functional principle of the system are represented in Figure 2.2.1.

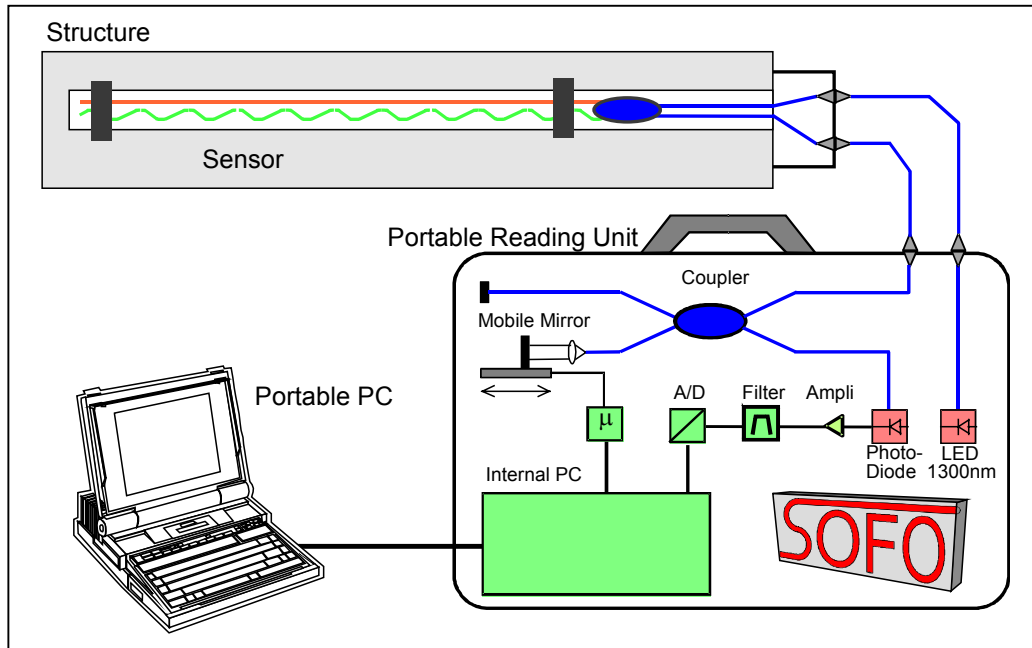


Figure 2.2.1: Set-up of the SOFO System

The SOFO reading unit is composed of a light emitter (LED), a low-coherence Michelson interferometer with a mobile scanning mirror, optical components and an internal PC. The sensor generally consists of two singlemode optical fibers: the measurement fiber and the reference fiber. The measurement fiber is in mechanical contact with the host structure and follows its deformation, while the reference fiber, placed close to the measurement fiber, is loose and independent of the behavior of the structure. Any deformation of the structure will result in a change of the length difference of the two fibers.

Infrared light is emitted by the LED, sent through the singlemode optical fibre to the sensor, split by the coupler and injected into the two arms of the sensor. Then, the light reflects off the mirrors deposited on the ends of each of the fibres and returns through the coupler to the reading unit, i.e. to the compensating Michelson interferometer. The interfered light contains the information concerning the path difference between the measurement and the reference fibres. This difference is compensated using the mobile mirror and transmitted to the external PC. By successively repeating the measurements, it is possible to determine the evolution of the deformation of the structure under observation.

2.3 Standard Sensor - description

The standard SOFO [6] sensor is composed of two zones, the active zone which measures the deformations, and the passive zone that serves as the carrier of information between the active zone and the reading unit. The sensor is schematically represented in Figure 2.3.1.

The active zone is limited by two anchor pieces and consists of two optical fibers placed in a protection tube. The anchor pieces have a double role: to attach the sensor to the monitored structure and to transmit the deformation from the structure to the sensing fiber. The measurement fiber is pretensioned between the anchor pieces in order to measure the

shortening of the structure as well as its elongation. The reference fiber is independent of both the measurement fiber and the deformation of the structure, and its purpose is to compensate for temperature changes. The length of active zone of the Standard Sensors is limited between 20cm and 10m. Out of these limits it is difficult to guarantee the independence of the measurement and reference fibers.

The passive zone transmits the information from the active zone to the reading unit. It is composed of one siglemode fiber, connector and coupler, all protected by a plastic tube. The coupler is placed in the passive zone of the sensor, close to the anchor piece in order to increase the precision and to facilitate the manipulation during the measurement. The length of the passive zone can vary from several tens of centimeters to several tens of meters, depending on the necessities. If the passive zone is very long a simple fiber optic cable can extend it to up to 5km. The protective plastic tube allows an easy manipulation, a fast installation and a very good protection of the sensors during the installation and long-term use of the system.

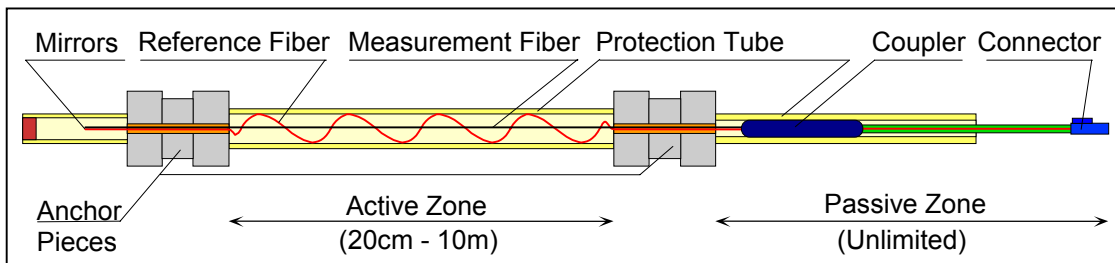


Figure 2.3.1: Standard SOFO Sensor

The standard SOFO sensors may be installed on the surface of a steel, wood or existing concrete structure or embedded in fresh concrete or mortar. The sensors are sufficiently robust to survive pouring and vibrating of the concrete.

2.4 SOFO sensor measurement

The sensors are ready to measure immediately after their installation on the structure. A measurement is initialised by the external PC, using the SOFO DB software. One measurement takes less than 10 seconds. When accomplished, it is represented on the PC screen in form of one central and two lateral peaks that represent the envelopes of the interference fringes. The distance between the central and the lateral peaks is proportional to the absolute value of the length difference between the measurement and the reference fibre. A typical measurement is represented in Figure 2.4.1 a).

The first measurement carried out on an installed sensor shows only the initial difference between the measurement and the reference fibres. This measurement is considered as a "zero" measurement. If the structure deforms, the deformation is transmitted to the sensor, the length of the measurement fibre is changed, and consequently the difference between the measurement and the reference fibre is changed accordingly, as the length of the reference fibre remains unchanged. The deformation of the structure is now easily calculated by subtraction of the "zero" measurement from the measurement of the deformed structure. This principle is represented in Figure 2.4.1 b) with regard to the measurement represented in Figure 2.4.1 a) as a "zero" measurement.

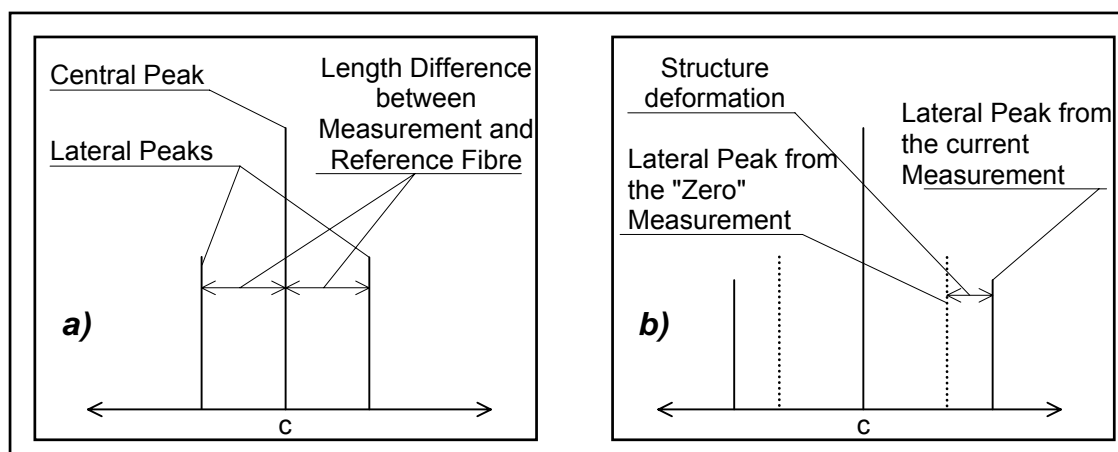


Figure 2.4.1 a) Schematic Representation of a SOFO Measurement and b) Determination of the Deformation of the Structure relative to the "Zero" Measurement

2.5 Performances of SOFO system

The following table resumes the principal features of the SOFO system.

<i>Parameter</i>	<i>SOFO characteristics</i>
Measurement basis	20cm to 10m for Standard Sensors
Resolution	2 μ m
Precision	Better than 0.2% of the measured deformation
Dynamic range of the sensors	1% elongation, 0.5% shortening for Standard Sensors
Dynamic range of the reading unit	Up to 80mm in elongation and shortening
Cable length (information carrier)	Up to 5 km
Temperature sensitivity	Insensitive, self-compensated sensors
Long-term stability	Good, drift not observable over at least five years
Acquisition time	Less than 10 seconds
Automatic and remote monitoring	SOFO makes possible a permanent, automatic and remote static monitoring
Environmental influences	Insensitive to humidity, corrosion, vibration, electro-magnetic fields
Construction material	Adapted to the monitoring of all types of conventional civil engineering materials (concrete, steel, wood)

Table 2.5.1: Specifications of SOFO Measurement System

In addition, we note that the SOFO system is well adapted to the use in in-situ conditions. The reading unit is portable, battery powered and waterproof, making it suitable for the dusty and humid environments usually found in most building sites.

2.6 References

- [1] Inaudi D., *Fiber Optic Sensor Network for the Monitoring of Civil Structures*, Ph.D. Thesis N°1612, EPFL, Lausanne, 1997
- [2] Inaudi D., Vurpillot S., *SOFO: Surveillance d'ouvrages par senseurs à fibres optiques*, IAS: Ingénieur et Architecte Suisse, 121^{ème} année, numéro 26, pp. 522-529, 6 décembre 1995
- [3] Vurpillot S., Inaudi D., Ducret J.-M., *Bridge Monitoring by Fiber Optic Deformation Sensors: Design, Emplacement and Results*, Smart Structures and Materials, SPIE Vol. 2719, pp. 141-149, San Diego, USA, 1996
- [4] Inaudi D., Vulliet L., Pflug L., Vurpillot S., Wyser A., *Low-coherence interferometry for the monitoring of underground works*, 1995 North American Conference on Smart Structures and Materials, Volume 2444, pp. 171-178, San Diego, 1995
- [5] Kronenberg P., Casanova N., Inaudi D., Vurpillot S., *Dam Monitoring with Fiber Optic Deformation Sensors*, Smart Structures and Materials, SPIE Vol. 3043, pp. 2-11, San Diego, USA, 1997
- [6] Inaudi D., Vurpillot S., Casanova N., Osa-Wyser A., *Development and Field Test of Deformation Smart Structures and Materials*, Smart Structures and Materials, SPIE Vol. 2721, pp. 138-148, San Diego, USA, 1996

3 Concrete at early and very early age

3.1 Introduction

Concrete is the most used material in civil engineering. Therefore, a good knowledge on its mechanical properties and behaviour is essential. Concrete is subjected to ageing and its mechanical properties change during the whole its life. The change is particularly accentuated during the first hours after pouring when it transforms from a plastic (non-solidified) to a solid material.

The objectives of this Chapter are firstly to present the different phases of the concrete life as well as their consequences and, secondly to define the research domain of the part of this thesis concerning the characterisation and deformation measurements of the concrete at early and very early age.

3.2 Composition of concrete

Fresh concrete is a fluid multiphase mixture of different components. It consists of cement, water and aggregate (sand and gravel), but contains a small amount of air, too. Furthermore, certain additives can be added to the basic mixture in order to improve or change certain characteristics of the concrete (workability, setting time etc.).

	<i>Mass [%]</i>	<i>Density [kg/m³]</i>	<i>Young modulus [GPa]</i>	<i>Poisson's ratio ν</i>	<i>TEC [$\cdot 10^{-5}$ 1/°C]</i>
<i>Cement</i>	10 - 20	~300	70	0.27	1.0
<i>Water</i>	4 - 10	1000	2.18*	0.5	20**
<i>CSH-gel</i>	***	2340	40	0.21	~1.0-1.6
<i>Aggregate</i>	70 - 80	1800-3000	10-150	0.3-0.35	0.1 - 1.5
<i>Air</i>	~0.001	~1.3	~0	0.5	367**
<i>additive</i>	0.2 - 5	-	-	-	0.1 - 1.5

*Bulk modulus, **Volume expansion, ***Replace cement and water in hardened concrete

Table 3.2.1: Concrete components and their properties

The mechanical properties of concrete such as strength, Young modulus, thermal expansion coefficient (TEC) and Poisson's ratio, depend directly on the mechanical properties of the components and on their proportion in the mixture. The proportion of water and cement is described as the water-cement ratio ω . Usual limits of proportion and the mechanical properties of components for ordinary concrete are represented in Table 3.2.1 [1,2,3,4].

In Table 3.2.1 only the quantity of aggregate is quoted. However note that the grain-size composition of the aggregate has a very important role with regard to the rheological properties of fresh concrete (notably workability) and the mechanical properties of future hardened concrete.

3.3 Hydration process

After mixing the components, the concrete life begins. The composition of cement and water is named cement paste. It is initially fluid, but gradually it transforms into a solid material. This transformation is caused by complex physical and chemical processes commonly named the hydration process or just hydration. The main product of the hydration process is CSH-gel, which represents in fact, hardened cement paste. The mechanical properties of CSH-gel are given in the Table 3.2.1.

The rate of the hydration process is not constant. It depends on the age of the cement paste, its temperature, chemical composition of cement, its finesse, admixture (silica fume, fly ash, etc.), additives (accelerators, retarders) and the water-cement ratio (ω).

Just after water is added to the cement the hydration process begins. The first reactions are very intense and a high amount of heat is released in a very short period. During the following hours (depending on type of the cement and additives), the chemical reactions slow down and the hydration process ceases. This period is called dormant period or induction period of concrete [4].

After the dormant period is finished, the period of intensive hydration starts. One percent of cement is hydrated two to five hours after the mixing [5], depending on the duration of the dormant period. Fifty to eighty percent of the cement is hydrated in the first seven days approximately. During this period, heat is liberated and the maximal heating of concrete occurs after 18 to 48 hours. Following this period the hydration process becomes slower because the hydration products envelop more and more the grains of the cement and water access to the unhydrated grains is more difficult. Therefore, a complete hydration of concrete could take several tens of years, and may never be achieved.

The advancement of the hydration process is parameterised by the degree of hydration α_h which is defined as fraction or percent of hydrated cement. Or more precisely as the ratio between water quantity absorbed by the hydration process and total water quantity indispensable to a complete hydration of cement. The evolution of the degree of hydration for a typical cement is schematically represented in Figure 3.3.1.

The hydration has numerous consequences such as thermal process (heating and cooling), maturity, setting of the cement paste, hardening and solidification of the concrete, variation of mechanical properties as well as the dimensions of concrete elements. Those consequences are described in the following sections.

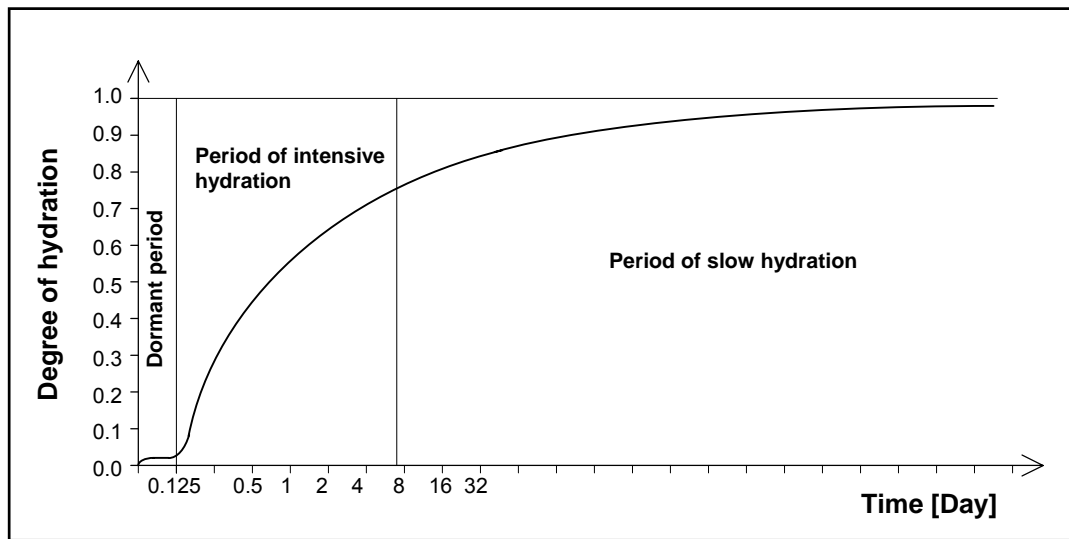


Figure 3.3.1: Evolution of the degree of hydration

3.4. Thermal effects

Hydration is an exothermic process. Nevertheless, the heating of concrete does not have the same intensity during whole hydration process. There are only two relatively short periods of intense heat release. The first one is almost instantaneous and it begins and ends just after the mixing of cement and water [5,6]. It is very intensive, but very fast and since the cement past is still fluid, its effect on future concrete behaviour remains negligible.

The second period of intense heat release begins after the dormant period has ended. It reaches its hottest moments (depending of the type of cement) in the next 12 to 48 hours and cools afterwards [5,6]. The second period of heating and cooling corresponds to the period of intensive hydration. During this period, the temperature of concrete increases and since concrete becomes hardened, parasite thermal stresses may appear. After the second period of intense heating, the period with low heating starts. It corresponds to the period of slow hydration. During this period the heating is practically over.

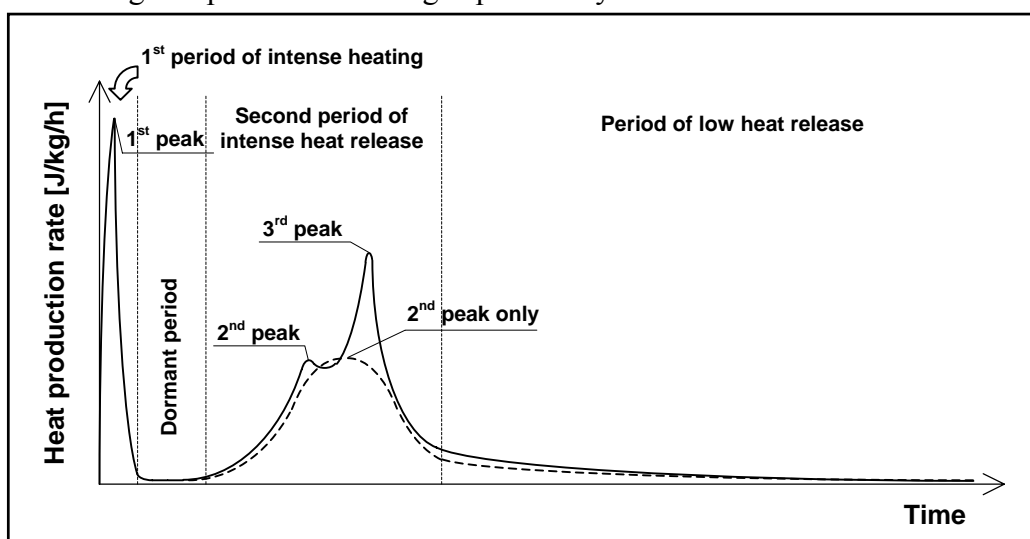


Figure 3.4.1: Schema of evolution of hydration heating of two different cements

In Figure 3.4.1 the evolution of the heat rate production is schematically represented for two different cements. The temperature of sample is maintained at 20°C. Figure 3.5.2 presents the temperature evolution of an ordinary concrete measured after pouring.

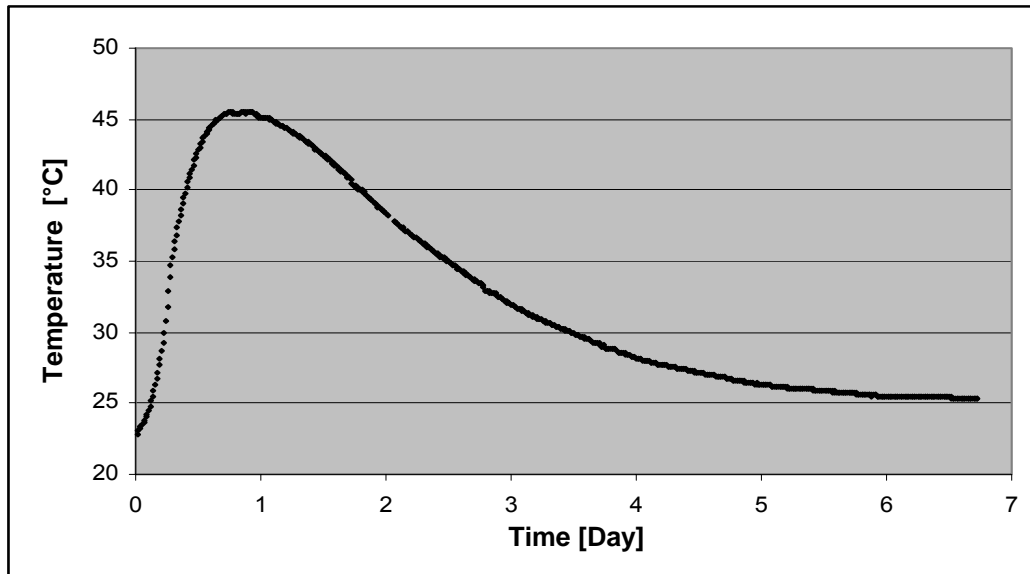


Figure 3.4.2: Temperature evolution of an ordinary concrete element measured from pouring

3.5 Maturity

The degree of hydration depends strongly on the temperature and the humidity of the concrete. Two samples of the same cement paste cured at different temperature and humidity have different degrees of hydration. The reason for this difference is the rate of chemical reactions that changes according to the environmental conditions. This means that the cement paste (and concrete) age depends on the manner of its ageing. Therefore the age is not a suitable parameter to describe the cement paste or concrete maturation. That's why we define the maturity.

The correlation between differently aged samples of the same concrete can be established using enlarged Arrhenius law [7], used in chemistry to describe the rate of chemical reactions. The maturity of the cement paste or concrete at the age t is defined by this expression as follows:

$$m(t) = \int_0^t e^{\frac{Q}{R} \left(\frac{1}{T_r} - \frac{1}{T(\tau)} \right)} \cdot \frac{1}{1 + a_c (1 - h(\tau))^{b_c}} d\tau, \quad (4.5.1)$$

where:

- t - Age [hours]
- $m(t)$ - Maturity at age t [hours]
- $e=2.7183\dots$
- Q - Activation energy of concrete [J/mol]
- $R=8.3144\dots$ J/mol/K - Universal gas constant
- T_r - Reference temperature [K]

T - Temperature of concrete [K]
h - Relative humidity [-]
 a_c, b_c - Coefficients [-]

The values usually employed in above expression are $T_r=293\text{K}$ (20°C) and $Q/R=3000$ to 6000K .

Samples made of the same cement and with the same composition theoretically have the same degree of hydration and the same mechanical properties at the same maturity. If the concrete is cured at 20°C with a relative humidity of 100% ($h=1$) then the maturity and the age of concrete are equal. Hence, for a concrete that ages in real, in-situ, conditions, the maturity can also be defined as the theoretical age achieved if it was cured at 20°C and a relative humidity of 100%.

3.6. Setting, solidification and hardening

The most important consequence of the hydration process is certainly the transformation of concrete from a multiphase fluid mixture to a solid multiphase composite. Even if it is not completely correct, the cement paste can be considered as the liquid part (in fact it is aqueous suspension) of fresh concrete and consequently the concrete transformation depends on the cement paste transformation.

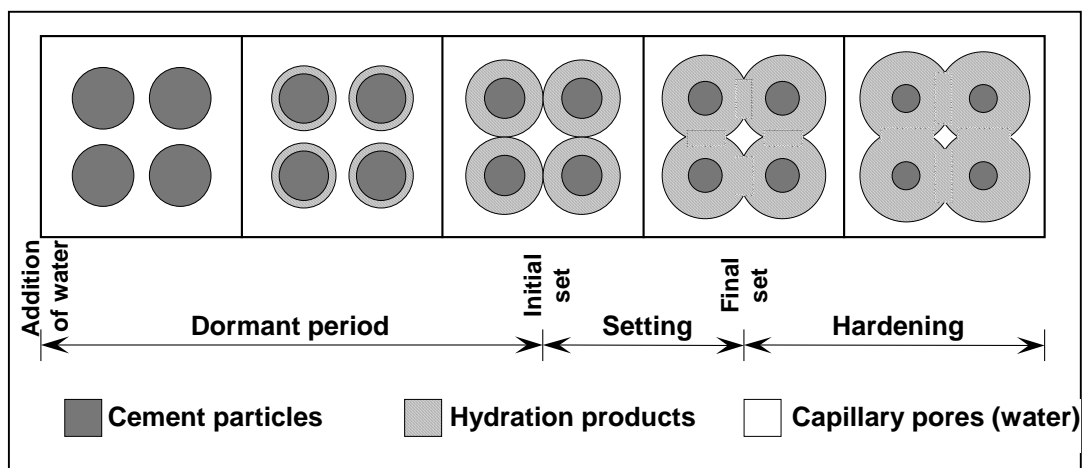


Figure 3.6.1: Stages of the cement paste [4]

In Figure 3.6.1 [4] the three stages of the cement paste are distinguished. The dormant period begins after the addition of water to the cement. During the dormant period the cement paste is liquid. Setting starts when the hydrated cement particles begin to be in mutual contact (initial set) and ends when the cement paste began solid (final set). During the setting period the cement paste is transforming from a liquid to a solid structure. The end of setting is defined by the Vicat test [8, 9]. After setting, the cement paste is solidified and continues to harden. The notion of setting is related rather to cement than to concrete. Anyway the setting of concrete is defined in American standards [10].

More suitable notions related to concrete are solidification and hardening or rigidification. Solidification refers to transformation from a fluid (non- solid) state to a solid state. While the solidification represents the transition from the non-solid to the solid state, the hardening or rigidification represents the increase of the stiffness i.e. increase of the Young modulus. More

precisely, the concrete is solidified if its plastic properties have disappeared but it is hardened if an imposed deformation generates the stresses. We note here that non-solidified concrete can have an initial stiffness due to the compacting and presence of aggregate. The hardening and the initial stiffness are additionally explained in more detail in the following Sections.

3.7. Early and very early age of concrete, hardening time

The period which begins with pouring and finishes when all thermal processes in concrete are calmed is considered here as the early age of concrete. It consists of the dormant period and the period of intense heat release, until concrete temperature is balanced with the environment temperature. The duration of the early age varies from a couple of days to several weeks depending on the thermal properties of the concrete components, the heat production potential of cement, the additives, the environmental conditions (temperature and relative humidity), the cure (thermoisolation) and geometry of the concrete element (massive and thick elements need more time to cool than thin elements).

The early age of concrete is an important period in the life of a concrete structure. Therefore during this period it is very important to take care of concrete, since a significant part of the hydration process and the mechanical properties (strength and stiffness) are developing at this stage. Due to the hydration process and the external influences, different types of deformation can appear. Residual and non-desirable stresses may also be generated. Since the strength of concrete at this stage is still low, the stresses can provoke cracking which affects the concrete resistance against unfavourable environmental conditions and decreases the durability of structure.

The period included in the early age, during which the concrete is still not hardened, is conventionally called the very early age. The measurements shows that during this period concrete owns a certain initial stiffness and strength (see Figures 3.9.1 to 3.9.3). The duration of the very early age is between several hours and one day depending mainly on the rate of hydration, concrete composition (notably the water-cement ratio) and curing conditions. Since the processes of solidification and hardening of concrete are continuous, it is difficult to precisely define the end of the very early age. It is not strictly defined in the literature. American norms propose the setting time of concrete [10]. We consider that the end of very early age corresponds to the cement paste representation as shown in Figure 3.6.1, Square 4. At this stage, the setting of the cement paste is done, the concrete is solidified and a certain strength is developed.

In this thesis, the end of the very early age of concrete is conventionally called the **hardening time** of concrete. Since the solidification and hardening are continuous transition processes, this time can not be precisely determined. However, the notion of hardening time is defined in this thesis for the purposes of discussion and is developed further in Chapter 6.

3.8. Evolution of mechanical properties of concrete - description

During the hydration process, all mechanical properties change, Young modulus E , Poisson's ratio ν , thermal expansion coefficient α_t , strength (compressive, tensile or shear), creep, fracture energy, etc. In this Chapter we limit the discussion to the first four properties mentioned above.

In Section 3.6 the principle of hardening is explained. During hardening, the Young modulus of the cement paste increases with a rate which depends on the advancement of the cement hydration [1,11]. It is accelerated during the period of intense hydration, and slows down afterwards. The evolution of the Young modulus of the concrete occurs in the same manner. It is a logical result of the interaction between the hardened cement paste and the aggregates.

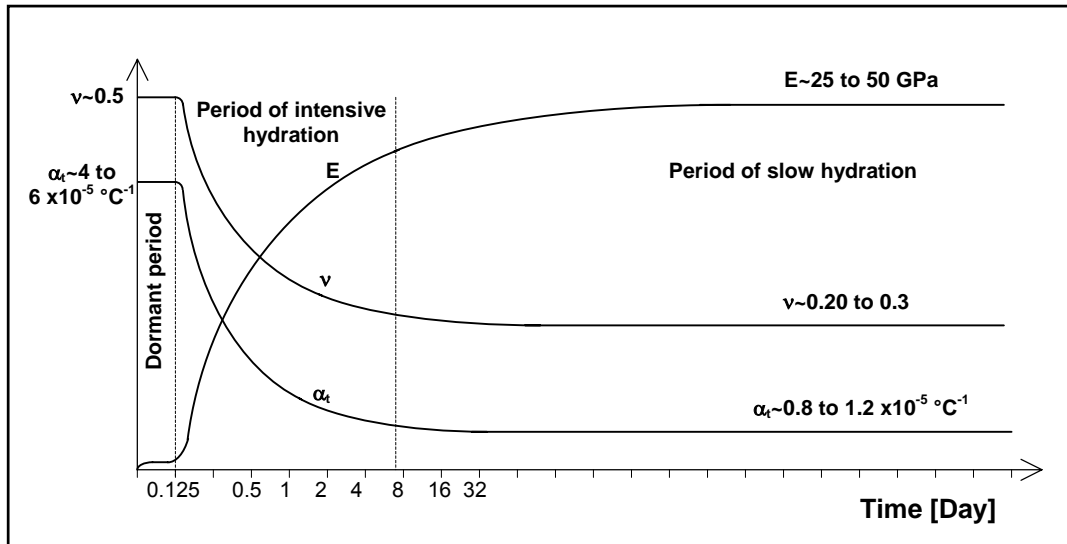


Figure 3.8.1: Schematic representation of the evolution of Young modulus E , Poisson's ratio ν , and thermal expansion coefficient α_t

The evolutions of the Poisson's ratio and the thermal expansion coefficient are entirely different. Both parameters decrease during the hydration process. After concrete mixing, the Poisson's ratio is equal to 0.5, which corresponds to a fluid material [11]. The more cement paste is solidified, the more the Poisson's ratio decreases. Thus, the decrease of the Poisson's ratio is significant during the phase of intensive hydration and less important thereafter.

The thermal expansion coefficient (TEC) also decreases with concrete ageing. After mixing of components, the concrete TEC is elevated due to the very high water TEC (see Table 3.2.1) [12]. During hydration, products with a TEC much lower than water TEC replace water and cement. That is why the TEC of concrete decreases. In Figure 3.8.1 the evolution of the three parameters is schematically represented.

The compressive, tensile and shear strength evolve in a manner similar (but not the same [11]) to the Young modulus. Therefore, the diagram of their evolution is similar to the diagram describing the evolution of the Young modulus represented in Figure 3.8.1.

3.9 Mechanical properties of concrete at very early age - initial stiffness and strength

The very early age begins with the pouring of concrete. The pouring is usually made during the dormant period and it consists not only of casting but also includes the compacting of concrete (by vibrating or manually). Immediately after the concrete is poured into the formwork, it is still fluid. When the construction work is finished, the grains of aggregate slowly move down, while the water and air move up. In this way an additional compacting is

performed. This process is defined here as the stabilisation period of concrete. The stabilisation period rarely surpasses two to four hours [13].

When stabilisation is finished, even if concrete is not hardened nor solidified, it is not fluid anymore. It is a multiphase mixture that is provided with certain initial stiffness and strength. The initial stiffness and strength have two origins, the first one refers to a cement paste and the second one to the aggregates.

Experimental research showed that the cement paste itself, even before the setting, has some initial stiffness and strength [5, 6, 14, 15, 16]. This is due to stabilisation, initial hydration reactions (coagulation), homogenisation and compacting of the cement grains. The first increase in cohesion appears only two hours after mixing of the paste [5]. In the following figures some experimental results are presented. Figure 3.9.1 [5] shows the shear strength versus the degree of hydration of the cement paste, and Figure 3.9.2 [6] the compressive strength evolution of cement paste mixed with siliceous aggregate, with or without plasticiser. In Figure 3.9.3 [14] the evolution of the Young modulus with respect to the degree of hydration is presented for the cement paste.

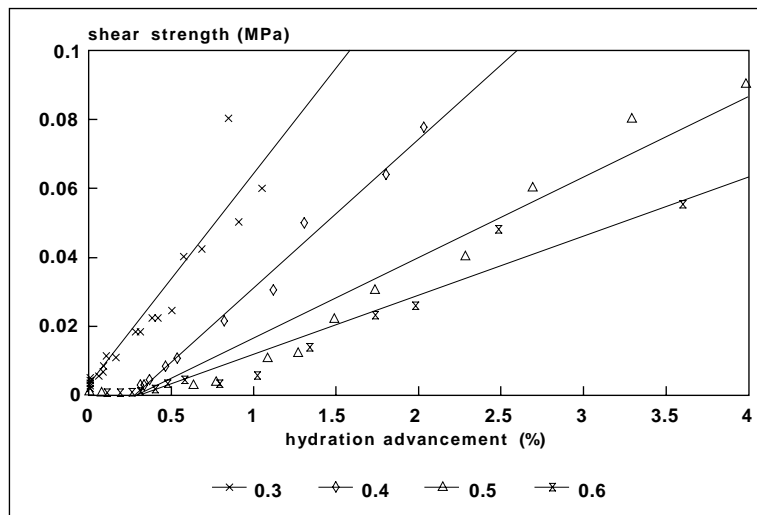


Figure 3.9.1: Evolution of the shear strength of cement pastes with water-cement ratio of 0.3, 0.4, 0.5 and 0.6 [5]

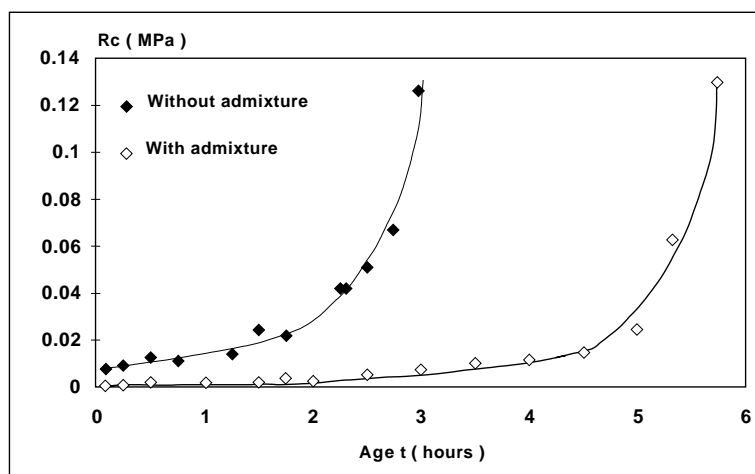


Figure 3.9.2: Evolution of the compressive strength of cement pastes with and without plasticiser [6]

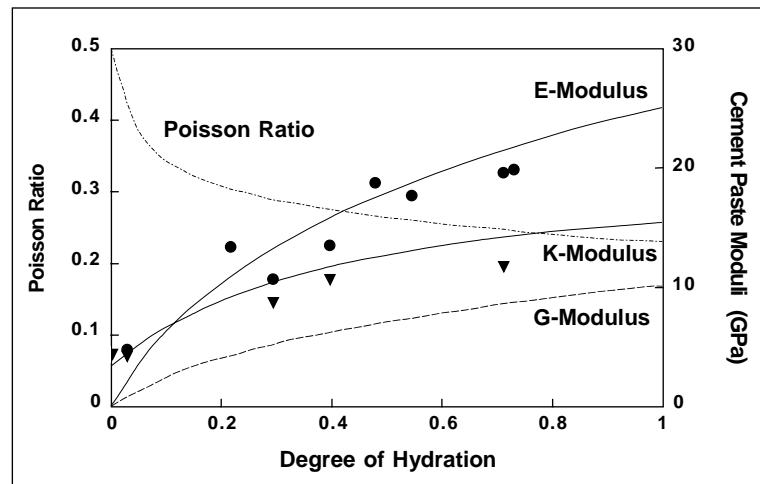


Figure 3.9.3: Evolution of the mechanical properties of a cement paste, points (circles and triangles) represent measurements, lines represents calculated values [14]

The aggregate makes up to 70-80% of the concrete mass. If compacted, it yields to the initial stiffness and compressive strength of the very early age concrete [17]. The aggregate forms the skeleton (see Figure 3.9.4) which owns, itself, the stiffness and a kind of compressive strength. If one puts a weight on the surface of the skeleton it will not submerge into the aggregate. Moreover, it is not possible to move an object submerged in the middle of the skeleton without a certain force. The more the object is deep in the skeleton, the more the force has to increase.

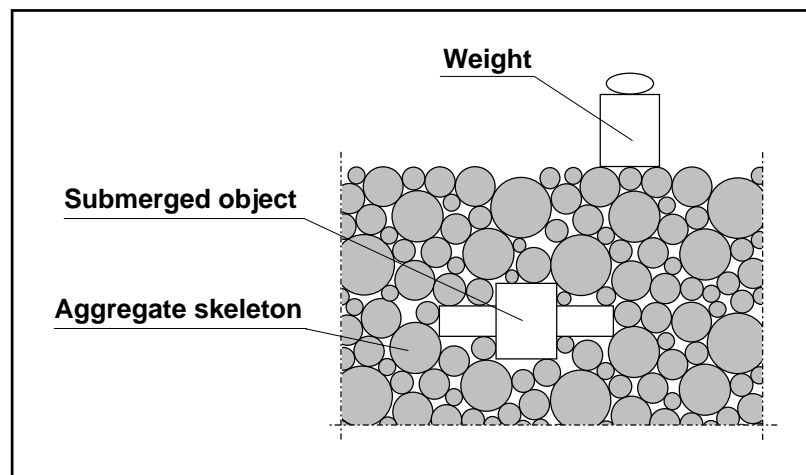


Figure 3.9.4: Schema of an aggregate skeleton

The initial stiffness and strength of the early age concrete are not easy to measure because of the non-hardened state of the concrete. They mainly depend on type and amount of cement, compacting and the mechanical properties of the aggregates, the water-cement ratio and the additives (plasticisers). The hardening phases of concrete, stiffening, and strength development at the very early age are schematically represented in Figure 3.9.5.

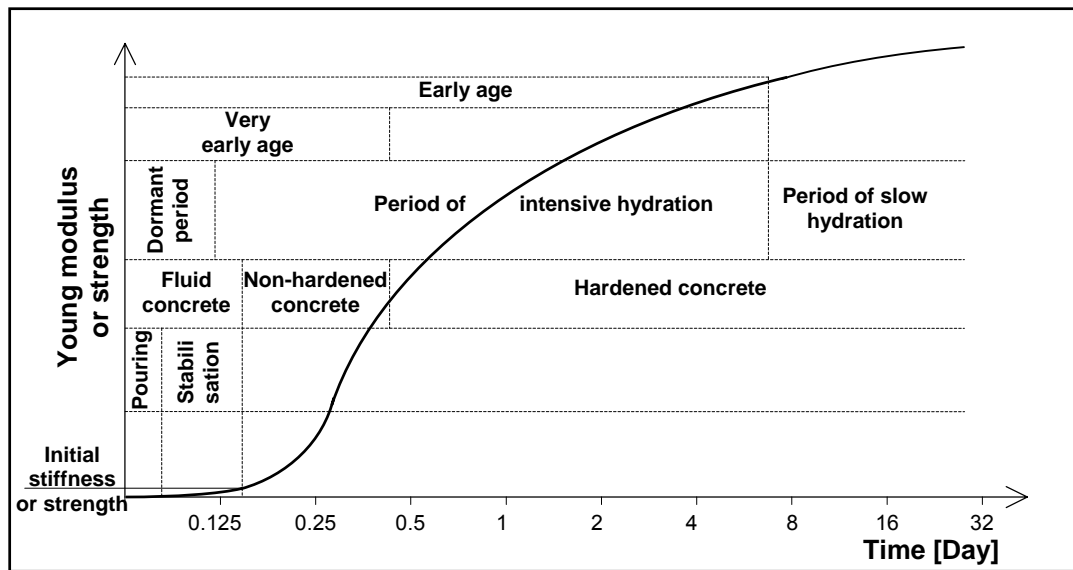


Figure 4.9.5: Hardening phases of the concrete at the very early age

The conclusion carried out from this brief presentation is that even for very low values of the degree of hydration we can consider the cement paste as a material with its own initial strength and stiffness.

3.10. Deformation of concrete at the early and very early age

The early age deformation of concrete is provoked by internal and external causes that have mechanical, thermal or hydraulic origins [12, 18, 19, 20]. The sources of the early age deformation are presented in Table 3.10.1.

	<i>Mechanical</i>	<i>Thermal actions</i>	<i>Hydraulic actions</i>
<i>Internal</i>	-	Hydration heat	Hydration hydraulic processes
<i>External</i>	Load	Ambient temperature variation, natural or artificial	Ambient humidity variation, natural or artificial

Table 3.10.1: Origins of the early age deformation

Six following forms of the early age deformation are distinguished [19, 20]:

- Plastic shrinkage,
- Autogenous shrinkage,
- Drying shrinkage and swelling,
- Carbonatation shrinkage,
- Thermal deformation (expansion and contraction),
- Load and creep deformation.

Some of them could appear simultaneously or sequentially. In this case, their sum represents the total deformation. Each deformation appearance, its origin and consequences, are described as follows.

Plastic shrinkage

The plastic shrinkage can appear before solidification, while the concrete still retains its plastic properties. It is caused by premature loss of water due to evaporation or absorption of water by dry porous material (soil or existing concrete) which is in contact with the observed concrete.

Plastic shrinkage affects only superficial parts of the concrete. It could provoke superficial cracks. It is avoided by using appropriate cure techniques (protection by napes or regular moisten).

Autogenous shrinkage

Autogenous shrinkage is a direct consequence of the chemical and physical processes provoked by hydration. The volume of the hydrated cement paste is approximately 8 to 12% smaller than the initial volume of utilised water and cement (see Figure 3.10.1) [21]. This diminution of volume does not change the apparent dimension of the hardened paste but rather increases its porosity.

The volume of hydrated cement paste is capillary porous. The water utilised for hydration is consumed from the pores. The consumption of water increases the capillary pressure and as consequence, the apparent volume additionally decreases. This diminution of volume is called self-drying shrinkage. Thus autogenous shrinkage is a consequence of chemical shrinkage and self-drying shrinkage. The apparent autogenous linear shrinkage of concrete is less than that of cement paste, due to the relatively small content of the cement paste in the volume of concrete, and it achieves approximately $100 - 300 \mu\epsilon$ ($100 - 300 \times 10^{-6}$) [20].

The consequences of autogenous shrinkage are identified at macro and micro level. At macro level, the external dimensions of concrete are changed and if the deformation is restrained (hyperstatic structures) parasite self-stresses are generated. In the case of isostatic structures the concrete structure changes its dimensions without self-stressing. At micro level, due to the diminution volume of the cement paste which is restrained by the aggregates, additional micro-cracks are generated. The autogenous shrinkage is an entirely intrinsic phenomena which occurs quasi-uniformly in the whole volume of the cement paste. It can not be avoided because it is in the nature of hydration.

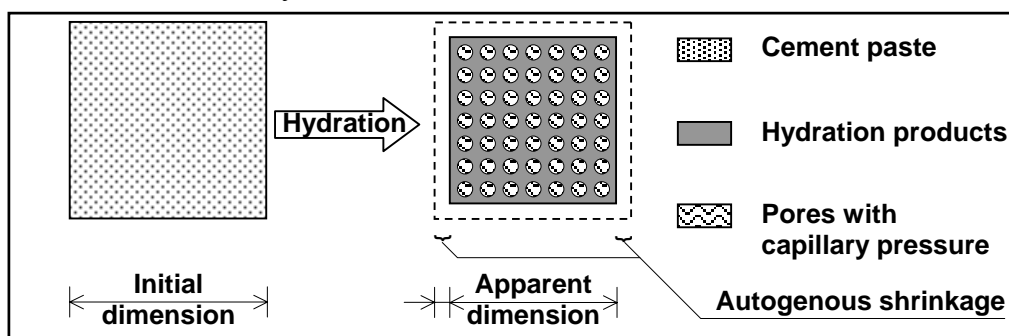


Figure 3.10.1: Schema of the autogenous shrinkage mechanism of the cement paste

Drying shrinkage and swelling

The best-known types of deformations are certainly the drying shrinkage and the swelling. They develop in solidified concrete as a result of the free pore water exchange with the environment (evaporation or absorption, natural or artificial i.e. industrial).

The drying shrinkage and the swelling arise from the faces which are in contact with dry or humid air. Hence the phenomenon is not uniform in the whole volume of concrete and consequently, it provokes internal stressing of concrete even in isostatic structures. Due to those internal stresses, cracks could appear on the contact surfaces.

During the early age, the drying shrinkage can be avoided if the concrete is cured (e.g. protected by napes). However, it is inevitable after the cure is ended, during the exploitation of the structure.

Carbonatation shrinkage

The carbonatation shrinkage develops only in the layers of concrete exposed to air with relative humidity limits of 30 to 70%. Carbonatation shrinkage is caused by the chemical reaction of hydration products with carbon gas from the air.

Under the actions of drying and moistening the carbonatation shrinkage is coupled with drying shrinkage and provokes very fine cracks. Effects of carbonatation shrinkage are superficial and can be avoided during the early age using the same manner of cure as in case of drying shrinkage.

Thermal deformation

A concrete structure is exposed, during the whole life, to external thermal influences caused by ambience temperature variations, sun radiance, or artificially by industrial heating. The result of these influences is thermal deformation of the structure. It causes self-stressing in the case of hypersatatic structures. Rapid thermal variation (heating or cooling) could cause self-stressing in massive elements of isostatic structures too. It may also provoke cracks, but since it is usually predictable, serious damage can be avoided.

Thermal processes due to hydration affect the structures at the early age. In ideal adiabatic conditions, the heat develops uniformly in the whole volume of the concrete. Nevertheless, in real structures, thermal exchanges with the environment cause a thermal gradient. The warmth of the concrete layers close to surface is lower than in the layers far in the middle of the concrete. This temperature difference in the concrete volume causes not only uneven advancement of the hydration, but also dangerous self-stressing in the very important phase of concrete life, when the full strength has not been yet developed. Recent research shows that the early age thermal cracking is the origin of several phenomena that imperil durability and shorten the lifespan of the structure.

Thermal stresses are notably dangerous in the case of large structures (e.g. dams) and hybrid structures (steel - concrete or existing concrete - new concrete structures). Serious damage can be avoided using a cement with low hydration heat and appropriate cure.

Load and creep deformation

The deformation generated by loads is mainly composed of elastic and viscous (creep) part. The elastic deformation is predictable (can be calculated), while the creep is difficult to determine notably during the early age because it is still evolving. At the early age it is usually possible to avoid external load deformation.

Total deformation

The total deformation of concrete is the sum of all the different deformations which appear simultaneously. It is always composed of at least two different types of deformation. In Figure 3.10.2 periods of apparition of different types of deformation are represented.

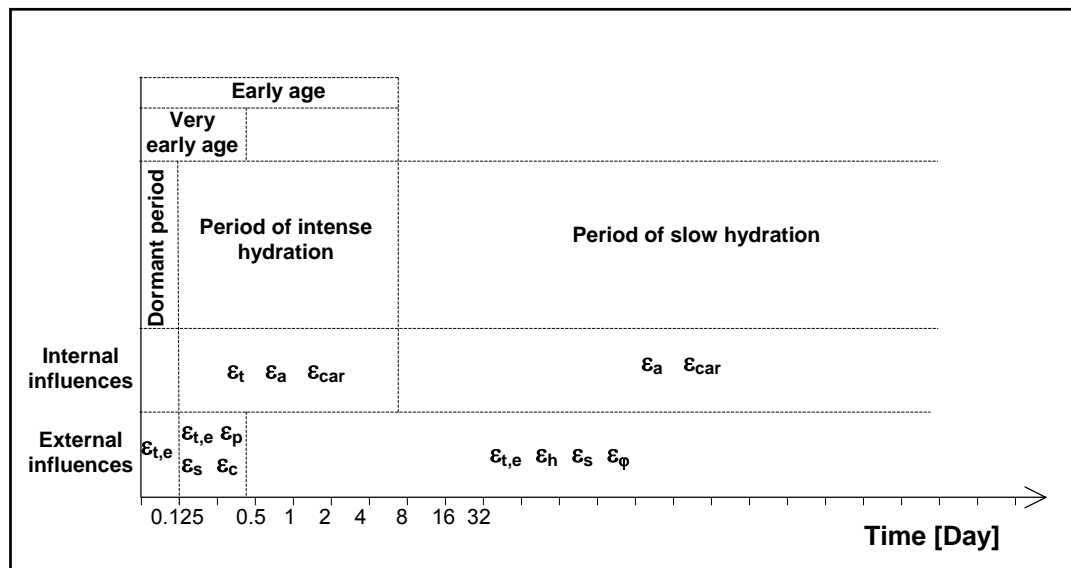


Figure 3.10.2: Periods of apparition of different types of deformations

In Figure 3.10.2 the notation is as follows:

- ϵ_t – Deformation due to hydration heat (expansion and contraction),
- ϵ_a – Autogenous shrinkage,
- ϵ_{car} – Carbonatation deformation,
- $\epsilon_{t,e}$ – Deformation due to external thermal influences (expansion and contraction),
- ϵ_p – Plastic shrinkage,
- ϵ_h – Deformation due to external hydraulic influences (swelling and drying shrinkage),
- ϵ_s – Elastic deformation due to loads
- ϵ_ϕ – Deformation of creep.

Figure 3.10.2 shows the possible combination of deformation at the different stages of concrete life. It is not possible to have all types of deformation during the whole life of the structure. Furthermore, some of them can be avoided as previously explained. However it is very important to take account of them in order to build a safe and durable structure.

3.11 Concluding remarks

In the previous sections we have presented several phenomena related to concrete at early and very early age. In this section we present important conclusions that serves as a basis in the research of the standard sensor- concrete interaction at early and very early age.

- The total deformation of the very early age concrete is inevitable because its thermal and autogenous components are in the nature of hydration. Its evolution mainly depends on the concrete composition, cement properties and the manner of curing. The early age deformation is the cause of the early age cracking, therefore it is important to measure it, and if possible to separate the thermal and autogenous deformations.

- The hardening time of concrete is defined as the end of very early age. There is no established procedure for the hardening time measurement.

- Even when non-hardened, concrete possesses an initial strength and stiffness due to initial strength and stiffness of the cement paste and the aggregate skeleton. Referring to research presented previously, we can consider that the cement paste, for a degree of hydration of 0.01 (2 - 4 h after the mixing), with water-cement ratio in usual limits (0.3 to 0.6) has an initial compressive and shear strength of 10 KPa, and an initial Young modulus of 0.2 GPa. The initial stiffness of concrete is certainly higher due to the aggregate skeleton. However, the above mentioned values for stiffness and Young modulus are adopted in this thesis in order to estimate the interaction between the very early age concrete and the standard SOFO sensor.

The objectives defined in Section 1.2 concerning the monitoring of concrete structures at early and very early age are repeated here, in the last sentence of each point mentioned above.

3.12 References

- [1] Neville A. M., *Properties of concrete*, Pittman International, 1975
- [2] Muravljev M., *Gradjevinski materijali*, Naučna knjiga, Beograd, Yugoslavia, 1989
- [3] Muravljev M., *Tehnologija betona*, Gradjevinska knjiga, Beograd, Yugoslavia, 1992
- [4] Soroka I., *Portland Cement Paste and Concrete*, The Macmillan Press Ltd, 1979
- [5] Nonat A., Mutin J. C., *From hydration to setting*, Thermal Cracking in Concrete at Early Age, RILEM International Symposium, p.p. 171-191, Munich, Germany 1994
- [6] Legrand C., Wirquin E., *First developments of strength in a microconcrete*, Thermal Cracking in Concrete at Early Age, RILEM International Symposium, p.p. 89-100 Munich, 1994
- [7] Bazant Z. P., Najjar L. J., *Nonlinear water diffusion in non saturated concrete*, Materials and Structures, Vol.5, N°25, pp. 1-20, 1972
- [8] *SIA 162*, Swiss Norms
- [9] *ASTM 04.01*, US Norms
- [10] *ASTM 04.02*, US Norms

- [11] De Schutter G., Taerwe L., *Degree of hydration-based description of mechanical properties of early age concrete*, Materials and Structures, Vol.29, p.p. 335-344, July 1996
- [12] Schöppel K., Springenschmid R., *The Effect of Thermal Deformation, Chemical Shrinkage and Swelling on Restraint Stresses in Concrete at Early Age*, Thermal Cracking in Concrete at Early Age, RILEM International Symposium, p.p. 215-220, Munich, 1994
- [13] Acker P., *Comportement mécanique du béton: apports de l'approche physico-chimique*, Rapport de recherche LPC N°152, LCPC, Paris, Juillet 1988
- [14] Paulini P., Gratl N., *Stiffness formation of early age concrete*, Thermal Cracking in Concrete at Early Age, RILEM International Symposium, p.p. 63-70, Munich, 1994
- [15] Fouad, F. H., H. Furr L., *Behaviour of Portland Cement Mortar in Flexure at Early Ages*, Properties of Concrete at Early Age, Editor J. F. Young, p.p. 93-113, American Concrete Institute, 1986
- [16] Hansen W., *Static and Dynamic Elastic Modulus of Concrete as Affected by Mix Composition and Compressive Strength*, Properties of Concrete at Early Age, Editor J. F. Young, p.p. 115-137, American Concrete Institute, 1986
- [17] De Larrard F., Ferraris C. F., *Rhéologie du béton frais remanié: II - Relations entre composition et paramètres rhéologiques*, Bulletin des laboratoires des Ponts et Chaussées, Vol. 214, p.p. 69-79, LCPC, Paris, Mars - Avril 1998
- [18] Acker P., *Les retraits du Béton, Origines physiques et paramètres influents, Analyse par type d'ouvrage et mode de mise en oeuvre*, Rilem GMC, LCPC, Paris, Avril 1995
- [19] Acker P., *Les retraits du béton: Origines Physiques, Rôle des paramètres de Composition, Formulation de Bétons a Faible Retrait*, Pontes mixtes, Annexe 1, p.p. 71-84, SETRA, Bagnaux - France, Septembre 1995
- [20] Aïtcin P.-C., Neville A., Acker P., *Les différents types de retrait du béton*, Bulletin des laboratoires des Ponts et Chaussées, Vol. 215, p.p. 41-51, LCPC, Paris, Mai - Juin 1998
- [21] Buil M., *Comportement physico-chimique du système ciment-fumées de silice*, Annales de l'ITBTP, n°483, pp. 19-29, 1990

4 Numerical models for Standard Sensor and concrete at very early age

4.1 Introduction

In order to evaluate the interaction between the Standard Sensor and the very early age concrete (in following text *sensor-concrete interaction*) numerical modelling and experiments are carried out. Numerical modelling serves as a basis to understand the behaviour of the Standard Sensor embedded in fresh concrete. To successfully perform numerical modelling it is necessary to know: the mechanical properties of both, the sensor and the very early age concrete (E , ν , α_t ,...); the mechanical behaviour (linear, elastic, plastic etc.) of the sensor and concrete; also a powerful tool to calculate the deformation and stresses provoked by interaction is required. In this chapter the numerical models of the sensor and the concrete are presented.

4.2 Numerical model for Standard Sensor

The behaviour of the sensor depends on the mechanical properties of its components. Three components influence the behaviour of the sensor (see Section 2.3 and Figure 4.2.1): the plastic tube, the optical fibres and the anchor pieces. The optical fibres are not in direct contact with the concrete, and are difficult to model due to their small dimensions. Therefore, the plastic tube and the measurement optical fibre are replaced with an equivalent material named, for the purposes of this thesis, "sensor" which equivalent mechanical properties are calculated using Equations 4.2.1 and 4.2.2.

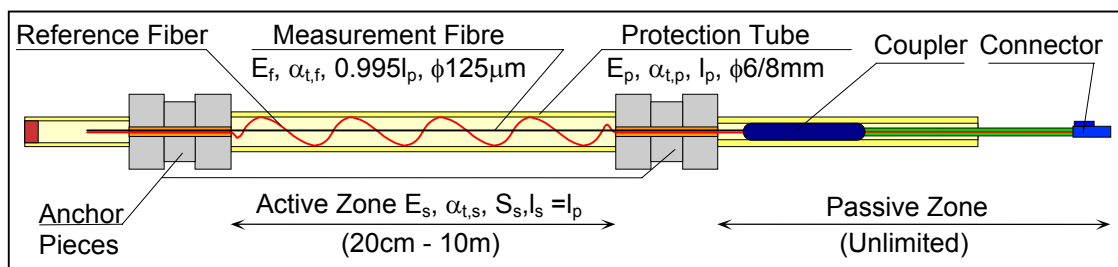


Figure 4.2.1: Standard Sensor, components, notation and dimensions

The properties of all components are relatively stable in time. Only the plastic (PVC) tube may change the Young modulus depending on the ambient humidity. For the humidity of the fresh concrete, we can use the module of humid plastic as a definitive value. The mechanical behaviour of PVC is visco-elastic. Since the deformation of the sensor is imposed by concrete, the maximal stresses in both sensor and concrete, are generated before the relaxation of the PVC, i.e. after the primary, elastic deforming of PVC. Therefore, the behaviour of the sensor is considered as linearly elastic in the numerical modelling process. Mechanical properties of the sensor and its components are given in Table 4.2.1 and represented in Figure 4.2.1.

	Young modulus [GPa]	Section [m²]	Stiffness [KNm/m]	α_h [·10⁻⁵°C⁻¹]	ν
Steel (anchor pieces)	210	3.142·10 ⁻⁴	66·10 ³	1.2	0.33
Optical fibre	72	1.227·10 ⁻⁸	0.89	0.05	-
PVC tube	1	2.199·10 ⁻⁵	21.99	15.00	0.4
Sensor	1.04	2.200·10 ⁻⁵	22.88	14.44	0.4

Table 4.2.1: Mechanical properties of the sensor and its components

The length of the Standard Sensor is not unique, it may be between 20 cm and 6 m long depending on the requirements. Therefore, sensor stiffness is represented as *KNm/m* in Table 4.2.1. The sensor stiffness is calculated using the following expression:

$$S_s = E_s \cdot A_s = l_s \cdot \left(\frac{E_f \cdot A_f}{l_f} + \frac{E_p \cdot A_p}{l_p} \right), \quad (4.2.1)$$

where:

E_s, E_f, E_p - Young modulus for sensor, optical fibre and PVC respectively,

A_s, A_f, A_p - Sections of sensor, optical fibre and plastic respectively,

l_s, l_p - Length of sensor and plastic respectively, $l_s = l_p$

l_f - Length of optical fibre, $l_f = 0.995l_p$ (optical fibre is 5% prestressed),

S_s - Sensor stiffness.

Thermal expansion coefficient (TEC) of the sensor is calculated as follows:

$$\alpha_{t,s} = \frac{\alpha_{t,f} \cdot E_f \cdot A_f + \alpha_{t,p} \cdot E_p \cdot A_p}{E_f \cdot A_f + E_p \cdot A_p}, \quad (4.2.2)$$

where:

$\alpha_{t,s}, \alpha_{t,f}, \alpha_{t,p}$ - TECs of sensor, optical fibre and plastic respectively.

The reference fibre does not influence the stiffness nor the thermal expansion coefficient (TEC, α_h) of the sensor since it is completely loose in the protective plastic tube.

4.3 Simplified numerical model for concrete at very early age

4.3.1 Introduction

Concrete can be treated on three levels: micro-, meso- and macro-level. The molecular study of the concrete (cement paste) defines the analysis at the micro-level. Thus the hydration is considered as a set of chemical reactions and physical processes. If the concrete is considered as an inhomogeneous multiphase material during the very early age and as an inhomogeneous composite afterwards, analysis is performed at the meso-level. Finally, at the macro-level the concrete is considered as a visco-elastic homogenous material, non-hardened during the very early age, and hardened afterwards. Hence, the macro level analysis is the most suitable for engineer applications.

The micro-level analysis is not of interest in this research. The sensor-concrete interaction is rather a problem that requires meso-level analyses in order to draw macro-level conclusions. However, meso-level modelling at the very early age is not easy to perform, it requires many parameters and the utilisation of the finite element method (FEM).

While the sensor properties are easily determined and unchangeable during exploitation, the concrete properties depend on the age, notably during the very early age. Thus, we have to know the evolution of the concrete mechanical properties during the very early age. Several models which describe the evolution of mechanical properties of concrete can be found in the literature. The CEB-FIP Model [1] describes the evolution of the concrete properties with regard to age, while the model given by De Schutter and Taerwe [2] describes the evolution with regard to the degree of hydration. Both models are macro-level models. Therefore, they are not suitable for modelling of sensor-concrete interaction. Moreover, the evolution of the concrete TEC is not included in these models.

For the above presented reasons, we have chosen a meso-level model, based on the Composite model for two materials [3] and enlarged to Multiphase model for the concrete [4]. The model describes the evolution of concrete properties versus the degree of hydration. However, it does not include the evolution of the TEC. Hence, a new model for TEC evolution has been developed. The model is called Extended Multiphase (EM) model, and is compatible with the Multiphase model.

The Composite, Multiphase, and EM models are presented in following sections.

4.3.2 Composite and Multiphase models

The Multiphase model enables the modelling of concrete mechanical property evolutions versus the degree of hydration with the exception of the TEC evolution. We have not found in the literature any model for evolution of TEC versus degree of hydration. In this section we present the Composite model and its extension to the Multiphase model. In the next section we develop a model able to predict the evolution of TEC. It is named the Extended Multiphase (EM) model.

The Multiphase model treats the concrete at the meso-level, as a composite material, but computes the mechanical properties that are applicable at macro-level. This modelling is, therefore, more realistic than simple macro-level models. The basis of the Multiphase model is a Composite model for two materials. Therefore, we present the Composite model first.

Composite model

The aim of the Composite model is to compute the equivalent (effective) mechanical properties of an inhomogeneous material, consisting of a matrix and spherical inclusions. In this way the original composite material is replaced with an equivalent homogenous material with equivalent mechanical properties. We suppose that all mechanical properties of the inclusion and the matrix are known. Unknown mechanical properties of an equivalent material are calculated using the Composite model based on the assumption that the equivalent material should store the same strain energy as the original materials - the inclusion and the matrix [3]. Figure 4.3.2.1 show the idea of model.

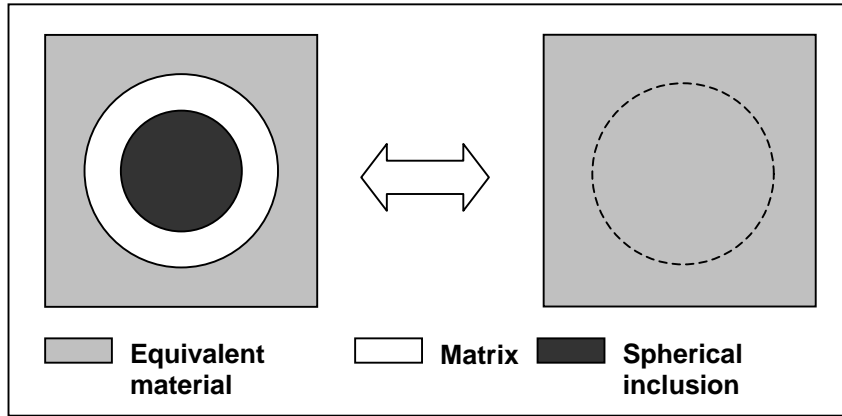


Figure 5.3.2.1: Model with spherical inclusion

More details concerning the final expression of calculus are found in [3]. We present here only a brief summary of derivation of expression [4].

The effective bulk modulus of the equivalent material is calculated as:

$$K_e = K_m + \frac{c \cdot (K_i - K_m)}{1 + \frac{(1-c) \cdot (K_i - K_m)}{K_m + \frac{4}{3}G_m}}, \quad (4.3.2.1)$$

where:

c - Concentration of volume, $c = V_i/V_m$, V_i, V_m - volumes of inclusion and matrix, K_i, K_m - Bulk moduli of inclusion and matrix respectively.

The shear modulus of the equivalent material is obtained as a solution of the following quadric equation:

$$A \cdot \left(\frac{G_e}{G_m} \right)^2 + 2B \cdot \left(\frac{G_e}{G_m} \right) + C = 0, \quad (4.3.2.2)$$

where: G_e , G_m is the shear modulus of the equivalent material and matrix respectively, and A, B, C are constants calculated as follows:

$$A = 8 \left(\frac{G_i}{G_m} - 1 \right) \cdot (4 - 5v_m) \cdot e_1 \cdot c^{\frac{10}{3}} - 2 \left[63 \left(\frac{G_i}{G_m} - 1 \right) \cdot e_2 + 2e_1 \cdot e_3 \right] \cdot c^{\frac{7}{3}} + 252 \left(\frac{G_i}{G_m} - 1 \right) \cdot e_2 \cdot c^{\frac{5}{3}} - 50 \left(\frac{G_i}{G_m} - 1 \right) \cdot (7 - 12v_m + 8v_m^2) \cdot e_2 \cdot c + 4(7 - 10v_m) \cdot e_2 \cdot e_3$$

$$B = -2 \left(\frac{G_i}{G_m} - 1 \right) \cdot (1 - 5v_m) \cdot e_1 \cdot c^{\frac{10}{3}} + 2 \left[63 \left(\frac{G_i}{G_m} - 1 \right) \cdot e_2 + 2e_1 \cdot e_3 \right] \cdot c^{\frac{7}{3}} - 252 \left(\frac{G_i}{G_m} - 1 \right) \cdot e_2 \cdot c^{\frac{5}{3}} + 75 \left(\frac{G_i}{G_m} - 1 \right) \cdot (3 - v_m) \cdot e_2 \cdot v_m \cdot c + \frac{3}{2} (15v_m - 7) \cdot e_2 \cdot e_3,$$

$$C = 4 \left(\frac{G_i}{G_m} - 1 \right) \cdot (5v_m - 7) \cdot e_1 \cdot c^{\frac{10}{3}} - 2 \left[63 \left(\frac{G_i}{G_m} - 1 \right) \cdot e_2 + 2e_1 \cdot e_3 \right] \cdot c^{\frac{7}{3}} + 252 \left(\frac{G_i}{G_m} - 1 \right) \cdot e_2 \cdot c^{\frac{5}{3}} + 25 \left(\frac{G_i}{G_m} - 1 \right) \cdot (v_m^2 - 7) \cdot e_2 \cdot c - (7 + 15v_m) \cdot e_2 \cdot e_3,$$

and

$$e_1 = (49 - 50v_i v_m) \left(\frac{G_i}{G_m} - 1 \right) + 35 \frac{G_i}{G_m} (v_i - 2v_m) + 35(2v_i - v_m),$$

$$e_2 = 5v_i \cdot \left(\frac{G_i}{G_m} - 8 \right) + 7 \left(\frac{G_i}{G_m} + 4 \right),$$

$$e_3 = \frac{G_i}{G_m} \cdot (8 - 10v_m) + (7 - v_m).$$

Finally, Young modulus and Poisson's ratio of the equivalent material are [3]:

$$E_e = \frac{9K_e \cdot G_e}{3K_e + G_e}, \quad (4.3.2.3)$$

$$v_e = \frac{3K_e - 2G_e}{2(3K_e + G_e)}. \quad (4.3.2.4)$$

Multiphase model

The concrete is a multiphase composite material. The proportion of its components varies depending on the degree of hydration. This variation is represented in Figure 4.3.2.2 [4].

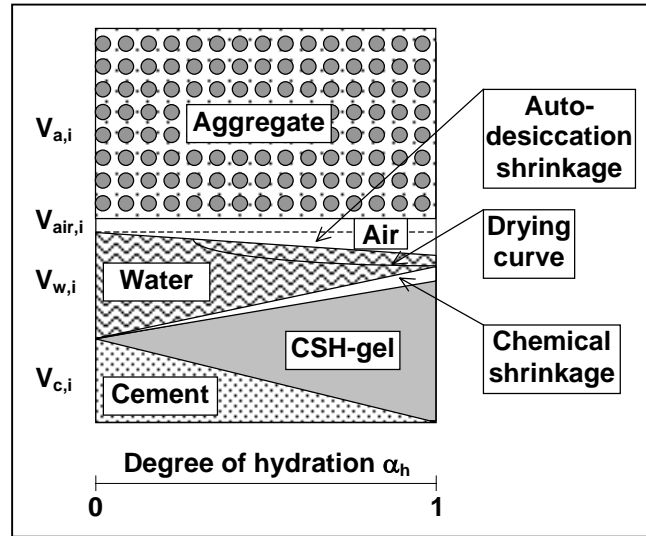


Figure 4.3.2.2: Fractional concrete volume [4]

For a certain value of the degree of hydration α_h the volume of each component is calculated using the following equations [4]:

$$\left. \begin{aligned} V_c(\alpha_h) &= V_{c,i} \cdot (1 - \alpha_h) \\ V_{\text{CSH}}(\alpha_h) &= V_{c,i} \cdot [1 + F_{\text{ww}} \cdot (1 - F_s)] \cdot \alpha_h \\ V_{\text{air},i}(\alpha_h) &= V_{c,i} \cdot F_{\text{ww}} \cdot F_s \cdot \alpha_h \\ V_w(\alpha_h) &= V_{w,i} - V_{c,i} \cdot F_{\text{ww}} \cdot \alpha_h \end{aligned} \right\}, \quad (4.3.2.5)$$

where:

V denotes volume and indexes

i - initial ($\alpha_h = 0$),

c, - cement (non hydrated),

CSH -CSH-gel,

air - air volume (sucked air, volume equal to auto-desiccation shrinkage),

w - water (cappilar water),

F_{ww} - volumetric water demand ratio, $F_{\text{ww}}=0.80$ to 0.82 (depends on type of cement) [5],

F_s - shrinkage ratio, $F_s=0.23$ to 0.25 (depends on type of cement) [5].

We notice that the volume of aggregate V_{ai} remains unchanged during hydration.

When the correlation degree of hydration vs. volumetric composition is established, it is possible to extend the Composite model to the concrete. For each value of the degree of hydration α_h , the volumetric composition of components is determined using Equation (4.3.2.5), and the Composite model is applied by repeating the Equations (4.3.2.1) to (4.3.2.5) following the algorithm presented in Figure 4.3.2.3.

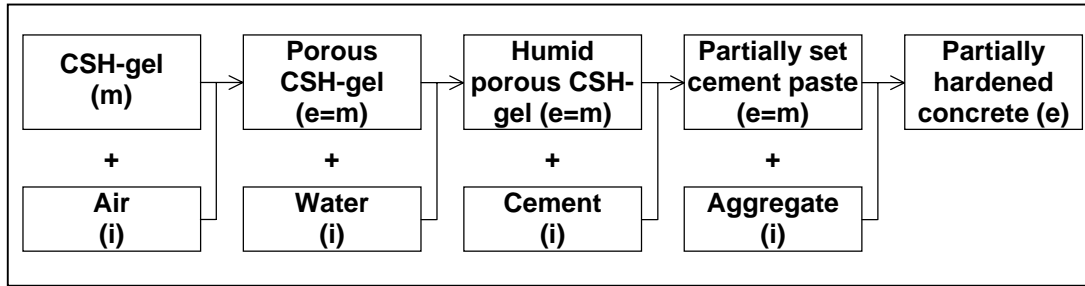


Figure 4.3.2.3: Computing procedure for Multiphase model

In Figure 4.3.2.3 (i) denotes the material treated as inclusion, the (m) - matrix and (e) - equivalent material.

The Multiphase model has three important shortcomings. All concrete components are considered as linearly elastic materials. Cement, aggregate, water and air inclusions are considered to be spherical. The matrix is considered as solid during the very early age. In spite of these shortcomings, a comparison between the model and experimental results is encouraging for α_h bigger than 0.1. For a degree of hydration less than 0.1, the model gives an underestimated value of Young modulus, but the estimation of the bulk modulus is still very good. The comparison between the model and the experimental results is given in Figure 3.9.3 (Chapter 3).

4.3.3 Development of Extended Multiphase (EM) model

The thermal deformation is very important at very early age. In the literature there are no models which describe the evolution of the TEC. The prediction of hardened concrete TEC is given by [6]. The model for composite materials [3] can also be applied to a hardened concrete. The research shows that the TEC of the concrete varies very much at early and very early age [7,8]. Therefore, to successfully model the sensor-concrete interaction, it is indispensable to establish a correlation between the TEC and degree of hydration.

The TEC of concrete depends on the mechanical properties of its components (cement, aggregate, water, etc.), the age of concrete, its internal humidity and ambience temperature range. A new model called EM model, inspired by Composite and Multiphase models, is developed and presented in this section. The model considers only the mechanical properties of concrete. The results obtained by EM model are compared with those obtained by FEM modelling and TEC prediction model for hardened concrete proposed by Emanuel and Hulsey [6]. It is also compared with experimental results found in the literature and the measurement carried out on hardened concrete specimen. The comparisons are presented at the end of the section.

Development of TEC model

The idea is similar to the case of the Composite model. We observe two materials with different TECs. The first material is considered as inclusion, the second one as a matrix (see Figures 4.3.2.1 and 4.3.3.1) and we look for an equivalent material with equivalent TEC.

If the temperature of the biphasic matrix-inclusion increases by 1°C , both materials deform. Consequently, a stress p appears on the interface. The TEC of the equivalent material is

calculated as ratio between the change of the external radius of the matrix Δr_m and the initial value of the external radius r_m (see Figure 4.3.3.1). In order to determine the deformation of the matrix Δr_m , firstly the stress p has to be determined. This is done using the method of forces and theory of elasticity [9].

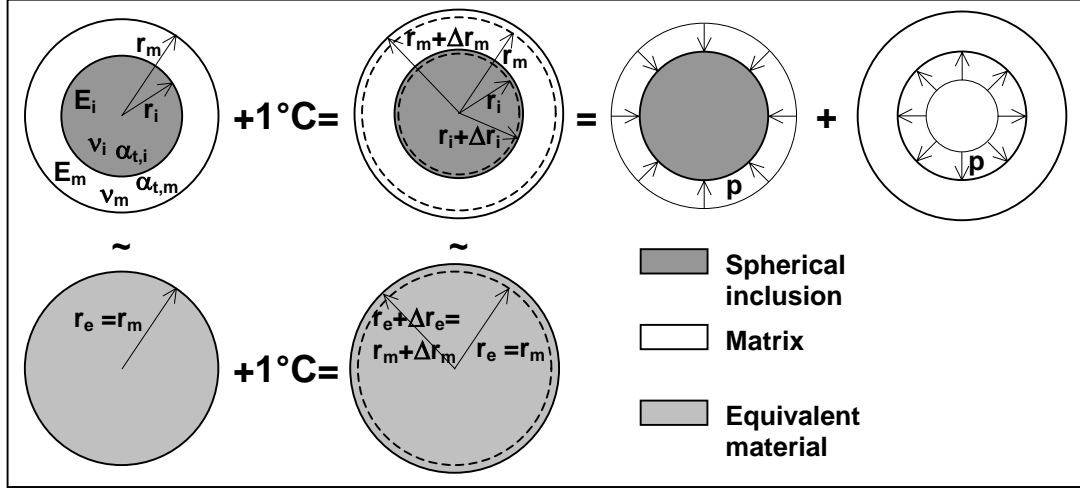


Figure 4.3.3.1: Schema of calculus of TEC for an equivalent material

The stresses in the inclusion produced by p are [9]:

$$\left. \begin{aligned} \sigma_{r,i}(r) &= -p = \text{const.} \\ \sigma_{\theta,i}(r) &= -p = \text{const.} \end{aligned} \right\}, \quad (4.3.3.1)$$

and in the matrix are [9]:

$$\left. \begin{aligned} \sigma_{r,m}(r) &= -p \cdot \frac{r_i^3 \cdot (r_m^3 - r^3)}{r^3 \cdot (r_m^3 - r_i^3)} \\ \sigma_{\theta,i}(r) &= p \cdot \frac{r_i^3 \cdot (2r^3 + r_m^3)}{2r^3 \cdot (r_m^3 - r_i^3)} \end{aligned} \right\}, \quad (4.3.3.2)$$

where indexes i and m denote inclusion and matrix respectively, σ_r normal stress in radial direction, σ_θ normal stress in tangential direction, p stress on the interface and r radius.

The strain fields are defined as:

$$\left. \begin{aligned} \varepsilon_{r,i}(r) &= \frac{\sigma_{r,i}(r)}{E_i} - 2v_i \cdot \frac{\sigma_{\theta,i}(r)}{E_i} + \alpha_{t,i} \cdot \Delta T = -(1-2v_i) \cdot \frac{p}{E_i} + \alpha_{t,i} \cdot \Delta T = \text{const.} \\ \varepsilon_{\theta,i}(r) &= (1-v_i) \cdot \frac{\sigma_{\theta,i}(r)}{E_i} - v_i \cdot \frac{\sigma_{r,i}(r)}{E_i} + \alpha_{t,i} \cdot \Delta T = -(1-2v_i) \cdot \frac{p}{E_i} + \alpha_{t,i} \cdot \Delta T = \text{const.} \end{aligned} \right\}, \quad (4.3.3.3)$$

and in the matrix as:

$$\left. \begin{aligned} \varepsilon_{r,m}(r) &= -\frac{p}{E_m} \cdot \frac{r_i^3}{r^3 \cdot (r_m^3 - r_i^3)} \cdot \left[(1+v_m) \cdot r_m^3 - (1-2v_m) \cdot r^3 \right] + \alpha_{t,m} \cdot \Delta T \\ \varepsilon_{\theta,m}(r) &= \frac{p}{E_m} \cdot \frac{r_i^3}{r^3 \cdot (r_m^3 - r_i^3)} \cdot \left[\left(\frac{1+v_m}{2} \right) \cdot r_m^3 + (1-2v_m) \cdot r^3 \right] + \alpha_{t,m} \cdot \Delta T \end{aligned} \right\}, \quad (4.3.3.4)$$

where ε denotes the strain, E - Young modulus, α_t the TEC and ΔT the temperature variation.

The displacement of the points of inclusion at the interface are calculated using the following expressions:

$$\left. \begin{aligned} \varepsilon_r &= \frac{\partial u}{\partial r} \\ \varepsilon_\theta &= \frac{u}{r} \end{aligned} \right\}, \quad (4.3.3.5)$$

where u denotes the radial displacement.

The displacement of the points of inclusion is

$$u_i(r) = \left[-(1-2\nu_i) \cdot \frac{p}{E_i} + \alpha_{t,i} \cdot \Delta T \right] \cdot r, \quad (4.3.3.6)$$

and at the interface

$$u_{i,i} = -(1-2\nu_i) \cdot \frac{p}{E_i} \cdot r_i + \alpha_{t,i} \cdot \Delta T \cdot r_i. \quad (4.3.3.7)$$

Finally the displacement of the points of the matrix is:

$$u_m(r) = \frac{p}{E_m} \cdot \frac{r_i^3}{r^2 \cdot (r_m^3 - r_i^3)} \cdot \left[\left(\frac{1+\nu_m}{2} \right) \cdot r_m^3 + (1-2\nu_m) \cdot r^3 \right] + \alpha_{t,m} \cdot \Delta T \cdot r, \quad (4.3.3.8)$$

and at the interface

$$u_{m,i} = u_m(r_i) = \frac{p}{E_m} \cdot \frac{r_i}{(r_m^3 - r_i^3)} \cdot \left[\left(\frac{1+\nu_m}{2} \right) \cdot r_m^3 + (1-2\nu_m) \cdot r_i^3 \right] + \alpha_{t,m} \cdot \Delta T \cdot r_i, \quad (4.3.3.9)$$

or if $c = V_i/V_m$ as in equations (4.3.2.1) we obtain:

$$u_{m,i} = \frac{p}{E_m} \cdot \frac{r_i}{(1-c)} \cdot \left[\left(\frac{1+\nu_m}{2} \right) + (1-2\nu_m) \cdot c \right] + \alpha_{t,m} \cdot \Delta T \cdot r_i, \quad (4.3.3.10)$$

The stress p is calculated from the condition that at the interface $u_{i,i} = u_{m,i}$ i.e.

$$p = \frac{(\alpha_{t,i} - \alpha_{t,m}) \cdot \Delta T}{\frac{\frac{1+\nu_m}{2} + (1-2\nu_m) \cdot c}{(1-c) \cdot E_m} + \frac{1-2\nu_i}{E_i}}, \quad (4.3.3.11)$$

and the displacement of the external points of matrix are:

$$u_e = u_m(r_m) = \left[\frac{3}{2} \cdot (1 - \nu_m) \cdot \frac{\alpha_{t,i} - \alpha_{t,m}}{\frac{1 + \nu_m}{2c} + (1 - 2\nu_m) + \frac{1 - c}{c} \cdot \frac{E_m}{3K_i}} + \alpha_{t,m} \right] \cdot r_m \cdot \Delta T. \quad (4.3.3.12)$$

Since $r_m = r_e$, the TEC of the equivalent material $\alpha_{h,e}$, is given in the following form:

$$\alpha_{t,e} = \frac{\varepsilon(\Delta T)}{\Delta T} = \frac{u_e}{\Delta T} = \frac{3}{2} \cdot (1 - \nu_m) \cdot \frac{\alpha_{t,i} - \alpha_{t,m}}{\frac{1 + \nu_m}{2c} + (1 - 2\nu_m) + \frac{1 - c}{c} \cdot \frac{E_m}{3K_i}} + \alpha_{t,m} \quad (4.3.3.13)$$

In the last two expressions, Young modulus and Poisson's ratio are replaced by bulk modulus using the expression:

$$K_i = \frac{E_i}{3 \cdot (1 - 2\nu_i)}. \quad (4.3.3.14)$$

The TEC model is completed using the schema presented in Figure 4.3.2.3, as in the case of the Multiphase model. Since the Multiphase model allows for the computation of the Young and bulk moduli as well as the Poisson's ratio, it is indispensable to integrate it in the algorithm. The model consisting of TEC model and Multiphase model is in fact an extension of the Multiphase model. Therefore it is called the Extended Multiphase model (EM). The EM model is compared with the results obtained by the finite element method (FEM) and experiments. The comparisons are presented in the following subsections.

Comparison with FEM model

In order to compare the accuracy of TEC and EM models, comparison with finite element method (FEM) is performed. This comparison is carried out as a part of the FEM modelling of the sensor-concrete interaction. Hence, more details concerning the used FEM method are found in Chapter 5. This FEM model is chosen because it performs calculus on material consisting of matrix and inclusions. However its performances are limited and its shortcomings are:

- Only 2 dimensional analysis (2D) is possible,
- Permitted difference in diameter between the biggest and the smallest inclusion is approximately 3 times,
- It is not possible to model the changes in time of mechanical properties of material.

The composition of simulated concrete is given in 5.2.2.1 and grain size in Figure 5.2.2.1 (Chapter 5). 2D FEM modelling is carried out using two materials, the mortar matrix and the aggregate inclusions. Due to the second shortcoming only grains of aggregate with diameter size of 9 to 32 mm are modelled as inclusions. Grains with a diameter smaller than 9mm along with the cement paste are considered as a matrix. The change of mechanical properties of the mortar matrix is calculated using EM model. Mechanical properties are calculated for different values of degree of hydration: 0.01, 0.05, 0.10, 0.50 and 1.00, and are presented in

Table 5.2.3.1 (Chapter 5). The mesh of finite elements and the schema of simulated bimaterial concrete specimen are represented in Figure 4.3.3.2.

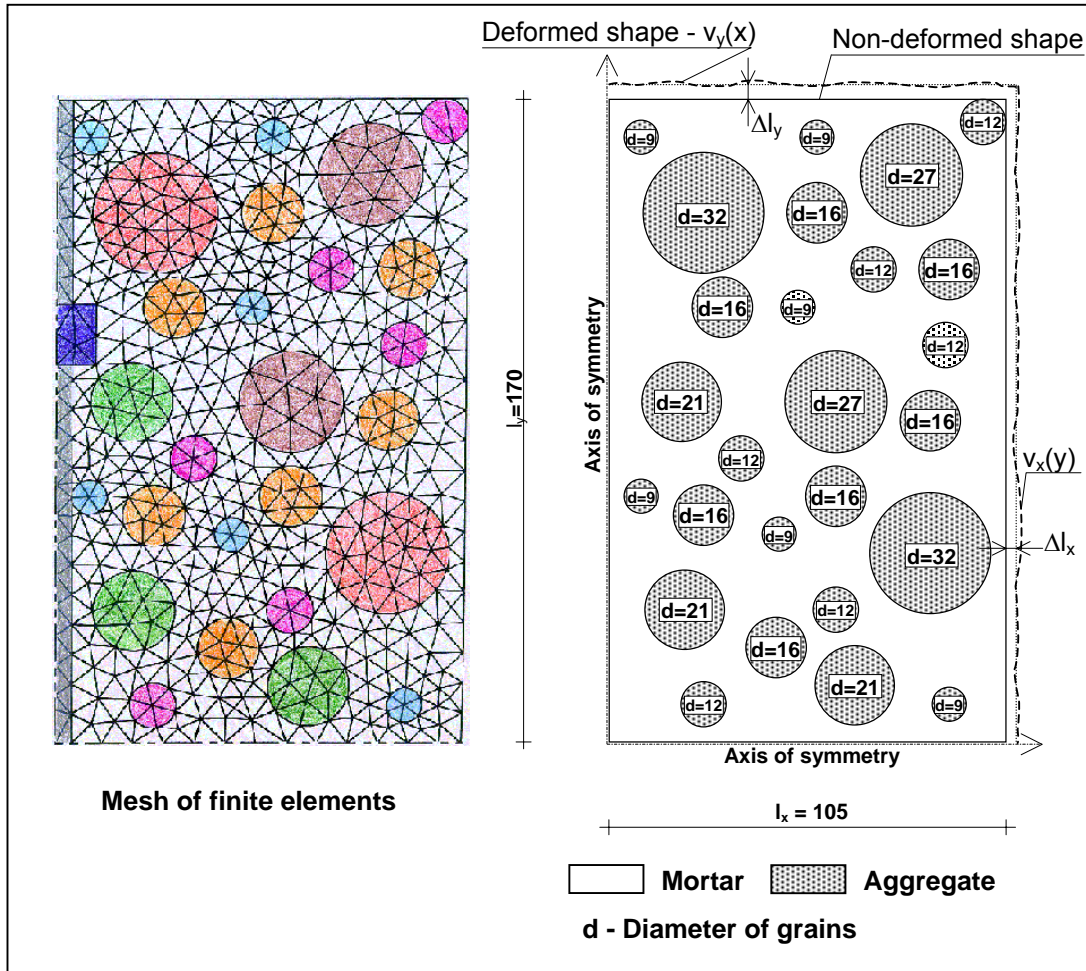


Figure 4.3.3.2: Finite element mesh and schema of modelled concrete specimen

The temperature variation of 170°C is imposed on the specimen and the displacement of border points is observed. A high temperature is imposed in order to increase the precision of the calculated displacements of the border points of the specimen. The thermal expansions of the specimen, Δl_x and Δl_y in both directions, x and y , is calculated as an average value of the border displacements $v_x(y)$ and $v_y(x)$. The average strains ε_x and ε_y are calculated as ratio between the thermal expansion Δl_x and Δl_y and the corresponding initial linear dimension l_x and l_y . (see Figure 4.3.3.2). Finally, the thermal expansion ratio α_t is calculated as ratio between the average strain and temperature of 170°C . Precisely:

$$\Delta l_x = \frac{1}{l_y} \cdot \int_0^{l_y} v_x(y) dy ; \Delta l_y = \frac{1}{l_x} \cdot \int_0^{l_x} v_y(x) dx ; \varepsilon_x = \frac{\Delta l_x}{l_x} ; \varepsilon_y = \frac{\Delta l_y}{l_y} \quad (4.3.3.15)$$

$$\alpha_{t,x} = \frac{\varepsilon_x}{\Delta T} ; \alpha_{t,y} = \frac{\varepsilon_y}{\Delta T} . \quad (5.3.3.16)$$

The results obtained by FEM modelling are compared with results obtained by EM model, if this last is performed if includes complete aggregate grain size distribution. Comparison is presented for different values of degree of hydration α_h in Tables 4.3.3.1 and 4.3.3.2 for x and y direction respectively. Graphical representation of the tables is given in Figures 4.3.3.3 and 4.3.3.4.

α_h	0.01	0.05	0.10	0.50	1.00
EM model, $\alpha_{t,x} [\cdot 10^{-5} \circ C^{-1}]$	1.7406	1.5900	1.4452	1.0900	1.0039
FEM $\alpha_{t,x} [\cdot 10^{-5} \circ C^{-1}]$	1.8715	1.6364	1.4630	1.1140	1.0372
Dispersion of FEM model	0.0879	0.0682	0.0530	0.0208	0.0138
Relative error [%]	6.99	2.83	1.22	2.16	3.21

Table 4.3.3.1: Comparison of results obtained by the EM model and FEM modelling in the x direction

α_h	0.01	0.05	0.10	0.50	1.00
EM model, $\alpha_{t,x} [\cdot 10^{-5} \circ C^{-1}]$	1.7406	1.5900	1.4452	1.0900	1.0039
FEM $\alpha_{t,x} [\cdot 10^{-5} \circ C^{-1}]$	1.8418	1.6169	1.4504	1.1113	1.0359
Dispersion of FEM model	0.0304	0.0188	0.0131	0.0045	0.0031
Relative error [%]	5.49	1.66	0.36	1.92	3.09

Table 4.3.3.2: Comparison of results obtained by the EM model and FEM modelling in the y direction

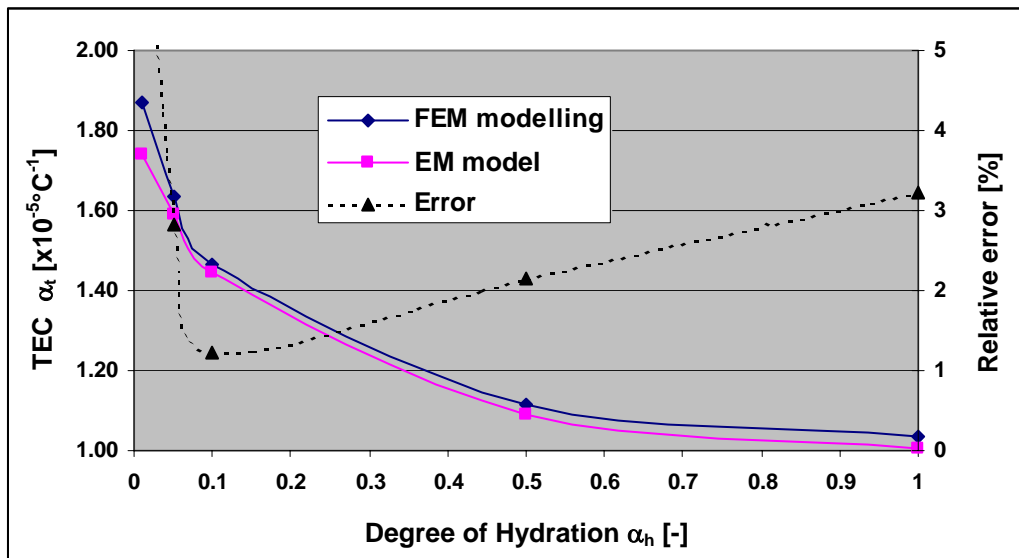


Figure 5.3.3.3: Comparison of results obtained by the EM model and FEM modelling in the x direction

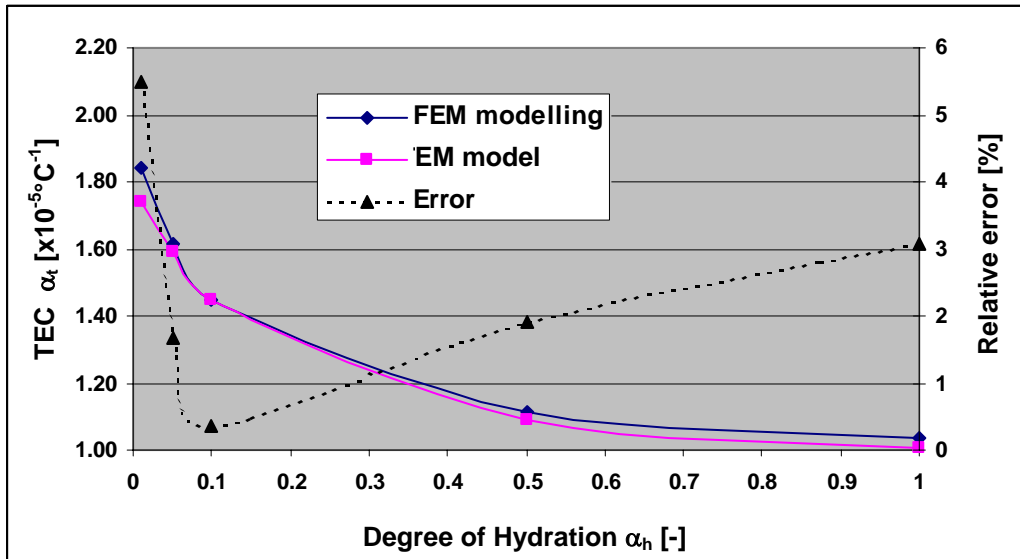


Figure 5.3.3.4: Comparison of results obtained by the EM model and FEM modelling in the y direction

The presented results shows that the compared models are complementary. The correlation coefficient is $R^2 > 0.99$. The results obtained by EM modelling are slightly underestimated, but the relative error do not exceed 7%, for degree of hydration less than 0.05, and 5% for degree of hydration higher or equal to 0.05.

Comparison with TEC prediction model for hardened concrete

The TEC prediction model is based on experimental results and proposed by Emanuel and Hulseley [6]. It is applicable to hardened concrete, thus only comparison with EM for value of degree of hydration $\alpha_h=1.00$ is reasonable. The concrete composition is the same as in the case of EM comparison with the FEM. The TEC of hardened concrete is computed using following expression [6]:

$$\alpha_{t,c} = f_T \cdot [f_M \cdot f_A \cdot \beta_{CP} \cdot \alpha_{t,CP} + \beta_a \cdot \alpha_{t,a}], \quad (5.3.3.17)$$

where:

$\alpha_{t,c}$ - TEC of hardened concrete,

$\alpha_{t,CP}$ - TEC of saturated hardened cement paste, $\alpha_{t,CP} = 1.08 \cdot 10^{-5} \text{ } ^\circ\text{C}^{-1}$,

$\alpha_{t,a}$ - TEC of aggregate,

f_T - correction factor for temperature alterations (1.0 for controlled environment; 0.86 for outside exposure),

f_M - correction factor for moisture content of cement paste (1.0 for saturated paste; 1.9 for moisture content of 60-75%; 1.2 for moisture content of 0%),

f_A - correction factor for age of cement paste (1.0 in case of saturated cement),

β_a - proportion by volume of aggregate,

β_{CP} - proportion by volume of cement paste, $\beta_a + \beta_{CP} = 1$.

The TEC of concrete in our case ($\alpha_{t,a}=0.85\cdot 10^{-5}\text{°C}^{-1}$, $\beta_a=0.73$, $\alpha_{t,CP}=1.08\cdot 10^{-5}\text{°C}^{-1}$, $\beta_{CP}=0.27$, $f_M=1.2$, $f_T=f_A=1$) obtained by expression (5.3.3.17) is 0.970. This value is less than 4% different from the value obtained by EM model (see Tables 4.3.3.1 and 4.3.3.2).

The comparison with TEC prediction model confirms the accuracy of the EM model for hardened concrete. We close this paragraph by noting that the TEC prediction model does not consider bonding of aggregate with the cement paste matrix.

Comparison with experimental results found in literature

The results obtained by EM model are compared with the experimental results found in the literature [7]. Since the mechanical properties of concrete utilised in the experiment are not known, only qualitative comparison is possible. Furthermore the EM model computes the evolution versus degree of hydration, while the experimental results are presented with respect to maturity. The evolution of TEC obtained by EM model and already presented in Figure 4.3.3.4 is given in more details in Figure 4.3.3.5. The experimentally measured evolution of TEC is presented in Figure 4.3.3.6 [7].

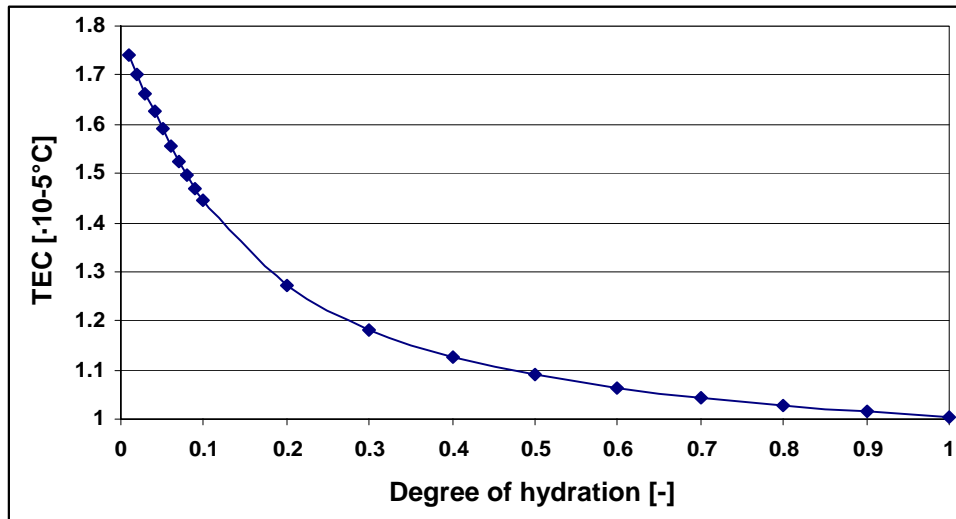


Figure 4.3.3.5: TEC evolution computed using EM model

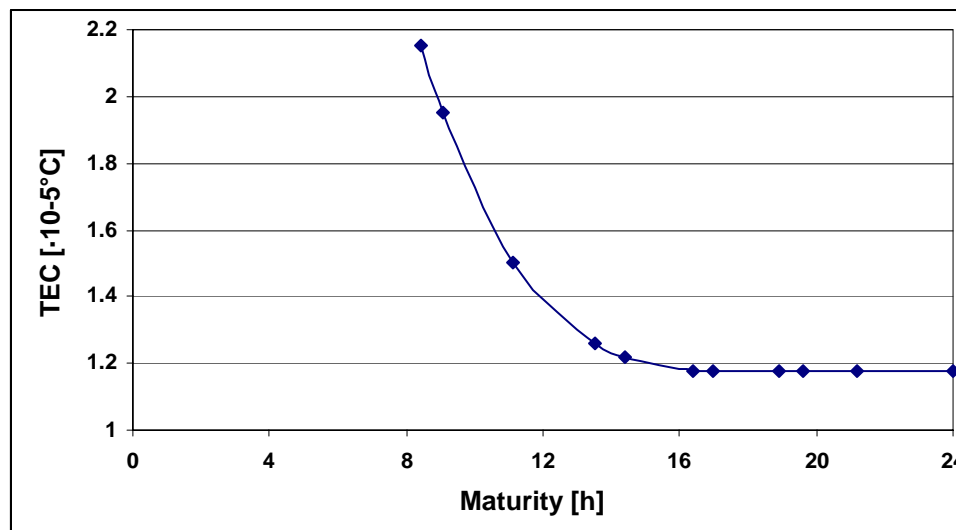


Figure 4.3.3.6: TEC evolution, measured experimentally

In both figures the curves are decreasing. The difference is in shape. The experimental results shows the stabilisation of the TEC at a maturity of 16 h. It is probably due to the structure of pores that allows the free deforming of water, and as a consequence, the rate of water in the final value of TEC is reduced.

The measurement presented in Figure 4.3.3.6 has started at a maturity of 8 h when the concrete becomes hardened. We can consider that the degree of hydration of concrete was at least 0.05 at this time. At maturity of 16h, we estimate degree of hydration of 0.2 to 0.25. Since the EM model predicts well the value of TEC for values of degree of hydration approaching 1 (see next paragraph), we conclude that TEC values obtained by the EM model are overestimated for degree of hydration α_h in limits 0.2 to 1. The error decreases from 20% ($\alpha_h = 0.2$ to 0.25), to approximately 5% ($\alpha_h \sim 1$). Therefore some corrections have to be performed on the EM model in further research.

Comparison with measurement performed on hardened concrete specimen

A specimen of concrete with known mechanical properties of aggregate is poured and its TEC is measured in the laboratory oven. The estimated degree of hydration during the period of measurement is approximately 0.9. The concrete composition of the specimen, as well as the mechanical properties of concrete components are presented in Table 4.3.3.3.

	<i>Mass [%]</i>	<i>Density [kg/m³]</i>	<i>Young modulus [GPa]</i>	<i>Poisson's ratio ν</i>	<i>TEC [$\cdot 10^{-5} 1/^\circ\text{C}$]</i>
Cement	15.13	300*	70*	0.27*	1.0*
Water	7.56	1000	2.18 ^{#+}	0.5	20 ⁺
CSH	-	2340	40*	0.21*	1.08*
Aggregate	77.31	2700	70	0.35	1.3
Air	~0	~0	~0	0.5	367 ⁺

* Values taken over from literature [4,6] # Bulk modulus + Volume expansion coefficient [10]

Table 4.3.3.4: Mechanical properties of concrete components

The specimen was poured in a rubber workform that's why its shape is not completely cylindrical (see Figure 4.3.3.7). It is equipped with three fibre optic sensors and two thermocouples. Each sensor consists of the measurement and the reference fibre glued to the plaques which are screwed to the specimen (see Figure 4.3.3.7, only one sensor is presented). The sensors are equidistantly placed in circumference of the specimen. The deformation of the specimen is determined as the mean value of the three measurements. The first thermocouple is installed in the core of the specimen and the second one at the surface. Thus, the thermal gradient of the specimen is monitored. Measurements are registered only if the thermal gradient core - surface is lower than 0.5°C. Schema and dimensions of the specimen are presented in Figure 4.3.3.7. In order to simplify the schema only one sensor is presented.

Three cycles of heating and cooling are performed in limits 4 to 45°C. During the first heating period the specimen has performed negative deformation (shrinkage) of approximately 1.12‰ due to the evaporation of water. This first cycle of heating is not considered in the determination of the TEC. The correlation temperature - deformation is presented in Figure 4.3.3.8.

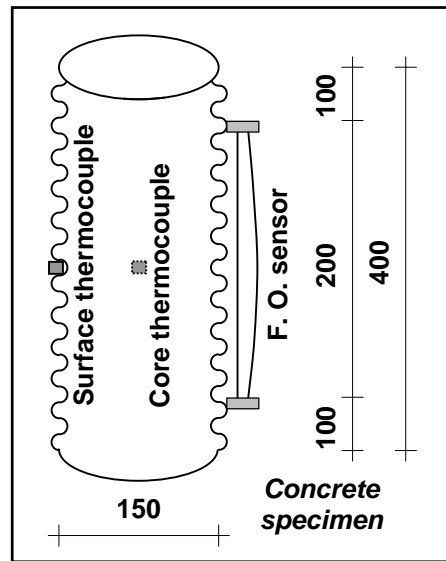


Figure 4.3.3.7: Schema of tested specimen

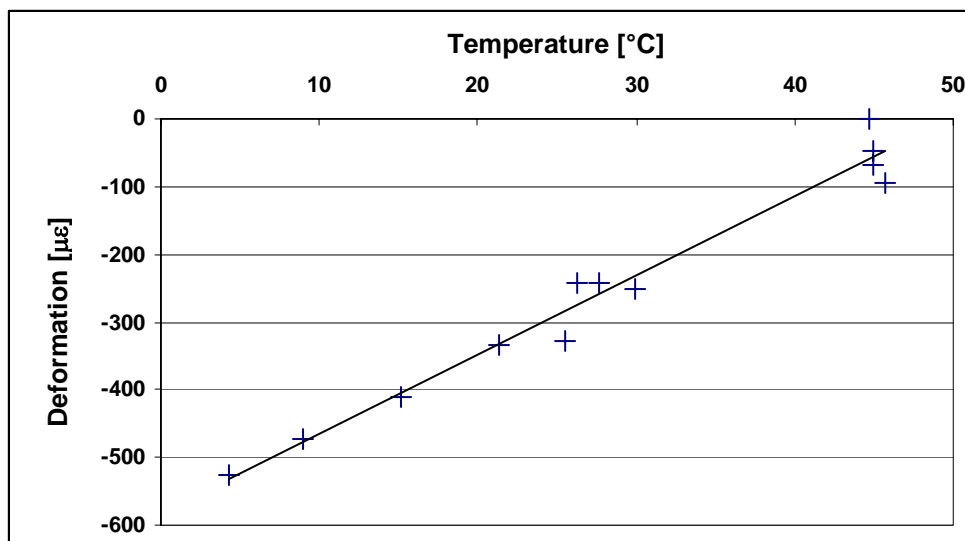


Figure 4.3.3.8: Correlation temperature - deformation of specimen

The TEC is calculated as the coefficient of regression, and the obtained value is near the $1.170 \cdot 10^{-5} \text{ } ^\circ\text{C}^{-1}$ with the coefficient of correlation $R^2=0.9706$. In Figure 4.3.3.8, we note dispersion of the measured values for the temperature of 45 °C caused by the evaporation of the specimen.

The evolution of TEC calculated by EM model is presented in Figure 4.3.3.9. Two values corresponding to degree of hydration of 1.0 are presented in this Figure. Higher value ($1.337 \cdot 10^{-5} \text{ } ^\circ\text{C}^{-1}$) to concrete with moisture content of 100%, and the lower value ($1.276 \cdot 10^{-5} \text{ } ^\circ\text{C}^{-1}$) to concrete with moisture content of 20%.

The measurement of the moisture content in the specimen could not be performed, but we assume that it is less than 20%. Hence the measured value of the TEC is compared with the value obtained by the EM model for the moisture content of 20%. The relative difference between the compared values is 9%. This proves a good prediction of the TEC of hardened concrete by the EM model.

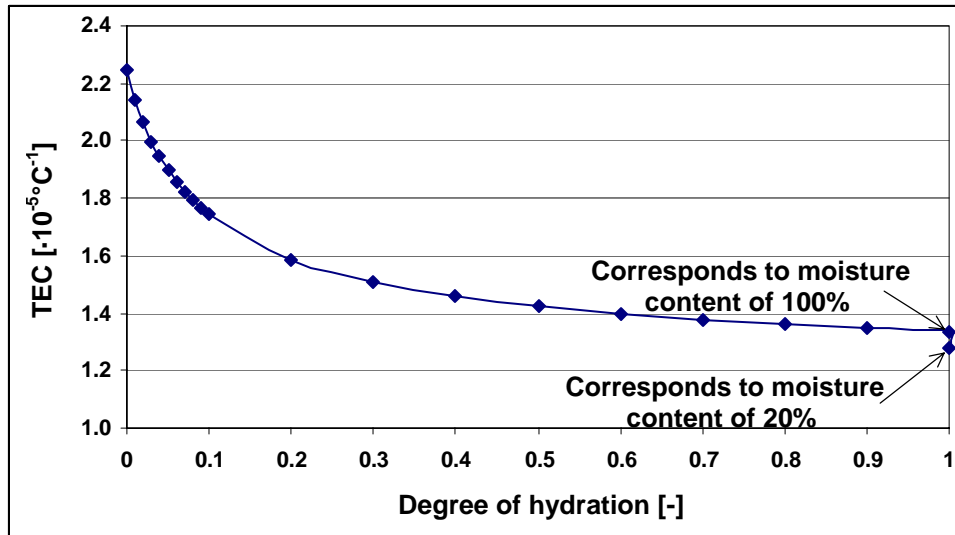


Figure 4.3.3.9: Comparison between the EM model and experimental results

The EM model has the same shortcomings as the Multiphase model. In spite of the shortcomings both the Multiphase and the EM models agree sufficiently with the experimental results and therefore, they are used for numerical modelling in this thesis.

4.4 Concluding remarks

In this chapter the mechanical properties of the Standard Sensor and the numerical model describing the evolution of mechanical properties of the early age concrete are presented. They are to be used in the research developed in the following chapters. The assumption of linear mechanical behaviour of materials is adopted due to sufficiently good agreement with experimental results.

The original contribution presented in this chapter is the development of the EM model. The model describes the evolution of the TEC of the concrete versus the degree of hydration. It is compared with FEM modelling, TEC prediction model for hardened concrete and experiments and the comparisons have proved its soundness.

The development of the EM model is not finished. Research continues in order to improve the model by adding corrections concerning moisture content and behaviour of water in pores.

4.5 References

- [1] CEB-FIP Model code, 1990
- [2] De Schutter G., Taerwe L., *Degree of hydration-based description of mechanical properties of early age concrete*, Materials and Structures, Vol.29 July 1996, pp 335-344

- [3] Christensen R. M., *Mechanics of composite materials*, Krieger publishing company, Malabar, Florida, 1991
- [4] Paulini P., Gratl N., *Stiffness formation of early age concrete*, Thermal Cracking in Concrete at Early Age, RILEM International Symposium, pp.63-70, Munich, 1994
- [5] Paulini P., *Zement-Kalk-Gips*, Nr.10, pp. 525-531, 1988
- [6] Emanuel J. H., Hulsey J. L., *Prediction of the Thermal Coefficient of Expansion of Concrete*, Journal of ACI, pp. 149-156, April 1977
- [7] Laplante P., Boulay C., *Evolution du coefficient de dilatation thermique du béton en fonction de sa maturité aux tout premiers âges*, , Materials and Structures, Vol.27, pp. 596-605, 1994
- [8] Schöppel K., Springenschmid R., *The Effect of Thermal Deformation, Chemical Shrinkage and Swelling on Restraint Stresses in Concrete at Early Age*, Thermal Cracking in Concrete at Early Age, RILEM International Symposium, p.p. 215-220, Munich, 1994
- [9] Timoshenko S. P., Goodier J. N., *Theory of Elasticity*, McGraw Hill International, 1970
- [10] *Formulaires et tables, Mathématique, Physique, Chimie*, Commissions romandes de mathématique, de physiques et de chimie, Editions de Tricorne, pp. 190-197, Genève, 1996

5 Interaction of Standard Sensor and concrete at early and very early age

5.1 Introduction

The concept of the SOFO system and the Standard Sensor was described in Chapter 2. The Standard Sensor is several orders of magnitude softer than hardened concrete. Thus, it measures deformation of a hardened concrete with high precision. The Standard Sensor does not perturb the strain field of the hardened concrete, and the concrete, being several orders of magnitude stiffer, entirely transmits the deformation to the Standard Sensor.

At the very early age, before hardening, the stiffness and strength of the concrete are low (see Chapter 3). The thermal processes are intense during this phase. The sensor thermal expansion coefficient TEC is greater than concrete TEC at the very early age. Due to thermal processes generated by hydration, both the sensor and the concrete are heating and deforming. The deformations of the sensor and concrete are not compatible due to their different TECs. The sensor squeezes into the concrete and stresses are generated. If the stresses exceed the strength of concrete or squeezing is significant, the sensor perturbs the strain field of the concrete at very early age, and measurements realised by sensor are not valid.

The aim of this chapter is to answer the questions: whether the SOFO system can be applied to non-hardened concrete, and what are the limits of application. This research is based on mathematical (numerical) models and experiments. Numerical research includes the influence of the sensor to a strain field of the concrete at early and very early age, evaluation of the transfer of deformation from concrete to the sensor, and estimation of the generated stresses in concrete. It is carried out using 3D finite element method (FEM) for modelling at macro-level and 2D FEM method for modelling at meso-level. The 2D modelling is also used to determine the accuracy of the EM model developed in Section 4.3.3.

Experimental research was performed in the laboratory. The aim of this research was to evaluate the numerical modelling and to define the limits of sensor application (minimal distance between two sensors, influence of the proximity of the rebars to the measurement etc).

The chapter closes with a discussion devoted to other monitoring systems which were designed for early and very early age concrete deformation monitoring.

The schema of research devoted to estimation of the sensor-concrete interaction is represented in Figure 5.1.1.

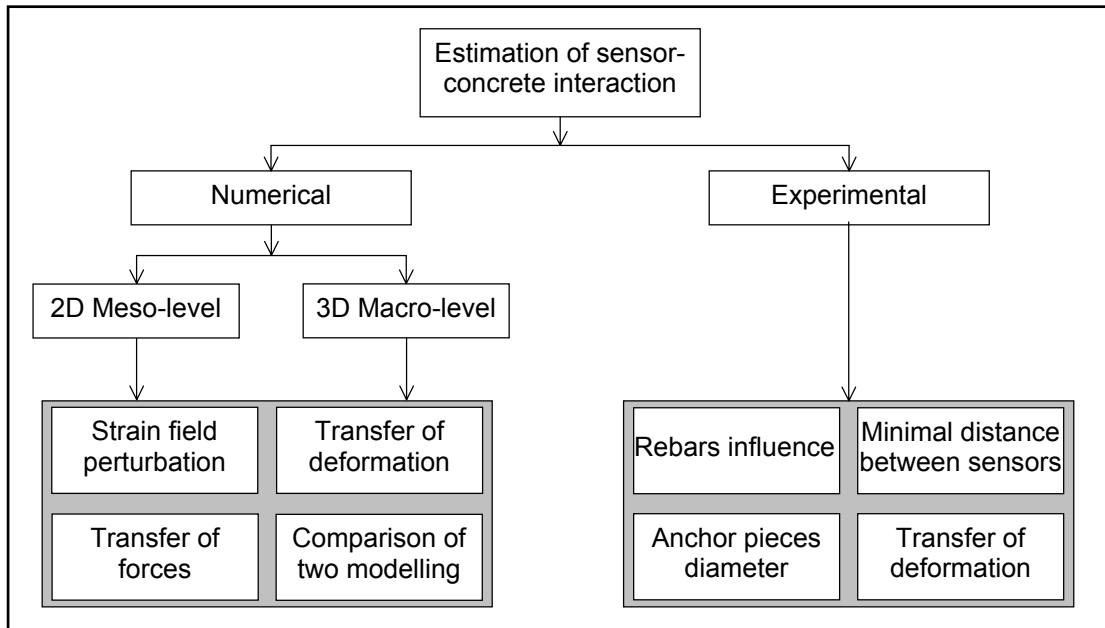


Figure 5.1.1: Schema of sensor-concrete interaction research

5.2 Numerical modelling of sensor-concrete interaction

5.2.1 Introduction

Numerical modelling consists of meso and macro modelling. In both cases two cylindrical specimens of concrete are compared. The first specimen does not contain sensors. The second specimen contains a sensor embedded in its middle. The specimens are exposed to temperature changes in order to simulate the internal deformation of concrete caused by hydration heating and autogenous shrinkage - the most important and unavoidable deformations at early and very early age.

The modelling is repeated for the following values of degree of hydration: 0.01, 0.05, 0.10, 0.50 and 1.00. For each value, the mechanical properties of concrete are calculated using the EM model presented in Chapter 4. For each degree of hydration, the deformation of the specimen containing the sensor is compared with deformation of the specimen without sensor.

Since the behaviour of concrete at very early age is visco-elastic, the best manner of modelling is to consider the concrete as a visco-elastic medium. The problem is that the viscous coefficient and the plastic limit evolve with concrete ageing, and it is too complicate to involve it in calculation. Therefore, in the presented modelling, the concrete behaviour is supposed to be linearly elastic. This assumption introduces an error in computing. Since the stresses provoked by the sensor-concrete interaction are low, it gives, however, a good approximation of the sensor's behaviour. The experimental research, presented in Section 5.3, has confirmed that the magnitude of the error is not significant.

5.2.2 Concrete composition

Both numerical modellings are performed using concrete with the same simulated mechanical properties. The composition and mechanical properties of each component of concrete are represented in Table 5.2.2.1, and the grain-size curve in Figure 5.2.2.1.

	<i>Mass [%]</i>	<i>Volume [%]</i>	<i>Young modulus [GPa]</i>	<i>Poisson's ratio ν</i>	<i>TEC [$\cdot 10^{-5} 1/^{\circ}\text{C}$]</i>
<i>Cement</i>	12.39	0.10	70	0.27	1.0
<i>Water</i>	6.20	0.15	2.18*	0.5	20**
<i>CSH-gel</i>	-	-	40	0.21	1.2
<i>Aggregate</i>	81.41	.73	50	0.25	0.85
<i>Air</i>	-	0.02	0.0001*	0.5	367**

*Bulk module

**Volumetric coefficient

Table 5.2.2.1: Proportion and mechanical properties of the concrete components

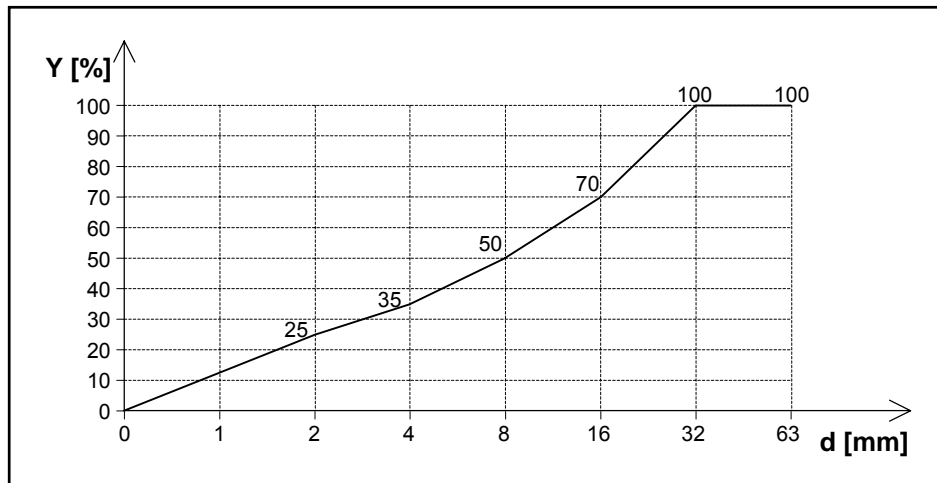


Figure 5.2.2.1: Grain-size distribution curve

5.2.3 2D FEM modelling at meso-level

Suitable software for 3D FEM modelling of concrete at meso-level is described in [1]. Unfortunately it was not possible to "embed" and model the sensor using this model due to problems related to the generation of the mesh. Therefore, 2D FEM [2, 3] modelling is carried out using the software presented in the next paragraphs.

As described in the introduction of this chapter the objective of 2D FEM modelling is to compare the deformation of two specimens. The first one is without any sensor and the second one contains the sensor. The specimens are loaded by temperature, in order to simulate the internal early age deformation provoked by hydration heating and autogenous shrinkage. The mechanical properties, composition, grain-size disposition, and degree of hydration of both specimens are equal. In this way, any difference between compared deformations is caused only by sensor-concrete interaction.

The modelling was realised by FEM software named FORGE2 MULTIMATERIALS, developed at CEMEF - Ecole des Mines de Paris, Sophia Antipolis, France. The software was

designed to model large deformation of materials with elastic-viscoplastic behaviour. It uses 2D finite element code with iso-parametric six-node triangular elements (P2P0: Quadratic velocity, Constant pressure), plane strain (or axisymmetrical), updated Lagrangian method and automatic remesher. However, FORGE2 MULTIMATERIALS has some important shortcomings. Firstly, it was possible to model only grains of aggregate with diameter in limits 9 -32 mm as inclusions, the smaller grains are considered, along with the cement paste, as mortar matrix. Furthermore, grain-size composition is not simulated as continuous, but as discrete.

This software was chosen because it offers the possibility to model the concrete at the meso-level (mortar matrix with aggregate inclusions). Since only linear analysis is performed and only grains with diameter in limits 9-32 mm are treated as inclusion, this analysis is not completely accurate but, in combination with experimental results, allows a good estimation of the interaction between the Standard Sensor and the concrete at early and very early age. Furthermore, a 2D analysis is performed instead the 3D analysis, that additionally decreased the accuracy of modelling. The mesh consists of 1000 triangular plane elements. It is presented in Figure 4.3.3.2, Section 4.3.3.

Modelling of concrete

Since the grain sizes varies in a large spectra it was not possible to represent all of them as inclusions in the cement paste matrix. The water and air could not be treated separately for the same reasons. Therefore, we considered the mixture of cement, water, air and aggregate with a grain size less than 8 mm as a unique material called mortar. The aggregate grains with sizes bigger than 8mm were represented in form of spherical inclusions. The total number of grains represented as inclusions as well as their dimension are adjusted to satisfy the distribution curve and mass equilibrium represented in Figure 5.2.2.1.1 and Table 5.2.2.1.1, respectively.

The 2D FEM model is not suitable for the analysis of materials with time dependent properties. Hence, mortar properties for different values of degree of hydration are calculated using the EM model. FEM calculation is executed afterwards, for each degree of hydration separately. The evolution of mortar properties versus degree of hydration is represented in Table 5.2.3.1.

α_h	<i>0.01</i>	<i>0.05</i>	<i>0.1</i>	<i>0.5</i>	<i>1</i>
<i>E [GPa]</i>	2.662	6.879	10.428	23.713	29.136
<i>ν</i>	0.434	0.365	0.324	0.259	0.243
<i>$\alpha_t [-10^{-5} 1/^\circ\text{C}]$</i>	2.068	1.877	1.689	1.220	1.111

Table 5.2.3.1: Evolution of mechanical properties of simulated mortar

Thus, for a chosen value of degree of hydration α_h , the simulated concrete consists of only two materials, the mortar matrix and the aggregate inclusions (see Figure 5.2.3.2).

Modelling of sensor

The modelling of the sensor is based on properties presented in Table 4.2.1. Modification of Young modulus and the shape of the sensor are needed in order to adapt the sensor model of sensor to software performance and 2D analysis.

The anchor pieces are considered as cylindrical. Young modulus, Poisson's ratio and the TEC are the same as for steel, i.e. $E=210$ GPa, $\nu=0.3$ and $\alpha_h=1.2 \cdot 10^{-5} \text{ } ^\circ\text{C}^{-1}$. Both, the active and the passive zones of the sensor, consisting of PVC tube and optical fibres, are replaced by a full beam consisting of an equivalent material with the external dimension equal to the external dimensions of the tube and with the stiffness equal to the stiffness of active zone. This equivalent material is also called "sensor" material. The Young modulus of the equivalent (sensor) material is calculated using the following expression:

$$E_{\text{equ}} = \frac{E_s \cdot A_s}{A_{\text{equ}}} = \frac{22.88 \cdot 10^3}{\pi \cdot (4 \cdot 10^{-3})^2} = 455183137.2 \text{ Pa} = 0.455 \text{ GPa} \quad (5.2.3.1)$$

The TEC and Poisson's ratio remains the same as those of the PVC tube, $\alpha_h=14.44 \cdot 10^{-5} \text{ } ^\circ\text{C}^{-1}$ and $\nu=0.4$. Thus the sensor model consist of two qualities, the sensor built of equivalent material, and the steel anchor pieces.

Reduction from 3D to 2D

A last limitation is a 2D representation of 3D objects. In order to maintain the initial shape of the sensor, the 2D representation is a simple vertical projection of 3D objects to a plane. In consequence, the aggregate grains are treated as cylinders and the sensor as a prismatic body. This problem can not be avoided. It is schematically represented in Figure 5.2.3.1.

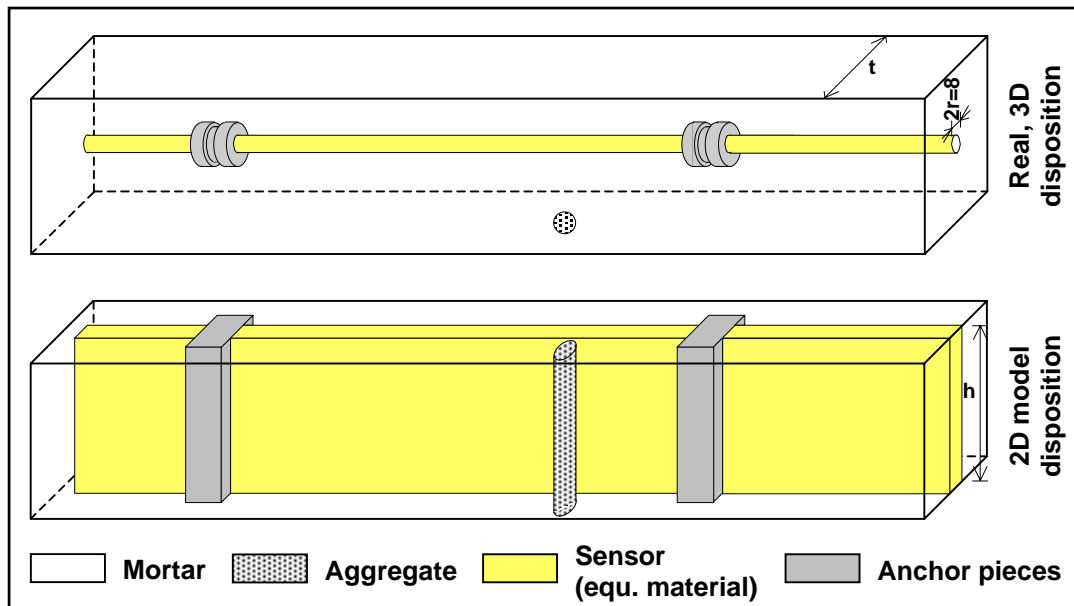


Figure 5.2.3.1: Problem of reduction from 3D to 2D

We can accept that mortar and aggregate Young moduli remains unchanged by 3D to 2D reduction, because in reality (3D) they are present in the whole volume of the specimen. On the contrary, the Young modulus of the sensor equivalent material has to be changed, because in reality the sensor occupies only the central part of the specimen. The changed Young modulus of the equivalent material is calculated using the following expression:

$$E_{\text{equ}} = \frac{E_s \cdot A_s}{A_{\text{equ}}} = \frac{22.88 \cdot 10^3}{8 \cdot 10^{-3} \cdot h} \quad (5.2.3.2)$$

In the last equation the magnitude of h is not defined. We suppose that this value is the same as the transversal dimension of specimen t . However, this is not completely correct, since the dimension t may be chosen differently. Therefore we have utilised for Young modulus of the sensor equivalent material the value obtained in 5.2.3.1. We take care that this value is high, and that the deformation obtained by computing using this value is overestimated.

The models of the specimens with and without sensor are represented in Figure 5.2.3.2. Only one quarter is analysed due to the biaxial symmetry.

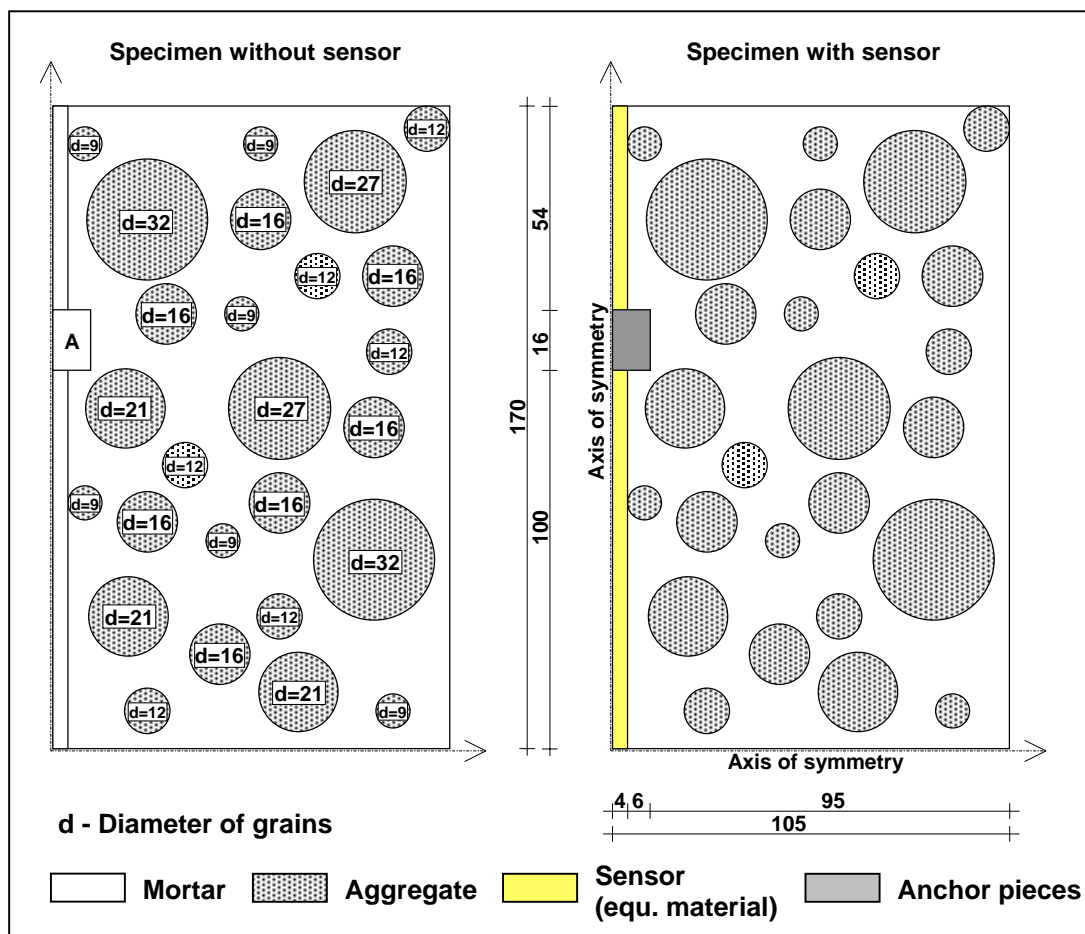


Figure 5.2.3.2: Modelled concrete specimens without and with sensor

5.2.4 3D FEM modelling at macro-level

3D FEM modelling has the same form as the 2D modelling, i.e. we will compare the deformation of two specimens, the first without and the second with the sensor, loaded by temperature variations. The mechanical properties, composition, grain-size disposition and degree of hydration of both specimens are also equal.

The modelling is realised by the software developed by FEMMASSE b.v., USA. The software is named HEAT 6.0, and is an extension of software HEAT 3.0 [4]. It is based on the non-linear finite element method [2, 3], but only the linearly elastic analysis is carried out as in case of 2D modelling. The elements employed in this modelling are plane quadrilateral with four Gauss points. HEAT 6.0 is conceived for 2D or axi-symmetrical analysis. Since the concrete is treated at macro level, as a homogenous material, the analysis becomes 3D axi-symmetrical. The mesh consists of 1107 square plane elements.

Modelling of concrete

Concrete is represented as homogenous linearly elastic material. The changes of mechanical properties are calculated for each degree of hydration using the Extended Multiphase model. Their evolution is represented in Table 5.2.4.1

α_h	0.01	0.05	0.1	0.5	1
E [GPa]	4.713	9.951	14.269	29.432	35.348
ν	0.408	0.345	0.308	0.254	0.242
$\alpha_t \cdot 10^{-5} 1/^\circ\text{C}$	1.741	1.590	1.445	1.090	1.004

Table 5.2.4.1: Evolution of mechanical properties of simulated concrete

Modelling of the sensor

The sensor is modelled in the same way as in the case of 2D modelling. The difference is that the sensor is treated as an axi-symmetrical cylindrical body. In Figure 5.2.4.1 the mesh of elements with sensor, anchor pieces and the concrete is represented.

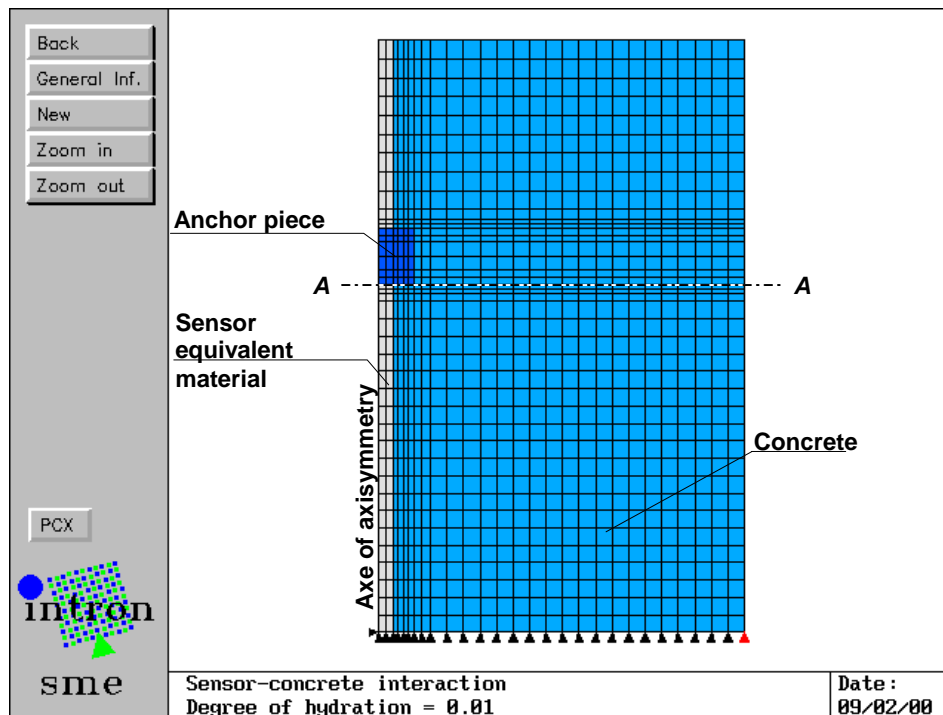


Figure 5.2.4.1: Mesh of elements for 3D modelling

The dimensions of all components are the same as in case of 2D modelling. Due to horizontal plane symmetry only the upper part of the specimen is analysed.

5.2.5 Results and discussion

Heating of the specimens for 2D and 3D analysis, with and without the sensor, is simulated. A temperature of 170°C is chosen in order to increase the precision of computing.

Transfer of deformation from concrete to sensor

The lower border displacements of the specimen anchor piece (specimen with sensor) is compared with the lower border displacement of the corresponding area of the specimen without sensor (denoted by A in Figure 5.2.3.2). The lower border is chosen because the measurement basis of the sensor does not include the anchor pieces. The comparison obtained through 2D modelling is shown in Table 5.2.5.1 and in Figure 5.2.5.1. The same type of data obtained by the 3D modelling is represented in Table 5.2.5.2 and Figure 5.2.5.2.

α_h	0.01	0.05	0.1	0.5	1
Without sensor [$\mu\text{m}/^\circ\text{C}$]	1.805	1.598	1.439	1.110	1.035
With sensor [$\mu\text{m}/^\circ\text{C}$]	1.931	1.665	1.486	1.126	1.047
Difference [$\mu\text{m}/^\circ\text{C}$]	0.126	0.067	0.046	0.017	0.012
Relative difference [%]	6.99	4.19	3.22	1.50	1.19

Table 5.2.5.1: Displacement of anchor piece vs. degree of hydration - 2D modelling

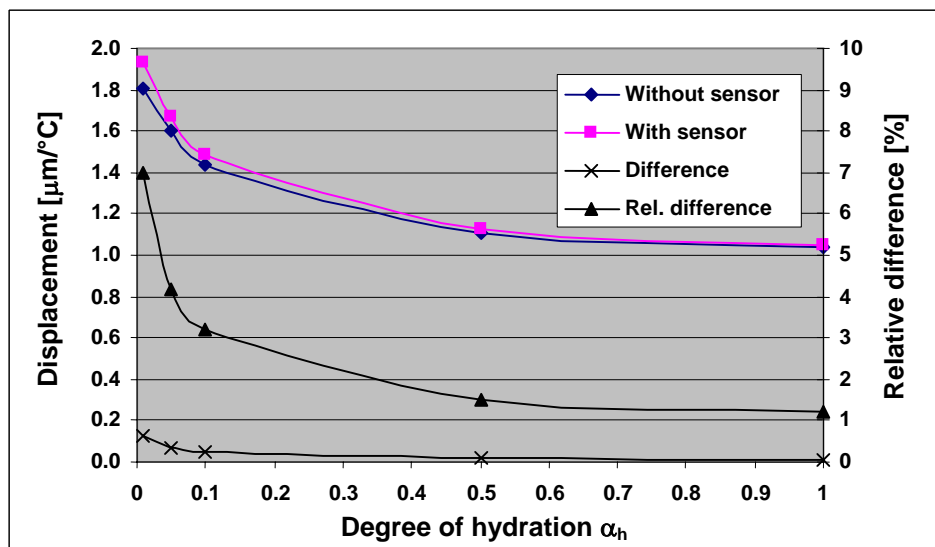


Figure 5.2.5.1: Displacement of anchor piece vs. degree of hydration - 2D modelling

α_h	0.01	0.05	0.1	0.5	1
Without sensor [$\mu\text{m}/^\circ\text{C}$]	1.741	1.590	1.445	1.090	1.004
With sensor [$\mu\text{m}/^\circ\text{C}$]	1.837	1.670	1.510	1.111	1.008
Difference [$\mu\text{m}/^\circ\text{C}$]	0.096	0.080	0.065	0.021	0.004
Relative difference [%]	5.52	5.05	4.51	1.91	0.41

Table 5.2.5.2: Displacement of anchor piece vs. degree of hydration - 3D modelling

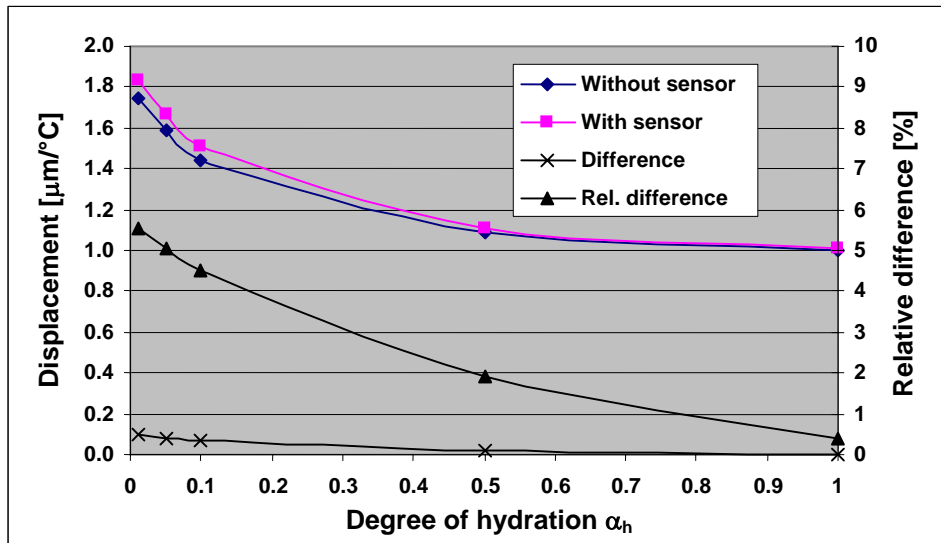


Figure 5.2.5.2: Displacement of anchor piece versus degree of hydration - 3D modelling

In Tables 5.2.5.1 and 5.2.5.2 the displacements are calculated as an average displacement of the anchor piece's lower border points.

In both cases of modelling, the relative difference between concrete deformation (corresponds to deformation obtained by specimens without sensor) and the deformation transferred to the sensor (corresponds to deformation obtained by specimens with sensor) does not exceed 7%, and decreases when the degree of hydration increases.

For a degree of hydration lower than 0.1, the relative difference is certainly overestimated. In the case of 2D modelling the value of sensor's Young modulus is overestimated due to reduction from 3D to 2.5D (see Section 5.2.3) while in 3D modelling there are no grains of aggregate to retain the deformation of the sensor.

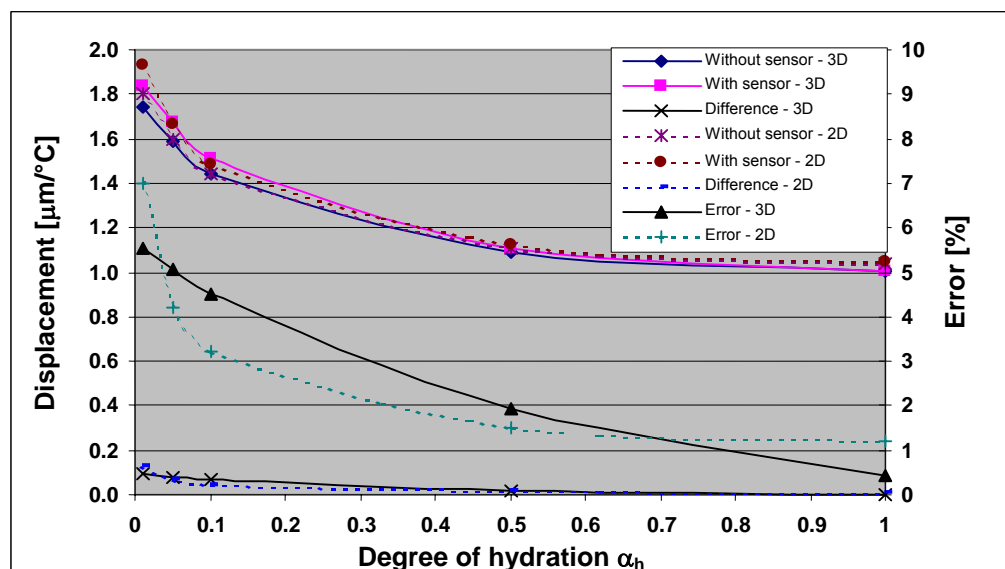


Figure 5.2.5.3: Comparison of 2D and 3D modelling

The comparison between 2D modelling and 3D modelling is represented in Figure 5.2.5.3. In this figure we note that relative difference decreases faster in the case of the 2.5D modelling even if Young modulus of sensor is overestimated. This phenomenon is a consequence of aggregate presence - the aggregate, being stiffer than the mortar retains the deformation of the sensor.

The conclusion carried out from 2D and 3D modelling is that a very good transfer of deformation from concrete to the Standard Sensor is confirmed. The difference in deformations per °C of samples with and without sensor is more than 15 times lower than resolution of SOFO system (2µm). Since the temperature rate per degree of hydration at very early age is limited 4-10 °C / 0.01, the resolution of the system is practically not achieved. This allows the use of the sensor for the deformation measurement of concrete at the early and very early age, for degree of hydration higher or equal to 0.01.

Transfer of forces

Due to temperature variation, a normal force is generated in the sensor. If the deformation of the sensor is completely restrained, the generated force induced by a temperature change of 1°C is calculated as:

$$F_{s,max} = -\alpha_{t,s} \cdot E_s \cdot A_s = -3.304N/^\circ C, \quad (5.2.5.1)$$

This force is entirely or partially transmitted to the concrete by means of the anchor pieces and lateral friction (see Figure 5.2.5.5). In consequence, stresses are generated in the concrete. The real distribution of stresses in concrete is very complex. The principal stresses distribution of the concrete surrounding the anchor piece obtained by 3D modelling for a degree of hydration of 0.01 is presented in Figure 5.2.2.5.

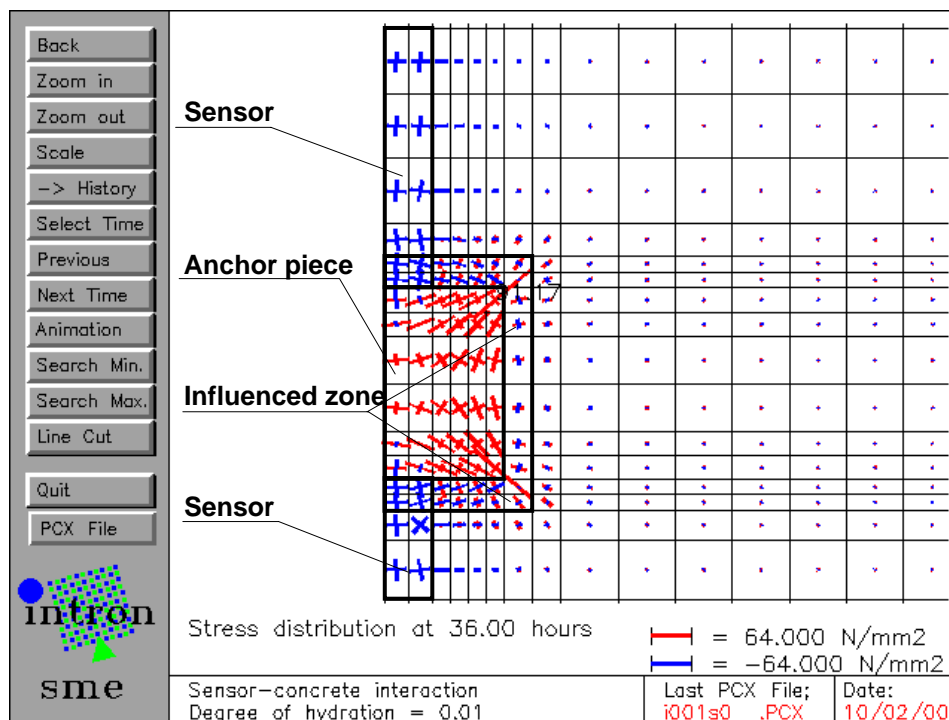


Figure 5.2.5.5: Stress distribution in surrounding of the anchor piece obtained by 3D modelling for degree of hydration of 0.01

In Figure 5.2.5.5 high stresses are observed in the anchor piece itself, the stresses in concrete surrounding the anchor piece (influenced zone) and sensor tube are less significant, and practically equal to zero in the zone 1 - 2 mm distant of the anchor piece. The origin of stresses generated in the influenced zone is the incompatibility of deformations of concrete and the anchor piece itself and not in global sensor behaviour. If only the anchor piece is embedded in concrete (without sensor) approximately the same stresses are generated. Since the anchor piece, embedded separately into the concrete, behaves as a grain of aggregate, these stresses are ignored during analysis.

The longitudinal normal stress in the sensor is practically constant. In fact the stress varies insignificantly through the section and along the sensor due to the precision of calculation. To simplify presentation and the calculation, the normal force in the sensor is calculated from the average deformation of the sensor, as follows:

$$F_s = \left(\frac{v}{l_s} - \alpha_t \cdot \Delta T \right) \cdot E_s \cdot A_s, \quad (5.2.5.2)$$

where:

F_s - normal force in the sensor,

v - displacement of the anchor piece presented in Tables 5.2.5.1 and 5.2.5.2,

l_s - initial length of the sensor,

ΔT - temperature variation, $\Delta T = 1^\circ\text{C}$,

$\alpha_{t,s}$ and $E_s \cdot A_s$ - TEC and stiffness of the sensor.

The evolution of the sensor normal force versus the degree of hydration is represented in Table 5.2.5.3. The shear stress at the sensor-concrete interface, obtained by simulation is zero. This means that the sensor normal force is transmitted to the concrete by means of the anchor pieces. Only when the compressive strength at the anchor piece-concrete interface is achieved, the frictional (shear) stresses at the interface will be generated. Thus, we can distinguish four stages of stress generation at the sensor-concrete and the anchor piece-concrete interfaces, depending on the magnitude of the normal force generated in the sensor. Those stages are schematically represented in Figure 5.2.5.6.

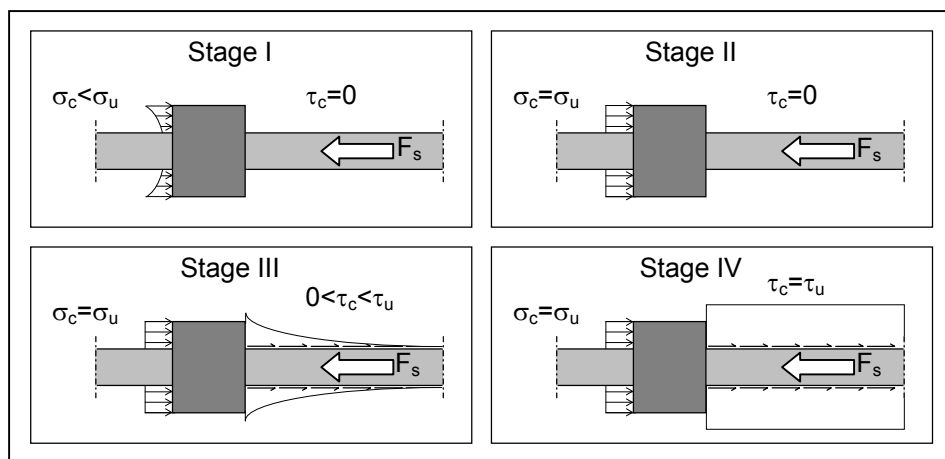


Figure 5.2.5.6: Stages in transfer of sensor normal force to the concrete

In Figure 5.2.5.6 σ_c and τ_c denote normal and shear stress in the concrete, σ_u and τ_u normal and shear strength of concrete and F_s is normal force in the sensor.

The normal and shear stresses in concrete are limited by compressive strength σ_u and shear strength τ_u . Hence, in order to guarantee the transfer of the normal sensor force to the concrete, the following inequality must be satisfied:

$$F_{s,max} < \sigma_u \cdot A_{int} + \tau_u \cdot O_s \cdot l_s / 2, \quad (5.2.5.3)$$

Where:

A_{int} - surface of anchor piece-concrete interface

O_s - circumference of the sensor plastic tube,

$l_s/2$ - half of the active zone length.

Maximal compressive stress in concrete appears at the contact interface between the sensor and the anchor pieces. Results obtained by FEM modelling are not easy to use because of anchor piece influence. For this reason the mean stress is calculated on the anchor piece-concrete interface using the following equation:

$$\sigma_{c,m} = \frac{F_c}{A_{int}}, \quad (5.2.5.4)$$

where:

$\sigma_{c,m}$ - mean normal stress on anchor piece-concrete interface (see Figure 5.2.5.6, Stage I),

F_s - the normal force in the sensor,

A_{int} - surface of anchor piece-concrete interface the surface of interface.

The stress, obtained as shown previously, is an overestimated approximation since the force generated in the passive zone of sensor and the lateral friction force on the anchor piece are neglected. The calculated mean stress is presented in Table 5.2.5.3.

α_h	<i>0.01</i>	<i>0.05</i>	<i>0.1</i>	<i>0.5</i>	<i>1</i>
Normal force in sensor [N/°C] (2D modelling)	2.862	2.923	2.964	3.046	3.064
Normal force in sensor [N/°C] (3D modelling)	2.884	2.922	2.958	3.050	3.073
Mean compressive stress on anchor piece [KPa/°C]	10.93	11.08	11.23	11.56	11.64

Table 5.2.5.3: Efforts in the sensor and the concrete according to numerical modelling

If the compressive strength is achieved frictional stress is activated. This generates the shear stress in the concrete. The magnitude of the frictional stress depends on the length of the sensor (see expression 5.2.5.3). In order to estimate the rate of this stress produced by a temperature variation, a minimal length of 20 cm is used. In this way the maximal average value of frictional stress is:

$$\tau_c = \frac{F_{s,\max}}{O_s \cdot l_s / 2} = 1.315 \text{ KPa} / ^\circ\text{C}, \quad (5.2.5.5)$$

This value of frictional stress provokes the same value of shear stress in the concrete, and according to experiments (see Figure 3.9.1) it is significantly lower than the shear strength of the very early age concrete (10 - 50 times for $\alpha_h=0.01$, depending of water-cement ratio).

We note that for a degree of hydration $\alpha_h=0.01$ and temperature change of 1°C the average compressive stress does not exceed the strength of the cement paste, according to the experiments (see Figure 3.9.2). Moreover, if the temperature change is greater than 1°C , the sensor normal force will be transferred to the concrete by means of friction. The transfer by friction is sufficient to transmit the sensor normal force to concrete even for $\alpha_h < 0.01$, and the capacity of the transfer by friction is in full measure to transmit the force even if the sensor is fabricated without anchor pieces. This validates results presented in the previous subsection (Transfer of deformation from concrete to sensor).

Strain field perturbation

The stiffness and the strength of concrete increase with ageing. In consequence, the sensor perturbs the strain field in the concrete for low values of degree of hydration more than for the high ones. For this reason we analyse here only the strain field perturbation for value of degree of hydration $\alpha_h=0.01$.

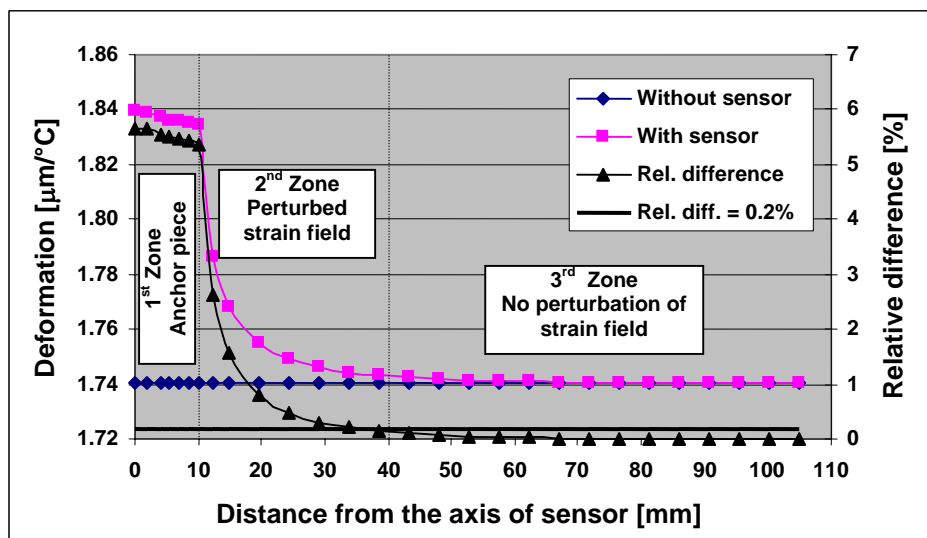


Figure 5.2.5.7: Perturbation of strain field of concrete caused by interaction with sensor, $\alpha_h=0.01$

Vertical displacements in the plain that is at the level of lower part of anchor piece (section A-A in Figure 5.2.4.1) are calculated and represented in Figure 5.2.5.7 for the 3D modelling. The displacement in cases with sensor, without sensor and their relative difference are also shown in the figure.

Three zones are distinguished. The first one includes the displacement of points of the anchor piece. The second zone is limited by anchor piece on one side and by the relative difference of 0.2% on the other side. The value of 0.2 is chosen because it corresponds to the precision of

the SOFO system. Finally the third zone is extended from the end of the second zone to the limit of the specimen.

The zone in which the strain field is perturbed is in fact the second zone. In terms of measurement precision it is not recommended to put another sensor in this zone (limit of 0.2% is chosen). This zone is, however, narrow it takes 40 mm, measured from the axis of the sensor. In reality this zone is even narrower because of viscous properties of very early age concrete.

5.2.6 Summary

Numerical modelling shows that the Standard Sensor is an appropriate device for deformation measurement of concrete at early and very early age. The difference between measurement and real deformation of concrete is estimated as lower than the resolution of the monitoring system, and decreases with concrete ageing. The perturbation zone of the concrete's strain field caused by the interaction with a sensor is less than 40 mm. The recommended distance between the axes of two sensors is, therefore, 5 cm. The stresses generated by sensor-concrete interaction do not exceed the strength of concrete at early and very early age. Hence there are no additional cracks generated by the interaction.

5.3. Experimental estimation of sensor-concrete interaction

5.3.1 Introduction

The numerical modelling, previously presented, confirm the ability of the Standard Sensor to measure the very early age deformation of concrete. Assumptions that simplify modelling have been adopted. The best way to control that they do not lead to inaccurate results is to perform the experiments. In this chapter the influences of rebars, mutual influence of two near sensors and influence of anchor pieces diameter to a measurement have been tested. These tests allow for indirect conclusions concerning the transfer of deformation from the very early age concrete to the sensor.

All tests were performed at the IMAC laboratory. Several concrete specimens were prepared and equipped with Standard Sensors also made at IMAC laboratory. To decrease the costs of tests, the sensors were made without the integrated coupler (see Figure 2.3.1), i.e. the coupler was installed externally, thus the passive zone between the active zone and coupler was approximately 20 to 50 cm long. In both cases, the handling of the passive zone after the pouring of concrete affected the measurement and the resolution is decreased to 5-10 μm instead of 2 μm . In this chapter we present only the results of measurements which were affected neither by handling of passive zone nor by other disturbing effects.

Each experiment concerns at least two of above cited influences: influences of rebars, mutual influence of two near sensors and influence of anchor pieces diameter to a measurement. Therefore, the tests are presented first, in their integral version. Thereafter, results concerning each of the influences are discussed separately.

5.3.2 Laboratory tests

Four tests were carried out. They are named P4, P5, Ex1 and Ex2. Standard Sensors with different lengths of active zone and different diameters of anchor pieces are fabricated and employed in tests. Only the sensors that functioned correctly are presented.

Tests P4 and P5

The dimensions of cross-section and concrete composition of specimens P4 and P5 are identical thus they are simultaneously presented in this subsection. The only difference is in initial temperature of specimens, which is 18°C for the specimen P4 and 5°C in case of specimen P5.

The concrete contained 350 kg/m³ of cement CEM II/A-L 32.5, aggregate 0-32mm and 1.2% plasticiser. The water-cement ratio was 0.48. The specimens were hybrid concrete-steel beams. Only the concrete part is presented in this subsection. The cross-section of concrete part of the specimens P4 and P5 is shown in Figure 5.3.2.1.

Two sensors, P41 and P42, with the active zone of 1m long were installed in the workform as presented in Figure 5.3.2.1. The other two sensors, P51 and P52, with an active zone of 1.5 m long, were installed in the workform of the specimen P5 (see also Figure 5.3.2.1). Thermocouple of type "K" was attached in the middle of sensors of specimen P5. Monitoring of the early age deformation of concrete was carried out during the first 150 hours in both cases. Thermoinsulating mats protected the specimens during testing.

To simplify this presentation all sensors are presented using the same image in Figure 5.3.2.1, but we note that they are embedded in two different specimens.

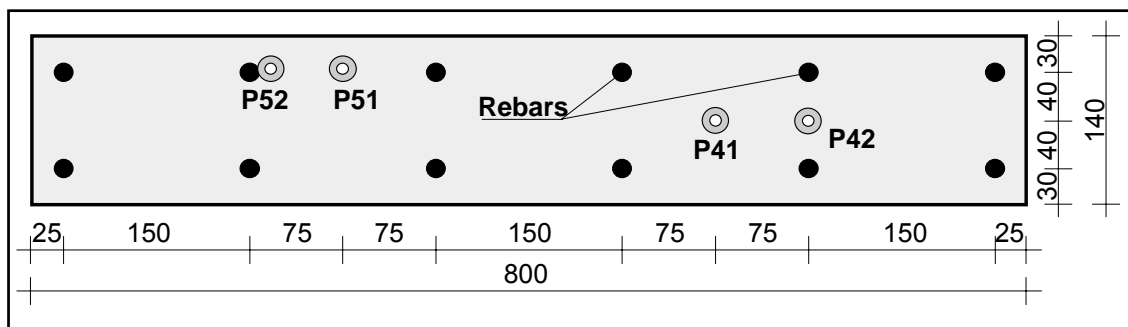


Figure 5.3.2.1: Cross section of specimens P4 and P5 and position of sensors P41, P42, P51 and P52

To estimate the influence of rebars the sensor P42 was placed between two rebars. The sensor P41 was placed in the middle of the concrete. It is assumed that the rebars do not have any influence to this sensor (min. distance from sensor to armature is higher than triple diameter of the biggest aggregate). Sensor P51 was placed between the rebars more distant than in case of sensor P41. Sensor P52 was attached to the reinforcement bar using plastic bands. The results of the measurements are presented in Figures 5.3.2.2-5. The deformation evolution of specimen P4, measured by sensors P41 and P42 during 150 hours, is presented in Figure 5.3.2.2. The difference between P41 and P42 during the first 24h is presented in Figure

5.3.2.3. The same types of diagrams as those used for specimen P5 are presented in Figures 5.3.2.4 (deformation evolution measured by sensors P51 and P52) and 5.3.2.5 (difference between measurements P51 and P52).

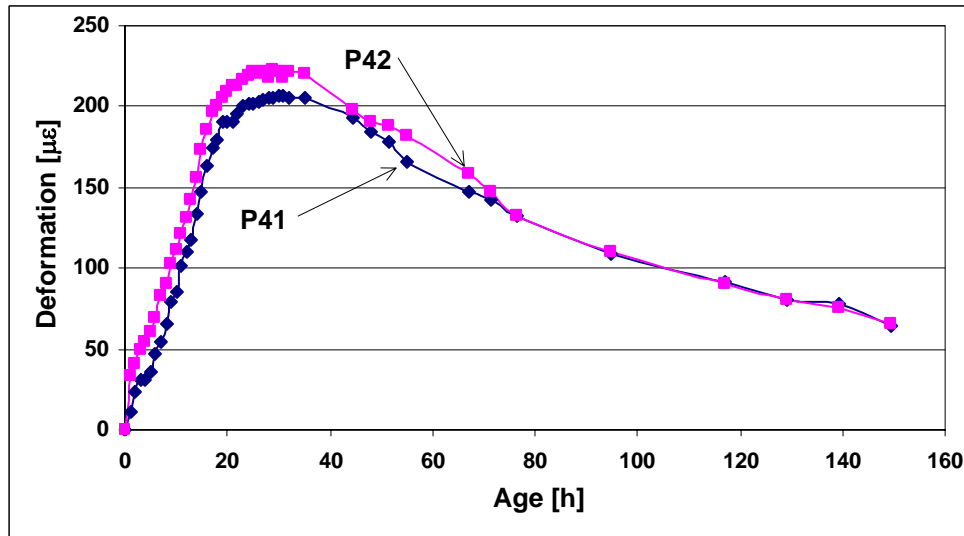


Figure 5.3.2.2: Deformation evolution of specimen P4 measured by sensors P41 and P42

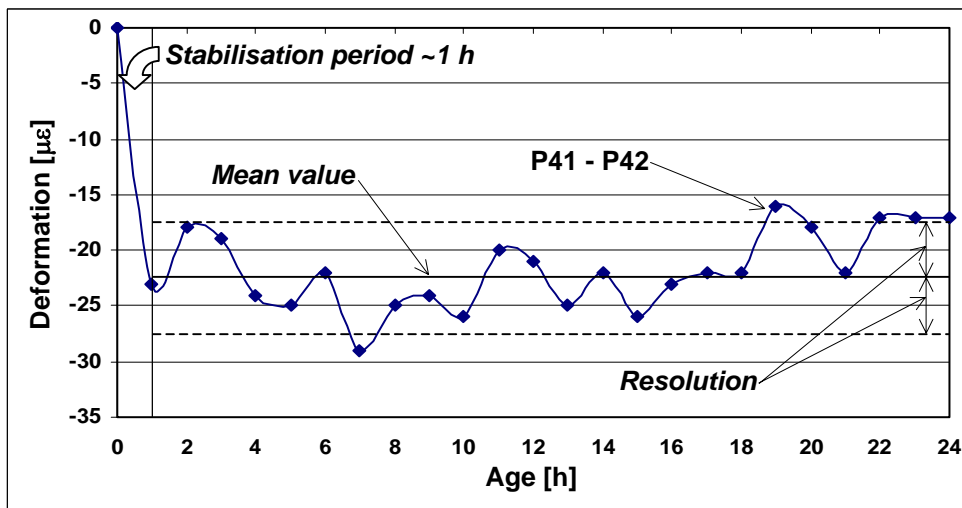


Figure 5.3.2.3: Difference between measurement of sensors P41 and P42 (P41 - P42)

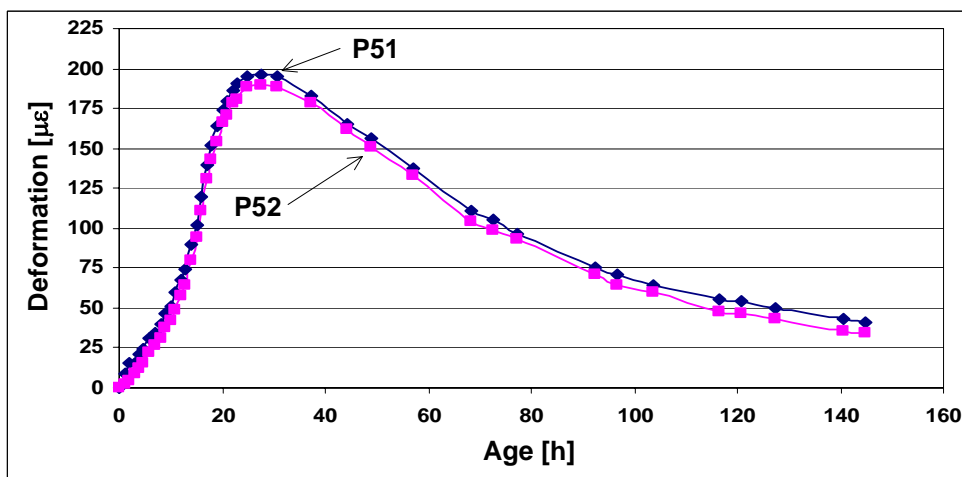


Figure 5.3.2.4: Deformation evolution of specimen P5 measured by sensors P5-1 and P5-2

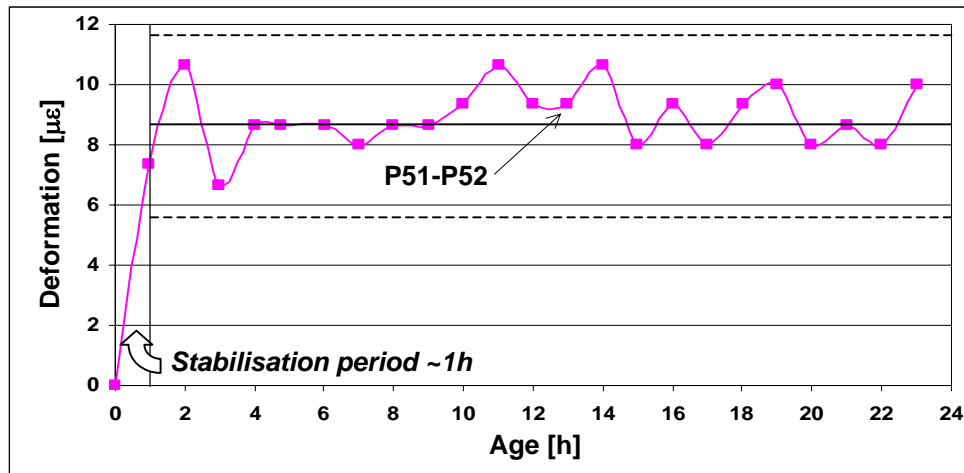


Figure 5.3.2.5: Difference between measurement of sensors P5-1 and P5-2 ($P5-1 - P5-2$)

Tests Ex1 and Ex2

As in the case of tests P4 and P5, test Ex1 and Ex2 were realised using specimens (slabs) with identical dimensions and concrete composition. The concrete contains 400 kg/m^3 of cement CEM I 42.5, water-cement ratio of 0.48, aggregate 0-32 mm, without additives.

Six 1.5 m long sensors were fabricated for this test: four Standard Sensors, Ex11, Ex12, Ex13 and Ex14, and two sensors, Pc6 and Pc8, with anchor piece diameters of 6 and 8 cm respectively. Note that Standard Sensor anchor pieces had a diameter of 2 cm. The early age monitoring was carried out during 70 hours. Sensors were placed in cross-section of non-reinforced concrete slab as shown in Figure 5.3.2.6.

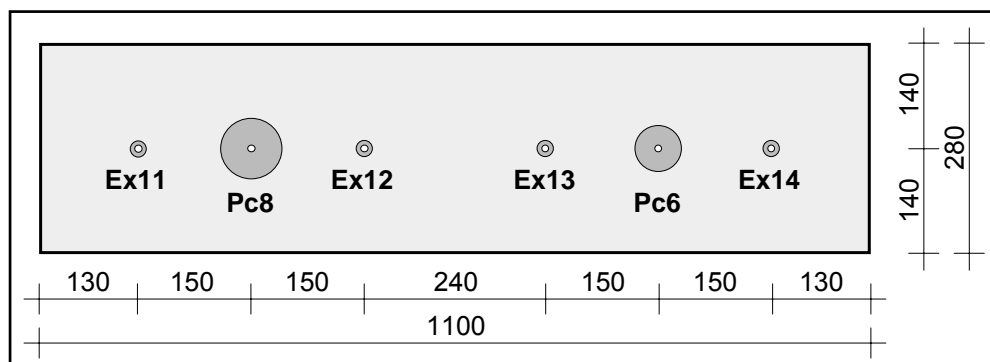


Figure 5.3.2.6: Disposition of sensors in concrete slab used for test Ex1

Results of measurements are presented in Figures 5.3.2.7-9. Deformation evolution measured by all sensors, Ex11-Ex14, Pc6 and Pc8, during 75 hours, is presented in Figure 5.3.2.7. The differences between Ex11, Ex12 and Pc8 sensor measurements during 17h is presented in Figure 5.3.2.8 while the same type of differences for the group of sensors Ex13, Ex14 and Pc6 is presented in Figure 5.3.2.9.

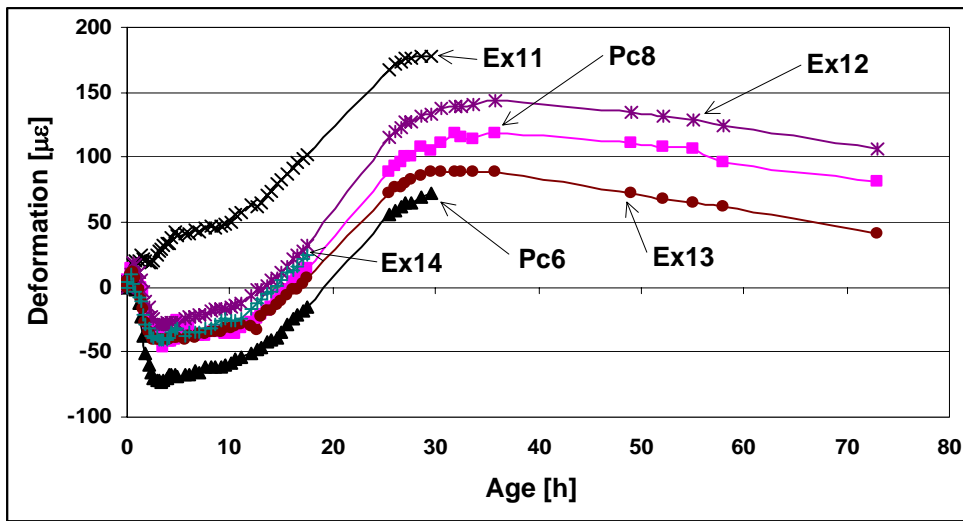


Figure 5.3.2.7: Deformation evolution of specimen Ex1, measured by sensors, Ex11-Ex14, Pc6 and Pc8

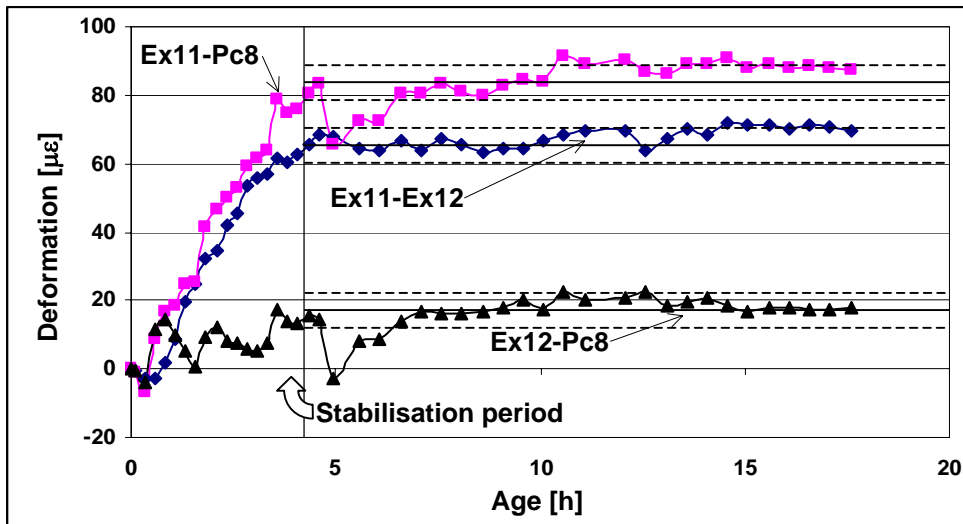


Figure 5.3.2.8: Differences between measurement of sensors Ex11, Ex12 and Pc8

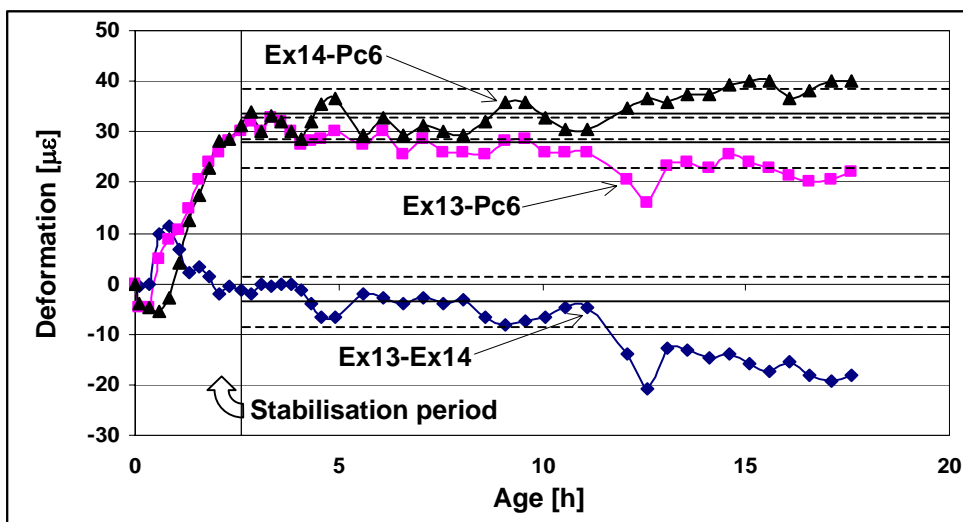


Figure 5.3.2.9: Differences between measurement of sensors Ex13, Ex14 and Pc6

In test Ex2 the 13 following sensors were compared:

- five 1.5 m long Standard Sensors, S1, S2, S3, S4 and S5
- two 1 m long sensors M1 and M2
- two 0.5 m long Standard Sensors D1 and D2
- two 1.5 m long sensors with the anchor piece diameter of 10 cm, P1 and P2
- two 1.5 m long sensors rigidified with still bars (d=2mm), R1 and R2

The sensors are placed in the concrete slab as presented in Figure 5.3.2.10. A thermocouple of type "K" was attached to the middle of each sensor (ts1, ts2 etc. see Figure 5.3.2.10). The early age monitoring was carried out during 120 hours. Results obtained by sensors reinforced with still bars were not of interest in this research, hence they are not presented.

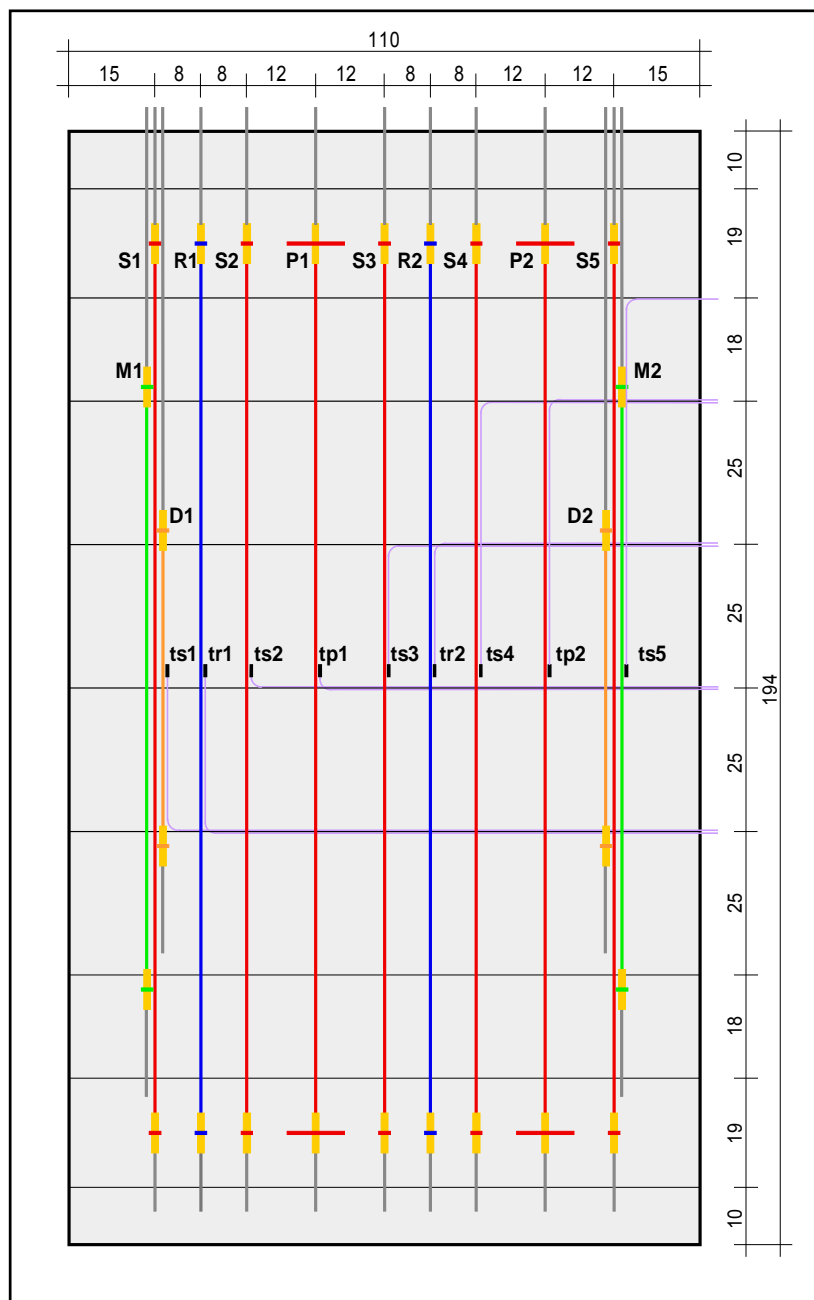


Figure 5.3.2.10: Vertical view to sensor position in concrete slab

Results of measurements are presented in Figures 5.3.2.11-15. Deformation evolution of specimen Ex2 measured by sensors S2, S3 and P1, during 115 hours after pouring, is presented in Figure 5.3.2.11 and deformation evolution measured by sensors S4, P2, S5, M2 and D2 in Figure 5.3.2.12.

The temperatures of upper and bottom surface of the specimen as well as the temperature of at level of sensor S3 are presented in Figure 5.3.2.13. Temperatures of other sensors are in limits of upper and bottom temperatures.

The differences between S5, M2 and D2 sensor measurements during the first 20 hours are presented in Figure 5.3.2.14. The differences between S2, S3 and P1 sensor measurements during the first 24 hours are presented in Figure 5.3.2.15. Finally the differences between S4, S5 and P2 sensor measurements during the first 20 hours are presented in Figure 5.3.2.16.

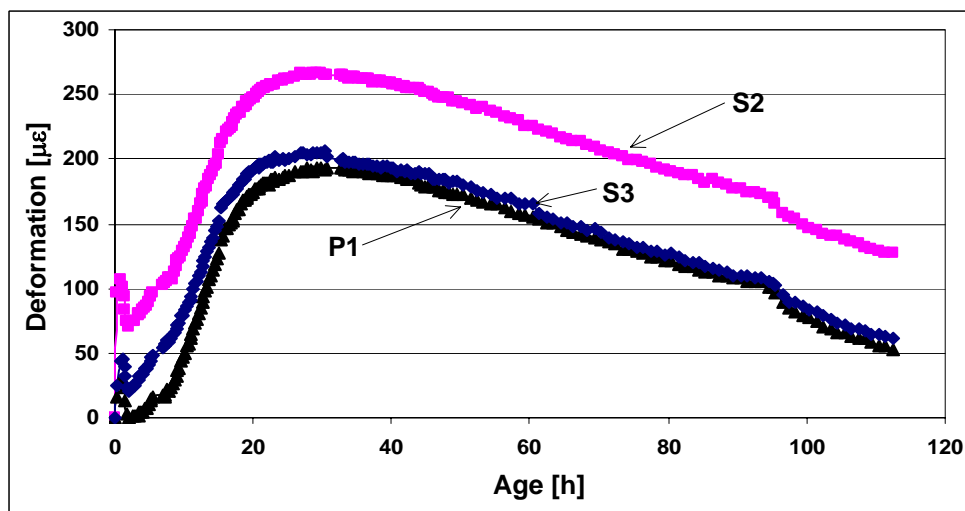


Figure 5.3.2.11: Deformation evolution of specimen Ex2 measured by sensors S2, S3 and P1

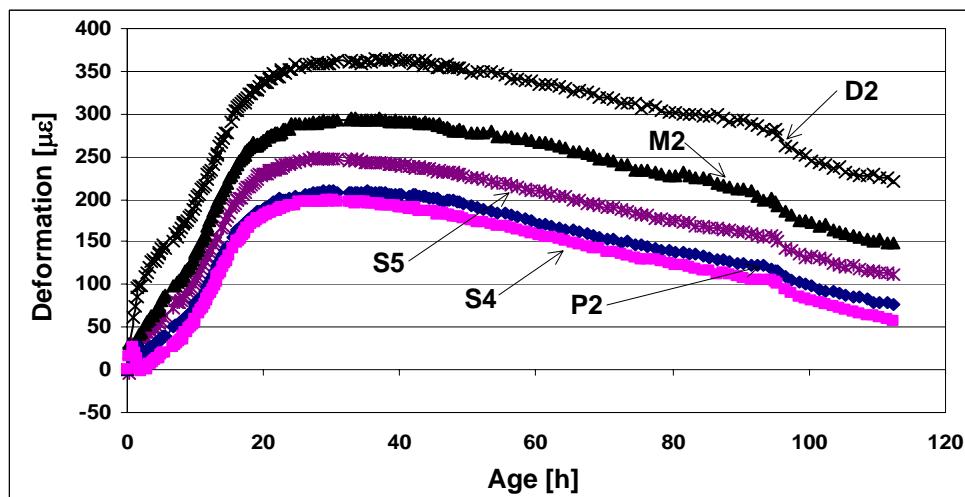


Figure 5.3.2.12: Deformation of specimen Ex2 measured by sensors S4, S5, P2, M2 and D2

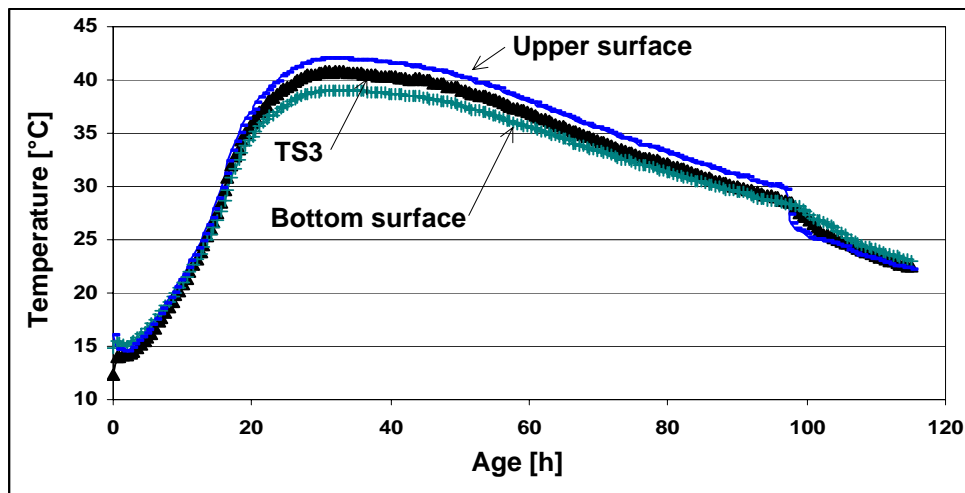


Figure 5.3.2.13: Temperature of specimen Ex2 measured by thermocouples at upper and bottom surface and by thermocouple TS3

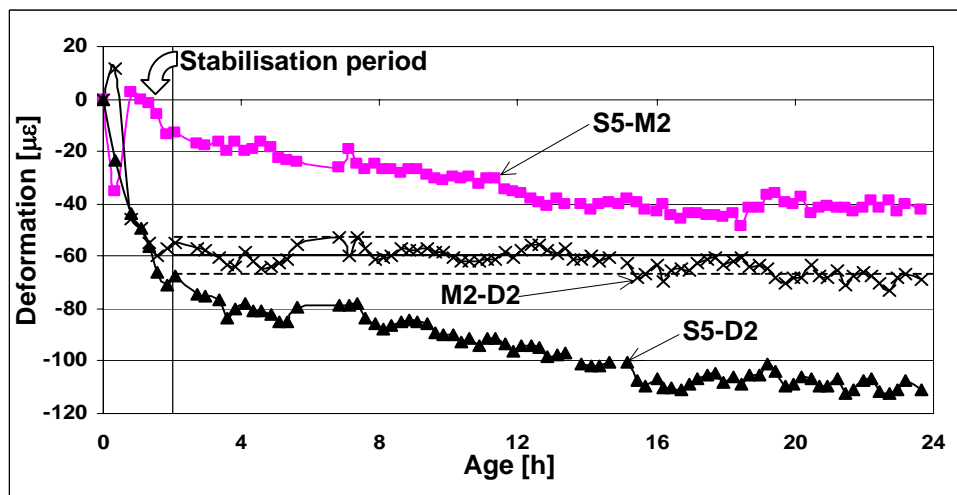


Figure 5.3.2.14: Differences between measurement of sensors S5, M2 and D2

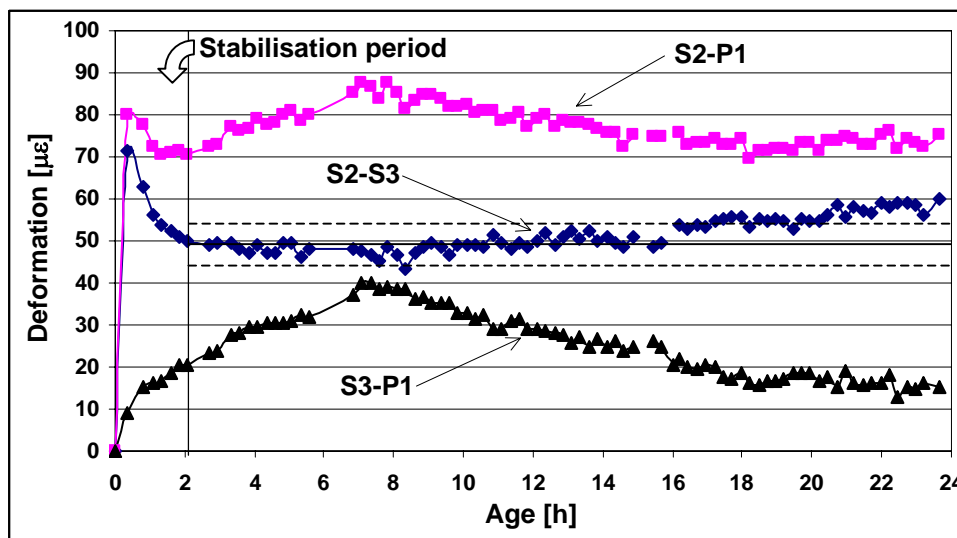


Figure 5.3.2.15: Differences between measurement of sensors S2, S3 and P1

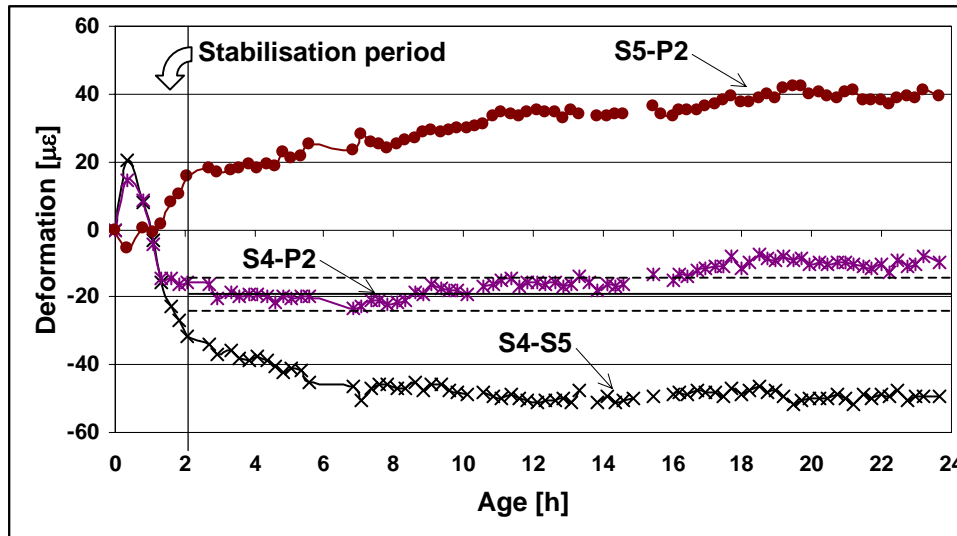


Figure 5.3.2.16: Differences between measurement of sensors S4, S5 and P2

General remarks

Only results, which were considered as to be accurate and interesting for this chapter, were presented. To understand better Figures 5.3.2.2-16 we give some general clarifications.

The above-presented measurements were taken 0 to 2 hours after the pouring of concrete. Therefore, the very early deformation during the stabilisation period of concrete is included in these measurements (see Section 3.9 and Figure 3.9.5). Since the deformation measured during this period is generated by accidental movement of aggregate grains (segregation) and water it cannot be considered as reliable. **Hence, the analysis of very early age deformation concrete must start after the period of stabilisation is finished.**

The duration of the stabilisation period depends mainly on the water-cement ratio, grain size composition, and additives (plasticisers). It rarely exceeds 2 to 4 hours and it is easy to detect using the Standard Sensor. During this period the measurements are chaotic and often elevated, if compared to measurements taken following the stabilisation period (e.g. see Figure 5.3.2.11). Two sensors, placed one close to the other start to measure the same of type deformation when the stabilisation period is finished (e.g. see Figure 5.3.2.14). The stabilisation period of the same concrete element can vary in different zones of the element (compare Figures 5.3.2.8 and 5.3.2.9) due to different times of pouring or external influences.

The stabilisation period is highlighted on each above presented figure representing deformation measurements. To accentuate the difference between diagrams that include and exclude the stabilisation period, the measurements shown in Figure 5.3.2.12 are represented one more time in Figure 5.3.2.17, this time excluding the stabilisation period.

In all experiments the measurements of the specimens were compared. Often the difference between measurements was approximately constant, i.e. the difference alternate around certain constant value. The range of alternations is two times higher than resolution of measurements since obtained as difference of two measurements. In order to highlight the constant and alternations, the mean value and the range of resolution are presented in each

diagram containing the differences of measurements. This is highlighted in Figure 5.3.2.3, but omitted in other figures in order to make the presentation of results clearer.

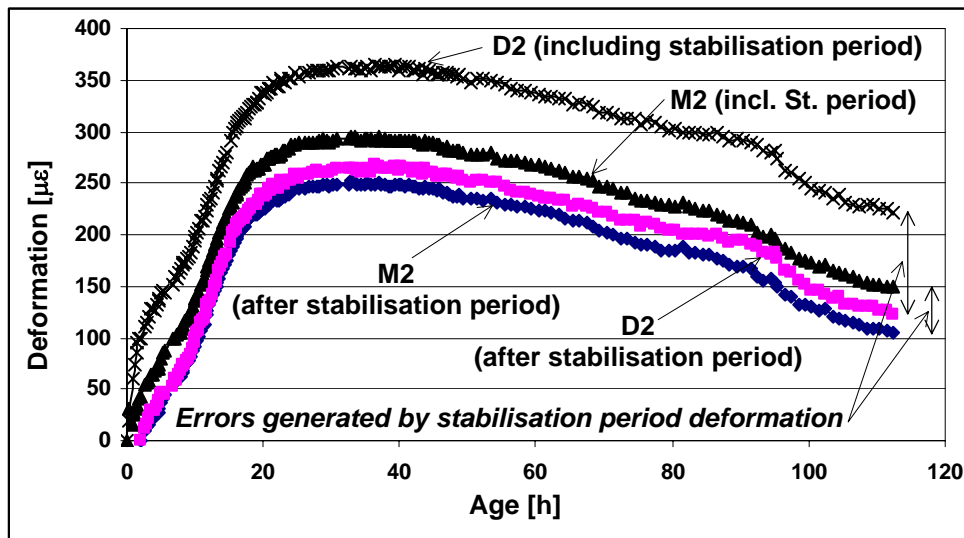


Figure 5.3.2.17: Deformation evolution of specimen Ex2 measured by sensors M2 and D2, with and without stabilisation period of concrete

Thermoisolating mats protected all specimens (P4, P5, Ex1 and Ex2) during testing. They also preserved the evaporation of water from the upper surface of concrete. Thus, drying deformation was avoided. Therefore, the total very early age deformation was composed of unavoidable thermal and autogenous deformation. This deformation was restrained by the workform and by the friction with the basis. Moreover, it was influenced by thermal gradients after the hardening of concrete. All this factors have to be considered during the analysis of results.

Results of the tests (P4, P5, Ex1 and Ex2) were utilised in order to estimate the different influences on a Standard Sensor measurement: the influence of rebars, mutual influence of two near sensors and influence of anchor pieces diameter. Transfer of deformation from the very early age concrete to the sensor was also indirectly estimated.

Results of tests and their consequences are discussed in next paragraphs. The contribution of the tests to each particular topic is schematically presented in Figure 5.3.2.18.

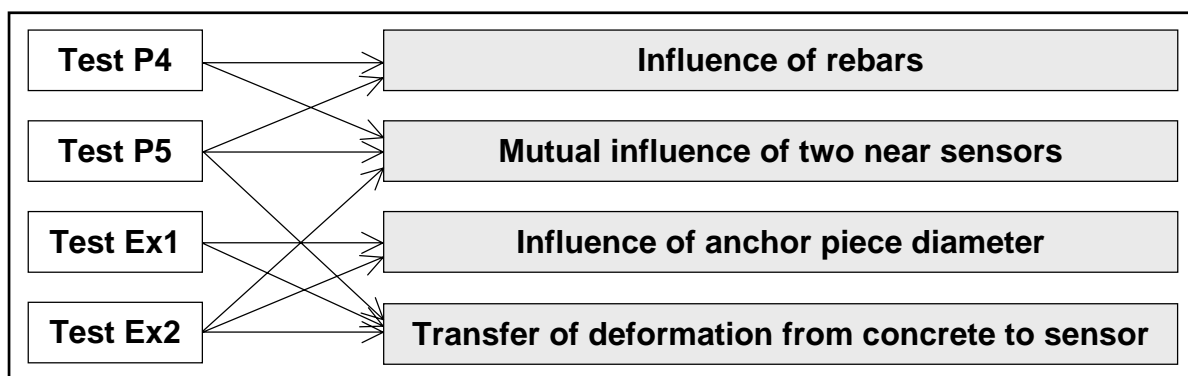


Figure 5.3.2.18: Contribution of tests P4, P5, Ex1 and Ex2 to each particular topic

5.3.3 Results and discussion

Influence of rebars to Standard Sensor measurement

Tests P4 and P5 evaluated the influence of rebars on sensor functioning during the very early age of concrete. The sensors employed during those tests were classified in three categories. The first category was the sensor considered as distant from the rebars and therefore, not influenced by them. The minimal distance of the first category sensors to the nearest rebar was bigger than $3d$, where d represents the maximal grain diameter of utilised aggregate. The sensor P41 was placed in the first category. The second category contained the sensors whose distance from rebars was lesser than $3d$, but were not placed next to rebars. The sensors P42 and P51 were arranged in the second category. Third category concerned the sensors which were placed next to a rebar, or attached to it. The sensor P52 was classified in third category.

The influence of rebars was estimated in two steps. The first step concerned the comparison between the first and the second category sensors (P41 and P42 respectively). In the second step the second category sensor (P51) was compared to the third category sensor (P52).

The first step comparison was given in Figure 5.3.2.3. The difference between the measurement taken by sensors P41 and P42 becomes constant after the stabilisation period (~1 hours) and remains approximately constant for 18 hours. Afterwards it slightly increases. We note that after 18 hours the concrete is certainly hardened and the very early age are finished.

The sensors P41 and P42 were placed at the same level in the concrete section. Therefore, it is assumed that they were subjected to the same surrounding conditions (see Figure 5.3.2.1) and than the very early age deformations of concrete were equal at this two points. Since the difference between compared sensors is approximately constant during the very early age, we conclude that the sensors measured approximately equal deformations and that the sensor of the second category was not influenced by rebars during the very early age. After the concrete was hardened, the deformation was additionally restrained by concrete therefore, the sensors measured the deformation of a solid element. Hence, measured deformations were different due to the influence of bending which is consequence of thermal gradient.

The second step comparison is presented in Figure 5.3.2.5. The discussion concerning this comparison is practically identical to the case of the first step.

The first step of comparison indicates that if the first category sensor can be considered as uninfluenced by rebars then the second category sensor can also be considered in the same manner. Also, the second step of comparison indicates that if there is no influence to the second category sensor than there is no influence of rebars to the third category sensor. The final conclusion of this paragraph is that there is no influence of rebars on the sensor. This conclusion is very important since the sensors are usually attached to rebars when employed for in-situ monitoring.

Mutual influence of two near sensors

The minimal recommended distance between two sensor obtained by numerical modelling is 40 mm. In the tests P4 and P5, the distance between Standard Sensors was greater than 40

mm. In Section 5.3.3 it is shown that the rebars do not influence the functioning of sensors. Since a rebar is several orders of magnitude stiffer than a sensor, it is reasonable to conclude that if the sensor is not influenced by the rebar, then it is certainly not influenced by another sensor.

Test Ex2 confirms the previous conclusion. In this test, sensor M1 is installed next to sensor S1, and sensors D2 and M2 are installed next to sensor S5 (see Figure 5.3.2.10). Sensors D2 and M2 are exposed to practically identical surrounding conditions and measure the same deformation after the stabilisation period (the difference is constant after 2 hours). The difference between other compared sensors (D2 and S5, and M2 and S5) shows a decreasing tendency probably due to different surrounding conditions: S5 is placed in the zone more influenced by workform restraining. This sensors behaviour together with the conclusion derived from tests P4 and P5, confirms the hypothesis that there is no mutual influence of two near sensors even if they are less than 4 cm away from each other.

Influence of anchor piece diameter

The influence of the anchor piece diameter was estimated in tests Ex1 and Ex2. These tests were performed in order to determine whether the sensor with bigger anchor pieces was more sensitive than the Standard Sensor, since the contact surface with concrete is larger. The sensors with anchor piece diameter of 6, 8 and 10 cm were tested.

Four groups of three sensors were observed (see Figures 5.3.2.6 and 5.3.2.10). Each group consisted of two Standard Sensors and one sensor with the anchor piece of diameter bigger than the standard diameter of the anchor pieces (2 cm). The sensor with bigger anchor pieces was placed between two Standard Sensors of the same group. Sensor measurements were compared separately for each group.

The first group consists of sensors Ex11, E12 and Pc8 (diameter of anchor pieces of 8 cm). The differences between measurements carried out by sensors of the first group are constant after the stabilisation period (see Figure 5.3.2.8). This confirms that the anchor piece of 8 cm does not influence the measurement.

The second group consisted of sensors Ex13, E14 and Pc6 (diameter of anchor pieces of 6 cm). These sensors were placed in the same concrete as the sensors of the first group, but they have stabilisation period shorter than the first group sensors. Two reasons this shorter stabilisation period are: The concrete surrounding the second group of sensor was poured before the concrete surrounding the first group of sensors, thus it started to stabilise earlier; The workform of the first group was not waterproof. Thus the water drained away and generated movement in the structure of concrete.

The differences between measurements carried out by sensors of the second group were constant after the stabilisation period (see Figure 5.3.2.8), but after approximately 11 hours there were some deviations. These were certainly generated by hardening of concrete and thermal gradient, as in case of test P4. Anyway, during the very early age there are no significant differences between measurements carried out by Standard Sensors and the sensor with an anchor piece of 6 cm.

The third group consisted of sensors S2, S3 and P1 (anchor pieces diameter of 10 cm, see Figure 5.3.2.10). After the stabilisation period (~2 hours) the sensor P1 behaved differently

from the Standard Sensors (see Figure 5.3.2.15). We suppose that it has probably been locally influenced by the inclining of the anchor piece generated by irregular deforming of different layers of the slab (probably caused by friction of concrete with the basis). Here, the influence of the anchor piece is unfavourable.

The Fourth group consists of sensors S4, S5 and P2 (anchor pieces diameter of 10 cm, see Figure 5.3.2.10). The behaviour of the sensor S5 was different to the behaviour of the other Standard Sensor S4 probably due to its position in the specimen. The difference between the measurement of sensors P2 and S4 is constant after the stabilisation period (~2 hours) and through the very early age (until ~14 hours, see Figure 5.3.2.16). No behaviour of the sensor P2 similar to behaviour of the sensor P1 is observed.

The general conclusion derived from the above presented tests is that the diameter of the anchor pieces does not increase sensitivity of the sensor. Moreover, if the diameter is bigger than 10 cm the effects are unfavourable.

Transfer of deformation from concrete to sensor

The good transfer of deformation from the very early age concrete to the sensor is confirmed indirectly by tests Ex1 and Ex2. The sensors D2 and M2 have different length active zone. Thus, available length for the frictional transfer of deformation (see Figures 5.2.5.6) is different for each sensor. In spite of this difference sensors D2 and M2 measure identical deformation (see Figure 5.3.2.14).

Moreover, in the case of sensors with a larger diameter of the anchor pieces, the contact surface for transfer by normal stresses is increased (see Figures 5.2.5.6). During the very early age the deformation measured using those sensors is identical to deformation measured using Standard Sensors. Hence, the anchor pieces with a diameter of 2cm provide sufficient contact with the interface.

Test P5 also indirectly confirmed a good transfer of deformation from concrete to the Standard Sensor. Sensor P52 was attached to the rebar using plastic bands. It measures deformations identical to those measured by sensor P51 which was not attached to the rebar.

Analyses presented in this section confirm that the transfer of deformation from the very early age concrete to the Standard Sensor is good.

5.3.4 Summary

Four laboratory tests were performed in order to test the different effects on the Standard Sensor measurement during the very early age of concrete. Influence of rebars, mutual interaction of two near sensors and anchor piece size were estimated. Obtained results show that all these influences do not affect the functioning of the sensor. Moreover, they confirm good transfer of deformation from the very early age concrete to the sensor which is in accordance with results provided by numerical modelling.

Segregation and stabilisation of concrete affect measurements carried out by the Standard Sensor. Therefore, only the measurements following the stabilisation period can be

considered as valid. No particular laboratory conditions were required during the tests, hence the Standard Sensor can be applied for in-situ very early age monitoring without restriction.

5.4 Other systems applied for in-situ monitoring of concrete at very early age

Very early age deformation is difficult to measure because of the changing viscosity and low stiffness of non-hardened concrete. A sensor employed for such kind of measurement has to be internal, embedded into the fresh concrete. Thus, external sensors such as classical strain gauges, omega gages, extensometers or LVDTs can not be applied in this case.

Even if the very early age deformation is difficult to measure, researchers in various laboratories have measured very early age deformation, more or less successfully[5, 6, 8]. However, in-situ application remains rare or limited.

In this Section requirements for a very early age deformation monitoring system are firstly discussed, and thereafter four different monitoring system utilised for very early age monitoring are presented.

The requirements for very early age deformation monitoring system are the following:

1. A sensor must be embedded into the fresh concrete.
2. The stiffness of sensor must be several orders of magnitude lower than that of the very early age concrete in order to avoid any perturbation of the concrete strain field and to guarantee good transfer of deformation from concrete to the sensor.
3. Thermal influences on the sensor itself must be cancelled. It is recommended to use self-compensated sensors.
4. Measurement basis (length) of sensor has to be sufficiently long (at least 3 times longer than the biggest diameter of the aggregate) in order to avoid local influences of aggregate, cracks and imperfections (air pockets etc.).
5. Since the concrete deformation evolves at very early age, it is recommended to use fully independent and automated monitoring systems.

The Standard Sensor as well as the SOFO system responds well to the above requirements. In the following paragraphs we present other systems applied in very early age concrete.

Vibrating wires are cheap and practical mean for deformation monitoring. However the application on very early age concrete has been unsuccessful. Two reasons are: The sensor is very stiff, and it is influenced by temperature changes.

The method developed by [8] is interesting, but measures the early age deformation only when concrete is hardened. The idea of this method is to fix strain gage to metallic beam, protect them and embed into the fresh concrete. This sensor is very stiff and does not guarantee good transfer of deformation from the very early age concrete to the sensor.

Fabry-Perot optical sensors [6,7] are more suitable for very early age deformation monitoring. However, they cannot fully self-compensate with respect to thermal influences and their

measurement basis is short. Therefore, utilisation of Fabry-Perot sensors remains limited to characterisation of mortars.

The Bragg grating optical sensor [9] has been successfully applied on very early age concrete structures. Although no complete fully automated monitoring system is still developed for in situ application, we believe it to be very promising.

5.5 Concluding remarks

Interaction of the Standard Sensor and the concrete at early and very early age has been numerically and experimentally tested. The results are presented in this chapter. Both, numerical and experimental research, have confirmed good transfer of deformation from the very early age concrete to the Standard Sensor. Numerical research supports the utilisation of the Standard Sensor for monitoring of concrete for a degree of hydration higher or equal to 0.01. It corresponds to the age of 2 to 5 hours after concrete mixing (for ordinary concretes). Experimental research has verified these numerical results. It supports the sensor as a means for the very early age concrete monitoring immediately after the end of stabilisation period, 1 to 4 hours after pouring.

Numerical and experimental tests also confirmed that there is no mutual interaction between two near sensors. Moreover experimental research has shown that there is no influence of near reinforcing bars to the sensor. This is very important because, for practical reasons, the simplest way to install the sensor in the structure is to attach it to the rebar before the pouring of concrete.

Important requirement of monitoring system and sensor designed for in-situ deformation monitoring of concrete structures at early and very early age are cited in the Section 5.4. The Standard Sensor responds very well to all those requirements and is, therefore, to be highly recommended.

5.6 References

- [1] Guidom A., *Simulation numérique 3D des comportements des bétons en tant que composites granulaires*, Ph.D. Thesis N°1310, EPFL, Lausanne, Switzerland, 1994
- [2] Zienkiewicz O. C., Taylor R. L., *La méthode des éléments finies: formulation de base et problèmes linéaires*, pp. 620, Afnor, Paris 1991
- [3] Hughes T. J. R., *The finite element method*, Prentice Hall, 1991
- [4] Roelfstra P. E., A numerical approach to investigate the properties of concrete - numerical concrete, Ph.D. Thesis N° 788, EPFL, Lausanne 1989
- [5] Boulay C., Paties C., *Mesure des déformations du béton au jeune âge*, Materials and Structures, vol 26, pp. 307 -311, 1993
- [6] Habel W. R., Jung M., Plohn J., Basedau F., *Non-Reactive Measurement of Mortar Deformation at Very Early Age by Means of Embedded compliant Fiber optic Micro*

Strain Sensors, 12th Engineering Mechanics ASCE Conf. Session Fiber Sensors for Condition Monitoring, La Jolla, CA, USA, 17-20 May 1998

- [7] www.fiso.com
- [8] Lindstedt H., Staffa M., Mesure d'allongements et d'évolution des températures au sein de parois en béton armé, CTM3/99, pp. 2-10, HBM, Darmstadt
- [9] Asnari F., *State-of-the-art in the Applications of Fiber-optic Sensors to Cementous Composites*, Cement and Concrete composites, Vol. 19, pp 3-19, 1997

6 Characterisation of concrete at very early age

6.1 INTRODUCTION

The main conclusion from the previous Chapter is that the Standard Sensor allows the measurement of concrete at very early age. In this Chapter research concerning the characterisation of concrete during the very early age is presented. The tests are carried out in the laboratory and in-situ, using the Standard Sensor.

The characterisation presented in this Chapter is based on deformation monitoring. Therefore the early age total deformation monitoring is presented first. The definition and the methods for measurement of hardening time of concrete are then proposed. Follows the discussion related to the monitoring of the evolution of the TEC and the separation of thermal and autogenous deformation from the total deformation.

During laboratory tests, the cure of specimens is realised without any special attention in order to approximate in-situ conditions.

6.2 MONITORING OF TOTAL EARLY AGE DEFORMATION OF CONCRETE

The total deformation of concrete at early age depends of different factors, such as concrete composition, curing, loads etc. (see Section 3.10), and is composed of different types of deformations such as thermal, autogenous, drying deformation etc. If the evolution of one of parameters varies, the evolution of the total deformation will vary too. It is difficult to separate each particular deformation from the total deformation. Nevertheless, monitoring of the total deformation can give rich information concerning the concrete at early and very early age. Therefore in the next subsections some characteristic cases are presented and discussed.

6.2.1 *Typical deformation of concrete at early and very early age*

Typical total early and very early age deformation is analysed for the concrete element Ex2. Composition of the concrete as well as dimensions of the element are presented in more details in Section 5.3.2. This concrete element was monitored using the Standard Sensors and

a "K" thermocouple. During the monitoring, the concrete element has been thermally and hydro isolated. Therefore two component of total deformation are dominant: thermal and autogenous deformation (see Chapter 3). The total deformation was restrained by the workform and friction with the basis. Evolution of total deformation measured by the sensor S4 as well as temperature evolution is represented in Figure 6.2.1.1. The first twelve hours from Figure 6.2.1.1.(encircled area) are presented in Figure 6.2.1.2.

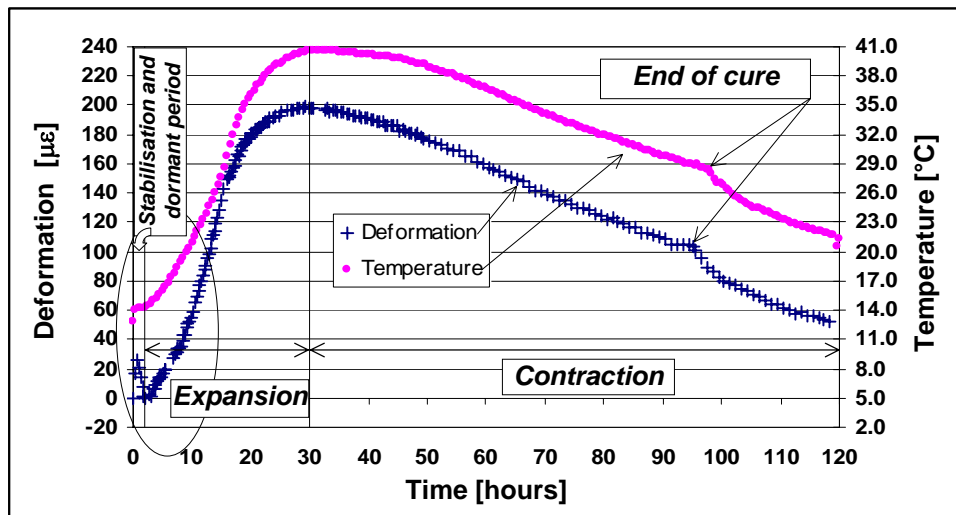


Figure 6.2.1.1: Typical ordinary concrete deformation and temperature evolution curves at early and very early age

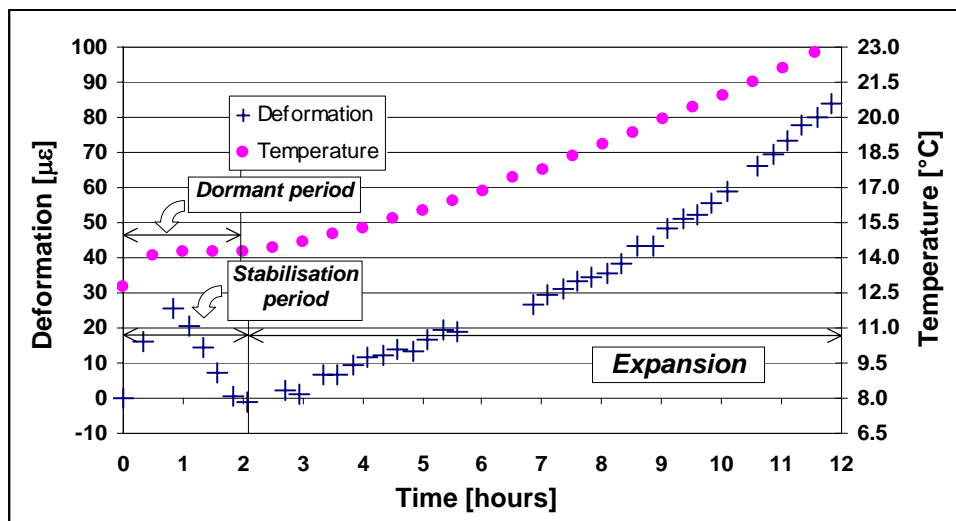


Figure 6.2.1.2: Encircled area from Figure 6.2.1.1 - Deformation and temperature evolution during the first twelve hours in the concrete life

In Figure 6.2.1.1 four periods are distinguished. The first one is the dormant period, the second is the period of stabilisation of the concrete, the third is the expansion period and the fourth is the contraction period.

During the first two hours approximately the temperature of concrete is constant, with exception of the first measurement which corresponds to the initial temperature of concrete.

The hydration process is practically paused, therefore this period corresponds to the dormant period. During the approximately same period, the Standard Sensor has registered important variations of the deformation. Since there are no other sources of deformation (temperature is constant and autogenous deformation is practically equal to zero) this variation is certainly the consequence of the segregation and stabilisation of the concrete. The end of the stabilisation period corresponds to the attenuation of the deformation variations. The end of the stabilisation period can not be strictly defined, since the stabilisation is a continuous process (e.g. in Figure 6.1.2.1, an earlier point could be also chosen to define the end of the stabilisation period). Moreover it is not uniform in the whole volume of the concrete element. However, the standard sensor can give good information related to the end of stabilisation. In Figure 6.2.1.2 the dormant and stabilisation period nearly coincide, but this is not a rule. They could be different, depending on concrete composition, manner of pouring and sensor position in the concrete (see Figures 5.3.2.7, 8 and 9 in Section 5.3.2).

The expansion period corresponds to the period of intense release of hydration heat. The concrete expands due to an increase of temperature. During this period the cement sets and the concrete rapidly hardens. If the concrete is restrained, the stresses start to be generated, especially after hardening.

When the period of intense discharge of hydration heat is finished, concrete cools and as a result of cooling it contracts. Since already hardened, during this period important tensile stresses are generated, and these stresses are often the origin of premature cracking. The Standard Sensor permits to determinate accurately the magnitude of the concrete expansion and contraction.

6.2.2 Monitoring in laboratory conditions

Test on old concrete - new concrete specimen

Test has been realised on a hybrid old concrete-new concrete specimen, named AA3. The geometry of the specimen AA3 is represented in Figure 6.2.2.1.

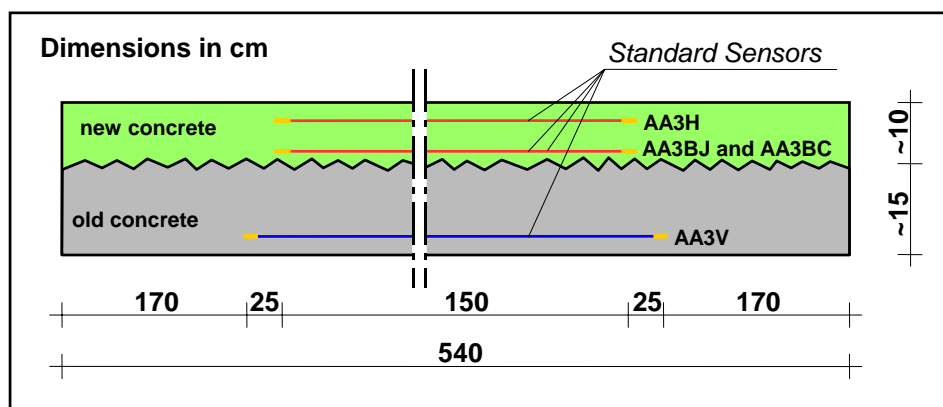


Figure 6.2.2.1: Geometry and sensor emplacement in hybrid old concrete-new concrete specimen AA3

The old concrete layer was poured two months before the new concrete. Its initial thickness was 17cm. In order to increase the interaction between the two concrete layers, its upper surface was treated by hydroblasting two days before the pouring of new concrete.

The new concrete consists of 300kg/m^3 of cement, type CEM I 52.5R, cement water ratio of 0.5 and aggregate from lake of Neuchâtel with maximal diameter of 16 mm. The new concrete is reinforced with bars $6\phi 14$. Two hours after the pouring the new concrete layer was covered for 105 hours with an isolating mat.

The specimen is equipped with thermocouples and standard SOFO sensors. The emplacement, length and names of the sensors are as shown in Figure 6.2.2.1. The sensors AA3BJ and AA3BC are placed at same level, but they are differently attached: the AA3BJ is free while the sensor AA3BC is fixed on the surface of the old concrete by means of iron corners (see also Figure 6.2.2.3). The deformation and the temperature of both layers were monitored during whole life of the specimen. The first four days are represented in Figure 6.2.2.2. During the first two days the deformation is registered every 30 minutes.

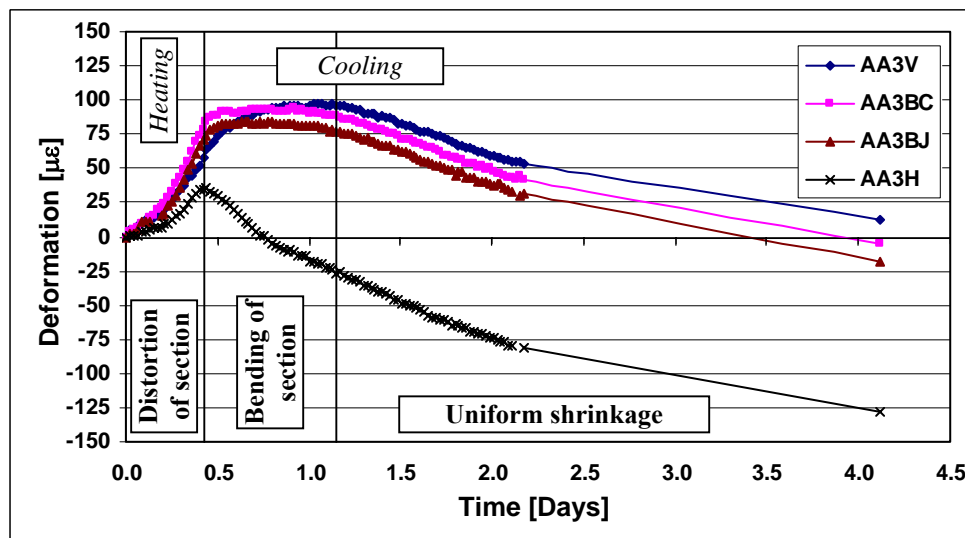


Figure 6.2.2.2: Early and very early deformation of new concrete and deformation of old concrete

Three types of curves are obtained. The first type curve (AA3V) describes the behaviour of the lower surface of the old concrete support.

The curves of second type (AA3BC and AA3BJ) are similar to first one, but there are some differences. They describe the behaviour of the interface where the temperature is the highest during the period of intensive thermal reaction of hydration. Therefore the deformation of the interface is greater than the deformation of the lower surface of the specimen. When the maximal temperature in the new concrete is reached, the deformation of the interface is firstly constant because of very slow cooling and finally the same as the deformation of lower surface of the support.

The third curve (AA3H) describes the deformation of the upper surface of the new concrete layer. This curve is remarkably different from the two previously described. The deformation of the upper surface achieves its maximum simultaneously with the maximal temperature of hydration, and after this maximum it decreases due to cooling and autogenous shrinkage.

Since the old and the new concrete are coupled, the contraction of new concrete generates tensile stresses in the new concrete. This contraction also provokes bending of the old concrete: the upper part of the cross section is compressed and the lower part is tensioned. Thus, the deformation measured by sensor AA3V continues to increase after the achievement of the maximal hydration temperature.

Three periods are distinguished in Figure 6.2.2.2. The first period is the period of intense hydration heat discharging. During this period due to the plastic properties of concrete and due to the non-uniform heating of concrete with respect to the height of the section, a distortion of the cross-section is remarked. The second period is characterised by non-uniform cooling. As a consequence the bending of the cross-section appears. Finally during the third period an uniform contraction is registered as a consequence of the shrinkage of the new concrete and very good interaction between two concretes. These three periods are more clearly presented in Figure 6.2.2.3 that represents the deformation distributed over the cross-section i.e. evolution of the cross-section: the first period is between curves 0 and 2, the second between curves 2 and 3 and the third period between curves 3 and 5.

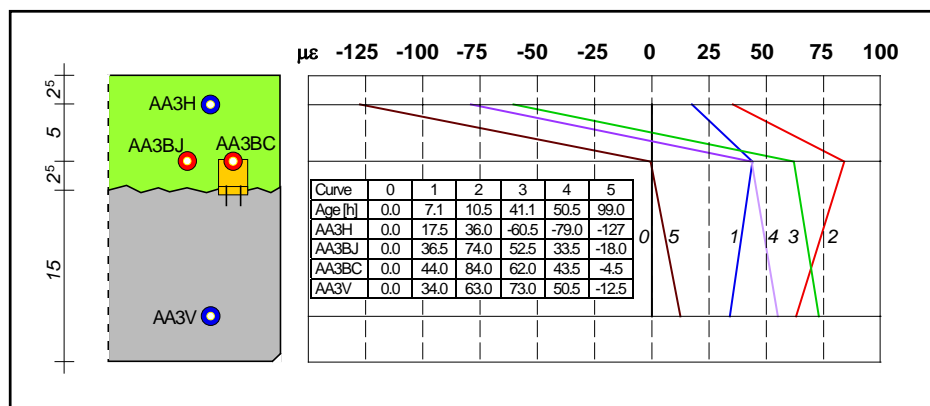


Figure 6.2.2.3: Evolution of the cross-section of the specimen AA3

Using the Standard Sensor the real behaviour of the hybrid specimen is understood. Distortion of the cross-section, evolution and final redistribution of the strain field are monitored and the magnitudes of thermal expansion and total contraction are measured in different zones of the cross-section. These measurement permitted the calibration of numerical FEM simulation of specimens using the software HEAT 6.0 (see Chapter 5) and numerical estimation of different components of total deformation. More details concerning this modelling are presented in [1 and 2].

Tests on steel - concrete specimens

In the previous paragraph we have shown how the early age monitoring helps to understand real behaviour of the structure. Here we compare concretes with different initial temperatures.

The hybrid steel-concrete specimens, called P6 and F2, are analysed. Both specimens are mixed with 350 kg/m^3 of the cement CEM I 52.5, the water cement ratio is of 0.48, granulate with maximal diameter of 32 mm, and 1.2% of plasticiser. These two concretes are different in two details: concrete for the specimen P6 is refrigerated to 5°C using the liquid nitrogen while 50 kg/m^3 of steel fibres DRAMIX is added to the concrete of specimen F2. The dimensions of the fibres are 35 mm of length and 0.35 mm of diameter. Both specimens are

cured in the same conditions after the pouring. Each specimen has the same length of 8.4 m, and the identical dimensions of cross section, as shown in Figure 6.2.2.4.

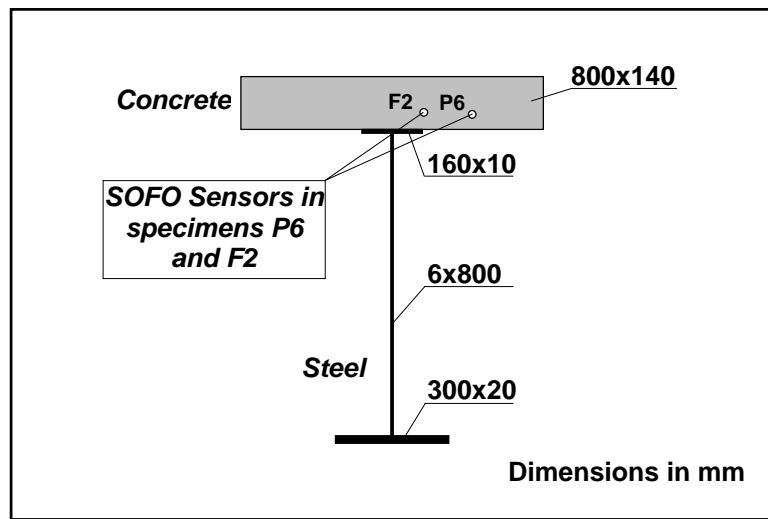


Figure 6.2.2.4: Cross-section of the specimens P5, P6 and F2

The specimens are equipped with thermocouples and Standard Sensors. The sensor emplacement in the cross-section is presented in Figure 6.2.2.4. Both sensors are presented in the same figure in order to facilitate the comparison.

In the longitudinal direction the sensor are centred in the middle of the specimens' spans. During the first two days the measurements of the sensor P6 is registered every 15 minutes and of the sensor F2 every 30 minutes. Afterwards the rhythm of measurement of the sensor F2 is unchanged while the measurements of the sensor P6 are registered less regularly. The monitored deformations of both specimens are presented in Figure 6.2.2.5.

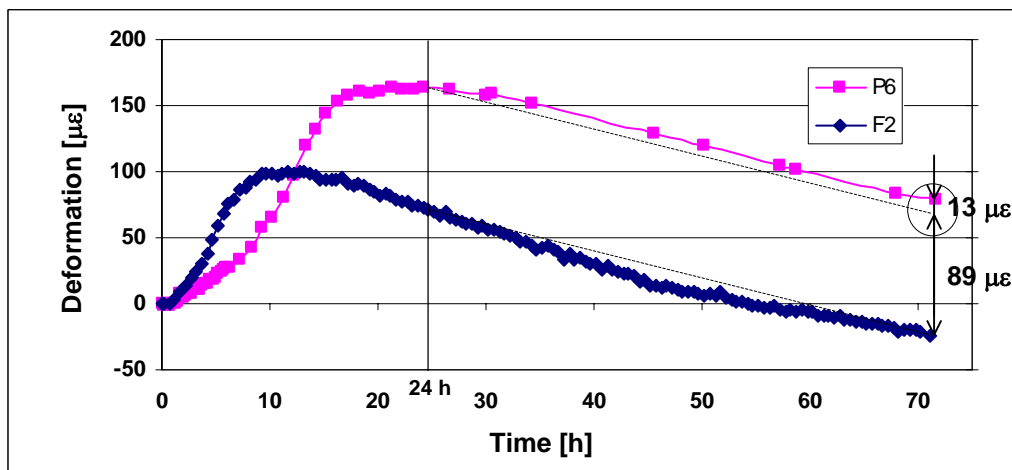


Figure 6.2.2.5: Behaviour of two different concretes cured in the same conditions

Initial, maximal and final (71 hour after the pouring) temperatures of specimens are presented in Table 6.2.2.1. The difference between very early age behaviour of specimens is noticeable in Figure 6.2.2.5. The difference between initial and final temperature is approximately equal

for both specimens (29.5°C for specimen P6 and 26.2°C for specimen F2). However, thermal expansion of the specimen P6 is higher for 75%. Moreover the maximum in expansion of specimen P6 is achieved 8 hours later than for the specimen F2. This difference in behaviour of specimens is consequence of their different initial temperature: the hydration process of refrigerated concrete was slowed down due to low temperature, therefore the period of intense heating was long, and since in this period the TEC of concrete is elevated, the thermal expansion of concrete is higher than in case of non-refrigerated concrete.

<i>Specimen</i>	<i>Initial temperature</i>	<i>Maximal temperature</i>	<i>Final temperature*</i>
P6	6.2	35.7	26.7
F2	26.1	52.3	33.1

* 71 hour after the pouring

Table 6.2.2.1. Initial, maximal and final temperatures of specimens P6 and F2

If we suppose that a monitoring systems using external sensor was applied on the concrete 24 hours after the pouring, then after 71 hours it would register a significantly smaller difference between specimen deformations (13 $\mu\epsilon$ instead 102 $\mu\epsilon$, see encircled area in Figure 6.2.2.5). The error obtained using such way of monitoring is very high (89 $\mu\epsilon$ > 87%) and it does not allow understanding of the different behaviour between the specimens. More details related to the described test are found in [3] and [4].

6.2.3 In-situ monitoring

Cut-and-cover tunnel Champ Baly

The cut-and-cover tunnel of Champ Baly is situated on the motorway A1, connecting Lausanne with Bern, in Switzerland. Construction work began in July 1998 and the end of the concrete pouring phase was in August 1999. The length of the tunnel is 230 m and the volume of used concrete is approximately 6000 m³. The concrete has been poured in twenty-one stages, i.e. nineteen 11.60 m long vaults and two 6 m long portals. The cross-section of the tunnel consists of two reinforced concrete vaults as shown in Figure 6.2.3.1 [5].

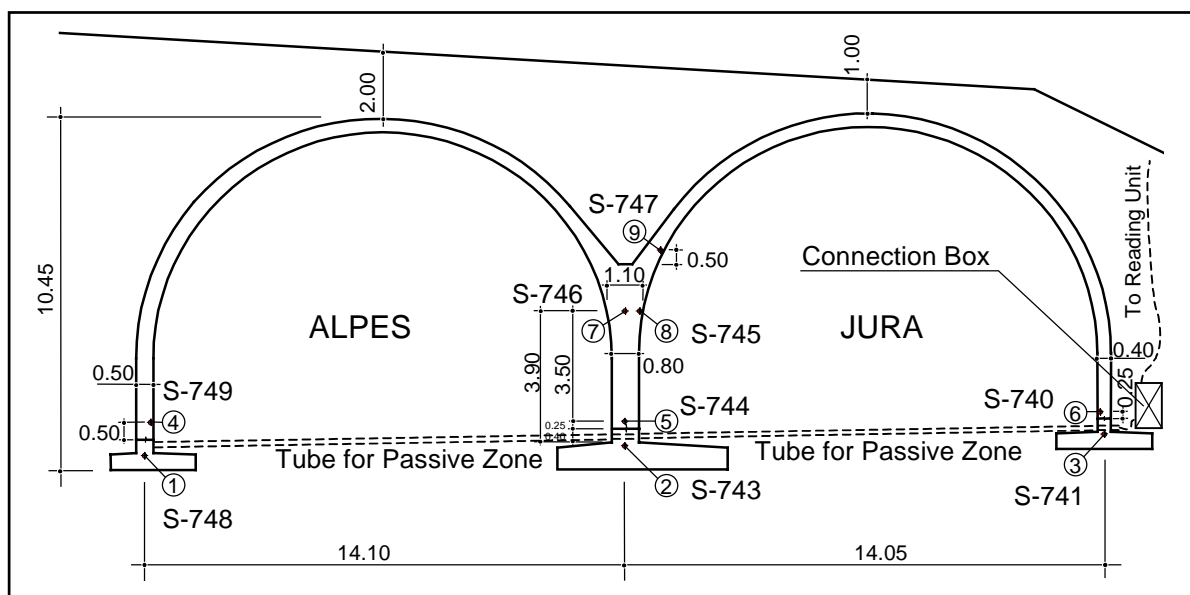


Figure 6.2.3.1: Cross section and sensor equipment of the cut-and cover tunnel Champ Baly [5]

The cross section of the tunnel has been equipped with nine 4 metres long Standard Sensors and nine thermocouples prior to the pouring of concrete, as shown in Figure 6.2.3.1. Each thermocouple is placed side by side to one sensor, which allows measuring the concrete temperature at each sensor location. In Figure 6.2.3.1 the thermocouples are represented by numbers (1, 2, ... 9) and the sensors by "S" followed by their respective serial number (S-740, S-741, etc.).

Sensors S-748, S-743 and S-741 are located in the foundations, which have been poured approximately three months prior to the vaults. The other sensors were mounted on the vault rebars a few days before the casting took place. The passive zones of the sensors are guided through plastic tubes to the connection box (see Figure 6.2.3.1). The reading unit is placed in a small portable chamber some twenty metres away from the tunnel. It is linked to the connection box by means of an optical cable.

The vaults early and very early age deformation was monitored during seven days following concrete pouring. Measurements were recorded automatically every 30 minutes. They are presented in Figure 6.2.3.2.

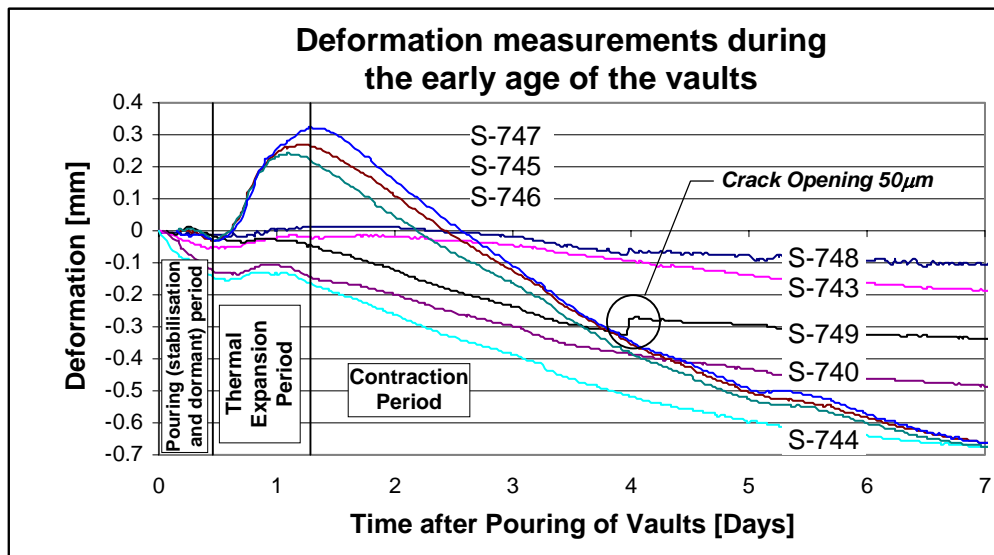


Figure 6.2.3.2: Early and very early age deformation of the tunnel cross-section

Three different periods during the early age deformation are distinguished and separated by lines in Figure 6.2.3.2. The first period corresponds to the pouring period. During this period the concrete is cast with the sensors measuring the corresponding deformation. A relatively small deformation due to the additional load of the fresh vault concrete is noticed with the sensors that measure the deformation of the foundation (S-748 and S-743). The deformation of the foundation is significantly smaller than the deformation measured with the sensors located in the lower part of the vaults (sensors S-749, S-744 and S-740). This is a consequence of the plasticity and rheology of fresh concrete. Finally the sensors that are higher in the vaults (S-746, S-745 and S-747) measured very small deformation due to the reduced load at their locations. Since the setting time is retarded, the new concrete is in a "dormant period" during the pouring period. This fact is also confirmed by the temperature measurements.

The second period in Figure 6.2.3.2 is the thermal expansion period. During this period the hydration process is activated, the temperature increases and induces the deformations too. While the deformation of the foundation is very small, the deformation of the lower parts of vaults is larger and the deformation of the upper parts of the vaults is very important. The smaller deformation of the lower parts of the vaults can be explained by their restraint of the foundations. The upper parts of the vaults are not confined and the concrete in these zones swells significantly. During this period the concrete sets and stresses are generated in the vaults.

During the contraction period the deformation generally decreases due mostly to the thermal contraction of concrete. During this period, a 50 μm wide crack opening was recorded by sensor S-749 and confirmed after visual inspection of the structure. The crack is a consequence of the vault-foundation interaction and the early age deformation provoked by thermal stress.

Different behaviours of the tunnel's different parts can be identified and described by three different types of curves shown in Figure 6. The first type concerns the foundation, the second type the lower parts of the vaults, and the third type the upper parts of the vaults. The deformation curves of the foundation and the lower parts of the vaults after the cooling are parallel and point to monolithic behaviour of the foundations and the vaults. The deformation curve of the upper parts of the vaults is not parallel to the other curves and indicate that the cross-section does not remain plane during early age deformations. Since the bonding between the vaults and the foundation can be assumed to be good, stresses are therefore introduced into the vaults. As a consequence, cracking of concrete may appear.

6.2.4 Summary

Diagrams that present real early and very early age deformation of concrete are presented in this Section. Tests are carried out in the laboratory and in-situ. Four characteristic periods are distinguished in diagrams: the dormant period, the stabilisation period, the thermal expansion period and the contraction period.

Thermal expansion and contraction is measured in laboratory and in-situ. Distortion of the cross section of structures as well as real mean strain distribution in structural elements are identified and quantified. These results are confirmed as essential for the calibration of numerical models.

The influence of elevated TEC during the very early age is confirmed in tests. Different behaviour of two equal concretes with different initial temperatures has proven this important characteristic of concrete at very early age. High difference between final thermal expansion deformations could not be accurately determined using traditional monitoring systems.

The moment of opening of cracks as well as the measurement of their width is recorded in-situ. Thus the early age cracking is detected and quantified.

The permanent monitoring of deformations using Standard Sensor, starting immediately after pouring provides accurate measurements that help to understand the real behaviour of concrete at early and very early age.

6.3 MONITORING OF HARDENING TIME OF CONCRETE

6.3.1 Introduction

The hardening time of concrete is defined in Section 3.7 as the end of the very early age. The idea of hardening time is presented on a simplified visco-elastic model of concrete at early and very early age. It consists of two elements [6], both composed of springs with linear elasticity (Hook) [7] and dashpots elements with linear viscosity (Newton) [7], as shown in Figure 6.3.1.1.

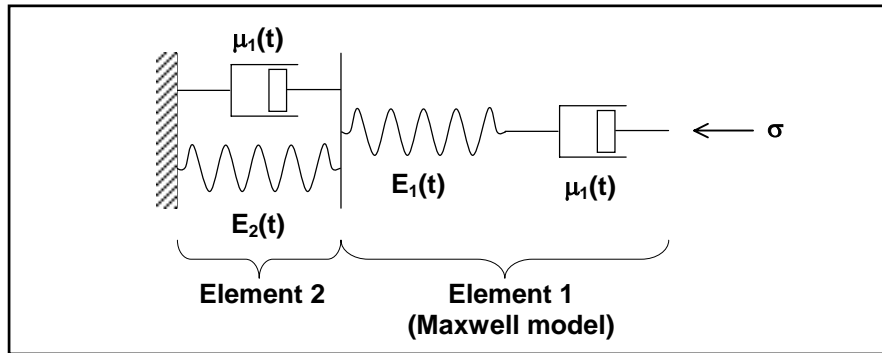


Figure 6.3.1.1: Simplified linear visco-elastic model of concrete

In Figure 6.3.1.1 notation is following:

t - age of concrete

$E_1(t)$, $E_2(t)$ - age dependent Young moduli

$\mu_1(t)$, $\mu_2(t)$ - age dependent coefficients of viscosity

σ - stress.

For this model, the following expression approximately describes the relation between strain and stress:

$$\varepsilon(\tau) = \frac{\sigma}{E_1(t)} + \frac{\sigma}{\mu_1(t)} \cdot \tau + \frac{\sigma}{E_2(t)} \cdot \left(1 - e^{-\frac{E_2(t)}{\mu_2(t)} \tau} \right) \quad (6.3.1.1)$$

where ε denotes strain and τ time measured from the moment when the stress σ is applied. We notice that this equation is only an approximation. Since the age t and the time τ evolve simultaneously, it would be necessary to make an integration. The aim of Expression 6.3.1.1 is to help explaining the idea of hardening time, therefore it is accepted in the following discussions.

In Expression 6.3.1.1 the first two terms on the right side of equation correspond to the first element, and the third term corresponds to the second element. The first term describes initial linear elastic deformation, the second term describes the linear creep and the third term describes the non-linear creep. It is important to note that the deformations described by the second and the third terms are different in maximal value: the second term can achieve unlimited values while the deformation described by third term is limited. Therefore the

deformation described by the second term is dominant until the concrete is not hardened (at very early age), while the third term describes rather the deformation dominant when the concrete is hardened. The deformation described by the first term is present before the concrete is hardened (initial stiffness of concrete, see Section 3.9), as well as in hardened concrete.

After the mixing of concrete, the Young moduli E_1 and E_2 as well as the coefficients of viscosity μ_1 , and μ_2 are low. Thereafter they increase rapidly, and when the coefficient μ_1 reaches an approximately infinite value, the concrete is practically solidified. Simultaneously, the Young modulus E_1 achieves a certain value. Thus the concrete is partially hardened and the very early age is finished.

It is important to notice that the deformation restrained before the hardening of concrete do not generate important stresses, because of relaxation (inversion of the second term). When the concrete is hardened, the relaxation is lower, and the stresses generated by restrained deformations could be significant. Hence, it is important to determine the hardening time of concrete.

The development of the Young moduli E_1 and E_2 and coefficients of viscosity μ_1 , and μ_2 with respect to the age of concrete is a continuous process. Therefore it is difficult to distinguish a particular moment corresponding to the end of very early age i.e. to the hardening time. In the literature we found definition of the setting time of concrete, based on penetration tests. In this Chapter we propose two original approaches for the determination and definition of the hardening time of concrete: the first approach concerns hybrid structures, and the second approach is more general, and applicable to all types of the structures. Both approaches are to be applied in-situ, and are close to the nature of reinforced concrete structures functioning.

6.3.2 Hardening time of concrete in case of hybrid structures

Hybrid structures are structures composed of two materials. The first material is often steel or existing (old) concrete, and the second material is the newly poured concrete. Steel-concrete structures are hybrid by conception, they are conceived in such way in order to exploit both materials in the best manner. If an existing (old) concrete structures has to be enlarged, strengthened or refurbished by adding a new concrete elements, new hybrid "old concrete-new concrete" structure arises. To facilitate narration, in the following text we use the term "the existing material" instead "the steel" or "the old concrete". The contact area of different materials is called interface.

Due to hydration of the new concrete, the very early age deformation develops and it is restrained by interaction with the existing material. Due to the dominant viscous behaviour of concrete at this stage, there are no important stresses generated by interaction.

During the new concrete hydration both materials deform, the new concrete due to hydration, and the existing material due to heat, transferred from new concrete. Before the new concrete hardening, the deformations of the new concrete and of the existing material are generally different since the interaction between them is weak, and the new concrete is viscous.

With ageing, the new concrete hardens, the interaction between the new concrete and the existing material starts and their deformations become less and less independent.

Furthermore, the difference of deformations of the new concrete and the existing material converge at the interface to a constant value. When this constant value is established, both materials deform equally. This means that a good interaction between them is created, and this is possible only if the new concrete is hardened.

Therefore, in case of hybrid structures, we propose the moment when the deformations of both materials (new concrete and existing material) at the interface begin to be equal as the hardening time of new concrete. In following two examples we present how to determine the hardening time of concrete in case of hybrid structures.

Hybrid old concrete - new concrete structure

Determination of the hardening time of new concrete is demonstrated using the specimen AA3 described in the Section 6.2.2. As mentioned, sensor AA3BC was fixed on the old concrete support, while sensor AA3BJ was independent of the old structure (see Figures 6.2.2.1 and 6.2.2.3). Therefore, during the new concrete very early age, the sensor AA3BC has measured the deformations of the old concrete, while sensor AA3BJ has measured the deformations of the new concrete, both at the interface.

Due to the different thermal expansion coefficients of two concretes and due to autogenous shrinkage of the new concrete, the unrestrained deformations of two materials are different. Since the new concrete at very early age is not hardened, the interaction with the old concrete is weak and the deformations are not fully restrained, i.e. they are different in the different material at the interface.

With ageing, the difference between deformations converges, and after a certain time it has begun to vary around a constant value. This means that after this time, both sensors measure the same type of deformation. Since the thermal expansion coefficients and shrinkage of two concretes are still different, this equality of deformation can only be explained by a very good mechanical interaction between old and new concrete. Consequently, after this time, the new concrete is hardened. Thus, one can say that the age when both sensors start to measure the same values corresponds to the hardening time of new concrete. This moment is appreciated in Figure 6.3.2.2.

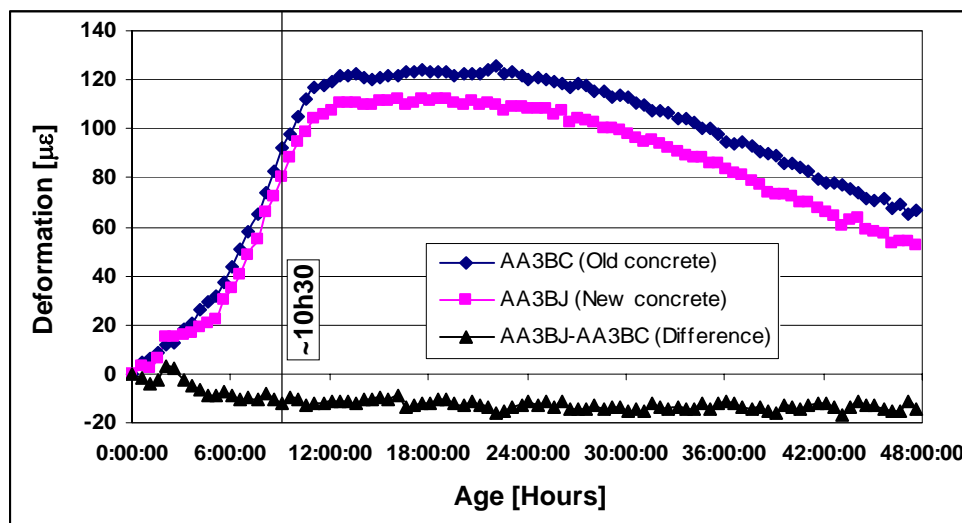


Figure 6.3.2.1: The (very) early age deformation and new concrete hardening time identification

In Figure 6.3.2.1 the early age deformations of both materials and their difference are presented. In order to present determination of the hardening time of new concrete in more details, in Figure 6.3.2.2 only the difference between measured deformations (shown also in Figure 6.3.2.1) and determination of new concrete hardening time are presented.

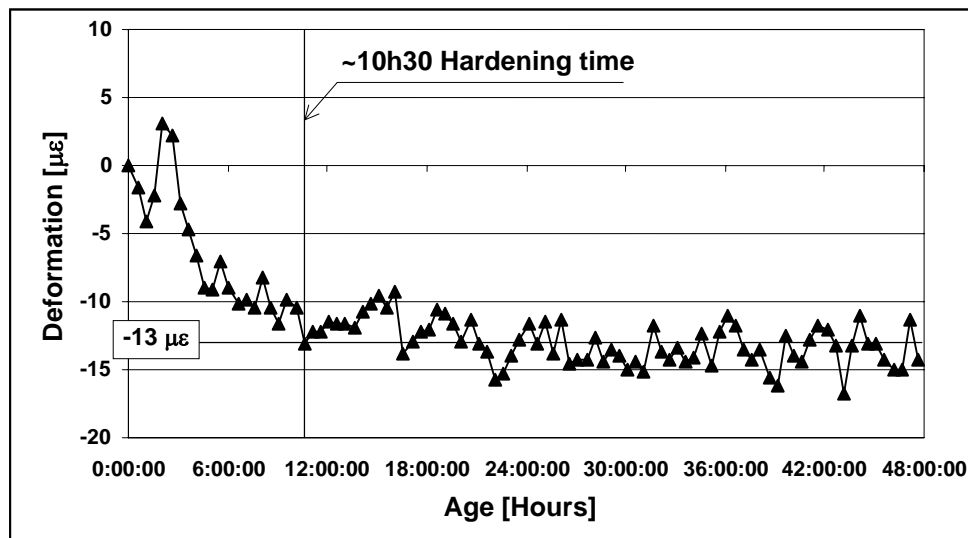


Figure 6.3.2.2: The difference between deformations of new and old concrete, and determination of new concrete hardening time

Hybrid steel - new concrete structure

In case of the hybrid steel - new concrete structures the reasoning is the same as in case of old concrete - new concrete structures. The hardening time of new concrete is monitored on the specimen F1, which contains the same concrete and has the length as the specimen F2 described in Section 6.2.2. The cross-section of the specimen and the placement of the sensors are presented in Figure 6.3.2.3.

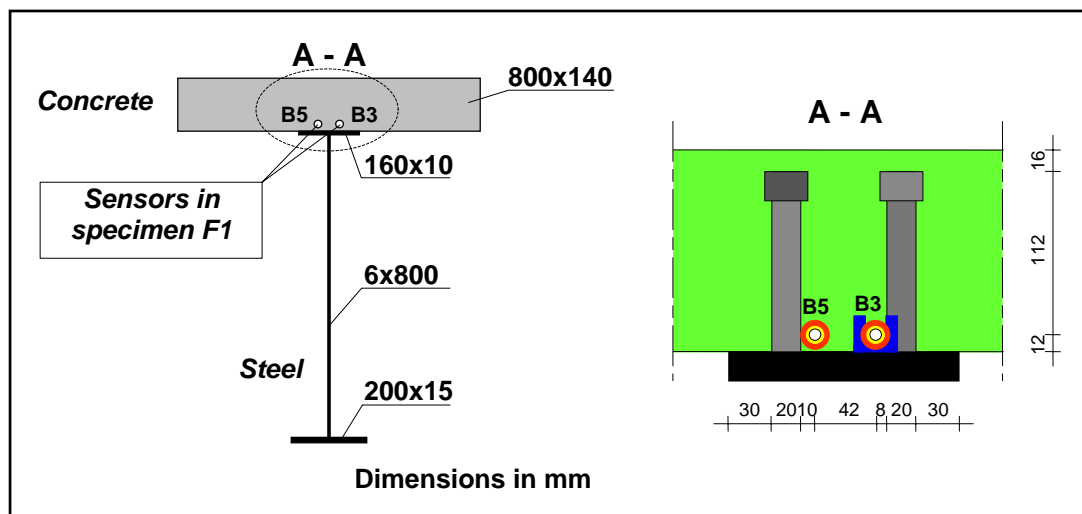


Figure 6.3.2.3: Cross-section and sensors placement of specimen F1

The 1.5 metres long sensors B3 and B5 have been positioned 720 mm from the end of the specimen. The sensor B3 is attached to iron corners welded to the steel (see Figure 6.3.2.3). In this way it measures the deformation of the steel support. The sensor B5 is placed into the

new concrete in order to measure its very early age deformation. The measurements are registered every 30 minutes. The measurements of both sensors and their difference are presented in Figure 6.3.2.4. The hardening time is successfully determined using the difference between the measured deformation. The difference between measured deformations is presented in more details in Figure 6.3.2.5.

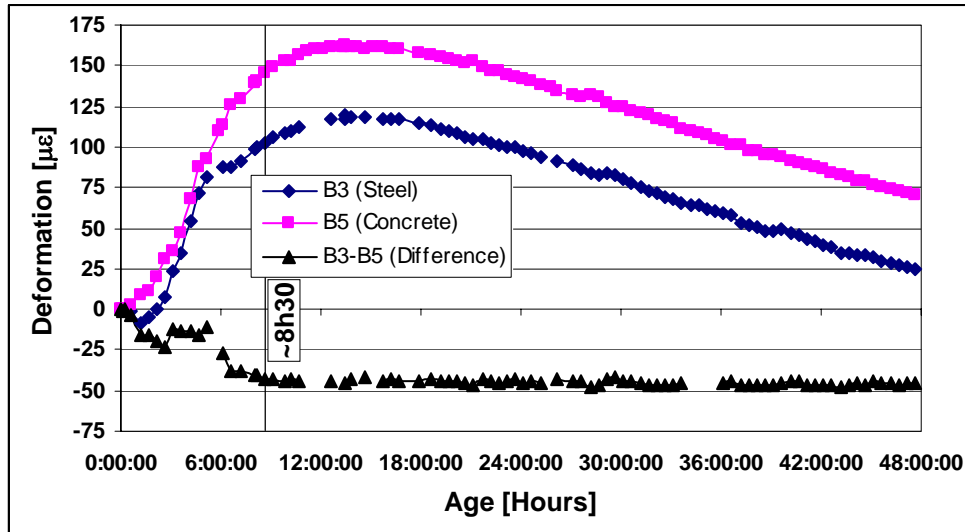


Figure 6.3.2.4: The (very) early age deformation of the specimen F1 and new concrete hardening time identification

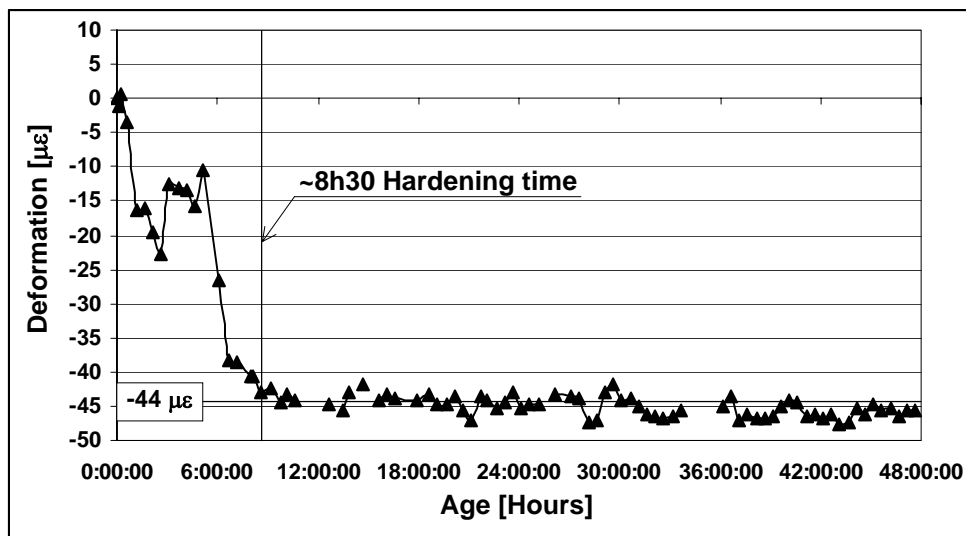


Figure 6.3.2.5: The difference between deformations of steel and new concrete and new concrete hardening time identification

6.3.3 Hardening time of concrete in general case

In this Section we propose a method for the determination of the concrete hardening time in a general case. A special sensor is developed for this method. It is called Stiff Sensor, since its stiffness is several order of magnitude higher than the stiffness of the Standard Sensor.

The idea is to place the Stiff and the Standard Sensor side by side and to compare their deformations. In the beginning, after the pouring of concrete, the Standard Sensor measures well the very early age deformation of concrete, while the Stiff Sensor deforms due to temperature of and interaction with concrete. However it does not follow exactly the very early age deformation evolution of concrete since it is stiffer than concrete at this stage. Therefore, before the hardening, the absolute value of the difference between measurements realised by the Standard and the Stiff Sensor is variable, but by ageing of concrete, it converges to a constant value.

When the concrete is hardened, it is sufficiently stiff to transfer the deformation to the Stiff Sensor too, and since both sensors measures an identical deformation (the deformation of concrete), the difference between their measurements becomes constant. The age when the difference between the Standard and the Stiff Sensor measurement becomes constant is proposed to be hardening time of concrete.

Stiff Sensor

The concept of the Stiff Sensor is the same as that of the Standard Sensor. The only difference is that the rigidity of protection tube must be several orders of magnitude bigger, and the thermal expansion coefficient must be different than the rigidity and the thermal dilatation ratio of concrete at the very early age. The stiffness of the tube guarantees the insensitivity of the sensor to the concrete very early age deformation, while the thermal expansion coefficient of the tube ensures incompatibility between the sensor thermal deformation and the concrete thermal expansion.

The Stiff Sensors are prepared and tested at IMAC-EPFL laboratory. The schema of the Stiff Sensor prototype is represented in Figure 6.3.3.1.

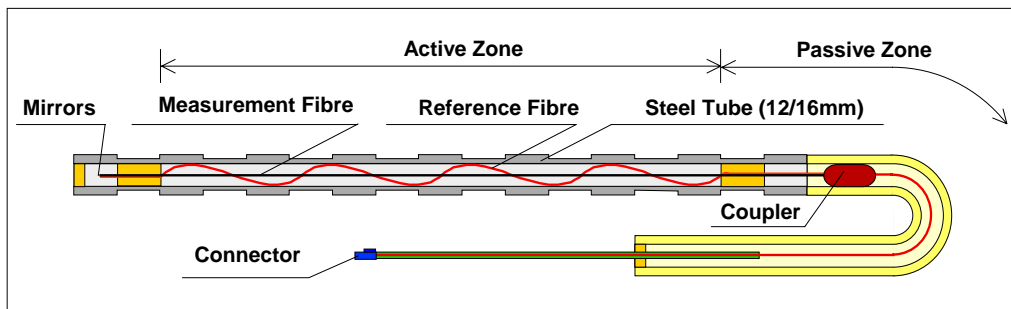


Figure 6.3.3.1: Schema of Stiff Sensor

A steel protection tube was used. There are two reasons for using a steel tube. The first is the very high stiffness of steel, and the second is the thermal expansion coefficient that is lower than that of concrete at the very early age. The endogenous shrinkage of concrete was not considered when choosing the material of the tube. Being made of steel, the Stiff Sensor has the same behaviour in the concrete as a non-anchored rebar.

Monitoring of hardening time

Two tests are carried out in order to measure the hardening time of the concrete. The disposition is fundamentally the same for each test, hence only one of them is described here in details, but results of all of them are presented.

Two packages consisting of the Standard Sensor, the Stiff Sensor and a "K" type thermocouple are placed in a formwork of a concrete slab as represented in Figures 6.3.3.2 and 6.3.3.3.

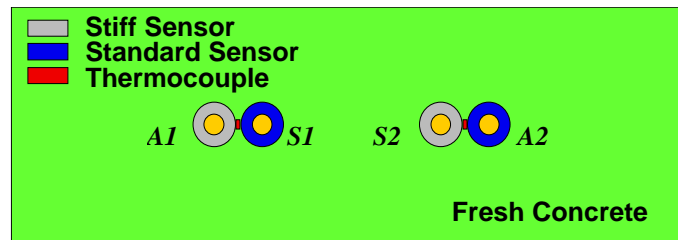


Figure 6.3.3.2: Emplacement of sensors in concrete slab (cross-section)



Figure 6.3.3.3: Pouring of concrete slab with thermocouple, Stiff and Standard Sensor

The dimension of the concrete slab is 38x110x200 cm. In order to decrease the influence of shrinkage due to evaporation and to increase the thermal expansion of concrete at very early age, the concrete was covered by isolation mats during the first forty eight hours. Deformation and temperature measurements were made during nine days. The ambient temperature was kept constant at 18°C.

The first experiment is realised in order to test the method. The concrete composition is unknown. The very early age deformation and the hardening time identification are shown in Figures 6.3.3.4 and 6.3.3.5 respectively.

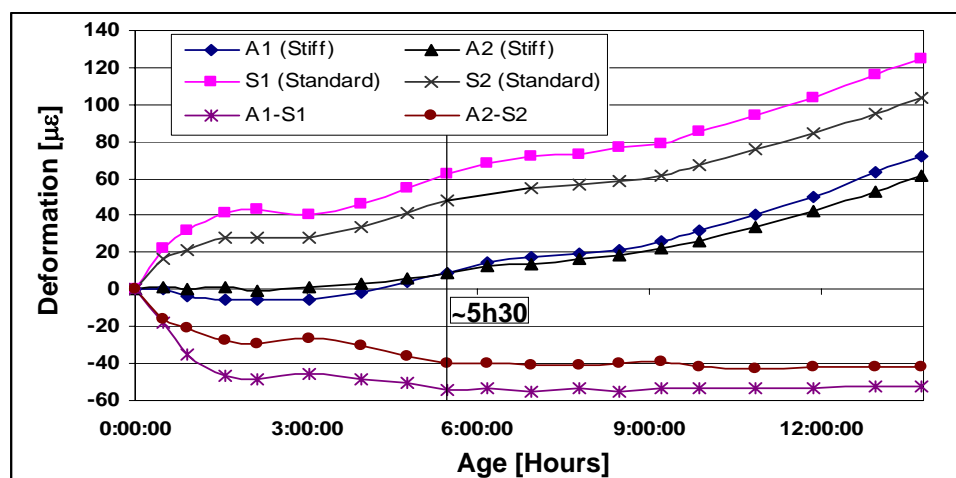


Figure 6.3.3.4: The very early age deformation of the concrete slab

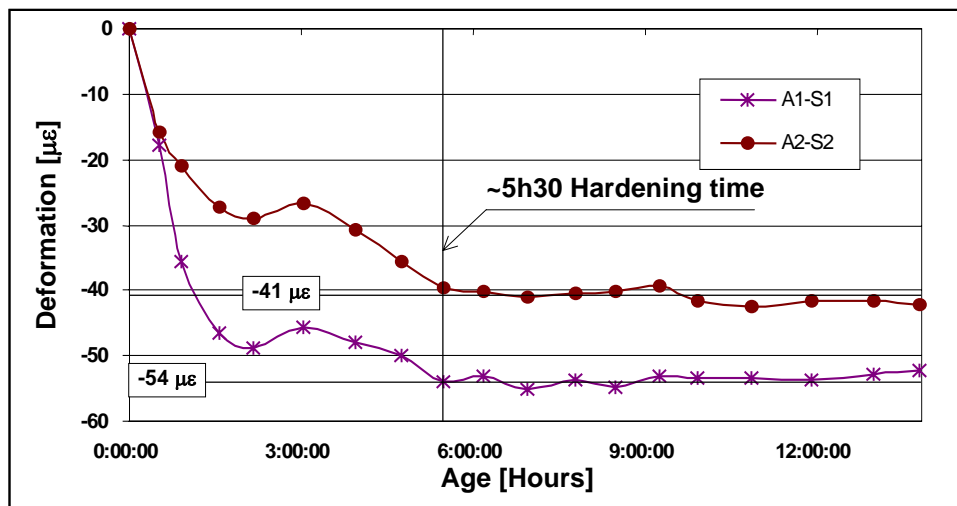


Figure 6.3.3.5: Identification of the hardening time of concrete using the Stiff Sensor

The measurements are registered every 30 minutes. The determined hardening time is approximately 5h30. The Stiff Sensor A1 has been prepared without the anchor pieces, while the Stiff Sensor A2 has two anchor pieces. Both sensors have measured the same hardening times, that prove the concept of the hardening time measurement. All sensors are 150 cm long.

The second experiment is realised using the same disposition. The used concrete is "Normo 4" according to Swiss norms, with a c/w ratio of 0.50 and the maximal diameter of aggregate grains of 32 mm. Unfortunately one of the Stiff Sensors was damaged during pouring, hence only the measurement made with one sensor are presented. In order to facilitate the presentation we will use the same notation, A1 for the Stiff Sensor and S1 for the Standard Sensor. All sensors are 60 cm long. The measurements are registered every 15 minutes. The very early age deformation and the hardening time are given in Figure 6.3.3.6.

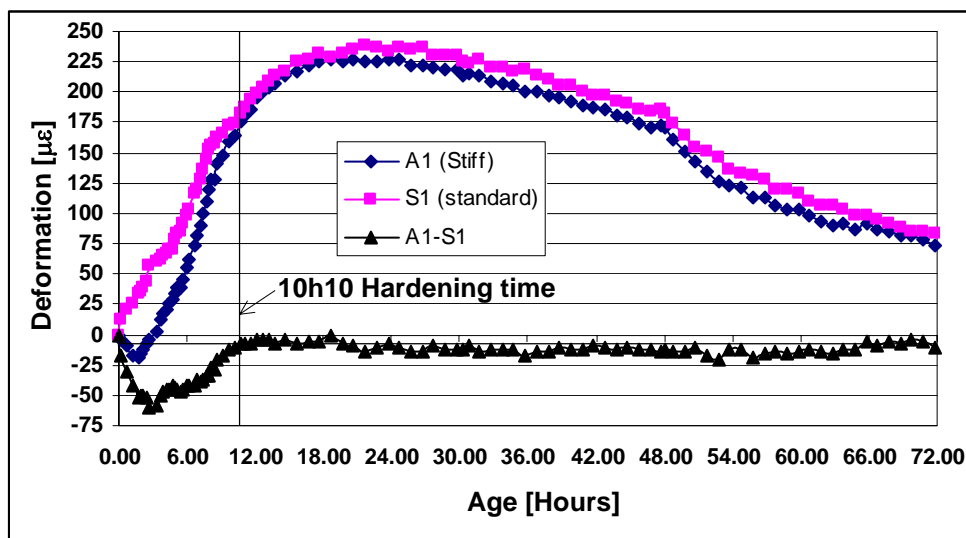


Figure 6.3.3.6: Very early age deformation of the concrete slab and determination of hardening time of concrete using the Stiff Sensor

Discussion

The presented experiments have confirmed the ability of the couple composed by a Stiff and a Standard Sensor to determine the hardening time of concrete. In the introduction of this Chapter we have noted that when the concrete is hardened the value of the coefficient of viscosity of the first element becomes practically infinite. Simultaneously the Young modulus reaches a certain value. Therefore the hardening time measured using the Stiff Sensor refers to a solidification of concrete, but also to a certain stiffening of concrete. This means that if we use another Stiff Sensor, which stiffness is different than the stiffness of the Stiff Sensors used in the presented experiments, the hardening time determined by this sensor will refer to another stiffening of concrete and will be different from hardening time obtained in these experiments.

In other words, the hardening time determined using the Stiff Sensor depends of its stiffness: if the stiffness of the Stiff Sensor is increased, the hardening time measured using this sensor is retarded, and vice versa, the sensor with low stiffness registers an earlier hardening time. The dependence of hardening time from the Stiff Sensor stiffness is more clearly presented in Figure 6.3.3.7.

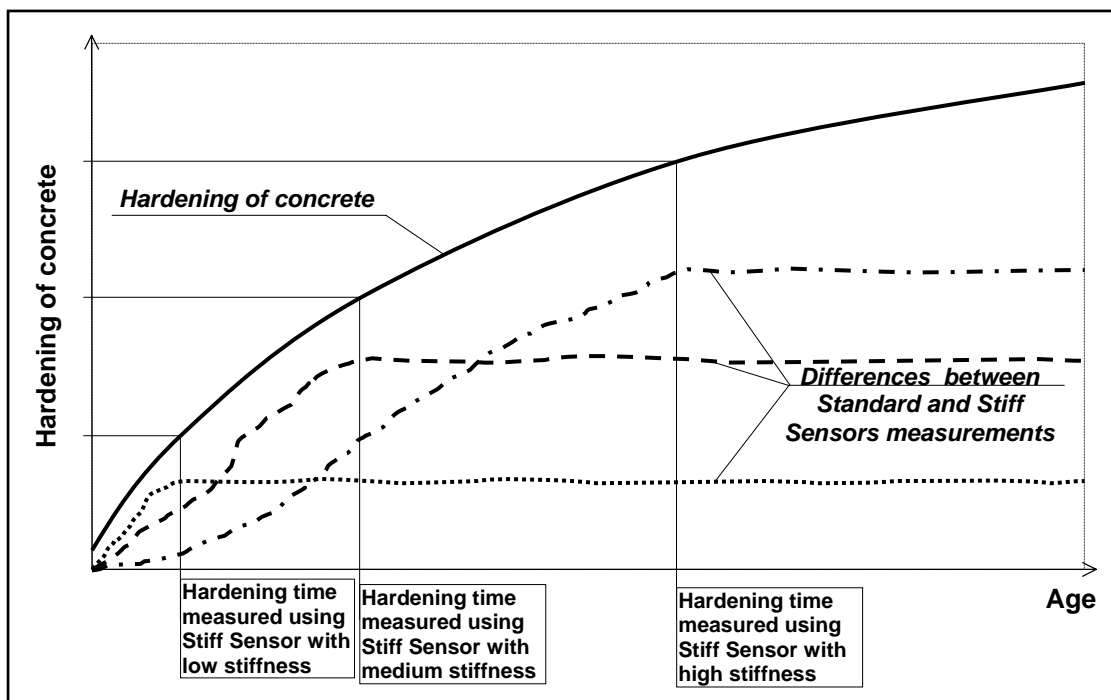


Figure 6.3.3.7: Supposed correlation between hardening time and Stiff Sensor stiffness

During the hardening (rigidification) of concrete the Young modulus increases (see Sections 3.6 and 3.7). Therefore the hardening time determined by Stiff Sensor also corresponds to the age when concrete achieves certain value of the elastic module. Using the Stiff Sensors with different stiffness it could be possible to qualitatively monitor the evolution of concrete hardening (rigidification) as shown in Figure 6.3.3.7. The quantification of the concrete elastic module at the hardening time needs establishing of correlation between the Stiff Sensor stiffness and the concrete Young modulus.

Recommendations

During the described tests the specimens have been cured (thermoisolated). The purpose of curing was the increase of concrete temperature which results in increase of the very early age deformation. In this way the difference between the new concrete and existing material in first case, and between the Standard and the Stiff Sensor in the second case, are emphasised. Neither curing nor any other special laboratory conditions are required to carry out the hardening time determination, therefore we suppose that it could be also carried out in-situ with no limits. However, it is recommend to use the sensors with measurement gage length as long as possible. In this way the resolution of the very early age deformation measurement is increased and the difference between measurements, indispensable to identify the hardening time of concrete, is more emphasised.

We propose two ways to use the Stiff Sensor for laboratory or in-situ applications. First possibility refers to both, laboratory and in-situ determination of the hardening time. The idea is to standardise the stiffness of the sensor in order to define a standard test for the determination of the hardening time. Existing similar standard tests are the Vicat test for cement paste setting and the standard penetration test for concrete setting (American Norms).

The second possibility refers to in-situ applications. Idea is to use a Stiff Sensor which stiffness is equal to the stiffness of the rebars. In this way, the hardening time corresponds to the moment when the monitored structure begins to behave as fully reinforced.

6.3.4 Summary

Hardening time is defined in this thesis as the end of the very early age. After the hardening time, the concrete is solidified and its Young modulus achieves a certain non-negligible value. Determination of the hardening time of concrete is important since after this moment significant stresses could be generated in early age concrete. These stresses are in origin of premature cracking of concrete that shortens the lifespan of concrete structures.

Since the processes of solidification and hardening of concrete are continuos, it is difficult to distinguish a particular moment corresponding to concrete hardening time. In this Chapter a definition and two original methods for hardening time determination are proposed. The first method is applicable only to hybrid structures, while the second method is applicable to all types of concrete structures. Both methods are laboratory tested and validated. To realise the second method, an original advanced sensor called Stiff Sensor has been developed.

The hardening time determined by the Stiff Sensor depends of the sensor's stiffness. Hence, more research in this domain is needed. Nevertheless, a standard test for the determination of the hardening time, similar to the Vicat and the penetration test, could be developed for laboratory and in-situ applications. Comparing with the penetration test, the method using the Stiff Sensor is advantageous since it is easier to apply, does not require direct access to the concrete and provides not only the hardening time, but also very early age deformation measurements.

6.4 TEC EVOLUTION MONITORING AT VERY EARLY AGE

6.4.1 Introduction

The TEC of concrete varies by ageing (see Section 3.8 and Section 4.3.3). At the beginning, after the mixing of concrete, it is relatively high (the TEC of fresh concrete is 2 to 5 times higher than the TEC of hardened concrete) but it rapidly decreases in the first 10 to 20 hours. Afterwards it is practically unchanged. Since the TEC of concrete is elevated during the period of intense hydration heating, it is the origin of important thermal deformations accumulated at very early age. This deformation can generate high tensile stresses that arise afterwards, during the contraction (shrinkage) period. The stresses provoke early age cracks that affect the durability of structures. That's why it is of interest to monitor the evolution of the TEC at very early age.

It is not easy to correctly monitor the TEC evolution. The thermal deformation of concrete is always coupled with autogenous deformation due to hydration, hence the problem of TEC evolution monitoring is in the separation of the thermal and the autogenous deformations. The solution of the first problem is given by [8]. However, monitoring presented by [8] have started eight hours after the pouring, when the concrete is already hardened.

In order to monitor the evolution of the TEC of concrete, an experiment is performed using the above-cited method. Measurements are carried out using the Standard Sensor in order to include the very early age. Several problems have appeared during the test, making it incomplete. Only a qualitative estimation of TEC evolution has been possible. The deadline of this thesis has made impossible the realisation of an improved test, but we believe it promising and therefore it is presented in this thesis. This experiment, as well as the explanation of the utilised method are presented in the following sections.

6.4.2 Principle of experiment

Two unavoidable types of deformation that appears simultaneously during very early age are the thermal and the autogenous deformation. Thermal deformation depends on the temperature and the TEC. While the temperature can be influenced by external conditions the TEC is an internal property of concrete as well as the autogenous shrinkage. Therefore, the evolution of the TEC and the autogenous deformation depends only of the evolution of hydration process, and this last depends on maturity (see Section 3.5). As a consequence, two specimens of the same concrete at the same maturity have equal TEC-s and autogenous deformation (shrinkage) even if they are cured differently. This principle is proven by [8] and serve as a basis for the separation of the thermal and autogenous deformation.

If all others types of deformation are avoided, the total deformation of concrete is given by following expression:

$$\varepsilon(m) = \varepsilon_a(m) + \varepsilon_t(m) = \varepsilon_a(m) + \int_0^m \alpha_t(\mu) \cdot \dot{T}(\mu) \cdot d\mu \quad (6.4.2.1)$$

where:

$\varepsilon(m)$ - total very early age deformation of concrete at maturity m

$\varepsilon_a(m)$ - autogenous deformation at maturity m

$\varepsilon_t(m)$ - thermal deformation at maturity m

$\alpha_t(\mu)$ - thermal deformation at maturity μ

$\dot{T}(\mu) = \lim_{m \rightarrow 0} \frac{\Delta T(\mu)}{\mu} = \frac{dT(\mu)}{d\mu}$ - first derivation of temperature T at maturity μ .

If two specimens of the same concrete are cured in different thermal conditions, at the same maturity they have equal autogenous deformation, equal TEC-s, but different thermal deformations. The deformations of these specimens are given by following expressions:

$$\varepsilon_1(m) = \varepsilon_a(m) + \varepsilon_{t1}(m) = \varepsilon_a(m) + \int_0^m \alpha_t(\mu) \cdot \dot{T}_1(\mu) \cdot d\mu \quad (6.4.2.2)$$

$$\varepsilon_2(m) = \varepsilon_a(m) + \varepsilon_{t2}(m) = \varepsilon_a(m) + \int_0^m \alpha_t(\mu) \cdot \dot{T}_2(\mu) \cdot d\mu \quad (6.4.2.3)$$

where indexes 1 and 2 denotes the specimens 1 and 2. By subtracting (6.4.2.3) and (6.4.2.2) we obtain:

$$\varepsilon_1(m) - \varepsilon_2(m) = \int_0^m \alpha_t(\mu) \cdot [\dot{T}_1(\mu) - \dot{T}_2(\mu)] \cdot d\mu, \quad (6.4.2.4)$$

and by derivation of equation (6.4.2.4):

$$d[\varepsilon_1(m) - \varepsilon_2(m)] = \alpha_t(m) \cdot d[T_1(m) - T_2(m)] \quad (6.4.2.5)$$

Finally, the TEC is calculated as:

$$\alpha_t(m) = \frac{d[\varepsilon_1(m) - \varepsilon_2(m)]}{d[T_1(m) - T_2(m)]} \quad (6.4.2.6)$$

The conclusion carried out from the previous discussion is that in order to monitor the evolution of the TEC of concrete it is sufficient to measure the total very early age deformation and temperature of two differently cured specimens, and afterwards to calculate the TEC using the expression (6.4.2.6). This expression is given by [8].

6.4.3 Laboratory monitoring of TEC evolution

The laboratory experiment of TEC evolution monitoring is performed. Two specimens of the same concrete are poured and the evolution of TEC is determined using the equation (6.4.2.6).

Concrete composition

The concrete used in this experiment is prepared using the cement CEM I 42.5, according to the Swiss norms. The crushed aggregate from the Arvel quarry is used in order to have the

grains with the same thermal expansion coefficient and elastic module. The grain-size curve of aggregate is presented in Figure 6.4.3.1.

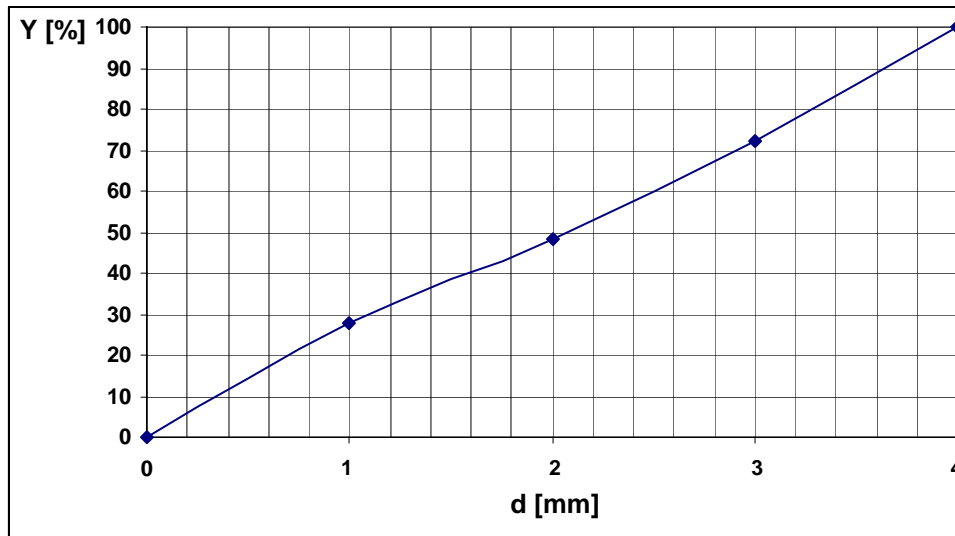


Figure 6.4.3.1: Grain size curve of aggregate

The water-cement ratio is 0.5. The proportions of all concrete components as well as their mechanical properties are given in Table 6.4.3.1.

	<i>Mass</i> [%]	<i>Elastic module</i> [GPa]	<i>Poisson ratio</i>	<i>TEC</i> [$\cdot 10^{-5} \cdot C^{-1}$]
Cement	15.13	70*	0.27*	1.0*
Water	7.56	2.18**	0.5	20***
Aggregate	77.31	70	0.35*	1.3
Air	~0	~0	0.5	367***

*Gussed **Compressive (Bulk) module ***Volume expansion coefficient [9]

Table 6.4.3.1: Proportion of components and their mechanical properties

Description of the experiment

The concrete is poured in two cylindrical specimens. To avoid any restraining of the specimen deformation, the workform is made of rubber, especially zigzag shaped as shown in Figure 6.4.3.2. Due to the special shape the workform deforms together with the concrete, without any restraining of the concrete deformation. The specimens have internal diameter of approximately 150 mm and height of approximately 400 mm.

Each specimen is equipped by a 200 mm long standard sensor and by "K" type thermocouple. Both sensors are placed in the middle of the specimen as shown in Figure 6.4.3.2. Measurements are registered every 15 minutes.

One of the specimens is cured in quasi-adiabatic conditions, placed in a special thermoinsulation box, while other is cured in ambient conditions. The thermally isolated specimen is called "TI" and non-isolated specimen is named "NI". Any evaporation of the

specimens during the very early age is prevented using plastic coverings. The workforms, thermoinsulation boxes and pouring of concrete are presented in Figure 6.4.3.3.

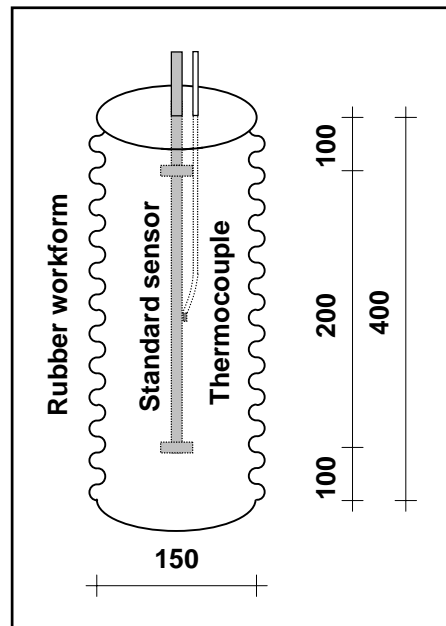


Figure 6.4.3.2: Shape and sensor equipment of specimens

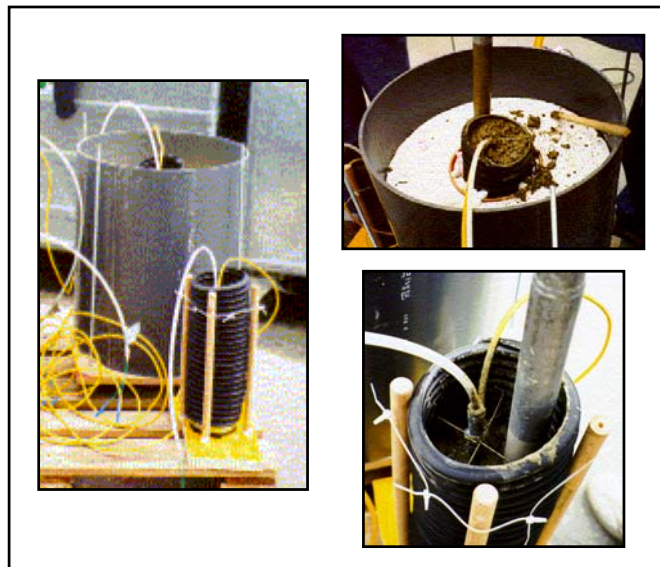


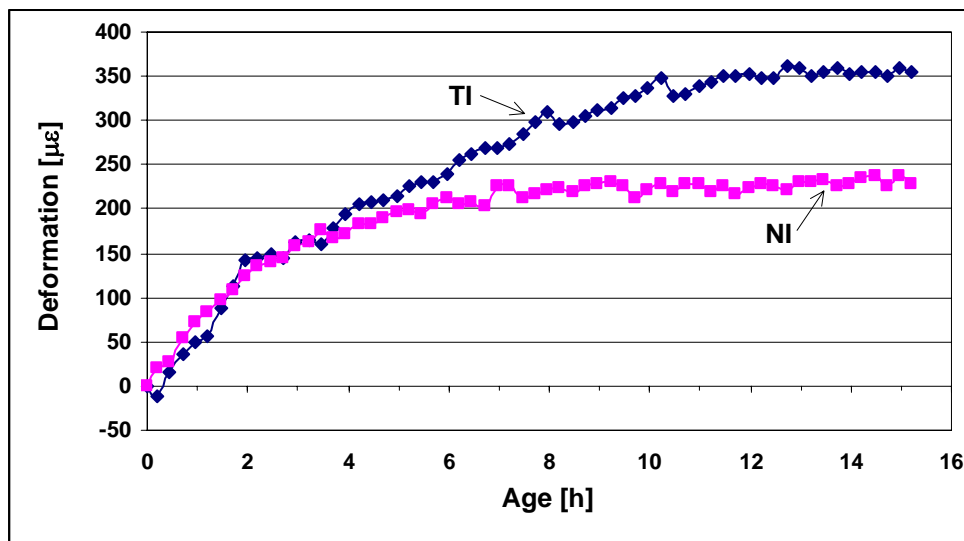
Figure 6.4.3.3: Workforms, thermoinsulation boxes and vibrating of concrete

Results and analysis of measurements

Several problems appeared during the test. All sensor used in this experiment are made with external coupler. Very long passive zone between the coupler and the active zone was source of perturbation and inaccuracy of measurements. Therefore only 15 hours following the pouring are valid. Later verifications have confirmed that the passive zone has been affected by temperature. This has increased the inaccuracy of the measurements.

Moreover, the deformation of non-isolated specimen NI has been restrained due to thermal gradient in specimen. Hence, the measured deformation of the specimen NI is lower than sum of pure thermal and autogenous deformation. However the influence of thermal gradient has not significantly affected the experiment.

Finally, there was a problem related to the gage length of sensors: it was only 20 cm long. Therefore the resolution of measurements is $10 \mu\epsilon$ ($2\mu\text{m}/0.2\text{m}$) and the accuracy of the difference between measurement is $20\mu\epsilon$. As a consequence, the measurement curves as well as curve that describe the differences between measurements (TI-NI) are not smooth (see Figures 6.4.3.4, and 6.4.3.5). Therefore the calculus of the first derivation of difference is not accurate. The evolution of specimens' deformation with respect to age is given in Figure 6.4.3.4. The evolution of the deformation difference of two specimens with respect to maturity (see Section 3.5) is given in Figure 6.4.3.5.



Figures 6.4.3.4: Evolution of deformation of thermally isolated (TI) and non-isolated (NI) specimen

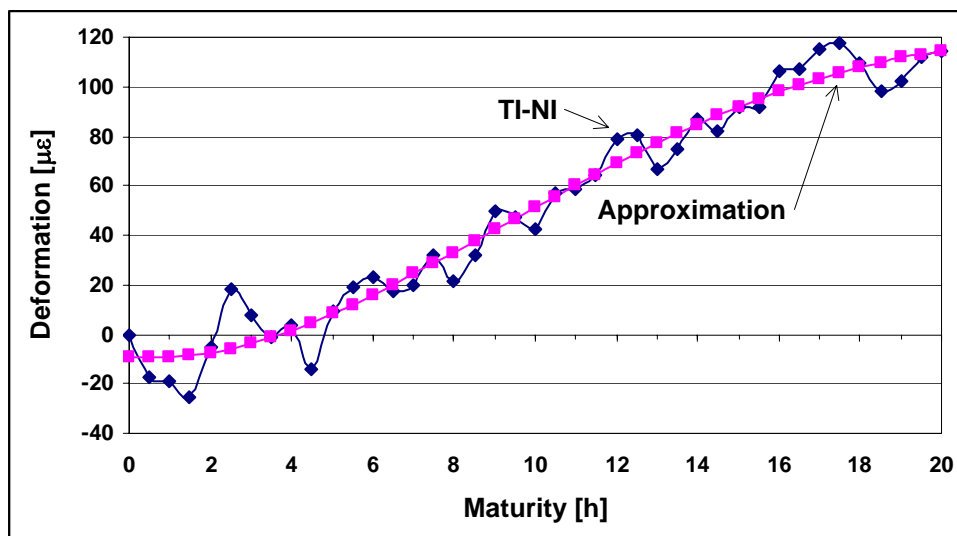
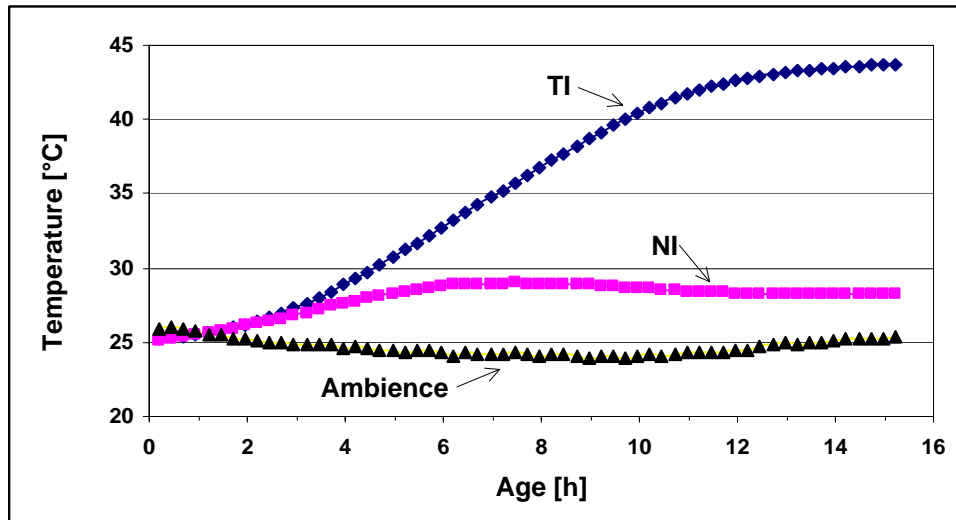


Figure 6.4.3.5: Difference (TI-NI) between deformations of thermally isolated (TI) and non-isolated (NI) specimen, and its approximation

All these problems have made impossible an absolutely accurate monitoring of the TEC evolution. Therefore only an approximate, qualitative estimation is carried out.

The temperature of non-isolated specimen achieves the maximum of 30°C, only 7 hours and 30 minutes after the pouring, while the isolated specimen achieves the maximum of 43.8°C approximately 10 hours later. The temperature evolution of specimens is shown in Figure 6.4.3.6.



Figures 6.4.3.6: Evolution of temperature of thermally isolated (TI) and non-isolated (NI) specimen

The maturity evolution of both specimens is calculated using expression 3.5.1. (see Section 3.5) and presented in Figure 6.4.3.7. During the first three hours the temperature evolution is equal for both specimens (see Figure 6.4.3.5) and therefore the maturity of both specimens is also equal during this period. Thus, the monitoring of TEC is possible only after the third hour.

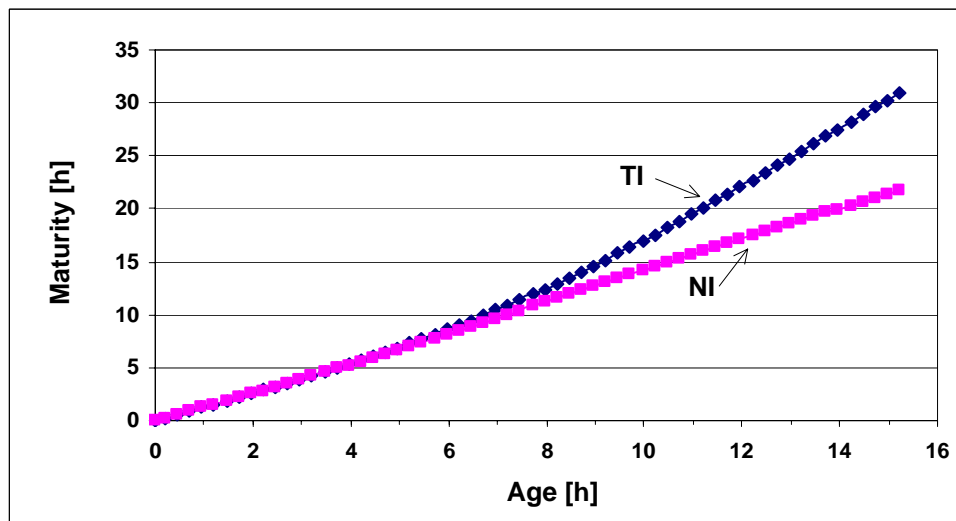


Figure 6.4.3.7: Maturity evolution of thermally isolated (TI) and non-isolated (NI) specimen

To make possible the application of the expression 6.4.2.6, the deformations and temperature as well as differences between the values of isolated and non-isolated specimen are calculated

with respect to maturity. The differences between deformations and temperatures are given in Figures 6.4.3.5 and 6.4.3.8 respectively.

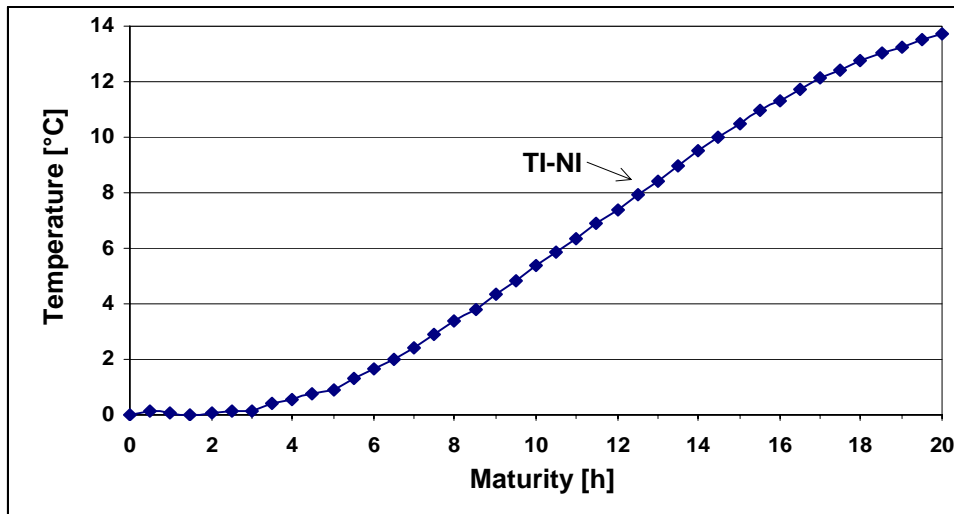


Figure 6.4.3.8: Difference (TI-NI) between temperatures of thermally isolated (TI) and non-isolated (NI) specimen

Since the resolution of measurement presented in Figure 6.4.3.5 is $20 \mu\epsilon$, the difference between two successive points on diagram 6.4.3.5 can vary a lot, even if the specimen is not really deformed. In this way, a direct application of the expression 6.4.2.6 was not possible. Therefore it is necessary to "smooth" the line representing the differences in Figure 6.4.3.5. The smooth line is obtained by 4th order polynomial mean quadratic approximation. This approximation is also presented in Figure 6.4.3.7. Now we have all elements to apply the expression 6.4.2.6 and to compute the evolution of the TEC of concrete at very early age.

Evolution of TEC of concrete at very early age

Using the expression 6.4.2.6 in finite differences form (i.e. substitution of d by Δ in formula), the evolution of the TEC of concrete is obtained with respect to maturity. The step of calculus is 1h. The evolution of the TEC of concrete is presented in Figure 6.4.3.9.

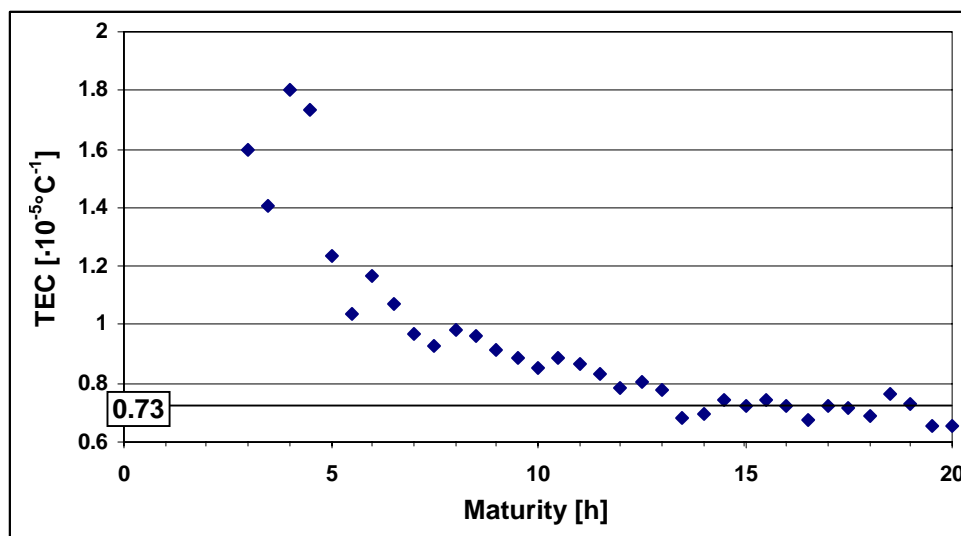


Figure 6.4.3.9: Evolution of concrete TEC with respect to maturity (non corrected)

The shape of the curve presented in Figure 6.4.3.9 corresponds well to the shape obtained by [8]. However the final value of TEC is lower than predicted: all component of concrete utilised in the test have TEC higher than obtained value of $0.73 \cdot 10^{-5} \text{C}^{-1}$ (see Table 6.4.3.1).

The EM modelling is performed in order to compare theoretical results with the test. Results obtained by EM modelling are presented in Figure 4.3.3.9, Section 4.3.3. They have confirmed that the value obtained in Figure 6.4.3.9 is certainly underestimated. The source of the error could be thermal influence to the passive zone of the utilised sensors or error in calculus which is consequence of separation of the autogenous shrinkage.

Therefore an other type of control was performed: The evolution of TEC is determined directly, without separation of autogenous shrinkage. Since the water cement ratio of concrete is 0.5, it is expected to obtain very low autogenous shrinkage. The diagram of deformation measured by specimen TI with respect to temperature is given in Figure 6.4.3.10.

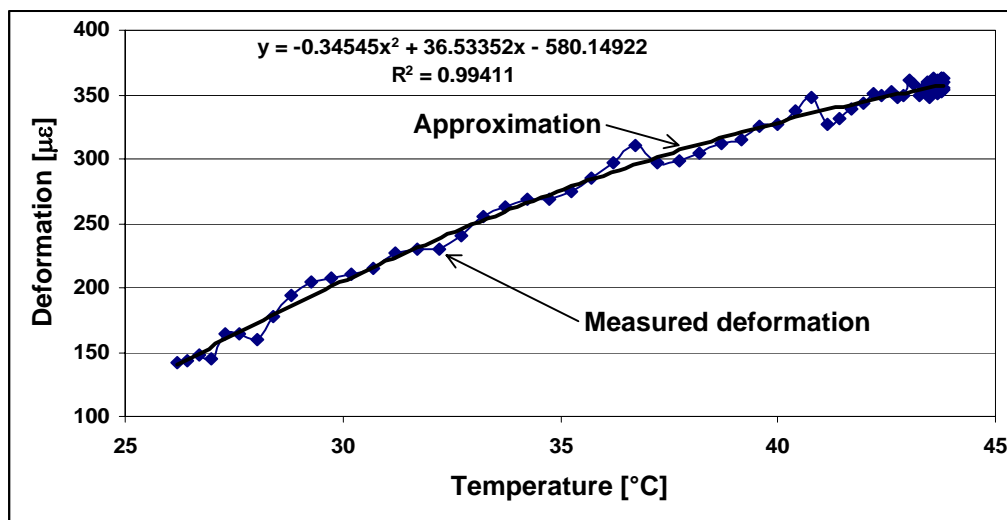


Figure 6.4.3.10: Deformation of specimen TI versus temperature

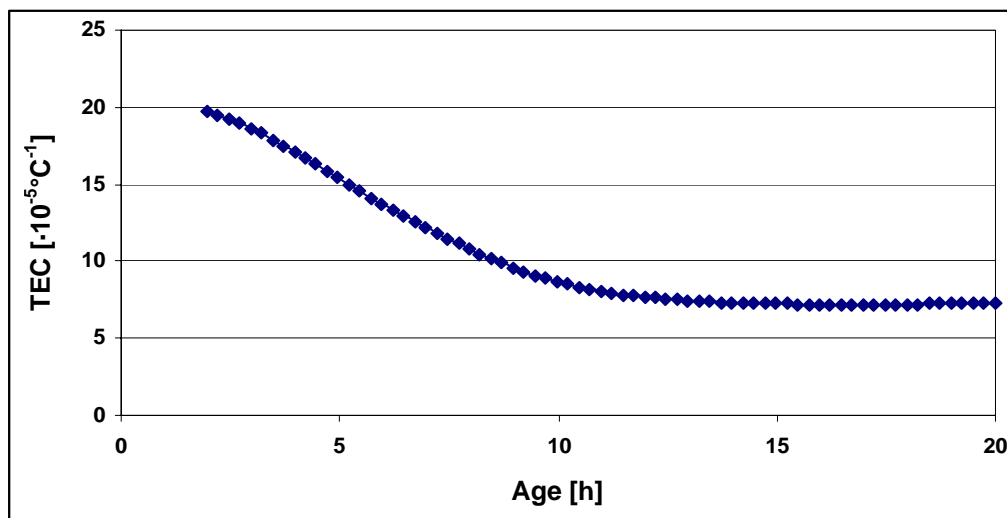


Figure 6.4.3.11: Deformation of specimen TI versus age

In order to calculate the evolution of the TEC, dependence of deformation with respect to temperature is approximated using 3rd order polynomial mean quadratic approximation. The TEC evolution is calculated as a first derivation of this approximation, and presented, with

respect to age, in Figure 6.4.3.11. Diagram of evolution obtained in such a way is practically identical to the diagram presented in Figure 6.4.3.9. Conclusions are following: first, as expected, the autogenous shrinkage of utilised concrete is negligible in the first 20 hours; and second, the source of error of measurement is in thermal influence to the passive zone between the coupler and the active zone of the sensor.

In order to improve the results, the influence of temperature to the passive zone is determined. After the 20th hour of maturity the TEC of concrete is stabilised. Therefore the TEC measured later is supposed to have the same value as for maturity of 20 hours, i.e. $0.73 \cdot 10^{-5} \text{ } ^\circ\text{C}^{-1}$.

Analysis of the results shows that measurements obtained between the 30th and the 54th hour could be supposed to be only affected by temperature. These measurements as well as the measured temperatures of specimen TI are presented in Figure 6.4.3.12.

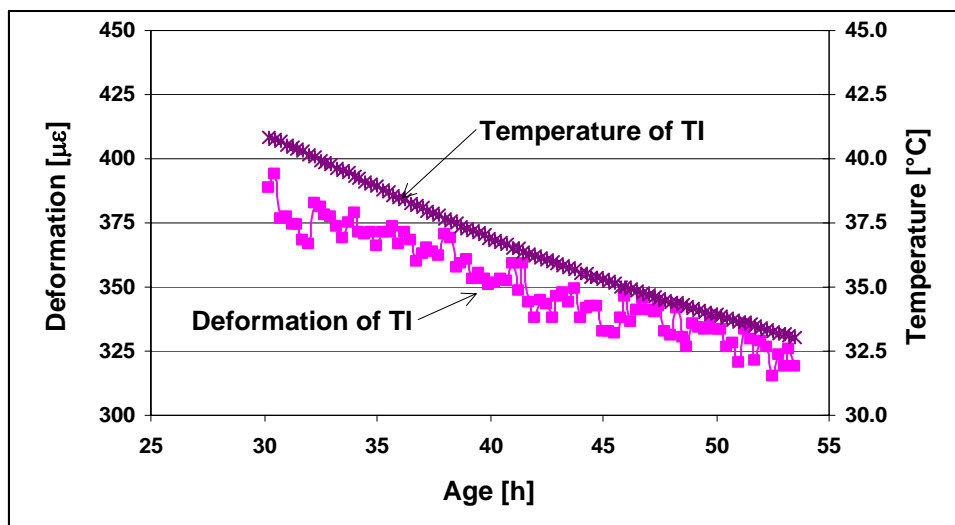


Figure 6.4.3.12: Deformation and temperature evolution specimens TI and NI, 30 to 54 hours after pouring of concrete

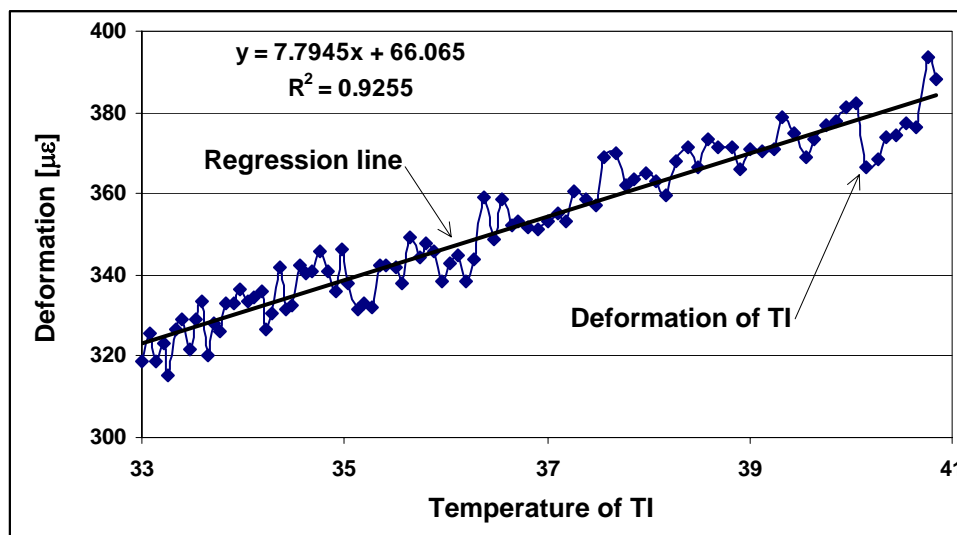


Figure 6.4.3.13: Correlation between deformation and temperature for specimen TI

The correlation between diagrams presented in Figure 6.4.3.12 is shown in Figure 6.4.3.13. This correlation is in fact the correlation between deformation and temperature. This correlation is not fully correct, since the autogenous deformation is not subtracted from total deformation. However the correlation helps to correct the results. The TEC obtained in this way is equal to $0.78 \cdot 10^{-5} \text{°C}^{-1}$. This value is close to that presented in Figure 6.4.3.9.

Since the sensors utilised in the test are affected by temperature, the real TEC of hardened concrete is determined using the specimens equipped with external sensors (see Figure 4.3.3.7, Section 4.3.3.). The obtained value is $1.17 \cdot 10^{-5} \text{°C}^{-1}$ (see Section 4.3.3.).

This last result shows that the influence of temperature to the sensor is approximately 0.39 to $0.43 \cdot 10^{-5} \text{°C}^{-1}$. If the diagram presented in Figure 6.4.3.9 is calibrated with the mean value of $0.41 \cdot 10^{-5} \text{°C}^{-1}$, the corrected evolution of TEC becomes as presented in Figure 6.4.3.14.

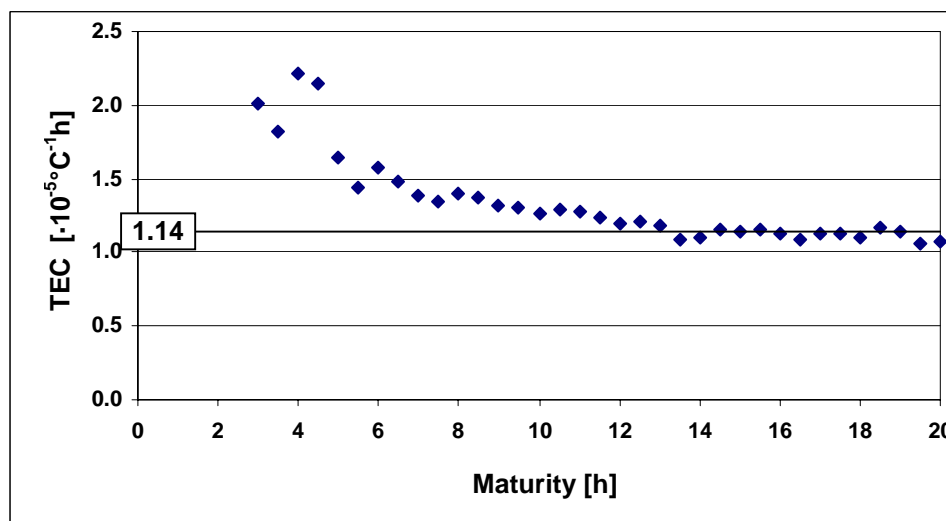


Figure 6.4.3.14: Evolution of concrete TEC with respect to maturity (corrected)

The diagram presented in Figure 6.4.3.14 corresponds well to experimental results found in the literature and to results obtained by EM model (see 4.3.3). However, this diagram is obtained using several corrections and suppositions concerning the results of the measurement. Therefore we consider that it represents the evolution of TEC only qualitatively but not quantitatively. In order to measure accurately the evolution of the TEC using the Standard Sensor, we give some recommendations in the following subsection.

Recommendations

To accurately monitor the TEC evolution of concrete at very early age we give following recommendations:

- To guaranty good and accurate measurement, the sensors with short passive zone between the coupler and the active zone have to utilised for deformation monitoring of specimens.
- To increase the resolution of measurements and to increase the accuracy of computing, the gage length of sensors, and consequently the height of specimens, has to be longer than 20 cm. We suggest a length of at least 50 cm.

- Each specimen has to be equipped with two to four Standard Sensors and thermocouples: one sensor and one thermocouple are to be installed in the middle of the specimen and other sensors and thermocouples are to be installed in circumference of the specimen. In this way the restraining of deformation due to thermal gradient could be controlled.

6.4.4 Summary

The method presented by [8] is adapted for standard sensor application. The evolution of the TEC of concrete is monitored from the third hour following the pouring. Unfortunately the measurements have been affected by several phenomena and the obtained evolution is only qualitatively estimated. In the last subsection of the previous section we have given recommendation for an accurate monitoring of the TEC evolution.

The results of the monitoring show qualitatively good agreement with the theory and numerical model. This is the first time that the evolution of the TEC of concrete is monitored from the third hour without special set-up, nor special laboratory conditions, therefore we think that this method could be easily adapted for in-situ application.

6.5 CONCLUDING REMARKS

In this chapter we have presented monitoring of three important characteristics of concrete at very early age using the Standard Sensor: total deformation, hardening time and thermal expansion coefficient.

In the Section 6.2, diagrams that present real early and very early age deformation of concrete are presented and discussed. Four characteristic periods are distinguished in these diagrams: the dormant period, the stabilisation period, the thermal expansion period and the contraction period. The importance of very early age monitoring has been confirmed by laboratory experiments and in-situ. It provides rich information concerning the very early age behaviour of structures, and helps to understand their real behaviour.

In the Section 6.3, the idea of hardening time of concrete is presented. The hardening time is defined as the end of very early age. It coincides with the moment when significant stresses could be generated in concrete. Two original methods for hardening time determination are proposed: the first is applicable only for hybrid structures while the second is applicable with no restrictions. Both methods are focused to practical applications. As logical consequence of this work, a standardised test for the hardening time determination, similar to Vicat and penetration test, could be developed for laboratory and in-situ applications.

In Section 6.4, a method for monitoring of thermal expansion coefficient (TEC) of concrete is presented. The method is laboratory tested. Due to some problems generated by different phenomena, only qualitative monitoring has been performed. However, the method is promising, and after the proposed improvements could allow the monitoring of the TEC that begins two to three hours after the pouring of concrete. Moreover, the method could be used not only for laboratory, but also for in-situ monitoring. It is easy to perform and does not require any particularly sophisticated equipment.

6.6 REFERENCES

- [1] Bernard O., Brühwiler E., *Analysis of Early Age Behaviour of a Hybrid Concrete Bridge Deck*, US-Canada-Europe Workshop on Bridge Engineering, Dubendorf and Zurich, July 14 -15, 1997
- [2] Bernard O., *Comportement à long terme des éléments de structures formés de bétons d'âges différents*, Ph.D. Thesis, EPFL, Lausanne, Switzerland, 2000 (*to be published*)
- [3] Blanc A., Gómez Navarro M., *Poutres mixtes à âme mince avec béton de fibres métalliques*, Rapport d'essai N°394, ICOM-EPFL, Juillet 1999
- [4] Monney C., Ducret J.-M., *Essais de poutres mixtes à âme mince*, Rapport d'essai N°357, ICOM-EPFL, Septembre 1999
- [5] Badoux M., Jaccoud J.-P., Fleury B., Simon N., *La tranchée couverte de Champ Baly - Projet pilote d'application de BHP*, Publication SIA D0160, 1999
- [6] Wittmann, F. H., *Personal communication*, 13.04.2000
- [7] Frey F., *Mécanique des matériaux (II)*, pp. 7.23-7.27, Cours de 3^e semestre, ISS, DGC, EPFL, Lausanne 1989
- [8] Laplante P., Boulay C., *Evolution du coefficient de dilatation thermique du béton en fonction de sa maturité aux tout premiers âges*, , Materials and Structures, Vol.27, pp. 596-605, 1994
- [9] *Formulaires et tables, Mathématique, Physique, Chimie*, Commissions romandes de mathématique, de physiques et de chimie, Editions de Tricorne, pp. 190-197, Genève, 1996

7 Advanced sensor designs

7.1 INTRODUCTION

The Standard Sensors can be used in a wide variety of applications and materials, but there are some special cases where its application is limited by its own dimensions or by the mechanical properties of the host structure. In order to extend the use of our system to these particular cases, special sensors have been developed. These sensors also allow knowledge extending related to real behavior of these structures and materials. Some of these new sensors open new measurement possibilities in cases where no traditional or fiber optic sensor is available.

In this Chapter we present four special sensors: Membrane, Long, Stiff and Displacement sensors. The Membrane Sensor is for use on laminated materials (e.g. membrane roofing). It is easy to install by simply gluing to the monitored structure. The Long Sensor has a measurement basis of several tens of meter and its purpose is the measurement of deformations in massive and large structures (dams, tunnels). The aim of the Stiff Sensor is to register the hardening (solidification) time of concrete. This time is determined by comparing the deformation of the Stiff Sensor with that of a Standard Sensor closely placed in the concrete at very early age. Finally, the Displacement Sensor is used to measure large displacements over short bases. It can be used for such cases where two parts of a structure move relatively one with respect to the other one. The Displacement sensor function accurately even if it is exposed to extreme environmental conditions (temperature of 1.4 K and vacuum). In particular, this sensor was developed to measure the internal displacements in the new CERN LHC cryo-dipoles. The design of these sensors is presented along with significant application examples.

7.2 MEMBRANE SENSOR

Introduction

Civil engineering is no longer the kingdom of a few building materials (stone, concrete, steel, timber). Many new building materials have been introduced and allow the construction of radically new types of structures.

Among others, thin plastic membranes are now a possible choice to cover large structures like exhibition spaces or sports arenas. The behaviour of such materials still presents a few uncertainties. The design, maintenance and safety of these structures call for a permanent monitoring of them.

In the literature, we did not find any reference to sensors developed in order to monitor the deformation of plastic materials in-situ. This deformation is indeed not easy to measure because of the thinness, low stiffness and the creep of plastics. Classical set-ups are unsuitable for automatic and permanent measurements on the structure itself.

Design criteria

As in case of the Standard Sensor, the Membrane Sensor has to contain two optical fibres, the measurement and the reference fibre. Both fibres are embedded between two plastic bands, assembled by the thermal fusion, executed at 250°C (see Figure 7.2.1). In order to guarantee the correct functioning of the sensor, the following conditions have to be satisfied:

- Very good deformation transfer from fused plastic bands to the measurement fibre;
- Independence of the reference fibre from the membrane deformations;
- Independence of the passive zone of both fibres from the membrane deformations, especially between the active zone and the coupler;
- Fast and easy installation.

Concept of the Membrane Sensor

The Membrane Sensor is composed of two zones: the active zone where the deformations are measured, and the passive zone that is used for connecting the sensor to the reading unit.

The active zone contains two optical fibres: the measurement fibre and the reference fibre. Both fibres are first placed between two plastic bands. A good transfer of deformation from the plastic bands to the measurement fibre is realised by means of two anchor plaques. The deformation of structure induces a deformation of sensor and changes the distance between the anchor pieces. This change is registered by the measurement fibre, detected in the reading unit, and represented on the data acquisition software. Placing the measurement fibre between plastic bands allows it to follow faithfully the behaviour and the deformed shape of the monitored plastic membrane without perturbing its strain field.

The measured fibre is glued to the anchor plaques using special two-phases thermo-cured glue. The glue has to be temperature resistant since during the fusion of the plastic bands the temperature increases until 250°C (see Figures 7.2.1 and 7.2.2).

The reference fibre should be independent of both the measurement fibre and the deformation of the structure, and its purpose is to compensate temperature influences. In order for reference fibre to be both, independent of deformation and protected during the fusion, it is not installed directly between the plastic bands, but is protected by a Teflon tube.

The measurement fibre attached to the anchor plaques and the Teflon tube with reference fibre are set between two plastic bands that are then fused together by heating. Both fibres exit from the active zone and continue to the passive zone. The length of active zone is

limited between 20cm and 2m. The maximal measurable deformation is of about 4% and is limited by the brittleness of the measurement fiber. This range is convenient for measuring the mechanical properties of many plastic materials. The sensor is schematically represented in Figure 7.2.1.

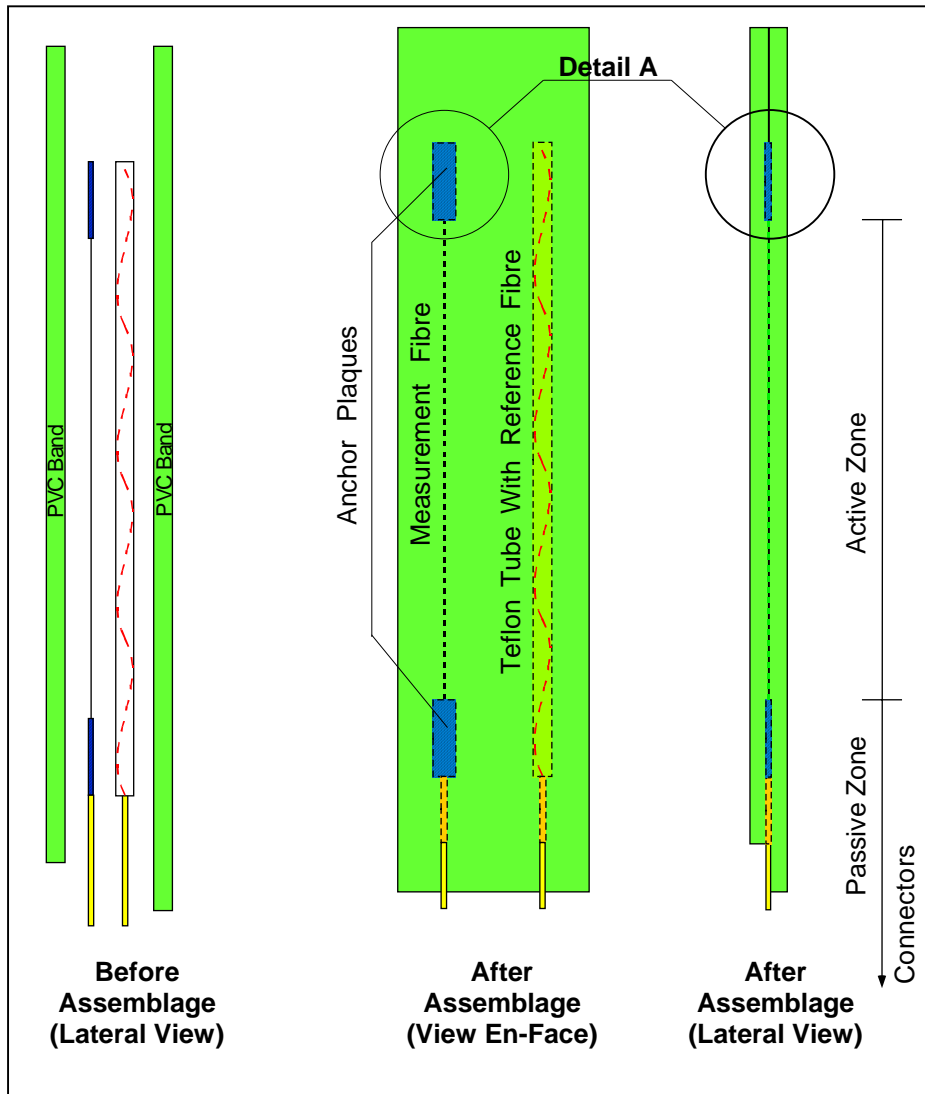


Figure 7.2.1: Conception and design of Membrane Sensor. Detail A: see next figure.

The passive zone transmits the information from the active zone to the reading unit. It consists of the coupler, optical cables and the connector. The length of the passive zone is practically unlimited (can be up to a few kilometres) and depends only on the distance between the sensor emplacement and the reading unit position. If this distance is very large (several tens of meters) the passive zone is extended by a simple fibre optic cable.

The manipulation and installation of sensor are very fast and easy. It is sufficiently to glue it to the monitored membrane by means of thermo-activated glue. Prototypes were tested in the laboratories of IMAC-EPFL and IMM-Lugano, the results are very positive and are presented in next sections.

Test of deformation transfer - anchor plaques

Different modes of deformation transfer from the fused plastic band to the measurement fibre are considered:

- By friction,
- By gluing,
- By anchor plaques.

The preliminary test has shown that the transfer of deformation from the assembled plastic bands to measurement fibre is not possible by friction alone. The measurement fibres with three different types of coating have been tested. The sliding of the fibres appeared in all cases at strains well below 1%.

The tests of deformation transfer carried out by direct gluing of fibre to the bands did not bring satisfying results, either. The sliding appeared again, due to very small gluing area.

Finally, tests using anchor plaques provided much better results. This solution has been retained and was used for all subsequent tests.

The anchor plaques are made of aluminium. To ensure their connection with the plastic bands, they are perforated (see Figure 7.2.2). Both extremities of the measurement fibre (polyimide coated) are glued in grooves previously machined in the middles of the plaques. The extremities of the grooves were especially treated to avoid damage to the fibres during the manipulation.

During the thermal fusion process, the plastic mass fills very well the perforations (see Figure 7.2.2) and the space around the plaques. As a result, a strain transfer between the plastic band and the anchor plaques is achieved. A Scheme of the anchor plaque is represented in Figure 7.2.2.

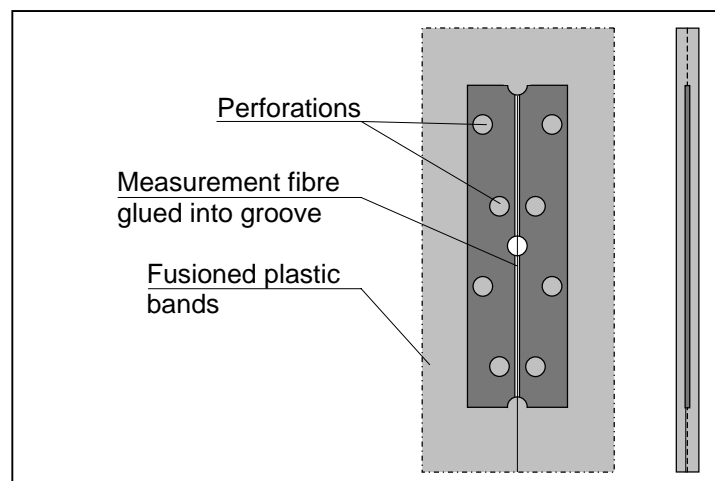


Figure 7.2.2: Anchor plaque between fused plastic bands
(represents detail A from Figure 7.2.1.)

Four Membrane Sensor specimens, named E1, E2, E3 and E4, with the active length of 25 cm are tested on a testing frame. The deformation is imposed to the Membrane Sensors step by step and deformation measurements are registered with the SOFO reading unit conventional

micrometer. The precision of these measurements has been of 0.3mm for the micrometer and 0.002 mm for the SOFO reading unit. Short and long term measurement were carried out. The testing set-up is presented in Figure 7.2.3.

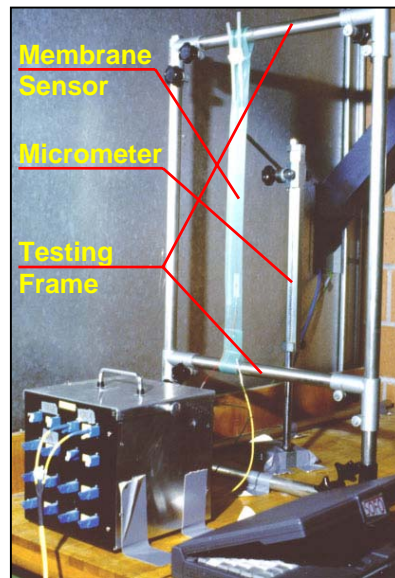


Figure 7.2.3: Membrane Sensor testing set-up

The short-term tests were carried out on all samples: E1, E2, E3 and E4. The behaviour of the samples was observed immediately after imposing the deformation. The samples were deformed and the deformation was measured, step by step, until a deformation of approximately 3.5% was achieved. Afterwards, the samples were relaxed, again step by step, and the measurement procedure was repeated.

Results have shown a correlation between Membrane Sensor and micrometer measurements of 99.6% - 99.9%. No sliding of the anchor plaques with regard to plastic bands is observed. The correlation between the Membrane Sensor and the micrometer obtained by specimen E1 is represented in Figure 7.2.4.

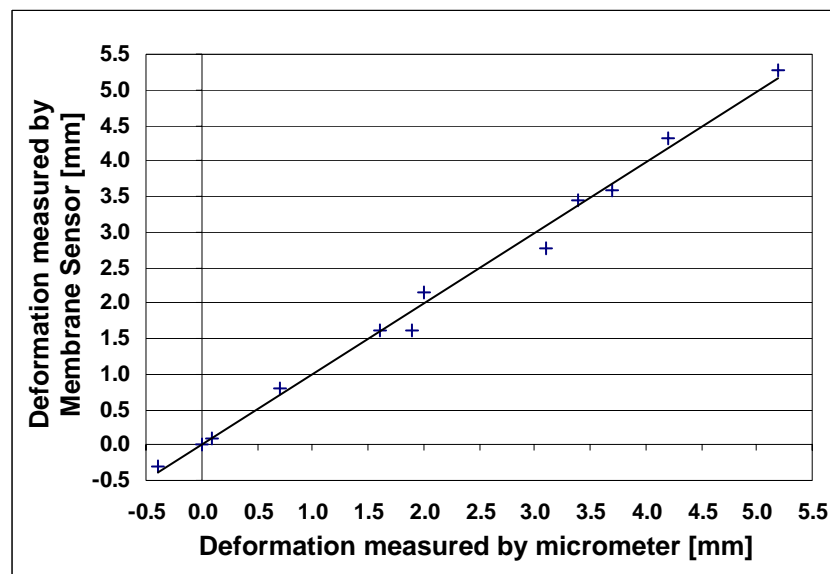


Figure 7.2.4: Correlation between Membrane Sensor and micrometer during short-term test

The goal of the long-term test was to register any creep of the sample and to prove the stability and the durability of the connection between the anchor plaques and the plastic bands.

If a constant deformation is imposed to the sensor, the distance between the anchor plaques is increased and a force is generated in the measurement fibre. This force perturbs locally the strain field around the anchor plaques, in the plastic part of the sensor. As a result the plastic creeps locally. The mechanism of creep is illustrated in Figure 7.2.5.

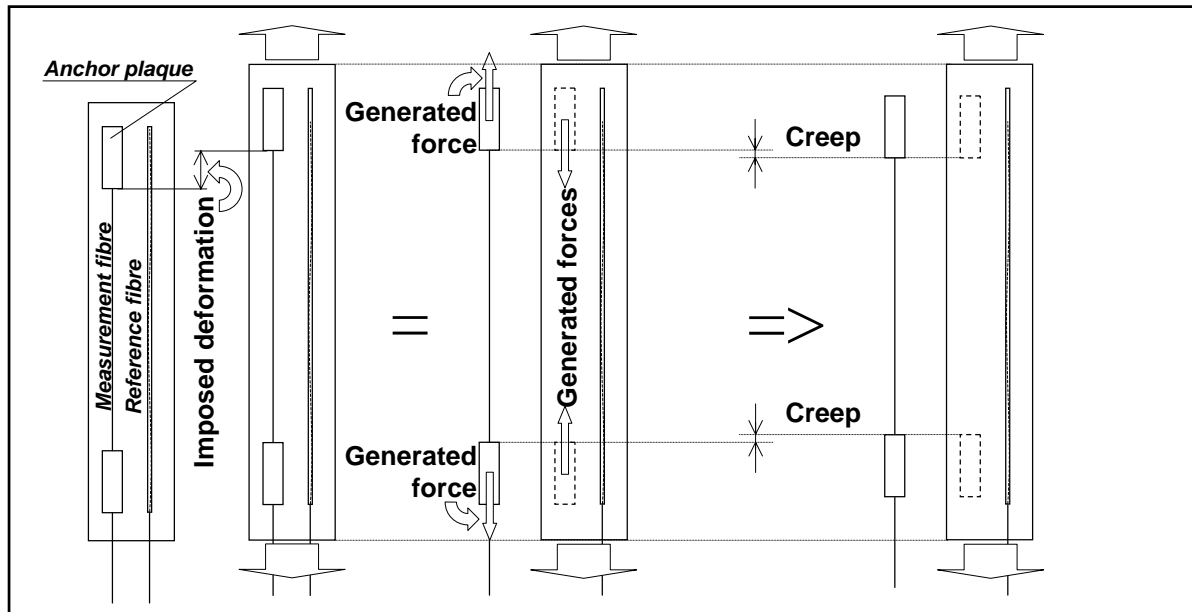


Figure 7.2.5: Mechanism of Membrane Sensor creep

The specimen E1 was deformed for about 3.0% in order to observe its creep. A significant creep is noticed after the first day. Later, it was less remarkable and finally minimised after ten days. The interaction between the anchor plaques and the plastic bands was as good as for the short-term test. The result of the creep test is presented in Figure 7.2.6. It has to be noticed that if the Membrane Sensor is installed on a membrane that does not creep, its creep will also be minimised.

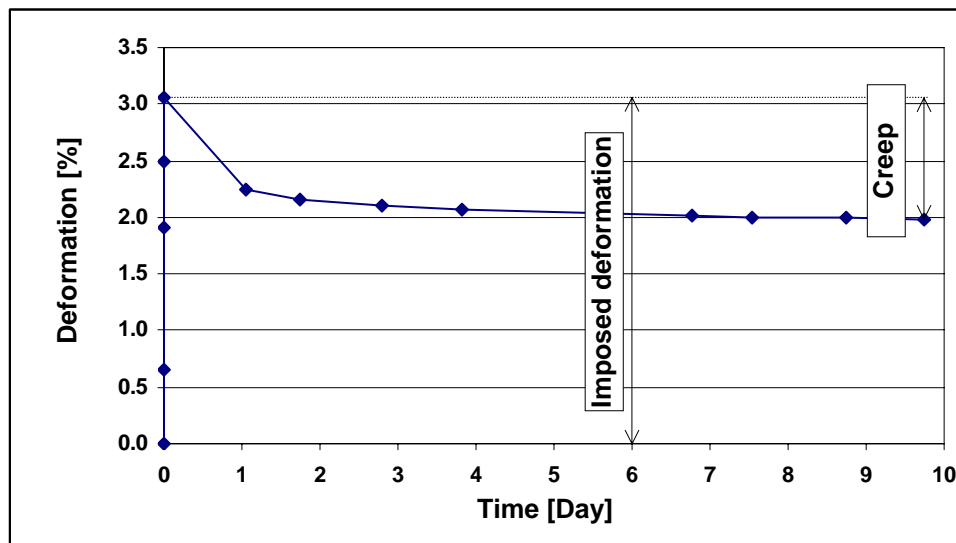


Figure 7.2.6: Result of long-term test

Load test

The thin plastic membranes are subjected to creep and therefore they can not withstand external loads if they are not reinforced. The reinforcing is frequently realised using Kevlar bands. The strength of reinforcing determines the capacity of the thin membrane structure or, in other words, if the reinforcing band fails than the structure it-self is endangered.

The long-term test has shown that the force in the measurement fibre influences the creep in the plastic bands. This creep could perturb the strain field of an observed element if it is made of a material that is also subject to creep. Therefore, it is not recommended to attach the Membrane Sensor to a zone without reinforcing. On the other hand, monitoring of the reinforcing bands is more important than monitoring of non-reinforced areas, because the reinforcing bands determine the capacity and deformed shape of a membrane structure.

In order to prove the adequacy of the Membrane Sensor to measure the deformation of reinforcing bands, the load test is performed. Two Membrane Sensors are tested. The length of active zones of the sensors was 1 m and 0.5 m, respectively. Both sensors are glued to a thin plastic membrane using thermal-activated glue, and the membrane is loaded by means of a hydraulic jack.

Figure 7.2.7 presents the equipment used for the installation of the sensor on the membrane: thermo-active glue, heat gun and roller.

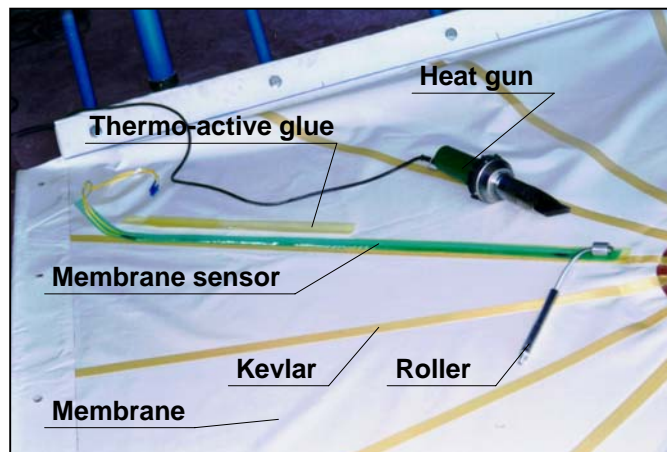


Figure 7.2.7: Membrane Sensor before gluing and gluing set-up

The longer sensor is positioned on the reinforcing Kevlar band and the shorter one is placed across the reinforcing bands, but its anchor plaques are glued over the bands. The design of the membrane and the emplacement of the sensors are represented in Figures 7.2.8.

The membrane is put in a stiff frame and pre-stressed in the horizontal plane. This set-up is shown in Figure 7.2.9. Vertical displacement is imposed step by step in the middle of the membrane by means of hydraulic jack (see Figure 7.2.9). Afterwards, the imposed displacement is removed, also step by step. The Membrane Sensors measured the deformations after each step. The results of these measurements are represented in Figure 7.2.10.

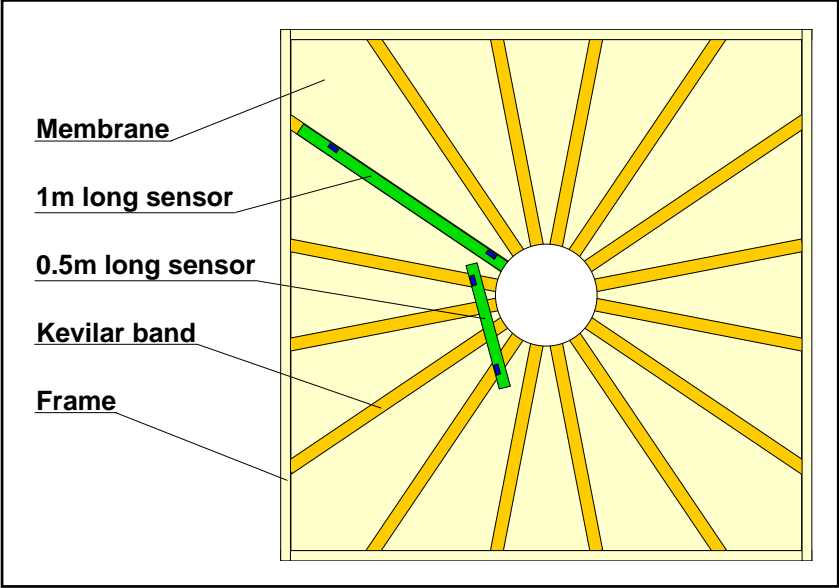


Figure 7.2.8: View to membrane and sensors emplacement

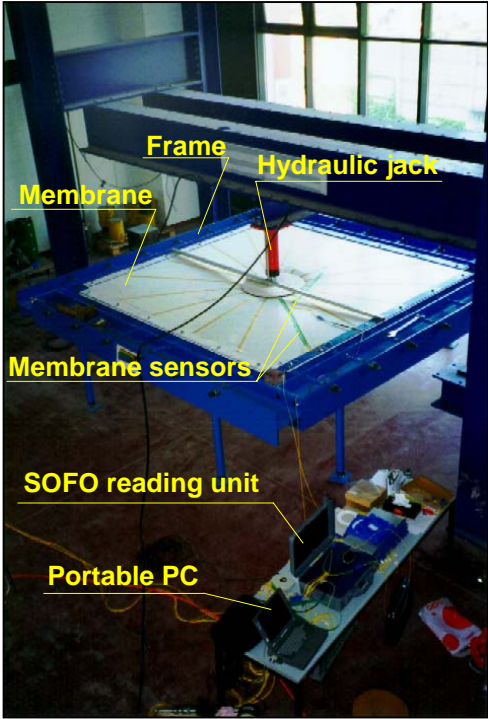


Figure 7.2.9: Disposition of load test

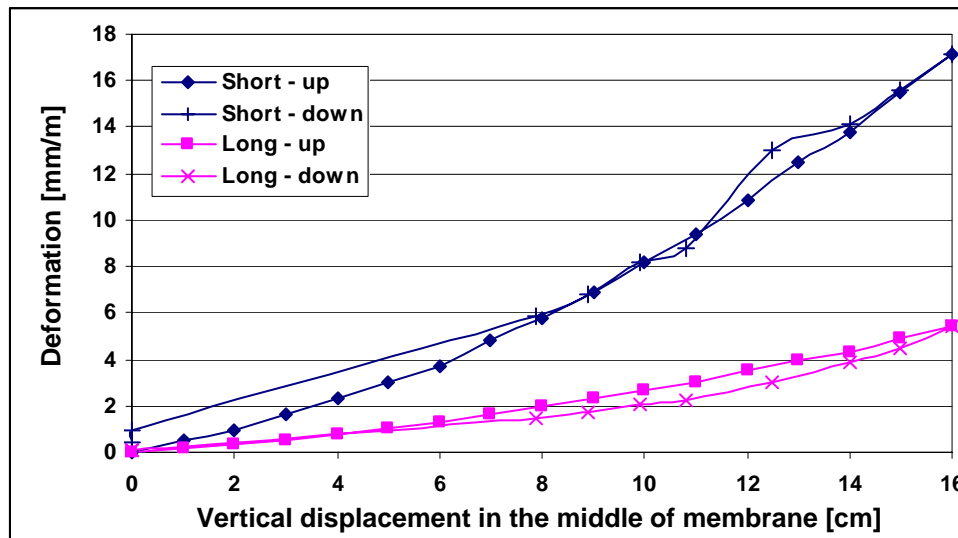


Figure 7.2.10: Results of load test

In Figure 7.2.10 the "Short - up", and "Long - up" denote the deformation measured by the longer (1 m long) and the shorter (0.5 m long) sensor, respectively, during the increase of the force. "Short - down" and "Long - down" correspond to the displacements recorded while removing the force. The steps of vertical displacement during the loading phase have been regular, each step equal to 1 cm. Contrary, the displacements while removing the load are not regular since it was difficult to control the hydraulic jack during this phase.

Result show a slight creep ($\sim 1.4\text{mm/m}$) measured by shorter sensor, when the displacement is removed. The membrane it-self was plastically deformed (folded) and the measured creep mainly originate from the slow membrane's return to its initial (non-folded) shape, but could also be influenced by the presence of the sensor. The longer sensor, attached to the Kevlar band, isd not register any significant creep. No sliding of the anchor plaques was noticed during the test. The measurement on the long sensor proves the ability of the Membrane Sensor to measure deformations of the reinforcing bands of plastic membranes.

More details related to above presented tests are given in [1].

Conclusions and remarks

From the presented tests, we conclude that a very good transfer of deformation from the assembled plastic bands to the measurement fibre can be realized by means of anchor plaques. The long-term test shows that the force in the measurement fibre influences the creep in the sensor's plastic part. This creep could perturb the strain field of a monitored element if this last is made of a material that is also subject to creep. Therefore it is recommended to attach the sensor to the parts of membrane that are not subjected to creep, i.e. to the reinforcing bands. Since the capacity and deformed shape of a membrane structure depends on the reinforcing bands behaviour, it is more important to monitor them than the non-reinforced parts of the membrane structure. The load test has proven the suitability of the Membrane Sensor for such kind of monitoring.

7.3 LONG SENSOR

Introduction

In order to understand the behaviour of very large structures such as dams or tunnels and to describe its deformed shape, it is important to measure deformations between two distant points in very long sections of a structure and/or to measure a relative displacement of the structure with regard to an external fixed point. This fixed point can be chosen several tens of meters deep in the ground, in a region non influenced by the presence of the structure.

Several conventional monitoring systems, such as rod extensometers [2], pendulums (normal or inverse), inclinometers, surveying networks, etc., exist and are used to monitor of large structures. However, some of them have certain drawbacks: delicate manipulation, sensitivity to temperature, humidity or electromagnetic fields, difficult installation, manual treatment of each measurement. Using an optical fibre measurement system it is possible to avoid all these inconveniences. Thus, the monitoring of large structures calls for the development of a fibre optic sensor with a very long active zone. Such a sensor, pragmatically called the Long Sensor, was developed in this thesis and is presented in following sections.

Design criteria

The sensor presented in this chapter is developed for use in existing structures, with idea to replace classical rod extensometers. Therefore the external dimensions of the sensor are limited by existing holes in which the rod extensometers are usually placed. In our case the maximum permitted external diameter of the sensor is 16 mm.

The anchorage of the sensor to the down-hole fixed point has to be the same as in case of the rod extensometer, i.e. using a bayonet system. Therefore the Long Sensor must be provided with torsional stiffness sufficient to transmit the force required to lock the bayonet system.

The length of the sensor is between 30 to 40 m and the transport, manipulation and installation may pose problems. It was decided to transport the sensor on a spool whose dimensions allow easy manipulation and fast installation. The diameter chosen for the spool is 155 cm, therefore the flexional stiffness of the Long Sensor has to allow winding on it.

The last limit was imposed by constructive problems. The measurement fibre of the Long Sensor has to be prestressed in-situ. Hence the upper anchor piece is fixed to the dam by means of a wedging screw. This system allows regulation of the measurement fibre prestressing, and rapid installation and dismantling.

Concept of Long Sensor

Maximal length of the active zone for the Standard Sensor is limited to 10m. The main problem for a sensor with an active zone longer than 10m is constituted by the friction between the reference and the measurement fibres that induces strains in the reference fibre and decreases the precision of the measurement.

In the case of a sensor with measurement basis longer then ten metres, the concept used for Standard Sensor (see Figure 2.3.1) can not guarantee the independence of the reference fibre

and the measurement fibre. It is therefore necessary to separate the fibres, and place them in different tubes. Two considered solutions are shown in figure 7.3.1.

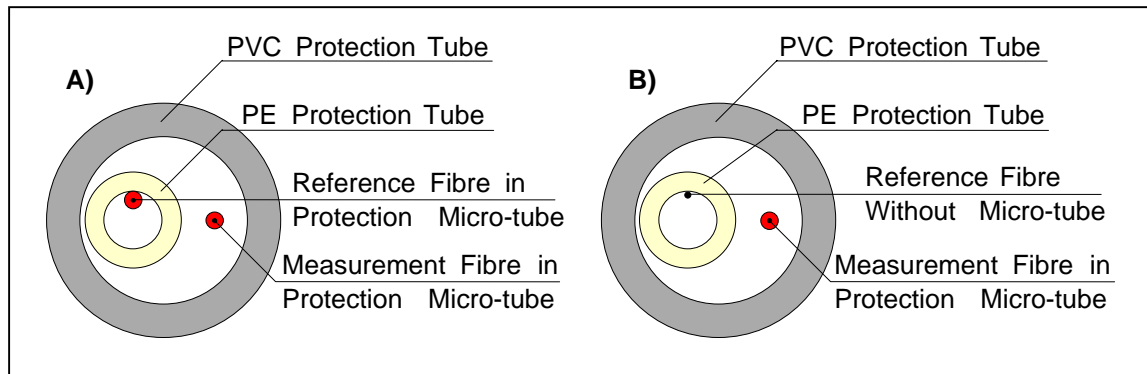


Figure 7.3.1: Cross-section of Long Sensor: A) First version, applied on sensor B3 and B) Final version, applied on sensor F3

The difference between the two solutions is the protection of the reference fibre. In the first version the reference fibre was protected by plastic micro-tube, but a creep of this micro-tube occurred during the measurements and perturbed the functioning of the reference fibre. Hence, the micro-tube was removed in the final version.

Being relatively fragile, the measurement fibre was firstly protected by a plastic micro-tube (external diameter 0.9mm). In order to separate the reference fibre from the measurement fibre, the reference fibre was put in a polyethylene (PE) tube (int./ext. diam. 3.0/5.0mm), and finally the whole assembly was protected inside by a PVC tube (int./ext. diam. 8.7/12.2mm). The reference fibre in the PE tube is helicoidally shaped as in case of the Standard Sensor (Figure 2.3.1).

In-situ test

Two Long Sensors, named B3 and F3, were built in order to replace two rod extensometers [2] in the Emosson dam in Switzerland. The external PVC tube is chosen in a way that satisfy all limits imposed by sensor installation and manipulation.

Since both sensors are installed inside the dam, we had to respect the local accessibility situation (dimension of elevator, doors, gallery,...). For the transport from the lab to the site, the sensors had been spun up on a wooden spool. A view to the Emosson dam and to one of two Long Sensors is shown in Figure 7.3.2.

In the dam, once the old mechanical extensometer was dismantled, the installation of the Long Sensors proceeded rapidly. The sensors had to be pretensioned in situ because of the manner of fixation: the upper anchor piece is connected to the dam by means of a wedging screw. The lower anchor piece is fixed to the rock using a bayonet anchor, the same used by the dismantled rod extensometer. Within half a day the sensors were installed and ready to measure.

When fabricating a sensor in the lab, it is very important to be aware of the climatic conditions present on the site. Especially for the Emosson dam gallery where the relative humidity goes up to 90% and the temperature is all the year round at about 5 °C. This

information, as well as the length of prestressing (approx. 0.5% of the length of the active zone of the sensor), have to be considered when the dimensions of the components of a sensor are defined.



Figure 7.3.2: Emosson dam and Long Sensor on transporting spool

In order to centralise the monitoring of the new sensors, situated at opposite ends of the dam, optic extension cords have been installed. In this way the two sensors can be measured from a common point without having to move the reading unit. Using this set-up, it is even possible to monitor the sensors automatically over a longer period of time without any human intervention.

The schema of the installed sensors and the principle of monitoring are given in Figure 7.3.3. The position of the sensors in the dam is presented in Figure 7.3.4.

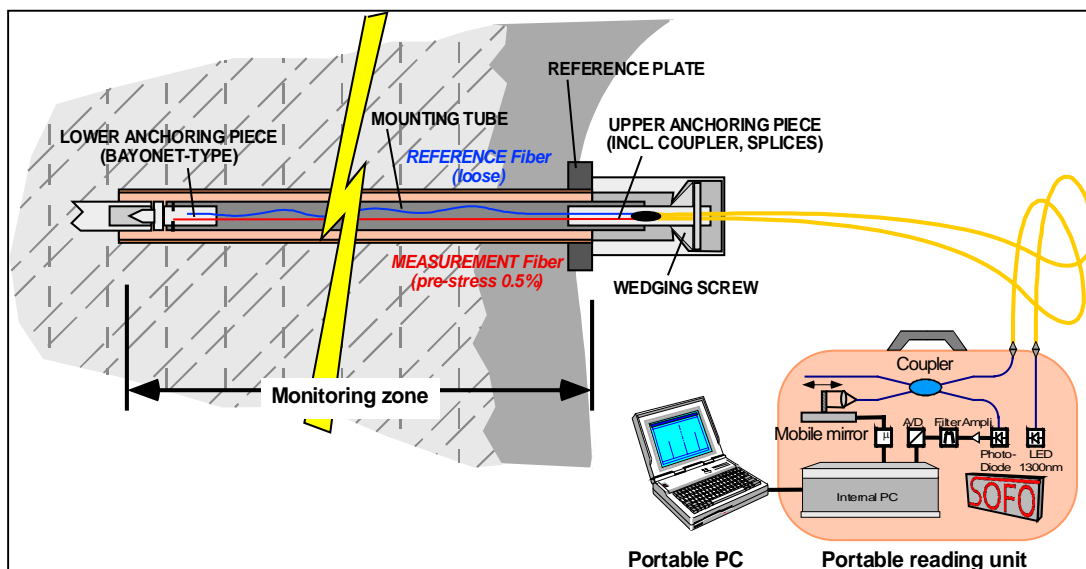


Figure 7.3.3: Schema of sensors and principle of monitoring applied in Emosson dam

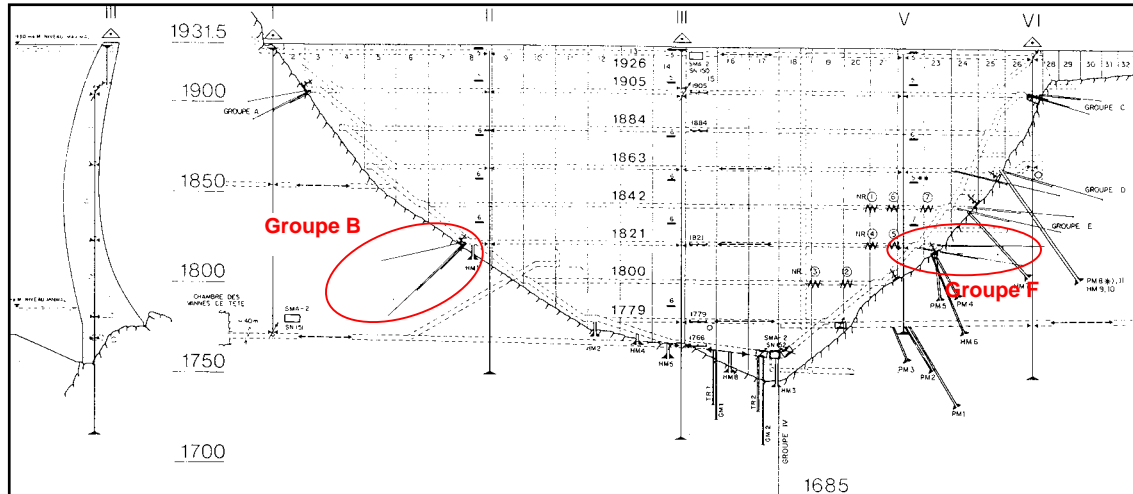


Figure 7.3.4: Position of sensors and rod extensometers in Eموsson dam

The Long Sensors B3 and F3, 39 m and 30 m long respectively, are mounted side by side with the rod extensometers B4 and F4. The monitoring started in October 1996. As mentioned previously, creep of the sensor B3 pushed us to improve the design of the Long Sensor. The improved design has been successfully applied to sensor F3, therefore only the results of this sensor are presented and analysed.

The 30 m Long Sensor F3 is placed close and parallel to the 60 m long extensometer F4. In order to compare more clearly the results of the measurements the deformation measured by extensometer is divided by a calculated correlation coefficient, which is equal to 2.0174. The improved F3 sensor was installed in October 1997. Its measurements, the measurement data of the extensometer, the difference between the Long Sensor and the extensometer and the water level in the dam are represented in Figure 7.3.5. The measurements are performed periodically once a month, with some exceptions.

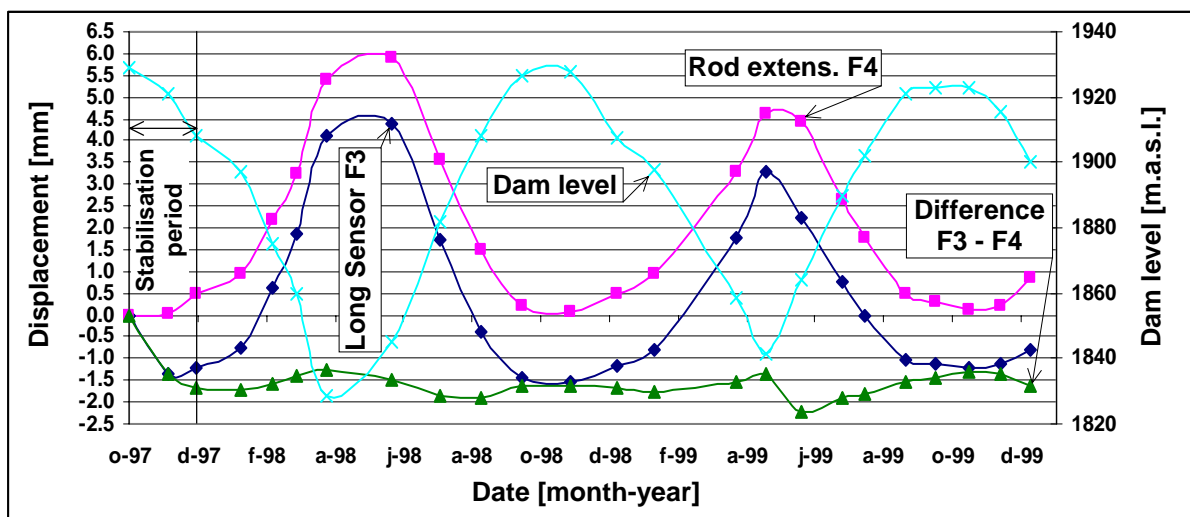


Figure 7.3.5: Measurements of rod extensometer F4 (divided by coefficient of correlation 2.0174) and measurements of Long Sensor F3

Some creep of the Long Sensor F3 has been noticed during the first two months following the installation (see Figure 7.3.5). This period is considered as a stabilisation period of the Long Sensor. The creep is due to residual stresses in the plastic parts of the sensor, the PVC and PE

tubes. The stresses are caused by transport and by the temperature and humidity differences between the sites of the Long Sensor fabrication (IMAC laboratory , 20°C, ~50% RH) and installation (Emosson dam, 5°C, ~90% RH). The stabilisation period is unavoidable if plastic pieces are used in the sensor design.

After two months the difference between the sensors begins to alternate around a constant value depending on the water level. These differences can be attributed to the different sensitivities of the sensors, but also to their different gage length. A comparison of the measurements after the stabilisation period is represented in Figure 7.3.6, and their correlation in Figure 7.3.7.

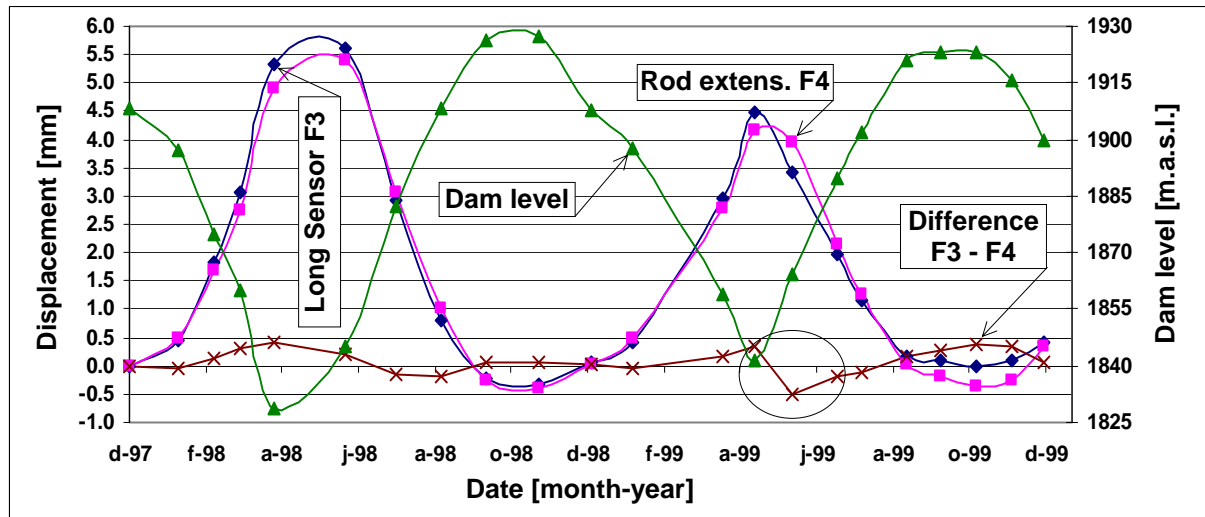


Figure 7.3.6: Comparison between measurements of rod extensometer F4 (divided by coeff. of correlation 2.0174) and measurements of Long Sensor F3 after the stabilisation period

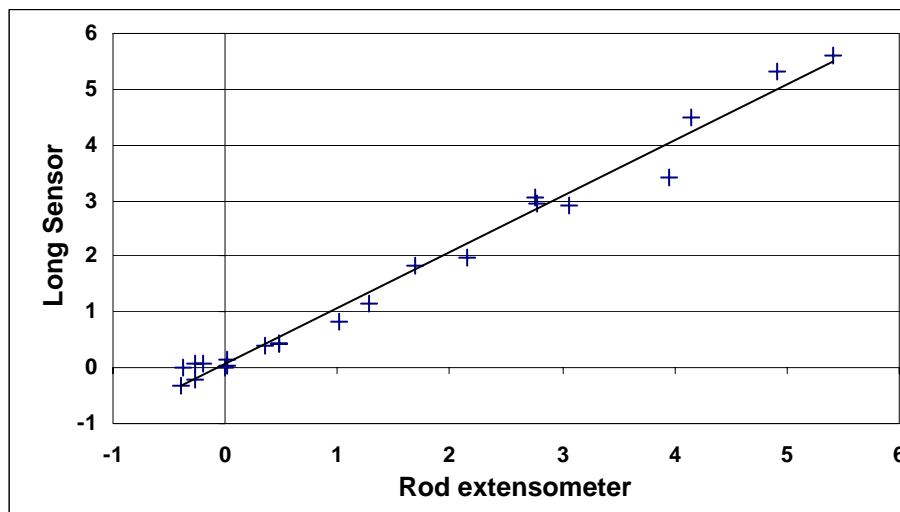


Figure 7.3.7: Correlation between measurements of rod extensometer F4 (divided by coeff. of correlation 2.0174) and measurements of Long Sensor F3 after the stabilisation period

Results given in Figures 7.3.6 and 7.3.7 show a very good agreement between the two compared systems and prove the correct functioning of the long SOFO sensor. The correlation is better than 99.2%. Moreover the response of the Long Sensor is faster than the rod extensometer response, meaning that the Long Sensor is more sensitive than the

extensometer. The lagging of the extensometer with regard to the Long Sensor is expected. It is a consequence of the friction between the extensometer and the walls of the hole in which it is placed. The biggest delay of the extensometer is registered just after the dam level starts to increase. At this time the force of friction changes sign, increasing the duration of inactivity of the extensometer. This effect is even more pronounced in the year 1999 (see encircled area in Figures 7.3.7).

The fact that the Long Sensor is more sensitive than the extensometer is more noticeable in Figure 7.3.8 representing the dependence of deformation with respect to the water level. The hysteresis of the Long Sensor being smaller than that of the extensometer indicates a better sensitivity of the Long Sensor. Colenco Power Engineering AG, official expert for monitoring of Emossion dam has performed statistical analysis of results provided by Long Sensor. The analysis has confirmed accurate functioning of the Long Sensor.

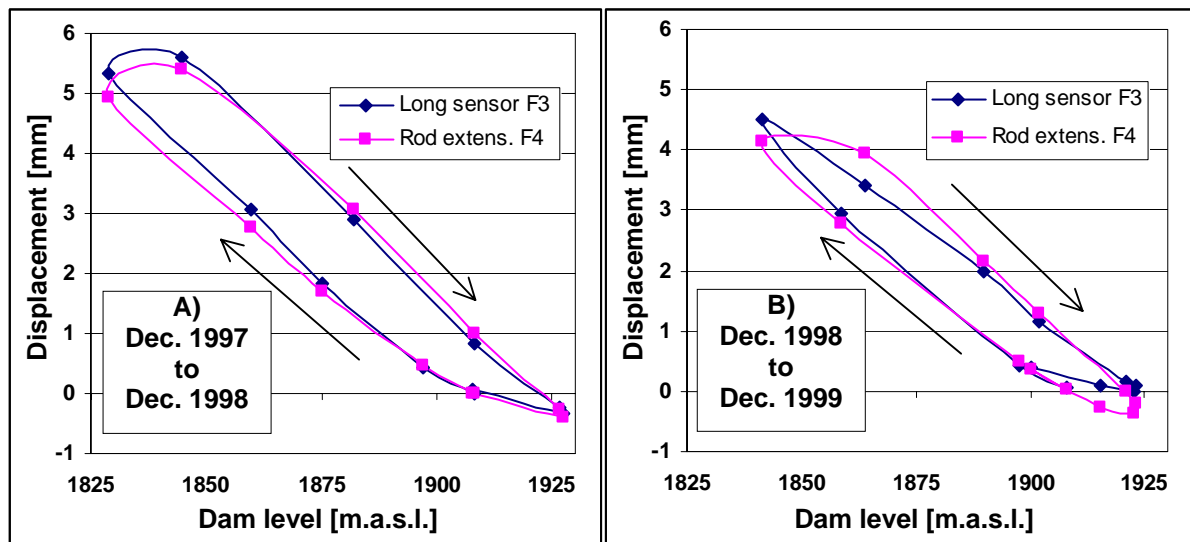


Figure 7.3.8: Measurements of Long Sensor F3 and rod extensometer F4 with respect to dam level; A) From Dec. 1997 to Dec. 1998 and B) from Dec. 1998 to Dec. 1999

More details related to the fabrication, testing, installation and measurements performed by the Long Sensor are given in [3].

Conclusions and remarks

The Long Sensor creeps right after the installation because of the deformation of the sensor's plastic parts during transportation. The creep stabilises after approx. 60 days. Therefore it is recommended to consider the measurement as valid only 60 days after the installation. Once stabilised, the Long Sensor continues to work correctly and achieves a very good correlation with the rod extensometer. It is the first time that a 30 metres Long Sensor has been implemented in a dam and compared with a classical monitoring system. The comparison proves its good functioning. The difference between two systems is always within $\pm 0.5\text{mm}/30\text{m}$, i.e. better than 2%.

The Long Sensor is more sensitive than the rod extensometer. It is also more precise than the rod extensometer (less hysteresis). Those facts and general advantages of the fibre optic monitoring system (long term stability, no calibration, insensitivity to electro-magnetic fields, no grounding required, possibility of permanent remote-monitoring, etc.), the use of the Long Sensor is recommended for dam monitoring.

7. 4 STIFF SENSOR

Introduction

The Stiff Sensor is destined to measure the hardening time of concrete. The problem of determination of hardening time is explained in details in Sections 3.7 and 6.3. In Section 6.3 we have proposed a method for the monitoring of the hardening time using a Stiff Sensor. The concept of the sensor, the results of the measurement and the ideas behind the tests are presented there. In this Chapter we only present tests related to the development of the sensor.

Design criteria

The procedure for the hardening time measurement, proposed in Section 6.3, consist of a comparison between deformation measurements of a Standard and a Stiff Sensor placed side by side in fresh concrete. The moment when the difference between their measurement becomes constant, corresponds to the hardening time of concrete. A suitable Stiff Sensor has to satisfy two main conditions:

- The thermal deformation of the Stiff Sensor must be different from the total deformation of concrete at very early age. This condition guarantees the incompatibility of the deformation measured by the Stiff and the Standard Sensors before concrete hardening. In this phase, the concrete is subjected to thermal and autogenous deformations, while the Stiff Sensor is subjected to its thermal deformation and to deformation transferred from concrete. If the deformation of concrete at very early age is equal to the one of the Stiff Sensor, there will be no mismatch and both sensors will measure the same deformations. Thus, the difference between the measurement will always be constant.
- The Stiff Sensor has to be several order of magnitudes stiffer than the concrete at very early age. This condition guarantees the mechanical independence of the Stiff Sensor before concrete hardening. The maximal value of Young modulus of hardened concrete is rarely higher than 50 GPa. In order to avoid an exaggerated cross-section of the Stiff Sensor, it is therefore sufficient to design a sensor with an Young modulus greater than 100 GPa.

Concept of the Stiff Sensor

The design of the Stiff Sensor is similar to the one of the Standard Sensor (see Figure 6.3.3.1). The Young modulus of the Stiff Sensor protection tube is several order of magnitudes bigger than the Young modulus of concrete, and the TEC of the tube is chosen to guarantee the incompatibility of the deformations between concrete and the Stiff Sensor.

Tests

The tests proving the principle of the hardening time measurement are presented in Section 6.3. Steel was used for the fabrication of the Stiff Sensors. Since the Young modulus of the steel is 210 GPa, the second of above cited criteria was satisfied.

The first criteria had to be tested. The dependence of the thermal deformations of the Stiff Sensor was compared with the very early age deformations of concrete.

Two 60 cm long Stiff Sensors, named A1 and A2, were exposed to temperature variation of approximately 40°C. The sensors are first heated to approximately 50°C, and afterwards cooled to approximately 10°C. The deformation were measured using the optical fibres installed in the sensor itself. A type "K" thermocouple has been attached to each sensor in order to measure its temperature. The precision of the temperature measurements was 0.5°C. The results are presented in Figures 7.4.1 and 7.4.2 for the sensors A1 and A2 respectively.

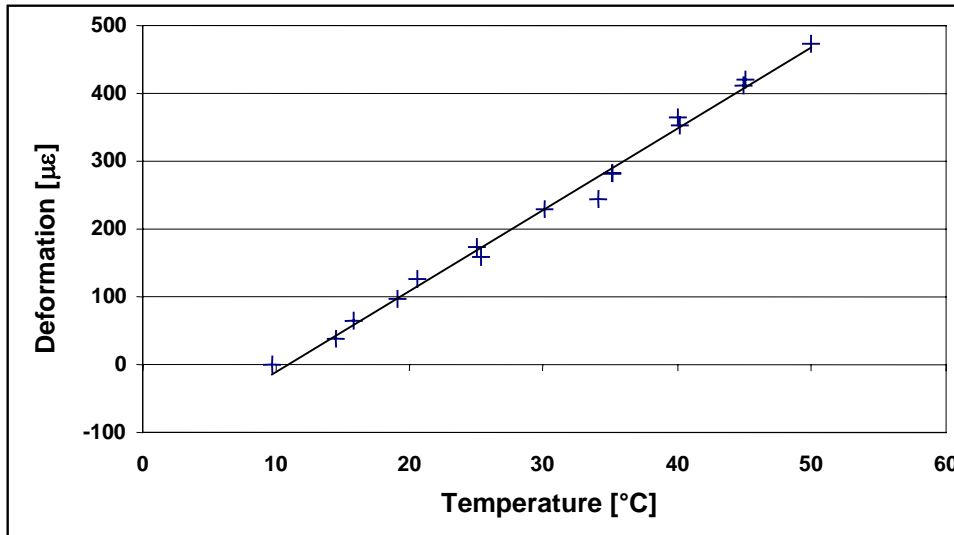


Figure 7.4.1: Correlation temperature-Stiff Sensor deformations for sensor A1

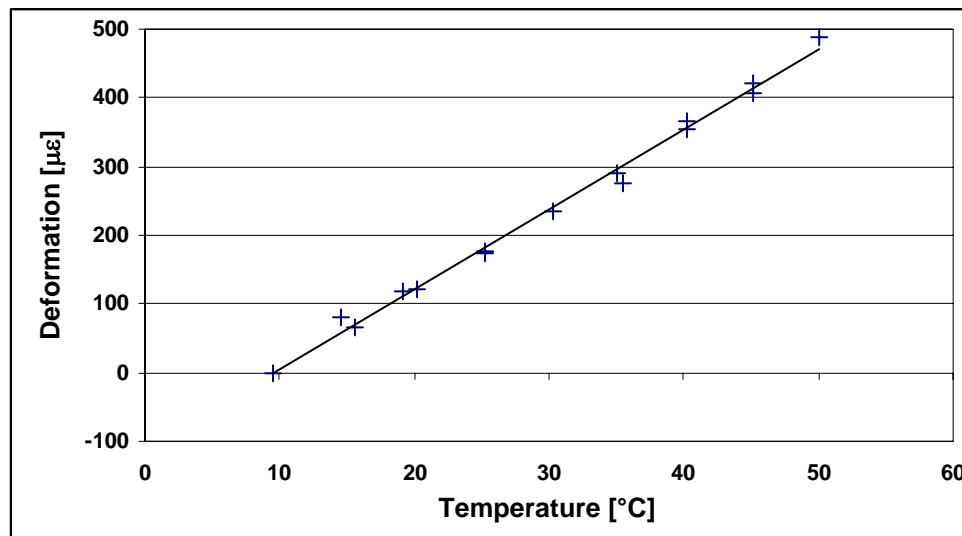


Figure 7.4.2: Correlation temperature-Stiff Sensor deformations for sensor A2

The results show a linear response of the Stiff Sensor. The degree of correlation for both sensors is 99.7%. The obtained values of TEC are $1.196 \cdot 10^{-5} \text{ } ^\circ\text{C}^{-1}$ for the sensor A1 and $1.157 \cdot 10^{-5} \text{ } ^\circ\text{C}^{-1}$ for the sensor A2. Those results are reasonable since the Stiff Sensor is made of steel, whose response is known to be linear and its TEC is approximately $1.2 \cdot 10^{-5} \text{ } ^\circ\text{C}^{-1}$.

The sensors A1 and A2 were used for the **second experiment** described in Section 6.3.3. Unfortunately, sensor A2 has been damaged 7 hours after the pouring. Hence only the results provided by the sensor A1 are presented in Section 6.3.3. To facilitate the reading of this Chapter these results are presented again in Figure 7.4.3, with the addition of the temperature

measurements. The temperature measurements were again carried out using the thermocouples. The set-up did not allow continuous temperature measurements.

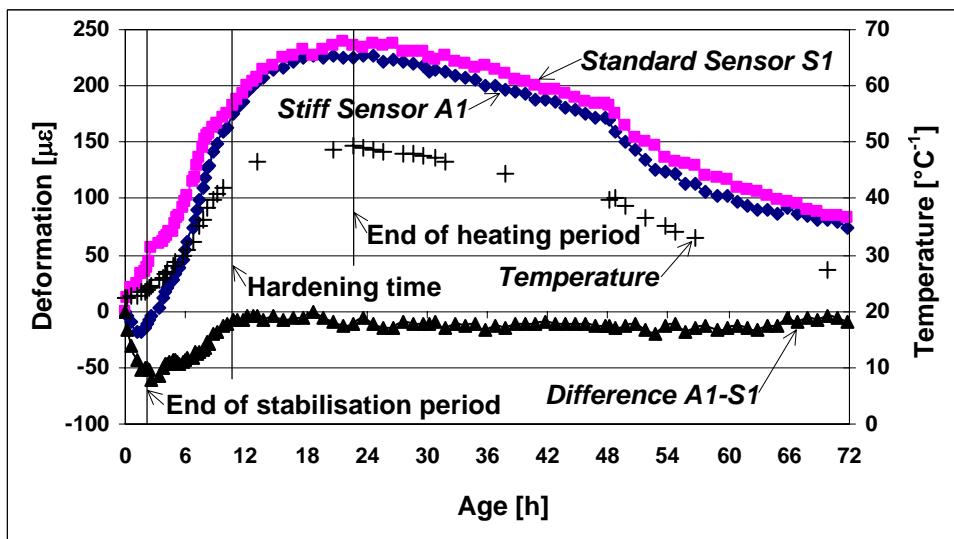


Figure 7.4.3: Very early age deformation, temperature and hardening time measurements of concrete slab

The correlation temperature vs. very early age of concrete used in the second experiment (see Section 6.3.3) is presented in Figures 7.4.4, 7.4.5 and 7.4.6. Figure 7.4.4 presents the correlation during the period starting with the end of stabilisation period (2 hours after the pouring) and ending at the hardening time. The correlation from the hardening time to the moment when the maximal temperature is achieved (end of heating) is presented in Figure 7.4.5. Finally the period of temperature decrease is shown in Figure 7.4.6.

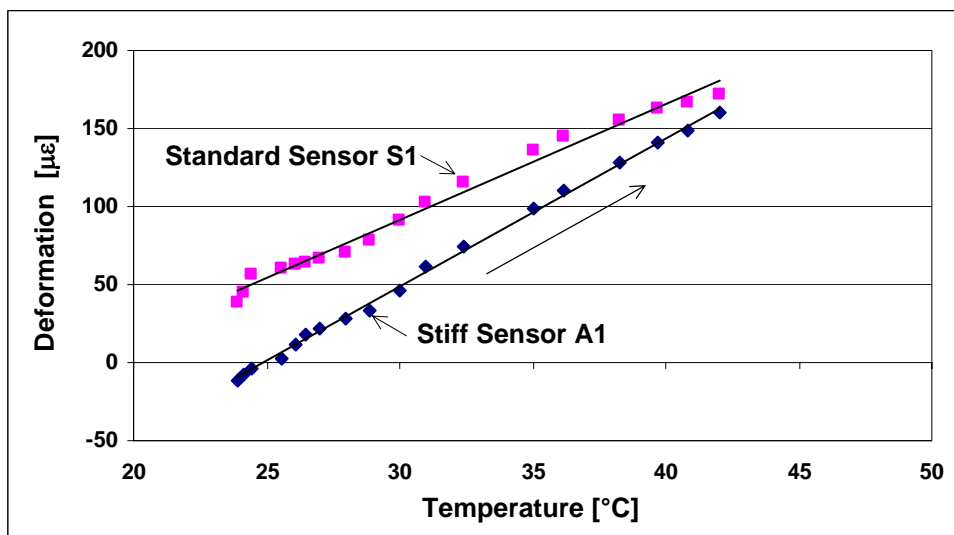


Figure 7.4.4: Correlation temperature-concrete very early age deformation, from stabilisation period to hardening time

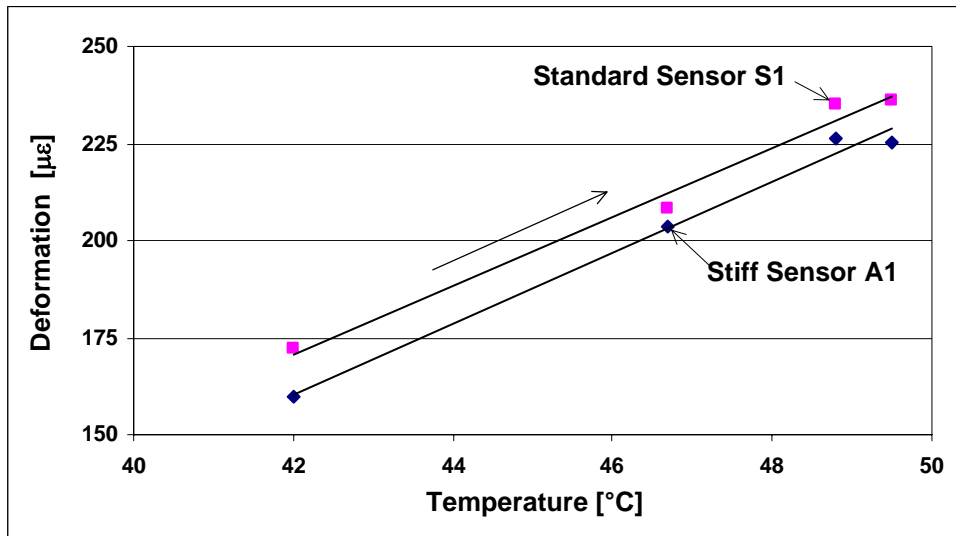


Figure 7.4.5: Correlation temperature-concrete very early age deformation, from hardening time to maximal temperature peak

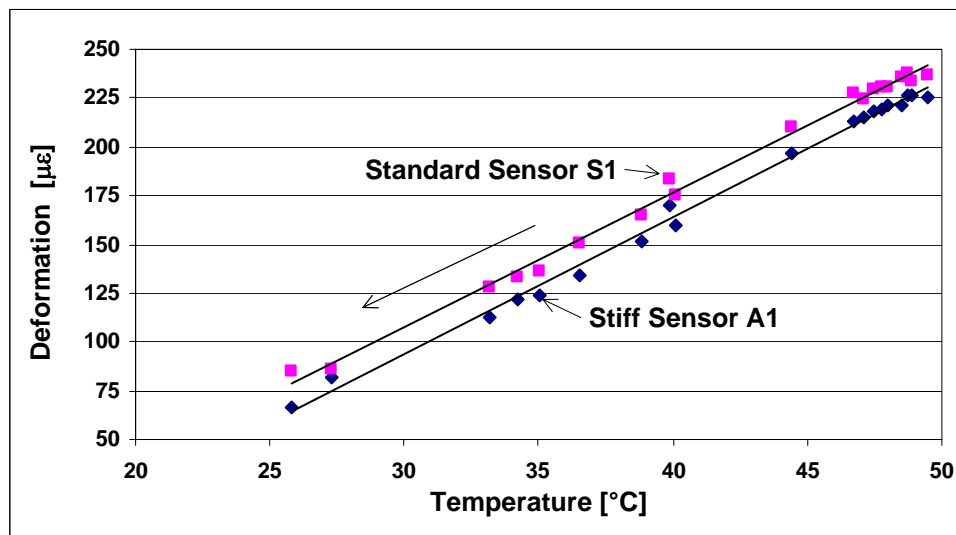


Figure 7.4.6: Correlation temperature-concrete very early age deformation, decreasing temperature period (cooling)

The early age deformation of concrete slab is consist of thermal and autogenous deformation. It is partially restrained by the walls of formwork and by the friction with its base. The deformations of Stiff Sensor are fundamentally thermal, but it is also restrained by the interaction with the surrounding concrete.

During the period delimited by the end of the stabilisation period and the hardening time, the coefficient of correlation between temperature and the Stiff Sensor deformations is $0.952 \cdot 10^{-5} \text{ } ^\circ\text{C}^{-1}$. This is about 20% less than the TEC determined for the sensor ($1.2 \cdot 10^{-5} \text{ } ^\circ\text{C}^{-1}$). It proves that the deformations of the Stiff Sensor are restrained by concrete. On the other hand, the correlation between the very early age deformation of concrete as measured by the Standard Sensor during the same period is $0.743 \cdot 10^{-5} \text{ } ^\circ\text{C}^{-1}$. This result proves that during the very early age there is no compatibility between the deformations of the Stiff Sensor and of the surrounding concrete. We notice that the TEC of concrete during this period is at list two

times higher than the above mentioned coefficient, but due to autogenous shrinkage, and especially due to restraining of deformation by the formwork, this coefficient is found to be smaller.

During the period delimited by hardening time and the end of heating, concrete is hardened, and therefore the coefficients of correlation of the Stiff Sensor and the concrete are approximately equal. The calculated values are $0.914 \cdot 10^{-5} \text{C}^{-1}$ and $0.886 \cdot 10^{-5} \text{C}^{-1}$ for the stiff and the Standard Sensors, respectively. The difference between them is only $\sim 3\%$. The calculated coefficients are smaller than the TEC of the Stiff Sensor. This proves the good functioning of the Stiff Sensor. Here we notice that the coefficient of concrete is higher in this phase than in the previous one, because concrete is hardened and the effect of the formwork restraining is therefore reduced.

During the period of cooling the thermal expansion coefficients are still approximately equal ($0.701 \cdot 10^{-5} \text{C}^{-1}$ for the Stiff Sensor measurement, and $0.689 \cdot 10^{-5} \text{C}^{-1}$ for the Standard Sensor measurement, the difference between them is less than 2%) and different than the TEC of the Stiff Sensor, again proving the soundness of the Stiff Sensor design. The coefficients are smaller than previously, since the TEC of concrete decreases with age.

A recapitulation of the calculated coefficients of correlation is presented in Table 7.4.1. All coefficients are calculated using a linear regression. The degree of correlation is for all cases better than 99%.

	<i>Correlation temperature - Stiff Sensor [$\cdot 10^{-5} \cdot \text{C}^{-1}$]</i>	<i>Correlation temperature - very early age deformation [$\cdot 10^{-5} \cdot \text{C}^{-1}$]</i>	<i>Difference [%]</i>
<i>Stabilisation period to hardening time (~2 to ~10 hours, Figure 7.4.4)</i>	0.952	0.742	28.30
<i>Hardening time to end of heating (~10 to ~23 hours, Figure 7.4.5)</i>	0.914	0.886	3.16
<i>End of heating to ~72 hours (Figure 7.4.6)</i>	0.701	0.689	1.74

Table 7.4.1. Recapitulation of coefficients of correlation temperature-deformation for the Stiff Sensor and concrete (as measured by a Standard Sensor)

Conclusions and remarks

Using a sensor pair made of one Stiff and one Standard Sensor, it is possible to determine the hardening time of concrete. The principle of functioning of the Stiff Sensor is based on incompatibility of its thermal deformation with the very early age deformation of concrete. This principle is confirmed by experiments. The correlation between the sensor properties (stiffness, length, etc.) and the Young modulus of concrete should be investigated in more detail in order to find an optimal compromise acceptable for all types of concrete. No special laboratory conditions are needed, therefore the Stiff Sensor can be used in-situ without restrictions.

7.5 DISPLACEMENT SENSOR

Introduction

All evidence indicates that new physics, and answers to some of the most profound scientific questions of our time, lie at energies around 1 TeV. To look for this new physics, the next research instrument in Europe's particle physics armory is the Large Hadron Collider (LHC). This challenging machine will use the most advanced superconducting magnet and accelerator technologies ever employed. LHC experiments are being designed to look for theoretically predicted phenomena.

European Organization for Nuclear Research (CERN) has been interested in measuring the relative horizontal displacements between the cold mass and the external vacuum tube called the vacuum vessel of the Large Hadron Collider (LHC) cryodipole. Due to the extreme environmental conditions (the displacement measurement must be made in vacuum and between two points with a temperature difference of more than 200°C) no adequate existing monitoring system was found for this application. It was therefore decided to develop a new optical sensor, called Displacement Sensor, suitable for this application.

Description of LCH

The LHC [5] will consist of two colliding synchrotrons installed in the 27 km tunnel. They will be filled with protons and two superconducting magnetic channels will accelerate them. To bend 7 TeV protons around the ring, the LHC dipoles must be able to produce fields of 8.36 Tesla. Superconductivity makes this possible. The LHC machine will contain around 2000 main ring superconducting magnets cooled at 1.9 K by super-fluid pressurized helium, mainly 15 m-long dipoles with their cryostats and 6 m-long quadrupoles. Figure 7.5.1 shows the concept of one of the 15 m-long LHC cryodipole.

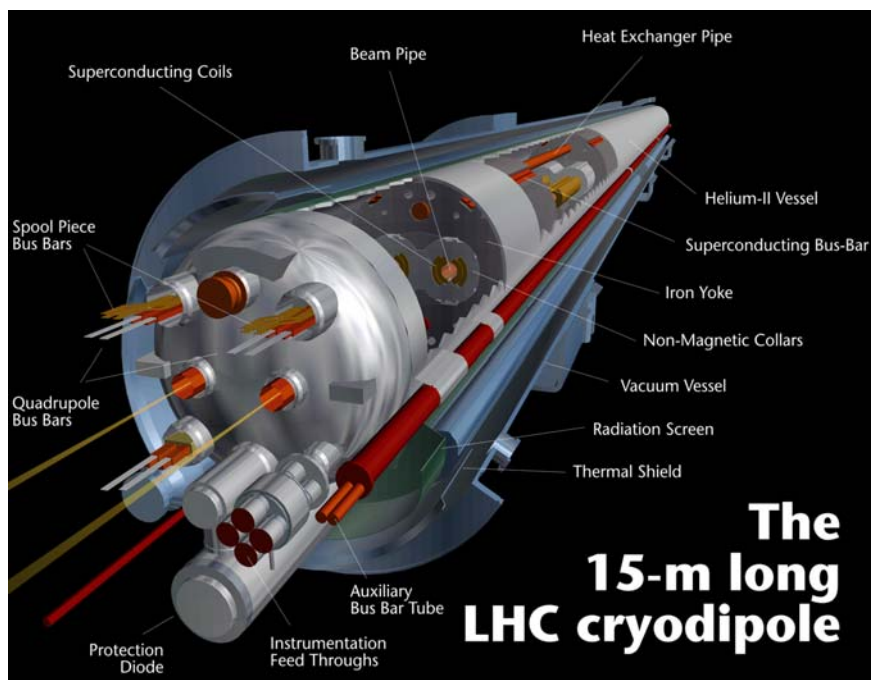


Figure 7.5.1: Concept of the LHC cryodipole [5]

The magnet dipole enclosed in the Helium Vessel with heat exchanger and cold bore tubes, forms the dipole cold-mass. The work temperature of the cold-mass is 1.9K. The cryostat of the dipole magnet consists of the three supports to position the cold mass, a radiation screen and a thermal shield both equipped with multi-layer super insulation, and a vacuum vessel. The dipole cold-mass assembled into the cryostat forms the Cryodipole Magnet. Figure 7.5.2 shows a cross section of the LHC 15 m dipole cryomagnet in the plane of an extremity support post.

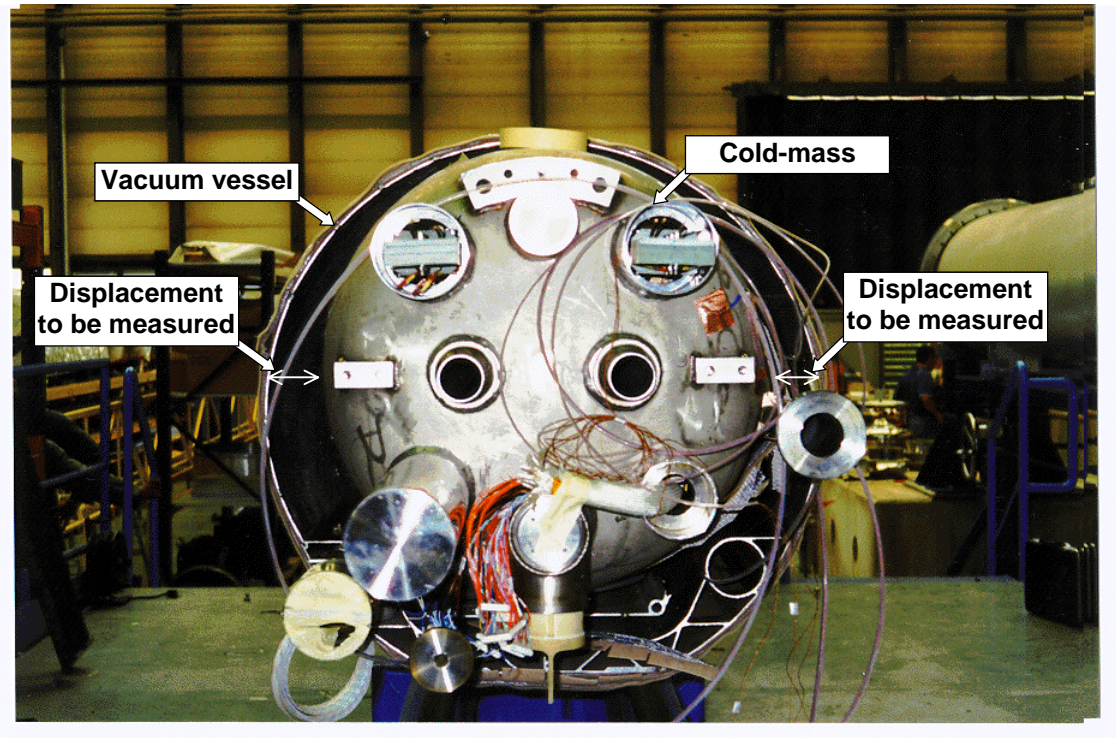


Figure 7.5.2: Cross section of the LHC dipole magnet

To insure the correct functioning of LHC it is necessary to know the real position of the cold mass in to the vacuum vessel. This allows positioning the particle beam relative to the surveying points placed on the external face of the vacuum tube. During cooling and increase of the magnetic field, the cold-mass changes its size, shape and position. The expected longitudinal deformation of the 15m long cold-mass will be of the order of 20 mm, caused mainly by thermal contraction. More difficult and more important is the determination of the horizontal displacement of its extremities (see Figure 7.5.2). This was the main goal of this work.

Design criteria

The extreme environmental conditions and the geometry have imposed several conditions to the displacement sensors:

- Since the longitudinal displacement is so important (20 mm), it is not possible to install an optical fibre between the vacuum vessel and the cold mass. Therefore it was decided to use a light beam propagating in the space between an optical head installed on the inner wall of the vacuum vessel and a mirror attached to the external surface of the cold mass.

Optical fibres are used as reference path in the optical head and to bring the light in / out of the vacuum tube.

- The solution requires the use of a mirror attached to the cold mass. The mirror must be undamaged to temperature of 1.9K
- The optical head consists of reference fibre, coupler, ferule, mirror and lens. The maximal permitted transversal dimension of the optical head is 30 mm because of space limitations.
- The optical head, installed in interior of the vacuum vessel is to be connected with the reading unit, which is in exterior, hence a special vacuum feedthrough must be conceived.
- All parts of the sensor must survive the vacuum without significant outgas.
- The sensor must guarantee an correct measurement even if the cold-mass mirror is subjected to tilt
- The working distance of the sensor is approximately 150 mm

All these problems are solved and presented in next subsections.

Concept of Displacement Sensor and feedthrough

Schematic representation and photo of the optical head without the covering as well as principle of functioning of the Displacement Sensor are presented in Figure 7.5.3.

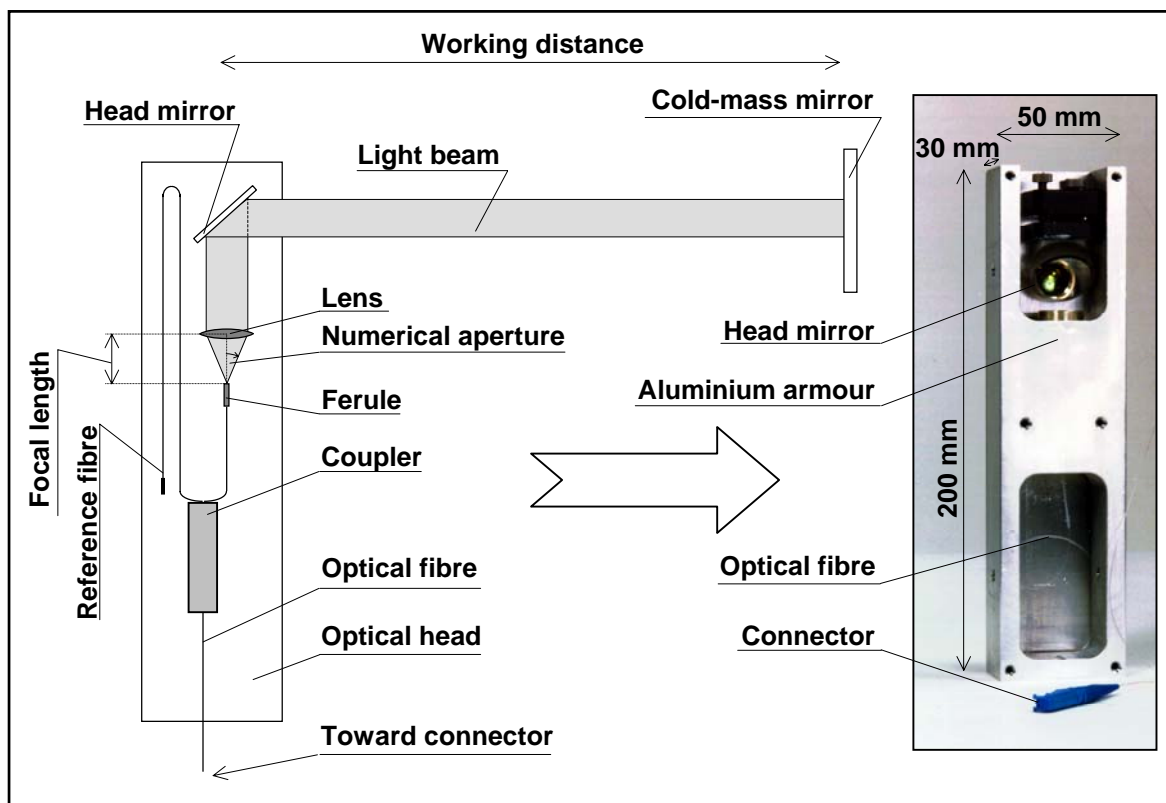


Figure 7.5.3: Schema, photo and principle of functioning of Displacement Sensor

The optical head is attached to the internal side of vacuum vessel. It consists of the coupler, reference fibre, ferule, lens and the head-mirror (see schema in Figure 7.3.5). All parts of the optical head are protected by aluminium armour. The other mirror is fixed on the cold mass.

The optical path and the reference fibre have about the same optical length and constitute a Michelson interferometer. This interferometer is demodulated using an existing SOFO path-matching readout system (see Chapter 2).

The optical head, including the reference fibre, is thermalised with the vacuum vessel hence it works under almost constant room temperature. The cold-mass mirror is subjected to temperatures as low as 1.9K ($\sim -271^{\circ}\text{C}$). Tests showed that an high quality mirror with gold coating could survive these extreme conditions without damaging.

The sensor works as follows: The broadband light coming from reading unit is split by the coupler. One path goes into the reference fibre while the second leaves the fibre trough a metallic ferrule which is collimated by the lens and pointed by the head mirror towards the cold-mass mirror. It reflects off the cold-mass mirror, goes back to the ferrule and is collimated on a point on the ferrule, close to the optical fibre end, but not on it. The reflected light travels back to the cold-mass and is finally reflected and collimated back in the optical fibre. Since the fibre core and the reflection point on the ferrule are conjugated points with respect to the lens-mirror system, the light is always reflected back to the fiber core after two passes, independently from the mirror tilt. The intensity of the re-coupled light will off course depend on the aperture-matching and will be reduced with increasing rotation of the mirror [6]. This setup ensures a back-coupling with high tolerance on the cold-mass mirror rotations and independence on its longitudinal translations. In general, a longer focal length of the lens will improve the angle range, but increase the head and beam size. The displacement is finally determined in the reading unit, as in case of the Standard Sensor.

Preliminary experiments are made with the aim to test the functional principle, and to determine the properties of the optical components of the sensor. The ferrule with numerical aperture of 0.25 and the lens with focal length of 25.4 mm allow sufficient back coupling efficiency. The dimensions of the optical head are 30x50x200 mm. The dimensions of the cold-mass mirror are 50x50x10 mm.

Feedthrough is made of a FCPC connector and corresponding mating adapter glued into an opening in steel feed. The gluing is realised using special vacuum resistant resin. This resin fills up all gaps around the connector and mating adapter. Schematic representation and photo of the feedthrough prototype are presented in Figure 7.5.4.

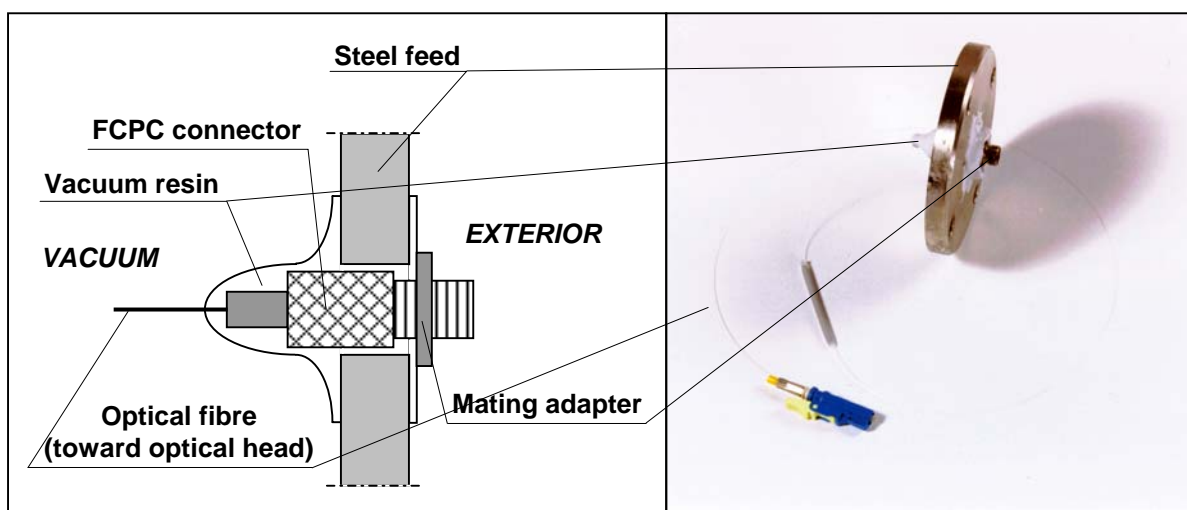


Figure 7.5.4: Schema and photo of feedthrough prototype

Laboratory tests

The following preliminary tests were carried out in order to certify the sensor before installation in the cryodipole prototypes:

- Resistance of the cold-mass mirror in low temperature conditions
- Behaviour of the materials constituting the prototype under vacuum
- Influence of vacuum to the optical head - cold-mass mirror alignment
- Acceptable tilt range

Resistance of the cold-mass mirror in low temperature conditions is tested at three different temperatures, at 75K using liquid nitrogen, at 20K using cryostat and at 4.2K using liquid helium. First two tests are carried out at IMAC and the third one at CERN. After all three tests there was no noticeable change when compared to a reference gold-coated mirror.

Behaviour of the materials constituting the prototype under vacuum is tested at IMAC using small vacuum chamber. The set-up consisting of the optical head and cold mirror and feedthrough is placed into the vacuum chamber. The set-up and vacuum chamber are shown in Figure 7.5.5.

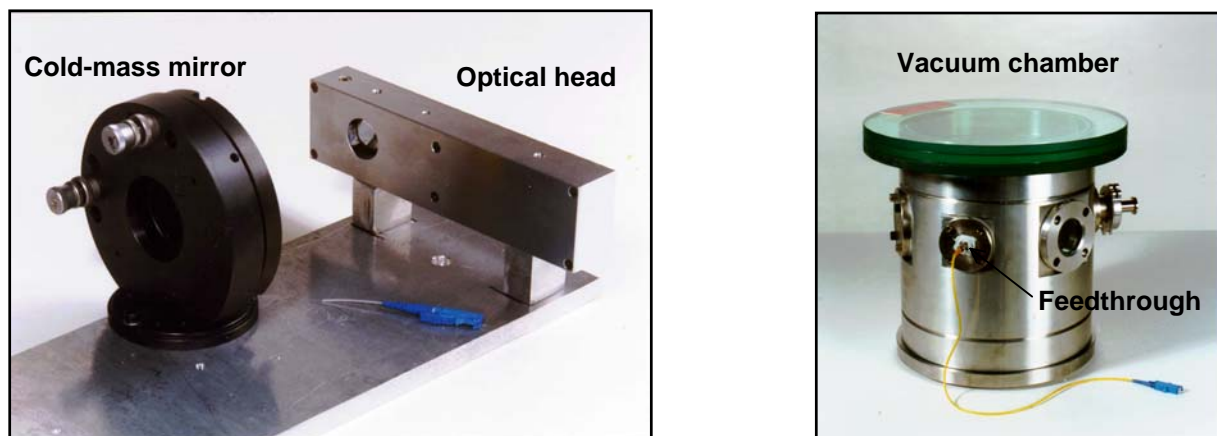


Figure 7.5.5: Optical head and cold-mass mirror placed in vacuum chamber, and chamber itself with installed feedthrough

Two phenomena are tested, the outgassing of all components and the leaking of the feedthrough.

Firstly, only the optical head and the cold-mass mirror are placed into the vacuum chamber, and vacuum is established. Afterwards, the feedthrough is installed and the experience is repeated. Results of both tests are presented in Figure 7.5.6.

No outgassing was observed during the first test. The pumping set-up has took approximately the same time to reach the final pressure ($2 \cdot 10^{-6}$) in the vacuum chamber as for empty chamber.

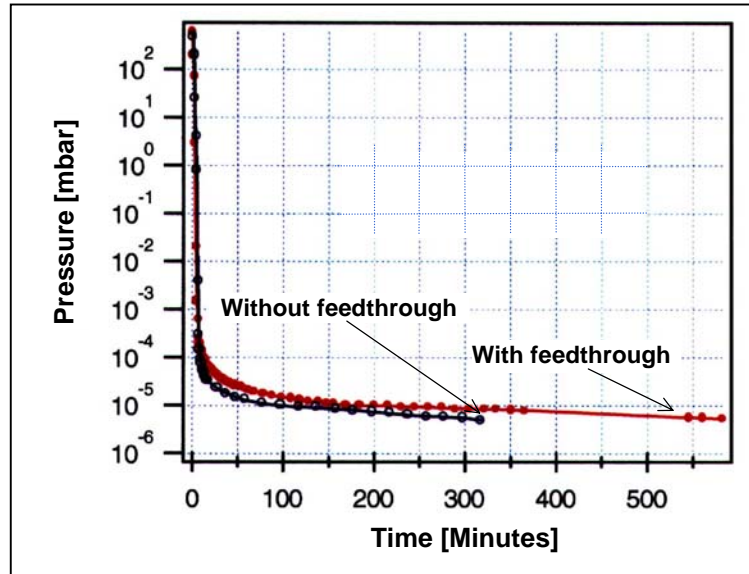
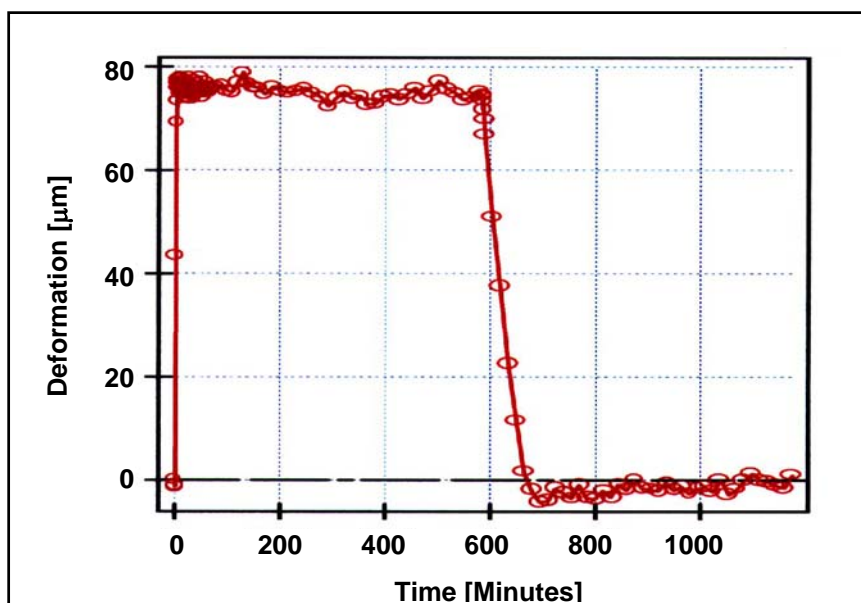


Figure 7.5.6: Vacuum tests of the prototype and the feedthrough

During the second test a small outgassing is observed: in Figure 7.5.6 a longer stagnation at a $1 \cdot 10^{-5}$ mbar pressure is noticed. The ultimate pressure is reached in 550 minutes instead of 300 minutes. This outgassing is small enough to be neglected in the LHC conditions (15 m long vessel). Moreover, the feedthrough does not leak since the pressure continues to decrease when the released gas is pumped out.

Influence of vacuum to the optical head - cold-mass mirror alignment is tested using the same set-up as in previous test.. The cold-mass mirror was aligned at atmospheric pressure and fixed at working distance of approximately 140 mm. The pressure is firstly decreased by pumping until the pressure of $5.4 \cdot 10^{-5}$ mbar is reached, and afterwards increased to the initial (atmospheric) pressure. Measurements are repeated during both phases of the test, and results with respect to time and to pressure are presented in Figures 7.5.7 and 7.5.8 respectively.



Figures 7.5.7: Displacement Sensor measurements with respect to time

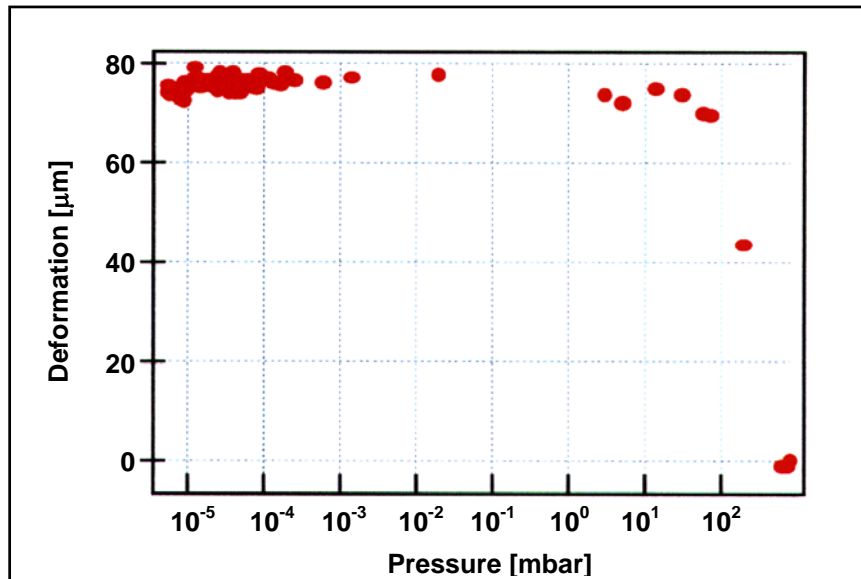


Figure 7.5.8: Displacement Sensor measurements with respect to pressure

The difference of approximately 80mm is noted when the pressure is changed. The origin of this difference is the change of the flight time of light. This change will not influence the measurement because it is easily corrected using the appropriate coefficient in reading unit. In the other hand, there was no losses of the optical signal, measured value was stable during the periods of stable pressure and when the atmospheric pressure is re-established the measurement is back to zero. Therefore, the alignment is not influenced by vacuum.

Acceptable tilt range was determined by simulating a mirror tilt with a rotation stage. In reality, the installation of the cold mass into the vacuum vessel, its cooling and the application of the electromagnetic field have as a consequence a torsion and an horizontal bending of the cold-mass. Thus the cold-mass mirror may be exposed to horizontal and vertical tilts. If the tilt exceed a certain value, the back-coupling efficiency might become insufficient to carry out a measurement.

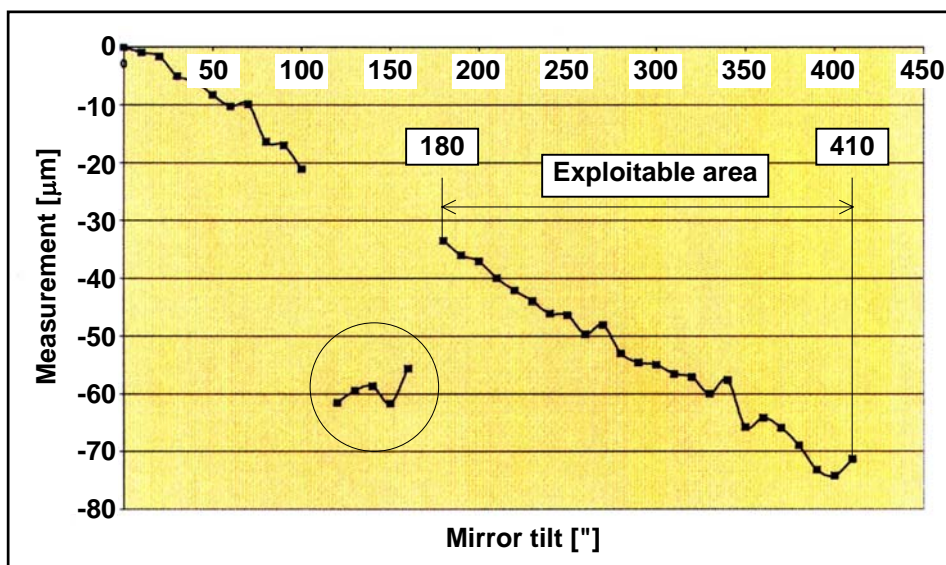


Figure 7.5.9: Horizontal tilt measurements

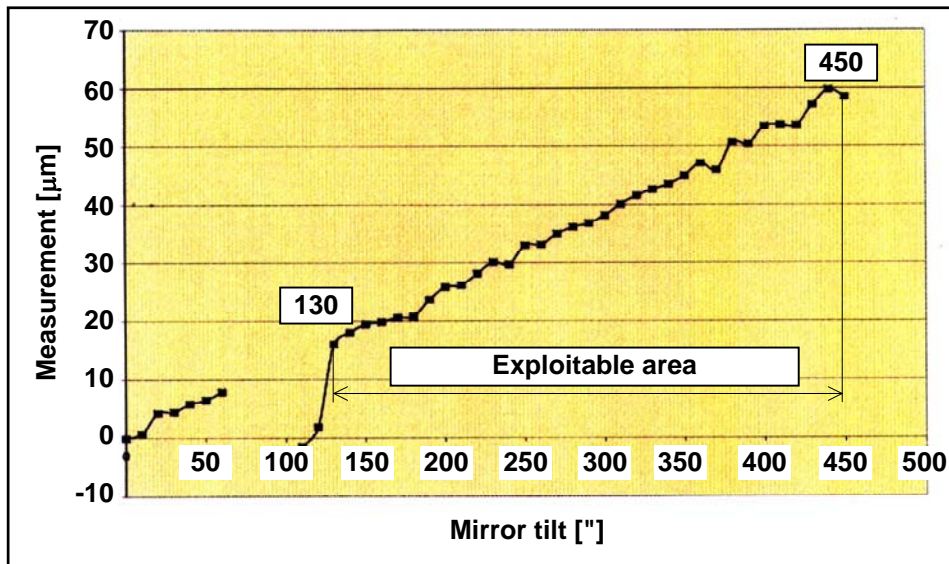


Figure 7.5.10: Vertical tilt measurements

The set-up used for this test is similar to the that shown in Figure 7.5.5. The cold-mass mirror is attached to the support which horizontal and vertical tilt is controllable and measurable. The tilt is imposed to the mirror and measurements are carried out with the optical head. Results are shown in Figures 7.5.9 and 7.5.10, for horizontal and vertical tilt respectively.

In both figures the correlation tilt - measurement is linear. This is caused by eccentricity between the light beam and axis of rotation of the mirror. Since the aim of the test is to determine the tilt range which allows return of the light to the optical head, this eccentricity is not of importance.

The usable measurement area is divided in two zones with a blind area in-between. This interruption is expected and corresponds to the light beam returning directly into the fibre after a single round trip. Therefore the area that is considered as exploitable for measurement begins after the interruption and finishes when the signal fades. This area, indicated in Figures 7.5.9 and 7.5.10, cover the range of 230" (1.12 mrad) for horizontal and 320" (1.55 mrad) for vertical tilt. These values are higher than the maximal tilt that can be tolerated in the cryodipole. The sensors should therefore cover the whole utilisation spectrum without the need of realignments.

In-situ application

Two optical heads have been installed in a test dipole in April 2000, the first one on the left side of the dipole and the second one on the right side of the dipole (see Figure 7.5.2). The installation proceeded without problems and the optical alignment required less than 30 minutes. A few days later the dipole was provided with end-caps and was displaced from the assembly hall to the testing hall. Figure 7.5.11 shows the recorded displacements during transportation. It can be noticed that most readings are symmetrical, indicating a rigid body motion of the cold-mass inside the vacuum vessel. Dissymmetrical deformation might be the result of temperature changes and deformations of the vacuum vessel. It can be noticed that a residual displacement of 0.05 to 0.1 mm was recorded at the end of the transport operation.

More details related to development of the Displacement Sensor can be find in [7].

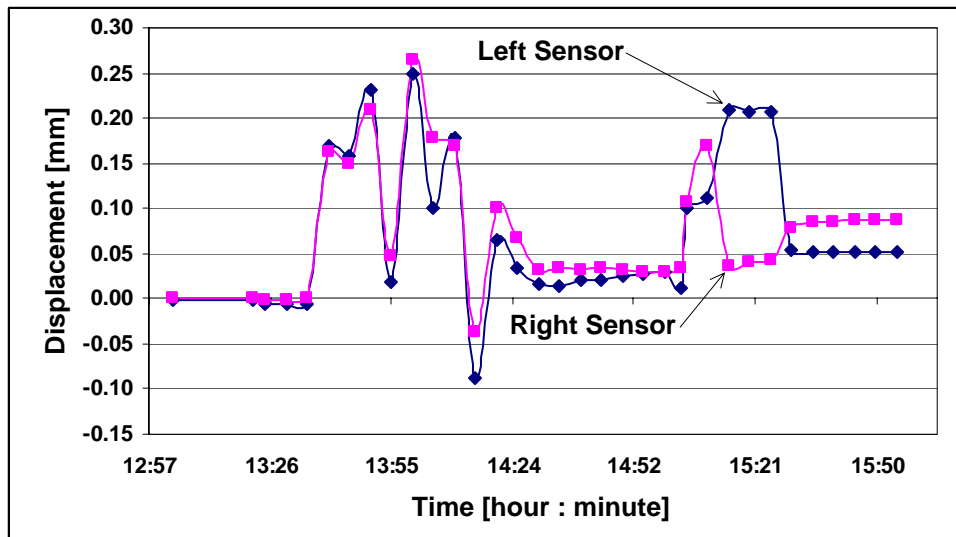


Figure 7.5.11: Measurements during dipole transport

Conclusions and remarks

The presented sensor extends the use of the monitoring system to displacement measurements in extreme environmental conditions. For this purpose the measurement fiber was replaced by a direct path in air and a bulk optical setup. The use of a double-pass optical setup allow the measurement even in the presence of significant rotations of the cold mirror. The sensor was successfully tested in conditions similar to the ones that will be encountered in the real experiment and in particular vacuum and cryogenic temperatures for the cold mirror.

Two Displacement Sensors have been installed in a prototype cryodipole and have measured the displacements of the cold-mass during transportation. This is the first monitoring performed on the LHC cryodipoles.

7.6 CONCLUDING REMARKS

Four new fibre optic interferometric sensors are presented in the Sections 8.2 - 8.5: the Membrane Sensor, the Long Sensor, the Stiff Sensor and the Displacement Sensor. They present original contribution of this thesis. Even if the principle of functioning of the sensor is similar, several different problems had to be solved during their development. The problems are caused by using of non-classical materials in Civil Engineering (thin plastic membranes), by dimensions of auscultated structure (Long Sensor), by the unusual aim of measurement (hardening time instead the deformation in case of the Stiff Sensor) and finally by extreme environmental condition (the Displacement Sensor).

Development of these sensors has widened the application domain of interferometric sensors in several directions. In the field of materials, the auscultation of membrane structures is possible using the Membrane Sensor. In domain of structures, large structures can be monitored using the Long Sensors. In domain of material characterisation, hardening time of concrete is detectable using a pair composed of the Standard and the Stiff Sensors. Finally, in

domain of application in extreme conditions, the displacement measurements are possible using the Displacement Sensor.

The Membrane, the Stiff and the Displacement Sensor are presently unique tools designed for in-situ application in their domains of monitoring. Only in domain of application of the Long Sensor we found other types of sensor, such as rod extensometer. However the Long Sensor is easier to install, more precise, and do not generate electromagnetic fields.

The spectre of sensors designed in this Chapter emphasises the applicability and adaptability of low coherence interferometric monitoring system SOFO developed at IMAC.

With the exception of the Membrane Sensor that was only tested in laboratory, all others sensors have been also tested on real structures with convincing results. Their installation proved to be rapid and simple and we believe that they have considerable potential for structural monitoring.

7.7 REFERENCES

- [1] Glisic B., Inaudi D., Kessi E., *Cloth Sensor: Transfer of Deformation from Assembled Plastic Bands to the Measurement Fibre*, Internal report, IMAC - EPFL, Lausanne, Switzerland, Oct. 1997
- [2] *Suggested Methods for Monitoring Rock Movements Using Borehole Exstensometers*, Int. Society for Rock Mechanics; Oxford, International Journal of Rock Mechanics and Mining Sciences, vol.15, no.6, pp. 305-368, 1978
- [3] Glisic B., Kronenberg P., Inaudi D., *Long Sensor: Installation of Two Long Sensors in Emosson Dam*, IMAC - EPFL, Lausanne, Switzerland, Jan. 1999
- [4] Glisic B., Simon N., *Monitoring of Concrete at Very Early Age Using Stiff SOFO Sensor*, Cement and Concrete Composites, Elsevier, Vol. 22, Issue 2, Pages 115-119, Oxford, UK, 1 Apr. 2000
- [5] www.lhc.cern.ch/, Official WEB site of LHC Division at CERN
- [6] Thévanaz L. et al., *Birefringence Measurement in Fibres without Polarizer*, Journal of Lightwave Technology, Vol. 7, No. 8, pp. 1207-1212, August 1989
- [7] Fakra S., *Deformation measurements on the LHC-CERN cryodipole: a SOFO sensor prototype*, Research report, IMAC-EPFL, Lausanne, 1999

8 Conclusions

The importance of in-situ deformation monitoring, from the construction of structure until the end of service, has inspired this thesis. It focuses on monitoring and characterisation of concrete structures at early and very early age as well as on special sensor development for specific applications.

Originality of this thesis focused in four successfully completed tasks:

- A new numerical model, called EM model, that describes the evolution of the thermal expansion coefficient (TEC) with respect to degree of hydration has been developed. The model is quantitatively compared with results obtained by 2D FEM, an existing model for TEC prediction of hardened concrete, and experiments and qualitatively compared with experimental results found in the literature. The comparison has validated the model.
- Interaction between the Standard Sensor and concrete at very early age is examined numerically and experimentally. Both approaches have shown that the Standard Sensor is a suitable device for deformation monitoring of concrete at very early age, from one to four hours after pouring, when the stabilisation period of concrete is finished.
- Laboratory and in-situ applications of the Standard Sensor as well as the newly developed Stiff Sensor help to characterise concrete at early and very early age. Total deformation of concrete, stabilisation period, early age thermal expansion and contraction as well as crack apparition, its magnitude and time of apparition are identified using the Standard sensor. It also helps to register the hardening time of concrete of hybrid structures. The Stiff Sensor, designed for concrete hardening time identification, is developed and its principle of functioning is experimentally confirmed. It makes a part of group of special sensors developed for specific applications.
- Three other special sensors are developed: The Membrane Sensor designed for in-situ monitoring of plastic membrane structures, the Long Sensor for displacement and deformation monitoring of very large structures and the Position Sensor for displacement monitoring in extreme environmental conditions - low temperature (1.9 K) and vacuum. All sensors are successfully laboratory tested. Moreover the Long Sensor and Position Sensor are successfully tested in-situ, the first one implemented in Emosson dam in Switzerland and the second one in Large Hadron Collider (LHC) at CERN.

This thesis provides scientific and technological contributions. Scientific contributions are:

- Increased knowledge concerning the real behaviour of concrete at very early age: identification of moment of interaction of concrete with other materials for hybrid structures; diagrams presenting the evolution of thermal expansion and contraction; distortion of section due to early age thermal effects.
- Characterisation of concrete at very early age: identification of the stabilisation period; determination of early age thermal expansion and contraction; definition and identification

of hardening time; monitoring of TEC evolution; and detection and quantification of early age cracks.

- Development and calibration of numerical models describing this characterisation: development of numerical model describing TEC evolution; and calibration of FEM.
- Understanding of real behaviour of special structures: identification of creep of membrane structures; and identification and determination of real and unpredictable horizontal displacement of LHC at CERN.

Technological contributions originate in the development of special sensors that are powerful tools for structural monitoring.

Further research related to this work could develop new sensors (Mortar Sensor), improve the Stiff Sensor and standardise its stiffness. Also an important task would be to conceive a method for real-time in-situ characterisation of concrete structures at early and very early age. The creation of standard procedures related to characterisation would be a logical conclusion of such research.

9 Bibliography

- **Acker P.**, *Comportement mécanique du béton: apports de l'approche physico-chimique*, Rapport de recherche LPC N°152, LCPC, Paris, Juillet 1988
- **Acker P.**, *Les retraits du Béton, Origines physiques et paramètres influents, Analyse par type d'ouvrage et mode de mise en oeuvre*, Rilem GMC, LCPC, Paris, Avril 1995
- **Acker P.**, *Les retraits du béton: Origines Physiques, Rôle des paramètres de Composition, Formulation de Bétons à Faible Retrait*, Pontes mixtes, Annexe 1, p.p. 71-84, SETRA, Bagneux - France, Septembre 1995
- **Aïtcin P.-C., Neville A., Acker P.**, *Les différents types de retrait du béton*, Bulletin des laboratoires des Ponts et Chaussées, Vol. 215, p.p. 41-51, LCPC, Paris, Mai - Juin 1998
- **Asnari F.**, *State-of-the-art in the Applications of Fiber-optic Sensors to Cementous Composites*, Cement and Concrete composites, Vol. 19, pp 3-19, 1997
- *ASTM 04.01*, US Norms
- *ASTM 04.02*, US Norms
- **Badoux M., Jaccoud J.-P., Fleury B., Simon N.**, *La tranchée couverte de Champ Baly - Projet pilote d'application de BHP*, Publication SIA D0160, 1999
- **Baron J., Ollivier J.-P.**, (sous la direction de), *La durabilité des bétons*, Presses de LCPC, Paris, France, 1992
- **Bazant Z. P., Najjar L. J.**, *Nonlinear water diffusion in non saturated concrete*, Materials and Structures, Vol.5, N°25, pp. 1-20, 1972
- **Bernard O., Brühwiler E.**, *Analysis of Early Age Behaviour of a Hybrid Concrete Bridge Deck*, US-Canada-Europe Workshop on Bridge Engineering, Dubendorf and Zurich, July 14 -15, 1997
- **Bernard O.**, *Comportement à long terme des éléments de structures formés de bétons d'âges différents*, Ph.D. Thesis, EPFL, Lausanne, Switzerland, 2000 (*to be published*)
- **Bertoncini A., Hammerschlag J.-G.**, *Personal communication*, February 2000
- **Blanc A., Gómez Navarro M.**, *Poutres mixtes à âme mince avec béton de fibres métalliques*, Rapport d'essai N°394, ICOM-EPFL, Juillet 1999
- **Boulay C., Paties C.**, *Mesure des déformations du béton au jeune âge*, Materials and Structures, vol 26, pp. 307 -311, 1993

-
- **Buil M.**, *Comportement physico-chimique du système ciment-fumées de silice*, Annales de l'ITBTP, n°483, pp. 19-29, 1990
 - *CEB-FIP Model code*, 1990
 - **Christensen R. M.**, *Mechanics of composite materials*, Krieger publishing company, Malabar, Florida, 1991
 - *Cours technique expérimentale en structures du génie civil*, ISS-EPFL, Lausanne, Oct.1998
 - **De Larrard F., Ferraris C. F.**, *Rhéologie du béton frais remanié: II - Relations entre composition et paramètres rhéologiques*, Bulletin des laboratoires des Ponts et Chaussées, Vol. 214, p.p. 69-79, LCPC, Paris, Mars - Avril 1998
 - **De Schutter G., Taerwe L.**, *Degree of hydration-based description of mechanical properties of early age concrete*, Materials and Structures, Vol.29, p.p. 335-344, July 1996
 - **Emanuel J. H., Hulsey J. L.**, *Prediction of the Thermal Coefficient of Expansion of Concrete*, Journal of ACI, pp. 149-156, April 1977
 - **Fakra S.**, *Deformation measurements on the LHC-CERN cryodipole: a SOFO sensor prototype*, Research report, IMAC-EPFL, Lausanne, 1999
 - **Fest E., Smith I.**, *Construction et modélisation des structures tensegrités*, Rapport Technique, IMAC - EPFL, Lausanne, Switzerland, 1999
 - *Formulaires et tables, Mathématique, Physique, Chimie*, Commissions romandes de mathématique, de physiques et de chimie, Editions de Tricorne, pp. 190-197, Genève, 1996
 - **Fouad, F. H., H. Furr L.**, *Behaviour of Portland Cement Mortar in Flexure at Early Ages*, Properties of Concrete at Early Age, Editor J. F. Young, p.p. 93-113, American Concrete Institute, 1986
 - **Frangopol D. M., Estes A. C., Augusti G., Ciampoli M.**, *Optimal bridge management based on lifetime reliability and life-cycle cost*, Short course on the Safety of Existing Bridges, ICOM&MCS, pp 112-120, EPFL, Lausanne, Switzerland, 1998
 - **Frey F.**, *Mécanique des matériaux (II)*, pp. 7.23-7.27, Cours de 3^e semestre, ISS, DGC, EPFL, Lausanne 1989
 - **Glisic B., Badoux M., Jaccoud J.-P., Inaudi D.**, *Monitoring A Subterranean Structure with the SOFO System*, 1st International Conference Long Road and Rail Tunnels, November 29 - December 1, 1999, Basel, Switzerland
 - **Glisic B., Inaudi D., Kessi E.**, *Cloth Sensor: Transfer of Deformation from Assembled Plastic Bands to the Measurement Fibre*, Internal report, IMAC - EPFL, Lausanne, Switzerland, Oct. 1997

-
- **Glisic B., Kronenberg P., Inaudi D.,** *Long Sensor: Installation of Two Long Sensors in Emosson Dam*, IMAC - EPFL, Lausanne, Switzerland, Jan. 1999
 - **Glisic B., Simon N.,** *Monitoring of Concrete at Very Early Age Using Stiff SOFO Sensor*, Cement and Concrete Composites, Elsevier, Vol. 22, Issue 2, Pages 115-119, Oxford, UK, 1 Apr. 2000
 - **Guidom A.,** *Simulation numérique 3D des comportements des bétons en tant que composites granulaires*, Ph.D. Thesis N°1310, EPFL, Lausanne, Switzerland, 1994
 - **Habel W. R., Jung M., Plohn J., Basedau F.,** *Non-Reactive Measurement of Mortar Deformation at Very Early Age by Means of Embedded compliant Fiber optic Micro Strain Sensors*, 12th Engineering Mechanics ASCE Conf. Session Fiber Sensors for Condition Monitoring, La Jolla, CA, USA, 17-20 May 1998
 - **Hansen W.,** *Static and Dynamic Elastic Modulus of Concrete as Affected by Mix Composition and Compressive Strength*, Properties of Concrete at Early Age, Editor J. F. Young, p.p. 115-137, American Concrete Institute, 1986
 - **Hammerschlag J.-G.,** *Mécanismes des réactions alcalis-granulats et leurs effets sur la structure du béton*, Service de recherches et conseils techniques de l'industrie suisse du ciment, 1999
 - **Hassan M.,** *Critères découlant d'essais de charge pour l'évaluation du comportement des ponts en béton et pour le choix de la précontrainte*, Ph.D. Thesis N° 1296, EPFL, Lausanne, Switzerland, 1994
 - **Hughes T. J. R.,** *The finite element method*, Prentice Hall, 1991
 - **Inaudi D.,** *Fiber Optic Sensor Network for the Monitoring of Civil Structures*, Ph.D. Thesis N°1612, EPFL, Lausanne, Switzerland, 1997
 - **Inaudi D.,** *Personal communication*, R+D Director of "Smartec SA"-Grancia, Switzerland
 - **Inaudi D., Vulliet L., Pflug L., Vurpillot S., Wyser A.,** *Low-coherence interferometry for the monitoring of underground works*, 1995 North American Conference on Smart Structures and Materials, Volume 2444, pp. 171-178, San Diego, 1995
 - **Inaudi D., Vurpillot S.,** *SOFO: Surveillance d'ouvrages par senseurs à fibres optiques*, IAS: Ingénieur et Architecte Suisse, 121^{ème} année, numéro 26, pp. 522-529, 6 décembre 1995
 - **Inaudi D., Vurpillot S., Casanova N., Osa-Wyser A.,** *Development and Field Test of Deformation Smart Structures and Materials*, Smart Structures and Materials, SPIE Vol. 2721, pp. 138-148, San Diego, USA, 1996

-
- **Inaudi D., Vurpillot S., Glisic B., Kronenberg P., LLoret S.,** *Long-term Monitoring of a Concrete Bridge with 100+ Fiber Optic Long-gage Sensors*, SPIE's International Symposium on Nondestructive Evaluation Techniques for Aging Infrastructure & Manufacturing, , Vol. 3587, Pages 50-59, Newport Beach, USA, 3-5, March 1999
 - **Kronenberg P., Casanova N., Inaudi D., Vurpillot S.,** *Dam Monitoring with Fiber Optic Deformation Sensors*, Smart Structures and Materials, SPIE Vol. 3043, pp. 2-11, San Diego, USA, 1997
 - **Laplante P., Boulay C.,** *Evolution du coefficient de dilatation thermique du béton en fonction de sa maturité aux tout premiers âges*, , Materials and Structures, Vol.27, pp. 596-605, 1994
 - **Legrand C., Wirquin E.,** *First developments of strength in a microconcrete*, Thermal Cracking in Concrete at Early Age, RILEM International Symposium, p.p. 89-100 Munich, 1994
 - **Lindstedt H., Staffa M.,** *Mesure d'allongements et d'évolution des températures au sein de parois en béton armé*, CTM3/99, pp. 2-10, HBM, Darmstadt
 - *Limitation de la fissuration au jeune age du béton dans des structures hybrides*, research report, MCS, IMAC et ICOM, EPFL, Lausanne, Switzerland, 2000 (to be published)
 - **Markey I. F.,** *Enseignements tirés d'observations des déformations de ponts en béton et d'analyses non linéaires*, Ph.D. Thesis N° 1194, EPFL, Lausanne, Switzerland, 1993
 - **Monney C., Ducret J.-M.,** *Essais de poutres mixtes à âme mince*, Rapport d'essai N°357, ICOM-EPFL, Septembre 1999
 - **Muravljov M.,** *Gradjevinski materijali*, Naucna knjiga, Beograd, Yugoslavia, 1989
 - **Muravljov M.,** *Tehnologija betona*, Gradjevinska knjiga, Beograd, Yugoslavia, 1992
 - **Nagesh M., Bhattacharjee B.,** *Modelling of Chloride Diffusion in Concrete and Determination of Diffusion Coefficients*, ACI Materials Journal, Vol. 95, N°2, April 1998
 - **Neville A. M.,** *Properties of concrete*, Pittman International, 1975
 - **Nonat A., Mutin J. C.,** *From hydration to setting*, Thermal Cracking in Concrete at Early Age, RILEM International Symposium, p.p. 171-191, Munich, Germany 1994
 - **Rastogi P.,** (edited by), *Optical Measurement Techniques and Applications*, Artech House Inc., Boston - London, 1997
 - **Paratte P.-A., Robert Ph.,** *Systèmes de mesure*, Traité d'électricité vol. XVII, Presses polytechniques romandes, Lausanne, 1986, pp. 4

-
- **Paulini P.**, *Zement-Kalk-Gips*, Nr.10, pp. 525-531, 1988
 - **Paulini P., Gratl N.**, *Stiffness formation of early age concrete*, Thermal Cracking in Concrete at Early Age, RILEM International Symposium, p.p. 63-70, Munich, 1994
 - **Radojicic A, Bailey S., Brühwiler E.**, *Consideration of the Serviceability Limit State in a Time Dependant Probabilistic Cost Model*, in "Application of Statistics and Probability", Vol. 2, pp 605-612, Balkema, Rotterdam, Netherlands, 1999
 - **Roelfstra P. E.**, A numerical approach to investigate the properties of concrete - numerical concrete, Ph.D. Thesis N° 788, EPFL, Lausanne 1989
 - **Schöppel K., Springenschmid R.**, *The Effect of Thermal Deformation, Chemical Shrinkage and Swelling on Restraint Stresses in Concrete at Early Age*, Thermal Cracking in Concrete at Early Age, RILEM International Symposium, p.p. 215-220, Munich, 1994
 - *SIA 162*, Swiss Norms
 - *SIA 462*, Swiss Norms
 - **Soroka I.**, *Portland Cement Paste and Concrete*, The Macmillan Press Ltd, 1979
 - *Suggested Methods for Monitoring Rock Movements Using Borehole Exstensometers*, Int. Society for Rock Mechanics; Oxford, International Journal of Rock Mechanics and Mining Sciences, vol.15, no.6, pp. 305-368, 1978
 - **Tazawa E., Iida K.**, *Mechanism of thermal stress generation due to hydration heat of concrete*, Transactions of the Japan Concrete Institute, 1983, vol. 5, p.p. 119-126
 - **Thévanaz L. et al.**, *Birefringence Measurement in Fibres without Polarizer*, Journal of Lightwave Technology, Vol. 7, No. 8, pp. 1207-1212, August 1989
 - *Thermal Cracking in Concrete at Early Age*, RILEM International Symposium, Munich, Germany, 1994
 - **Timoshenko S. P., Goodier J. N.**, *Theory of Elasticity*, McGraw Hill International, 1970
 - **Udd E.**, (edited by), *Fiber Optic Sensors, An Introduction for Engineers and Scientists*, A Willey-Interscience Publicatio, John Willey&Sons Inc. 1991, New York
 - **Vohra S.T., Althouse B., Johnson G., Vurpillot S., Inaudi D.**, *Quasi-Static Strain Monitoring During the "Push" Phase of a Box-Grider Bridge Using Fiber Bragg Grating Sensors*, European Workshop on Fiber Optic Sensors, Peebles, Scotland, July 1998
 - **Vurpillot S.** *Analyse automatisée des systèmes de mesure de déformation pour l'auscultation des structures*, Ph.D. Thesis N° 1982, EPFL, Lausanne, Switzerland, 1999

- **Vurpillot S., Inaudi D., Ducret J.-M.,** *Bridge Monitoring by Fiber Optic Deformation Sensors: Design, Emplacement and Results*, Smart Structures and Materials, SPIE Vol. 2719, pp. 141-149, San Diego, USA, 1996
- **Vurpillot S., Krueger G., Benouaich D., Clément D., Inaudi D.,** *Vertical Deflection of a Pre-Stressed Concrete Bridge Obtained Using Deformation Sensors and Inclinometer Measurements*, ACI Structural Journal, Vol. 95, No. 5, September-October 1998
- **Walther R., Miehlsbradt M.,** *Dimensionnement des structures en béton, Traité de génie civil*, Vol.7 pp. 3, Presses polytechniques et universitaires Romandes, Lausanne, 1990
- **Wittmann, F. H.,** *Personal communication*, 13.04.2000
- www.fiso.com, Official WEB site of Fiso Technologies
- www.lhc.cern.ch/, Official WEB site of LHC Division at CERN
- www.smartec.ch, Official WEB site of Smartec SA
- www.statistik.admin.ch/stat_ch/ber09/fufr09.htm, Official WEB site of Swiss Federal Statistic Office
- **Zienkiewicz O. C., Taylor R. L.,** *La méthode des éléments finies: formulation de base et problèmes linéaires*, pp. 620, Afnor, Paris 1991

Appendix: Monitoring system - basic notions

A1 INTRODUCTION

The aim of this chapter is to make a brief recapitulation of some basic notions concerning measurements, measurement techniques and monitoring systems. This recapitulation do not pretend to describe and classify measurements in details but only to make a general view to the subject and to introduce the reader in domain of measurements in order to facilitate the perception and comprehension of this thesis. Only the subjects closely related with thesis' principal objectives are moved on in following sections. They are estimated as essential and indispensable for understanding of the thesis' parts that concern measurements and development of different types of sensors. Being fundamental for presented research, the deformation and the displacement measurements are particularly described.

A2 WHAT IS A MEASUREMENT?

Objects with different physical properties (parameters) surround us. Some of those properties are intuitively apparent to anyone (e.g. dimensions, weight etc.). Other physical properties are not so clear (e.g. strain, stress, etc.), therefore they are defined by intuitively clearer ones (e.g. strain $\varepsilon = \Delta l / l$ where l is initial linear dimension of object and Δl is variation this dimension etc.). Certain properties can be quantified i.e. it is possible to attribute them a numerical value describing their magnitude. The property that can be quantified is also called parameter. To make feasible the quantification of a parameter it is necessary to establish a standard and a unit corresponding to the parameter. Thus the magnitude is equal to the number of units that this parameter consists of. A measurement of a parameter is the process of its quantification.

Example 1: If the object is a pencil and the (observed) parameter is its length, then the corresponding unit is 1 meter and the measurement is in fact the comparison between the length and the ruler. If we read value a on the ruler it means that the length consists of a meters i.e. the magnitude of the length is a .

A3 DIRECT AND INDIRECT MEASUREMENT

Generally a measurement can be carried out directly or indirectly. Direct measurement consists of immediate comparison of the observed parameter with the corresponding standard or with the objects that have the same type of parameter with the known magnitude. Often, the observed parameter is in correlation with some other parameter, called the encoding parameter. The correlation between observed parameter x and encoding parameter y can be represented as:

$$y=f(x), \quad (A3.1)$$

where f is function of correlation. If the function of correlation between observed and encoding parameter is established, it is possible to determine the magnitude of initially observed parameter by measuring the encoding property using the expression:

$$x=f^{-1}(y). \quad (A3.2)$$

Measurement made in a such way is indirect. In order to assure a correct measurement f has to be bijection.

Example 2: Let the observed parameter is the weight of an object m . If one uses the balance and puts the weights on one side and the object on the other side of the balance, the measurement is direct: unknown property is measured by comparing it with the objects with known property. The Example 1 is also example of direct measurement. If one uses the weighing machine with a spring and put the object on it, the spring will be deformed. Knowing the stiffness of the spring k and gravity acceleration g , it is possible to determinate the weight of the object by measuring the shortening of the spring Δl as follows:

$$m = \frac{k}{g} \Delta l . \quad (A3.3)$$

The measurement is indirect, i.e. by measuring the shortening, indirectly, one measures the weight. Here $f^{-1}(y) = \frac{k}{g} y$.

A4 ERROR OF A MEASUREMENT

Error refers to the difference between true value of magnitude of the observed parameter and the value measured by the measurement system. By origins, the errors can generally be classified in three groups: systematic, stochastic and accidental error [1].

Systematic error is a constant and noticeable error. It can be caused by construction error or measurement device, its calibration error or ageing, but also by some external influences as temperature or humidity variation. Systematic error appears during each repeating of measurement.

Stochastic error is non-predictable error caused often by chance. It is not possible to determine it neither a priori nor a posteriori but it is possible to determinate the maximal value of this error by statistical analysis. The real causes of the stochastic error are complex and are

result of several phenomena such are friction in mechanical part of measurement system, electro-magnetic perturbations etc.

Accidental error refers to an error caused by inattentive performing of measurement. Typical examples of accidental errors are wrong reading, measurement of a wrong point or incorrect utilisation of measurement device. The accidental error normally does not appear when the measurement is correctly repeated.

Example 3: It is supposed that the stiffness of the weighing machine spring in example 2 is 5% overestimated. All measurements made by this weighing machine show a systematic error of 5%. If during the measurement with a correct machine one touches the pan by chance, it causes an accidental error which can be corrected by repeating the measurement.

A5 MEASUREMENT SYSTEM

In order to carry out a measurement one can use different types of apparatus. Set of all devices destined to carry out a measurement is called measurement system. In case of direct measurement it is necessary to have a direct access with the standard (or objects with known measure) to the object which property has to be measured. In case where the direct access is not available or the standard for the observed property does not exist, one has to carry out an indirect measurement. The measurement system to be utilised to realise an indirect measurement is composed of different components: sensors, carriers of information, reading unit, analyser and interface. The sensor is in direct contact with the measured object. It transforms the magnitude of observed parameter to the magnitude of the encoding parameter (see Example 2). The carrier leads the information concerning the magnitude of the encoding parameter from sensor to the reading unit which decodes the information and retrieves the magnitude of the encoding parameter. The analyser transforms the measure of the encoding parameter to measure of observed parameter using the function of correlation. Finally, the measurement is visualised and presented to the operator by user interface.

The encoding property defines the principle of functioning of the sensor. If it is the electrical resistance we talk about electrical sensors, if it is an optical property, the sensor is optical, etc. Modern measurement systems mainly consist of electrical, inductive, mechanical, electro-mechanical, optical or fibre-optic sensors.

Example 4: Let the strain of an object is an observed parameter. It is internal parameter of the object therefore it is not possible to measure it directly. Let the measure of the strain is carried out using a measurement system based on the change of electrical resistance of a strained object. The system's components are given in the Table A5.1.

<i>Component</i>	<i>Appearance</i>
Sensors	Extensometer (metallic band)
Carriers of information	Electrical cables from sensors to the reading unit
Reading unit	Ohmmeter
Analyser	Digital multiplier integrated in the reading unit ($\epsilon=R\Omega$)
Interface	Digital screen integrated in the reading unit

Table A5.1 Example of measurement system components

A6 TIME DEPENDENT MEASUREMENT - ABSOLUTE AND RELATIVE MEASUREMENT

There are the parameters that change in time. If it is of interest to monitor the parameters' changes during certain period then the measurements have to be carried out several times during this period. The measurements interesting to be repeated in time are time dependent measurement.

Example 5: Measurement of a child's height during the grooving is time dependent measurement. Measurement of an adult is not essentially a time dependent measurement - the height of an adult does not change in time, hence it is not of interest to measure it.

Time dependent measurement can be rhythmic or arrhythmic. It is rhythmic if the delay between each two successive measurement is constant otherwise it is arrhythmic. A campaign of measurement is the set of all measurements (rhythmic or arrhythmic) carried out during certain period. If the campaign is managed during up to seven days it is a short-term measurement otherwise it is a long-term measurement. The evolution of a parameter from the moment τ is a long-term measurement, which consist of all measurement of this parameter done after the moment τ . Measurement or evolution is absolute if observed property did not exist before the moment τ , when the measurements have begun. Otherwise it is relative to measurement done in the moment τ . Evolution (absolute or relative) can consist of several short-term or long-term campaigns of measurements, rhythmically or arrhythmically realised.

Example 6: One measures a child's weight. The child is born in Sunday at 17h00. During the first week the measurement is repeated daily at 17h00. Following six months the measurement is repeated every Sunday at 17h00. Afterwards, until present, the measurements are done irregularly, depending of necessities. We have described three campaigns of measurements. The first two are rhythmic and third is arrhythmic. The first is a short-term while the second and the third are long-term campaigns. All three campaigns compose an absolute measurement (absolute evolution of the observed parameters) because the observed parameter (the child's weight) did not exist before the child's birth.

A7 MONITORING SYSTEM

A monitoring system is destined to follow the evolution of an observed parameter during a certain period. Consequently, it consists of all components of a measurement system (sensors, reading unit, etc.) and, in addition, a management subsystem. The components of a monitoring system can be separated or differently combined (e.g. sensor and carrier can make one device).

The purpose of the management subsystem is to manage the rhythm of measurements, to collect results of measurements and to make a partial or complete analyses of the results. The management subsystem can be manual or automatic. If all components of a monitoring system are automatic, the system is fully automatic. The SOFO measurement system is an example of fully automatic monitoring system.

A8 PROPERTIES OF A MONITORING SYSTEM: SENSITIVITY, RESOLUTION, PRECISION, DYNAMIC RANGE AND DRIFT

A measurement can never quantify exactly the observed parameter, but can only give an approximation of its magnitude. Furthermore, a measurement system destined to measure an observed parameter is not necessarily suitable to be applied for any cause (e.g. it is not reasonable to measure the height of a man using a mechanical micrometer).

The applicability and quality of measurement depends of performances of the measurement system, especially of sensors' and reading unit's performances, such are sensitivity, resolution, precision, dynamic range and drift. There is confusion in the literature concerning the definitions of mentioned performances, notably resolution and sensitivity [2,3,4,5]. Therefore the definition given in this thesis have not to be considered as absolute. They are rather adapted to the definition adopted by "Smartec SA", the vendor of the system SOFO [6]. Main properties of a monitoring system are represented in Diagram A8.1.

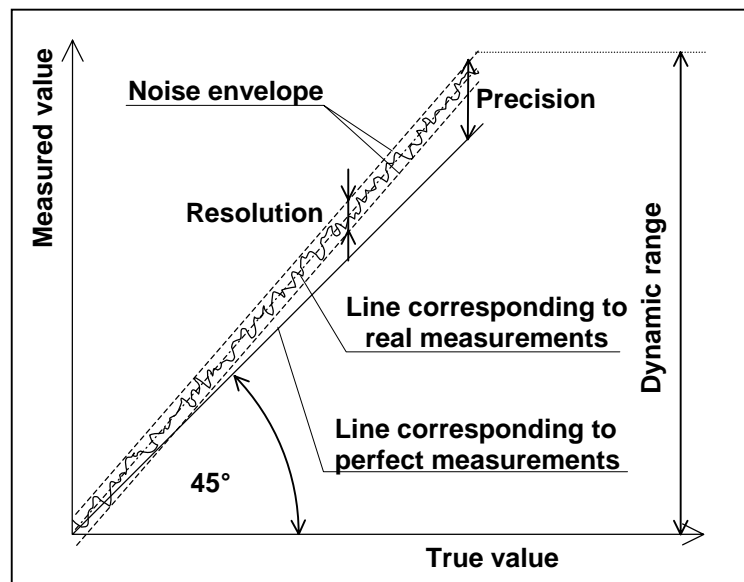


Diagram A8.1: Properties of a measurement system

In this thesis, for the practical reason, the sensitivity of measurement system for a given measured value is defined as the ratio dy/dx between variations of the encoding and the observed parameter [5, 7]. If the function of correlation is linear, the sensitivity is a constant equal to the first derivation of the function of correlation.

The maximum resolution [5, 7] in terms of magnitude of the observed parameter x is the minimum detectable change of the observed parameter Δx that can be perceived with the measurement system. This definition is often found in the literature as definition of sensitivity. It is calculated as the root mean square of the noise, where the noise represents the dispersion of the several measurements done without change of the magnitude of the observed parameter. The resolution defines the lowest limit of the measurement.

The precision refers to the ability of measurement system to measure the same value of an observed parameter if measurement is repeated several times. It represents the maximum

expected difference between measured and true value. It is calculated as the root mean square of this difference.

The dynamic range represents the maximal variation of the observed parameter that can be registered by measurement system.

Finally, the drift refers to long-term non-stability of a monitoring system. By ageing some components of measurement system, notably sensors can be subjected to degradation and as a consequence the measurement errors appear. The monitoring systems subjected to the drift can not be utilised for long-term measurements.

Example 7: In Example 2, let the minimal perceivable deformation of the spring is 0.5 mm, maximal deformation of the spring is 30 mm, and all parts of the weighing machine are made of steel, protected of corrosion and utilised in non-aggressive environment. Properties of the weighing machine are shown in Table A8.1.

<i>Property</i>	<i>Value</i>
Sensitivity [mm/kg]	g/k
Resolution [kg]	~k/g·0.5mm
Precision [%]	Have to be determined statistically
Dynamic range [kg]	k/g·30mm
Drift	Not expected due to the favourable conditions of utilisation

Table A8.1: Properties of the weighing machine presented as a measurement system

A9 DEFORMATION SENSOR

Civil structures change its shape when loaded. This change of shape provokes a displacement of each point of structure and a change of strain and deformation. These three parameters, displacement, strain and deformation, describe well the behaviour of a loaded structure, its functioning and current state. Therefore it is of interest to monitor them using an appropriated monitoring system.

Displacement refers to a change of distance between two points of the structure (relative displacement) or between one point of the structure and one fixed point in surroundings of the structure (absolute displacement). Displacement is a consequence of a simultaneous effect of stressing, thermal variations and sinking of the structure, but can also occur without stressing, e.g. due to thermal variations or sinking of isostatic structures. Sensors used to measure displacement, relative or absolute, are called displacement sensors. However, the sensors destined to measure the deformation can be often used as displacement sensors.

Strain refers to internal state of the structure and is a direct consequence of stressing. Sensor destined to measure strain is called the strain sensor. In reality, it is not possible to measure the strain of structures built of classical civil engineering materials (it is possible to measure it only on photoelastic materials). Thus the strain sensor is, in fact, a deformation sensor with short measurement basis l . If the variations of the strain field along the sensor are small, the (average) strain is calculated as:

$$\varepsilon = \frac{\Delta l}{l}. \quad (\text{A9.1})$$

Strain sensors give an information related to local behaviour of structure, and are very useful if the structure is built of a homogenous material or if we are interested to know local behaviour of structure. In case of inhomogeneous materials, e. g. concrete or composites, the strain field varies very much due to presence of components (e.g. aggregate in concrete), and it is more interesting to use sensors with longer measurement basis.

Deformation refers to an internal dimensional or shape variation of structure. It is consequence of simultaneous action of stressing and temperature variation, but can occur without stressing, only due to thermal variations in isostatic structures. Sensor destined to measure the deformation is called the deformation sensor.

Generally, the deformation sensors consists of a measurement basis that could be 10 centimetres to several meters long, or even several tens of meter, in case of large structures (geotechnical structures, dams, etc.). Making mainly indirect measurements, they contain a part of information carrier, too. The measurement basis is in contact with the structure to be monitored, following the behaviour of the structures. It is important to avoid any perturbation of the structure strain field by presence of sensor. It means that stiffness of the deformation sensor has to be several orders of magnitude inferior than stiffness of the structure material. Also, transversal dimension of sensor has to be minimal possible, and several order of magnitude inferior than length of the measurement basis. The sensor has to be attached to the structure in a way that guaranties good (complete) transfer of deformation from the structure to the measurement basis. If the strain field varies along the sensor, measured value gives an average strain value. The deformation sensors describe well the global behaviour of structure, therefore they are very useful in case of structures built of inhomogeneous materials. They are notably applied when a dimensional stability of structure is expected (e.g. bridges, dams etc.).

Any deformation sensor is subjected, itself, to thermal influences, because the temperature variations change eater length of components of the measurement basis or the encoding parameter. Temperature variations to the sensor have to be cancelled in order to increase precision and to carry out reliable measurements. In order to avoid thermal influences to the deformation sensor two approaches are frequently applied. First, the utilisation the sensors that are self-compensated - sensor components have low sensitivity to temperature variations or a temperature sensor is integrated in the deformation sensor in order annul the thermal influences. Second approach contents following procedure: temperature is measured simultaneously with deformation sensor readings, then the pure thermal influence to the sensor is calculated and each sensor reading is corrected with the calculated value. We note here that first method is more elegant and in the case of self-compensated sensor more precise than the second one.

A10 STATIC AND DYNAMIC DEFORMATION

Depending of the nature, the deformation of structure can be static or dynamic. The deformation is static if it changes sufficiently slowly that dynamical effects, essentially the acceleration of the structure points, can be neglected. The static deformation is provoked by static loads, material mechanical properties (e.g. creeping, relaxation, land sliding),

temperature variation. The rhythm of measurements in case of the static deformation is adapted to necessities.

The deformation is dynamic if the changes of deformation are fast and dynamical effects can not be neglected. It means that deformation changes several times during a very short period (1 to 10 seconds). Dynamic deformation is mainly caused by dynamic loads (earthquake, wind, machines e.t.c.). Frequencies for civil engineering structures are usually in the limits from 0.1 Hz to 30 Hz, but can extend to kilohertz for composite and metallic structures. A monitoring system chosen to control the behaviour of a dynamically loaded structure must be able to realise several readings each second depending of the acquisition time of a reading.

A11 CHOICE OF THE MONITORING SYSTEM

The choice of a monitoring system relies several factors. The most important are:

- monitoring system performances (resolution, dynamic range etc.)
- type of structure (bridge, dam, etc.)
- observed (monitored) parameter
- construction material (concrete, steel, wood etc.)
- environment conditions (in-situ or laboratory conditions)
- particularities of each structures.

In Table A11.1, characteristics of certain frequently used types or deformation monitoring systems are presented.

A12 REFERENCES

- [1] Muravljev M., *Gradjevinski materijali*, Naucna Knjiga, Beograd 1989. pp.99
- [2] Inaudi D., *Fiber Optic Sensor Network for the Monitoring of Civil Structures*, Ph.D. Thesis N°1612, Swiss Federal Institute of Technology Lausanne (EPFL), 1997
- [3] *Optical Measurement Techniques and Applications*, edited by Rastogi P., Artech House Inc., Boston - London, 1997
- [4] *Fiber Optic Sensors, An Introduction for Engineers and Scientists*, edited by E. Udd, A Wiley-Interscience Publicatio, John Willey&Sons Inc. 1991, New York
- [5] Paratte P.-A., Robert Ph., *Systèmes de mesure*, Traité d'électricité vol. XVII, Presses polytechniques romandes, Lausanne, 1986, pp. 4
- [6] Inaudi D., *Personal communication*, R+D Director of "Smartec SA"-Grancia, Switzerland
- [7] *Cours technique expérimentale en structures du génie civil*, ISS-EPFL, Lausanne, Oct.1998

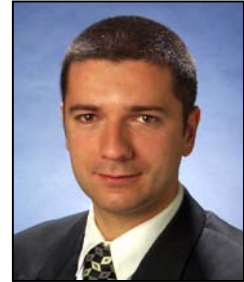
	<i>Measurement basis</i>	<i>Resolution</i>	<i>Dynamic range</i>	<i>Temperature sensitivity</i>	<i>Long-term aptitude</i>	<i>Automatic and remote monitoring</i>	<i>Construction material</i>	<i>Observed parameter</i>
<i>Vibrating wires</i>	10 - 20 cm	0.04 μm	0.4 cm	High, must be compensated	Good	Good	Steel, hardened concrete	Strain, deformation
<i>Strain gauges</i>	0.02 - 10 cm	1 $\mu\text{m}/\text{m}$	0 - 5 %	High, must be compensated	Drift	Good	Steel, hardened concrete	Strain, deformation
<i>Omega gauges</i>	5 or 10 cm	$\sim 2 \mu\text{m}/\text{m}$	2 mm	High, must be compensated	Depends of environment	Good	Steel, wood, hardened concrete	Strain, deformation, opening of localised cracks
<i>LVDT</i>	5 - 20 cm	10 - 1 μm	0.1 - 50 cm	High, must be compensated	Depends of environment	Good	Steel, wood, hardened concrete	Displacement, deformation
<i>Rock-meter</i>	0.3 - 250 m	10 μm	>5 cm	Depends of required precision	Good	Good if equipped with a LVDT	Rock, soil	Displacement, deformation
<i>Water level</i>	-	1 mm	1 - 20 cm	High, must be compensated	Bad	Bad	Steel, wood, hardened concrete	Relative displacement
<i>Brag grating</i>	0.5 cm - several m	1 $\mu\text{m}/\text{m}$	2%	High, must be compensated	Good	Good	Steel, wood, hardened concrete	Strain, deformation
<i>SOFO</i>	0.2 - 10 m	2 μm	8 cm	Self - compensated	Good	Good	Steel, wood, fresh (non-hardened) and hardened concrete	Strain, deformation, concrete very early age deformation

Figure A11.1: Comparison of characteristics of monitoring systems frequently utilised in Civil engineering

Curriculum vitae

PERSONAL DATA:

First name: **Branko**
Family name: **Glišić**
Date and place of birth: Oct. 8, 1969. in Valjevo, Serbia, Yugoslavia
Citizenship: Yugoslav



EDUCATION:

1997-2000 Ph.D. student at the Laboratory for Stress Analysis (IMAC), Swiss Federal Institute of Technology, Lausanne (EPFL)
1989-1996 University of Belgrade, Faculty of Mathematics, average grade 8.55 out of 10
1989-1994 University of Belgrade, Faculty of Civil Engineering, av. grade 9.15 out of 10

HONOURS AND PRIZES:

1996-2000 Ph.D. EPFL scholarship
1995 Awarded by the University of Belgrade as the best student in year of Faculty of Civil Engineering
1989-1994 Scholarship, Ministry for Education, state of Serbia
1986 Second Prize, Yugoslav Federal competition in mathematics

PROFESSIONAL EXPERIENCE 1996-2000:

Ph.D. Student, Assistant, and Project Co-ordinator at the Laboratory for Stress Analysis (IMAC), Swiss Federal Institute of Technology, Lausanne (EPFL)

Teaching activities:

- Teaching assistant for Mechanics of Structures and Solids, Statics and Dynamic Analysis of Structures I.
- Preparation, organisation and demonstration of exercises.
- Supervision of student projects
- Expert for several examinations.

Research activities:

- Development of advanced optical sensors of type SOFO for deformation measurements of different construction materials and structures.
- Deformation measurement and characterisation of concrete at early and very early age.
- Simplified numerical modelling of concrete at early and very early age.

Projects:

- Behaviour of concrete at early age and limitation of hybride structures cracking (mandated by Swiss Federal Department for Roads - OFROU)
 - Development of Membrane Sensor (mandated by Smartec SA)
 - Displacement monitoring of Emosson Dam (mandated by Electricit  d'Emosson SA)
 - Displacement monitoring of LHC Cryodipol (mandated by CERN)
 - Total Deformation monitoring of Cut-and-Cover Tunnel of Champ Baly (mandated by Roads and Highways Department of Canton of Vaud)
-

PROFESSIONAL EXPERIENCE 1995-1996:

Teaching Assistant at Department for Engineering Mechanics and Theory of Structures, Faculty of Civil Engineering, University of Belgrade

Teaching activities:

- Teaching assistant for Structural Analysis 1, Structural Analysis 2 and Theory of Plates and Shells.
- Preparation, organisation and demonstration of exercises. Preparation, organisation and evaluation of written examinations.

Research activities:

- Numerical modelling of dynamical response of cooling tower foundations using complex analysis.
-

Published papers

PROFESSIONAL PAPERS

Journals:

- **Monitoring A Subterranean Structure with the SOFO System**, B. Glisic, M. Badoux, J.-P. Jaccoud, D. Inaudi, *Tunnel Management International magazine, UK, Selected paper, (to be published)*
- **Monitoring of Concrete at Very Early Age Using Stiff SOFO Sensor**, B. Glisic, N. Simon, *Cement and Concrete Composites, Elsevier, Vol. 22, Issue 2, Pages 115-119, 1 Apr. 2000, Oxford, UK*

Conferences:

- **Development of a Displacement sensor for the CERN-LHC Superconducting cryo-dipoles**, Daniele Inaudi, Branko Glisic, Sirine Fakra, Walter Scandale, Juan Garcia Perez, Jaques Billan, *Optical Fiber Sensors 2000, Octobre 11 - 13 2000, Venise, Italy (to be published)*
- **Towards Monitoring of Dynamic Deformations in Civil Structures using SOFO Sensors**, Sandra Lloret, Daniele Inaudi, Branko Glisic, Ian Smith, *Trends in Optical Non-destructive Testing, 3-5 June 2000, Lugano, Switzerland*
- **Optical Set-up Development for the Monitoring of Structural Dynamic Behaviour Using SOFO Sensors**, Samuel Vurpillot, *SPIE's 7th Annual International Symposium on Smart Structures and Materials, March 2000, Newport Beach, USA*
- **Monitoring A Subterranean Structure with the SOFO System**, B. Glisic, M. Badoux, J.-P. Jaccoud, D. Inaudi, *1st International Conference Long Road and Rail Tunnels, November 29 - December 1, 1999, Basel, Switzerland*
- **Dam Monitoring Using Long SOFO Sensor**, B. Glisic, D. Inaudi, P. Kronenberg, S. Vurpillot, *Hydropower into the Next Century, October 18 - 20, 1999, Gmunden, Austria*
- **Bridge Deformation Monitoring with Fiber Optic Sensors**, D. Inaudi, N. Casanova, S. Vurpillot, B. Glisic, Sandra Lloret, *IABSE Symposium, Structures of the future – The search for quality, August 25 – 27, 1999, Rio de Janeiro, Brazil*
- **Packaging Interferometric Sensors for Civil Structural Monitoring**, D. Inaudi, B. Glisic, S. Vurpillot, *13th International Conference on Optical Fiber Sensors, April 12-16, 1999, OFS-13, Kyongju, Korea*
- **Long-term Monitoring of a Concrete Bridge with 100+ Fiber Optic Long-gage Sensors**, D. Inaudi, S. Vurpillot, B. Glisic, P. Kronenberg, S. Lloret, *SPIE's International Symposium on Nondestructive Evaluation Techniques for Aging Infrastructure & Manufacturing, 3-5 March 1999, Vol. 3587, Pages 50-59, Newport Beach, USA*
- **Special Sensors for Deformation Measurements of Different Construction Materials and Structures**, B. Glisic, D. Inaudi, P. Kronenberg, S. Lloret, S. Vurpillot, *SPIE's 6th Annual International Symposium on Smart Structures and Materials, 1-5 March 1999, Vol. 3670-78, Pages 505-513, Newport Beach, USA*

- **Soil-Structure Interaction Effects at the Pile Supported Cooling Tower**, M. Petronijevic, B. Glisic, *2nd National Congress on Computational Mechanics, 26-28 June 1996, Chania, Greece*
- **Dynamic Analysis of Pile Supported Cooling Tower**, M. Petronijevic, B. Glisic, *6th Symposium of the Macedonian Association of Structural Engineers, Vol. 2, ST55, 3-7 Oct. 1995, Ohrid, Macedonia*
- **Dynamic Stiffness of Ring Footing Founded on Piles**, M. Petronijevic, B. Glisic, *6th Symposium of the Macedonian Association of Structural Engineers, Vol. 2, ST54, 3-7 Oct. 1995, Ohrid, Macedonia*
- **Funkcije odgovora prstenastog temelja fundiranog na šipovima (Response Functions of Ring Footing Founded on Piles)**, M. Petronijevic, B. Glisic, *XXI Yugoslav Congress of Theoretical and Applied Mechanics, Vol. C, Pages 380-385, 29 May-3 June 1995, Niš, Yugoslavia (In Serbian)*

Reports:

- **Early Age Behaviour of Concrete and Limitation of Hybride Structures Cracking**, P. Mivelaz, S. Wolf, B. Glisic, J.-P. Lebet, O. Bernard, *MCS, IMAC et ICOM, EPFL, 2000 (In French - to be published)*
- **Long Sensor: Installation of Two Long Sensors in "Emosson" Dam**, B. Glisic, P. Kronenberg, D. Inaudi, *IMAC - DGC- EPFL, Pages 1-11 + Appendix 1-6, Jan. 1999, Lausanne, Switzerland*
- **Cloth Sensor: Transfer of Deformation from Assembled Plastic Bands to the Measurement Fibre**, B. Glisic, D. Inaudi, E. Kessi, *IMAC - DGC- EPFL, Pages 1-6 + Appendix 1-5, Oct. 1997, Lausanne, Switzerland*

NON-PROFESSIONAL PAPERS

Numismatics:

- **Zastitni znak u obliku nominalne vrednosti na novoj seriji švajcarskih novčanica (Security Features in the Form of Nominal Value on the New Series of Swiss Banknotes)**, Branko Glisic, *"Dinar" - Journal of Serbian Numismatic Society, No. 11, Pages 26-28, Belgrade Feb. 1999 (In Serbian and English)*
 - **Vladarska titula na novcu bosanskog kralja Stefana Tomaševica (Sovereign Title on Bosnian Coins of King Stefan Tomaševic)**, Branko Glisic, *"Dinar" - Journal of Serbian Numismatic Society, No. 10, Pages 16-17, Belgrade Oct. 1998 (In Serbian)*
-